COMPARATIVE NEUROANATOMY OF THE MAMMALIAN TRIGEMINAL SOMATOSENSORY SYSTEM

By

Eva Kille Sawyer

Dissertation

Submitted to the Faculty of the

Graduate School of Vanderbilt University

in partial fulfillment of the requirements

for the degree of

DOCTOR OF PHILOSOPHY

in

Neuroscience

August, 2016

Nashville, Tennessee

Approved:

Douglas Kilpatrick Abbot, Ph.D.

Vivien Casagrande, Ph.D.

Kenneth C. Catania, Ph.D.

Jon H. Kaas, Ph.D.

To my mother, Susan Kille; my father, Thomas Sawyer; and my sister, Lucy Sawyer; for supporting me throughout my education. And to Segundo Pablo Lema and his family, who in the midst of their tragedy made a generous choice of organ donation that allowed my family to be spared.

ACKNOWLEDGEMENTS

In my graduate school training I have had the opportunity to benefit from the guidance of many great mentors, most notably my thesis advisor Dr. Jon H. Kaas, and Dr. Kenneth C. Catania. Both of these mentors supported my development as a scientist and allowed me the freedom to shape my own research trajectory. I learned much from their examples of how to be a professional scientist, and I will always admire the passion they have for their work. In addition, I have benefited much from the rest of my thesis committee. Conversations with Dr. Vivien Cassagrande almost always draw out a way of looking at a problem that I had not considered, and I have yet to find a limit of her knowledge of neuroscience. Dr. Patrick Abbot's expertise lies outside of neurobiology, and yet he challenged me with questions that were so on point that they helped me develop the overall frame of this thesis. In particular, his question of "why these animals?" sent me in a direction that shaped my thinking about the future of comparative neurobiology.

I have had the opportunity to work with many wonderful, generous, intelligent and supportive lab mates. Every one of them devoted their time to teaching me a technique, critiquing my thinking, helping with my experiments, and/or talking me through mid-graduate school crises. Thank you to Dr. Pooja Balaram, Dr. Mary Baldwin, Dr. Mariana Gabby, Dr. Duncan Leitch, Dr. Chia-Chi Liao, Daniel Miller, Dr. Jamie Reed, Dr. Iwona Stepniewska, Emily Turner, Laura Trice, and Dr. Hui-Xin Qi.

Of those lab mates, I would particularly like to highlight the work of Laura Trice and Duncan Leitch. Without Laura's support as lab manager I could not have accomplished much of what is presented here. Her foresight and organization allowed the accumulation of the specimens in Chapter V. Without her tireless efforts to help me section, process and mount sections, I could not have completed the pinniped brain histology in Chapter III.

Duncan has been my partner through many of the most exciting and fun scientific moments of graduate school training, from learning about electrophysiology while helping him with his crocodilian projects, to catching moles in the wilds of Pennsylvania, to accompanying me to take publication-quality photos of sea lions and seals. He has also stood with me through the more dull parts. For example he

never tired of fixing my poor spelling and to my knowledge he has never thought less of me for all my errors. I thank him very much for his consistent assistance.

Other Vandervilt researchers also have supported me in graduate school. In particular, Vanderbilt faculty Dr. Anita Disney, Dr. Anna Roe, and Dr. Kenneth Schriver have provided me with critical feedback, support and career advice. In addition students Dr. Suzanna Avery, Terry Jo Bichell, Cassidy Cobbs, Dr. Juli Krueger-Fister, Dr. Sarah Lawson, and Barbara O'Brien, as well as postdoctoral researcher Dr. Diana Sarko, were valuable friends and colleagues.

The animal care staff and veterinarians I have worked with at Vanderbilt have been knowledgeable and devoted to the animals they care for. I thank them for the important work they do. I also thank the staff of the Vanderbilt Brain Institute for helping me navigate through the various requirements and logistical hurdles of graduate school; issues that are can be an underappreciated challenge of academia. Barbara Martin also deserves accolades. The entire Kaas lab owes her for her efforts, often behind the scenes, to sort through mountains of paper work and keep us on track.

Funding for the research presented here was provided by National Institute of Health (NIH) grant NS084706 to Eva K. Sawyer, NIH NS016446 to Jon H. Kaas, NIH grant 3T32MH64913 to Vanderbilt University and a National Science Foundation grant 0844743 to Kenneth C. Catania.

The Neural Systems and Behavior course at the Woods Hole Marine Biological Laboratory was very important to me. Woods Hole is a science haven. My time there allowed me to meet a broader scientific community and have 8 weeks in a new environment to access my goals in science. Numerous faculty of that course were important to me and they include but not are limited to Dr. Randy Bruno, Dr. Hans Hofmann, Dr. William Kristan, and Dr. Krista Todd. I learned from all the students of that course; one of the most important lessons was how lucky I am as a researcher in the United States. I have rarely been as exhausted as I was that summer (the biology-themed July fourth parade still seems like sleep deprivation-induced hallucination). I have also rarely been so content as I was that summer.

Before coming to graduate school, more mentors and friends have shaped my thinking as a scientist than I can thank here. But out of all those experiences, there were three big events that, had they worked out differently, would have likely precluded my interest or ability to pursue a graduate degree in Neuroscience. First, there was a time in my early education where I couldn't learn to read, my attempts at

writing were difficult for even myself to interpret, and I was nearly taken out of the regular education stream. It would have been easy to lose enthusiasm for education and lose any confidence in my own intelligence. I owe so much of my education to the caring support of Phyllis Bilus, Iris Fearon, Karen Louick, and Susan Swed. Not only did they get me through that patch and help me develop strategies to use going forward, but they helped me learn a lesson in perseverance that continues to serve me. The second important event was the excellent advanced placement biology course taught by Dr. Stephanie Tzall. Dr. Tzall, the first female scientist I had ever met, was able to take a difficult course that was taught far too early in the morning and show me the beauty of the Biology. Lastly, as an undergraduate in my junior year Dr. Stephen Emlen allowed me to enter his lab as a research assistant, which was the first time I had even considered research science as a career.

The Gower family has become my adopted family in Nashville. I thank them for their love and support, and I encourage them to move to San Francisco with me.

Lastly, I would like to thank my parents and sister. I come from a family of writers and artists, and these fine people found ways to support me as scientist even though it was well outside their expertise. Thank you for putting up with my long-winded explanations of esoteric topics that you weren't even interested in to begin with, and for your editing efforts even as my research veered into spinal trigeminal subnuclei, vesicular glutamate transporters, cortical somatosensory receptive fields, as well as all the other jargon-filled topics you have read about for my sake.

TABLE OF CONTENTS

PAGE

DEDICATION ii

ACKNOWLEDGEMENT iii

LIST OF TABLES ix

LIST OF FIGURE x

LIST OF ABBREVIATIONS xii

Chapter

I. Introduction 1

Model organisms and comparative biology 1
Trigeminal somatosensation in mice and rats 5
Trigeminal somatosensation in the california sea lion 7
Trigeminal somatosensation in the star-nosed mole 8
Trigeminal somatosensation in prosimian primates 10
Literature review of the somatosensory brainstem 11
Conclusion 12
References 12

II. The Somatosensory Brainstem, Thalamus, and Cortex of the California Sea Lion (*Zalophus californianus)* 17

Abstract 17
Introduction 17
Methods 20
Animals 20
Tissue preservation 21
Tissue processing 21
Antibody characterization 22
Image acquisition and analysis 24
Anatomical designations 24
Results 25
Peripheral nervous system 25
Central nervous system: 26
Discussion 31
Sea lion whiskers and the trigeminal somatosensory pathway 41
Sea lion limbs and the ascending body representation 43
Conclusions 46
Acknowledgements 50
References 50

III. ORGANIZATION OF THE SPINAL TRIGEMINAL NUCLEUS IN STAR-NOSED MOLES (*CONDYLURA CRISTATA*) 56

Abstract 56
Introduction 57

Methods 60
Animals 60
Electrophysiology and receptive field mapping 60
Histochemistry 61
Size of receptive fields 61
Reconstruction of star representations 61
Results 62
Anatomy of subnucleus interpolaris 62
Anatomy of subnucleus caudalis 68
Size of receptive fields 69
Discussion 69
Anatomy of the sensory star 77
Anatomy of subnucleus interpolaris 77
Anatomy of subnucleus caudalis 80
Size of receptive fields 84
Acknowledgements 85
References 85

IV. Subcortical Barrelette-Like and Barreloid-Like Structures in the Prosimian Galago (*Otolemur garnetti*) 90

Abstract 90
Introduction 91
Methods 95
Results 96
Vibrissae 96
Brainstem 97
Thalamus 97
Cortex 99
Discussion 113
Vibrissae 113
Brainstem 114
Thalamus 115
Cortex 116
Conclusions 117
Acknowledgements 118
References 118

V. Literature Review of the Anatomy of the Brainstem Somatosensory Nuclei in Mammals .....

Abstract 122
Introduction 122
Somatosensory pathways 123
Anatomical review 131
Major clade Monotremes, superorder monotremes 132
Major clade Marsupials, superorder Marsupials 133
Major clade Laurasiatheria, order Eulipotyphla 137
Major clade Laurasiatheria, order Carnivora 139
Major clade Laurasiatheria, order Chiroptera 140
Major clade Laurasiatheria, order Artiodactyla 141
Major clade Euarchontoglires, order Rodentia 142
Major clade Euarchontoglires, order Primates 145
Major clade Xenarthra, superorder Xenarthra 151
Major clade Afrotheria, order Hyracoidea 151
Major clade Afrotheria, order Proboscidea: 152
Major clade Afrotheria, order Sirenia: 155
Trends 156

Volumes of brainstem somatosensory nuclei are evolutionarily plastic 156
New nuclei are rare 157
Parcellation of tactile nuclei is common in the brainstem 158
Orientation of functional subdivisions within the cuneate nucleus may be plastic 161
Conclusions 161
Acknowledgements 162
References 162

VI. Conclusions and Future Directions 171

Somatosensory system of the California sea lion 171
Spinal trigeminal nucleus of the star-nosed mole 173
Trigeminal somatosensory system in the prosimian galago 174
Literature review of somatosensory brainstem nuclei in mammals 175
Consideration of methods 176
Overall conclusions 178
References 178

Appendix 180

LIST OF TABLES

Page

CHAPTER II

1. Antibodies used in this study. 23

CHAPTER IV

1. Antibodies used in this study. 94

LIST OF FIGURES

Page

CHAPTER I

1. The brainstem barrelettes, thalamic barreloids, and cortical barrels in a rat....6

CHAPTER II

1. The California sea lion body form....19
2. The peripheral trigeminal somatosensory system of the California sea lion....27
3. Schematic of the lemniscal somatosensory pathway....28
4. The trigeminal brainstem of the California sea lion....29
5. The dorsal column nuclei of the California sea lion....32
6. The somatosensory thalamus of the California sea lion....33
7. The external anatomy of the brain of the California sea lion....35
8. Example histology on coronal sections of the anterior sea lion cortex....37
9. The location of the presumptive somatosensory cortex....39
10. The size of a sea lion and a rat brainstem....47
11. Lateral view of the brain of a cat, dog, raccoon, and sea lion....48

CHAPTER III

1. The star and somatosensory brainstem of the star-nosed mole....58
2. Electrophysiology of the spinal trigeminal subnucleus interpolaris....63
3. Reconstruction of the ray representations in the spinal trigeminal subnucleus interpolaris....65
4. Neural tissue devoted to the representation of each ray, from the periphery to the cortex....70
5. Laminae in the spinal trigeminal subnucleus caudalis....71
6. Star and vibrissae representation in the spinal trigeminal subnucleus caudalis....73
7. Microlesions in the spinal trigeminal nucleus caudalis and corresponding receptive fields....75
8. Size of receptive fields in the principle sensory nucleus, spinal trigeminal subnucleus interpolaris and spinal trigeminal subnucleus caudalis....76
9. The peripheral sensory surfaces and somatosensory brainstem representations in rats and star-nosed moles....82

CHAPTER IV

1.Tactile hairs on the face of the Prosimian Galago....92
2. Whisker-related areas in the somatosensory brainstem....98
3. The somatosensory thalamus of the Prosimian Galago....100
4. Somatosensory mapping and cortico-thalamic tracing in Galago case 14-09....102
5. Somatosensory mapping and cortico-thalamic tracing in Galago case 14-13....104
6. Somatosensory mapping and cortico-thalamic tracing in Galago case 14-06....106
7. Somatosensory mapping and cortico-thalamic tracing in Galago case 14-3, left....108
8. Somatosensory mapping and cortico-thalamic tracing in Galago case 14-31, right....110
9. Summary of tracer accumulation in the somatosensory thalamus following injection in area 3B....112

CHAPTER V

1. Somatosensory pathways....124
2. Examples of anatomical visible somatotopic maps....126
3. Example stains....128

4. Mammal cladogram 129
5. Carnovore brainstems 134
6. Rodent brainstems 136
7. Primate brainstem 146
8. Ape brainstems 148
9. Manatee, Elephant and Hyrax brainstem 153
10. Summary of the organization of the cuneate nucleus 159

CHAPTER VI

1. Comparison of mouse and galago thalamus 177

LIST OF ABBREVIATIONS

5N	motor trigeminal nucleus
An	ansate sulcus
BN	Bischoff's nucleus
C	caudal
CC	Clark's column
Co	coronal sulcus
CO	cytochrome oxidase
Cru	cruciate sulcus
Cu	cuneate,
D	dorsal
DCN	dorsal column nucleus
DRG	dorsal root ganglion
Ecu	external cuneate nucleus
ES	ectosylvian sulcus
Gr	gracile nucleus
L	lateral
Lat	lateral sulcus
M	medial
Me5	mesencephalic nucleus
MG	substantia magnocellularis
MZ	substantia marginalis
PBS	phosphate buffered saline
PFA	paraformaldehyde
PrV	principal sensory nucleus
Ps	pseudosylvian sulcus
R	rostral
S1	primary somatosensory cortex
SG	substantia gelatinosa
SpVc	subnucleus caudalis
SpVi	subnucleus interpolaris
SpVo	spinal trigeminal subnucleus oralis
SpVt	spinal trigeminal tract.
SS	suprasylvian sulcus
STN	spinal trigeminal nucleus
TG	trigeminal ganglion
V	ventral
VGLUT1	vesicular glutamate transporter 1 protein
VGLUT2	vesicular glutamate transporter 2 protein
VIII	8th cranial nerve
VP	ventral posterior nucleus
VPL	ventroposterior lateral subnucleus
VPM	ventroposterior medial subnucleus.

CHAPTER I

Introduction

Mammals use their senses of pain, temperature, proprioception, and discriminative touch to perceive and interact with their environment. These modalities of somatosensation are mediated by an intricate system of sensory neurons that projects along a pathway from the periphery to the brainstem onward to the thalamus and the cortex, as well as to a network of other areas (Ebner and Kaas, 2015). Somatosensation to the face is particularly important behaviorally. For example, the head leads the body when moving through the environment, is the site of ingestion behaviors, and often has a significant role in communication. Many mammals have specialized somatosensory organs on their face, such as the prominent facial whiskers of rodents and pinnipeds or the tactile star of the star nosed mole (Catania, 1995; Sawyer et al., 2016; Vincent, 1912). Not only is touch to the face behaviorally important, but neuroanatomically, it is segregated from touch to the rest of the body. From the periphery, facial touch is mainly conveyed through the trigeminal nerve. In the brainstem, the face is represented nuclei that are distinct from the nuclei that represent the rest of the body. In the somatosensory thalamus, the representation of the face and body are sometimes deemed discrete nuclei, sometimes grouped more closely as subnuclei, but generally considered to be separate. This dissertation focuses on the comparative neuroanatomy of the pathways for touch arising from the face.

In this introductory chapter I will first review some general considerations about how species are chosen for research. I will then introduce each chapter by specifically explaining some of traits of the species reported on in Chapters II, III, and IV, and then presenting the reasoning behind the literature review in Chapter V.

MODEL ORGANISMS AND COMPARATIVE BIOLOGY

The use of animals for scientific research is an important tool in the biological sciences, and a small number of these species have been widely adopted as the main research animals in laboratories around the world (Alfred and Baldwin, 2015; Krebs, 1975). Commonly these animals include *C. elegans*, *Drosophila*, zebrafish, frogs, chickens, and representing the mammals, mice and rats (Bier and McGinnis, 2004). The choice of these

animals is not an accident; their fast development and easy care are well suited the logistical constraints of research. They are often referred to as "model organisms," in part because they provide a useful estimate, or model, of biological processes that occur in species that are less well suited for research. Given the focus on research related to human diseases, many models are meant to serve as a proxy for certain aspects of biological processes in humans. One reason model organisms have been so effective is that there is a deep homology in genetic information and protein function. Thus a tiny translucent nematode can be used as a model of tissue function in humans if we are looking at the level of the protein interactions and cellular metabolism.

One of the great advantages of model species is that their widespread adoption promotes the development of specialized techniques and equipment for use in these species. For example, from the first observation of heritable mutations in *Drosophila* in 1910 (Morgan, 1910), to the first knockout mouse in 1988 (Capecchi, 1989), to the genetic techniques available today (Alfred and Baldwin, 2015; Lawson and Wolfe, 2011; van der Weyden et al., 2011) there has been much progress in making genetic manipulations easier in these select species. The ability to manipulate the genetics of these animals expands the kinds of questions that can be asked in these organisms.

Despite the many advantages of model systems, the narrow focus on just a few species has its weaknesses. The current models are too few to well represent the diversity of life. In fact, because they were selected with a specific criterion in mind (ease of use in laboratories), they are also a biased sample of life. For example *Drosophila* embryos develop quickly, making them a convenient model for developmental biologists. However, one reason early *Drosophila* development can progress at such an elevated rate is because it is marked by an unusual process of nuclear divisions without cell membrane formation (Karr and Alberts, 1986). Thus, the quick development that makes *Drosophila* a convenient study animal also makes it less comparable to the rest of life that it is supposed to be modeling.

There is also a danger of embracing the methods so enthusiastically that one loses sight of the basic biology needed to answer the question. This can be seen in research that becomes focused on animals that lack the sensory abilities or the behavioral repertoire to answer the questions being asked. Examples include the development of models of social and language disorders in species that lack a strong social and vocal learning, or studying the dorsolateral prefrontal cortex in animals that lack that cortical area (Preuss, 1995).

The work of comparative biologists contrast with this model organism approach. Comparative biologists use the diversity of life and the phylogenetic histories of those species to answer questions about the patterns of life

and the mechanisms that generate those patterns. Comparative biologists also tend to pick their study animals in a different way than scientists that work on traditional model organisms. They often try to pick an animal that maximizes the traits that are relevant to the questions being asked. This tenent was famously stated by August Krogh, a comparative physiologist, who wrote, "For such a large number of problems there will be some animal of choice or a few such animals on which it can be most conveniently studied"(Krogh, 1929). This theme was echoed by Walter Heiligenberg, a neuroethologist, who advised his colleagues to study "champion species," by which he meant species that are particularly adept in a certain sensory or motor ability (Heiligenberg, 1991). He reasoned these species would have optimized the neural designs supporting those skills and that the optimized system will be at its most obvious in these animals. Thus an investigator is most likely to be able to recognize the neural substrate supporting the special abilities in these animals. For example, owls are champions of localizing the source of auditory signals. Using this logic, if you are interested in auditory localization, then owls are ideal to study because their exaggerated skills will make the relevant processes and anatomical substrates stand out in comparison to what you might find in an animal with mediocre auditory localization abilities (Heiligenberg, 1991; Konishi, 1986). Biologists who abide by these guidelines forgo the logistical convenience of laboratory animals to benefit from the strong signal-to-noise ratio in these champion animals.

But here too, is a problem. Just as model species have been selected because they are unusually amenable to laboratory life, champion species have been selected because they are convenient outliers. Krogh and Heiligenberg assert that these champion animals should be studied because in these species the question can be easily addressed, and the chance of finding a clear result is greater. Note that they do not say these species should be studied because they provide examples that are generalizable to the rest of life. Indeed, most animals are not champions. Studying sound localization in an owl will reveal the extremes of auditory capabilities across living organisms, and it may apply to other animals as well. However, it is also possible that the owl is uniquely capable because it is fundamentally different than other organisms. Whereas the deep homology of protein structure lends tentative support to the use of traditional model organisms to model cellular functions, it is more contentious to assume a similarly strong background of homology in auditory processing systems.

Other challenges to the study of less commonly researched species include fewer available methods, research tools that must be customized, the logistical hurtles of introducing new species into a research setting, and

animals that are more difficult to obtain. All this makes experiments difficult. In addition, the scientific community working on any one of these animals is small, and without a robust community progress is slow.

With recent advances with the CRISPR interference technique, limited genetic manipulation of some unusual animals is beginning (Cong et al., 2013; Doudna and Charpentier, 2014). These opportunities are exciting, but the methods available for unconventional animals will still lag behind those available for traditional species. CRISPR will not be new forever, and whatever the next new technique is, it will likely be first developed in the most common research animals. Barring a breakthrough, the methods available in less-studied species will always lag behind those available in the most commonly used research species. Given these critiques, comparative biologists working on unusual animals should be able to provide something that cannot be learned from a *C. elegans* or a mouse.

In pursuit of that goal, a recent National Science Foundation-sponsored gathering of leading comparative neurobiologists set out to make recommendations for the future of their field. This document, titled "Discovering General Principles Of Nervous System Organization By Comparing Brain Maps Across Species," makes several suggestions, including that research efforts should coalesce around specific "reference species" to anchor comparisons (Striedter et al., 2014). In their conception, these reference species include the current model organisms and additional species that should be selected for other strategic advantages. The selection criteria may be an animal's behavioral repertoire, or the availability of a well-annotated genome, or it could be the organism's phylogenetic position.

The authors make it clear they do not mean to limit research to these reference species, but they recommend that work outside of these species should be compared back to the references. Without such comparisons, studies of the seemingly exotic champion animals contribute little to a larger understanding of life. This is not to say they are unimportant; studies of specific species can be awe-inspiring, and these stories have an important role in that they help us appreciate the grandeur of that tangled bank teeming with life. However, with an extra step they can be more than just a method to raise awareness about nature's splendor. With an effort to link that knowledge to the rest of biology, the chaotic collections of similarities and differences can be placed within a larger context and patterns can emerge. These patterns will help us predict which neural features are likely to exist in animals that are not yet studied (Striedter et al., 2014).

This dissertation examines the comparative anatomy supporting the sense of touch to the face. This pathway has been extensively researched in laboratory rodents, the reference species for many parts of this thesis. The same pathway in other mammals has been largely unstudied. As such, I set out to examine the specific anatomy of three species that, together, covered a broad range of mammalian phenotypes for facial touch. These are the California sea lion (*Zalophus californianus*), the star-nosed mole (*Condylura cristata*), and the northern greater galago (*Otolemur garnetti*). In each case, I compare what can be learned in this non-reference species, to what is known in the laboratory rodents. The role of trigeminal somatosensation in the biology of the mice and rat, as well as the sea lion, star-nosed mole, and galago is summarized below.

TRIGEMINAL SOMATOSENSORY SYSTEM IN MICE AND RATS

Rats and mice have sturdy tactile hairs on their face, also called whiskers or vibrissae, which they use to explore the world around them (Ahl, 1986; Vincent, 1912). With these whiskers and the neural circuits associated with them, mice and rats acquire information related to the world near, but not in direct contact, with their skin. They can use this sensory array to determine information about the location, size, shape, and texture of objects (Brecht et al., 1997; Carvell and Simons, 1990; Guić-Robles et al., 1989; Prigg et al., 2002). When whiskers are artificially removed animals show pronounced behavioral changes including a change of posture to bring the snout into contact with surfaces and deficits in many domains, including locomotion, foraging, and fighting (Ahl, 1986). To explore, they sweep their facial vibrissae forward and backward in a "whisking" motion (Berg and Kleinfeld, 2003; Hill et al., 2008). This is an active process that has been compared to how humans may run their hands along a surface to access texture (Grant et al., 2014).

When the vibrissae come into contact with an obstacle, the pressure of that contact is transduced into an electrical signal at nerve endings in the vibrissae follicle. The follicles are innervated by neurons of the trigeminal, or fifth, cranial nerve. The trigeminal nerve projects to somatosensory nuclei in the brainstem, specifically the principal sensory nucleus and the spinal trigeminal nucleus (Clarke and Bowsher, 1962; Torvik, 1956). From the brainstem, the signals is relayed to neurons in the ventroposterior medial nucleus of the thalamus (Smith, 1973; Veinante et al., 2000). From the thalamus, the inputs are sent to the primary somatosensory cortex. In all of these locations, the punctate array of whiskers on the face is represented in a one-to-one manner by anatomically distinct

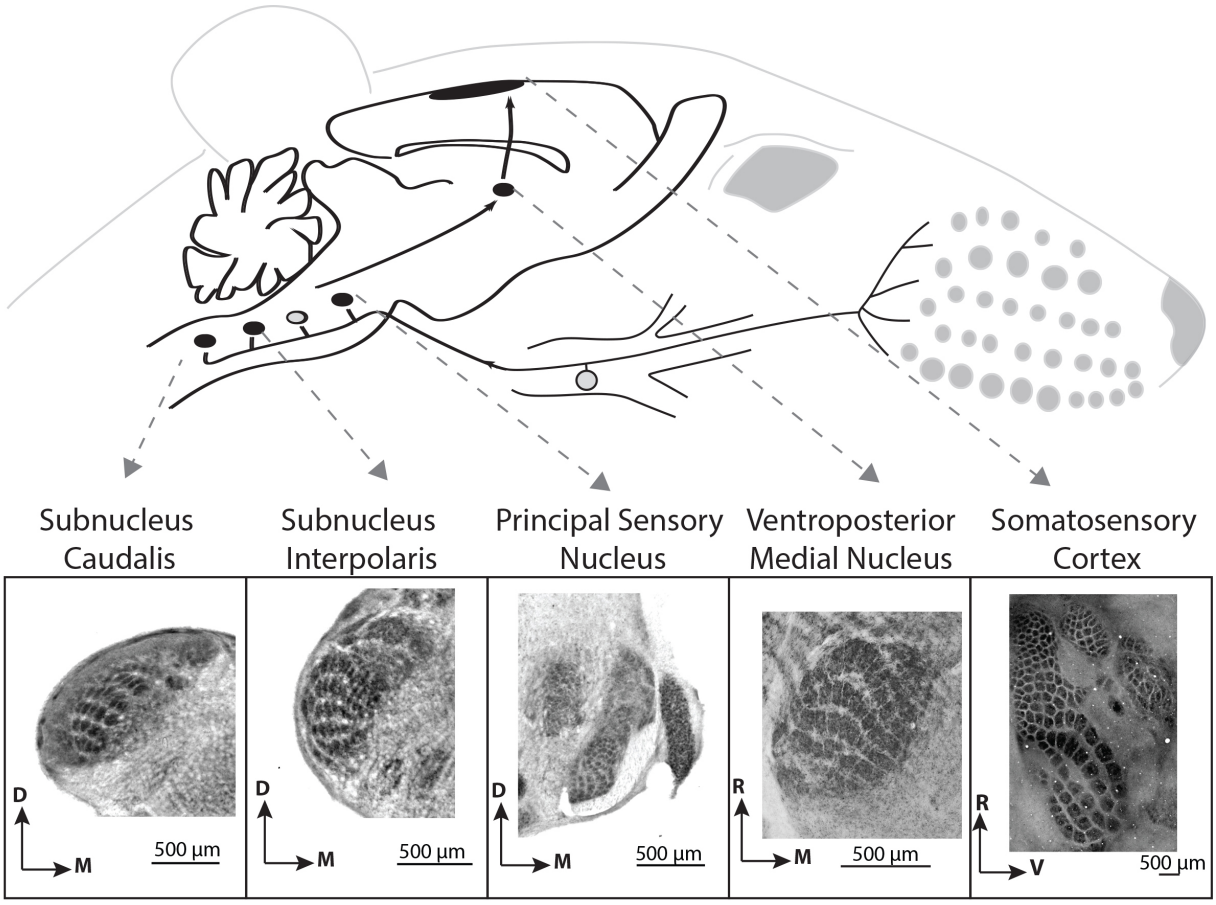

Fig. 1: The brainstem barrelettes, thalamic barreloids, and cortical barrels in a rat. The diagram at the top of the image shows the approximate location of the sections shown at the bottom of the image. All section were processed with cytochrome oxidase. D= dorsal, L= lateral, M= medial, R= rostral

units, called barrelettes, barreloids, or barrels in the brainstem, thalamus, and cortex, respectively (Ma, 1991; Van der Loos, 1976; Woolsey and Van der Loos, 1970). There are three distinct barrelette patterns in the brainstem, with one present in the principal sensory nucleus, another in the spinal trigeminal nucleus pars interpolaris, and the third in the spinal trigeminal nucleus pars caudalis. Thalamic and cortical somatosensory areas each have one visible whisker map.

The presence of these units provides some of the clearest examples of somatotopic mapping in mammals, as well as provides researchers with an anatomically visible and measureable phenotype to judge perturbations to development (Fox, 2008). In addition, the circuits contained in each barrel module are small and has distinct boundaries, allowing researchers to attempt to understand it at the level of the connections of individual cells. The ease of visualization of these whisker-related patterns makes the rodent whisker-to-barrel pathway an experimentally tractable system, which has been adopted by research programs worldwide for studies in realms such as neural plasticity, sensory processing, sensorimotor integration, and brain development (Ebner and Kaas, 2015; Fox, 2008; Krieger and Groh, 2015).

TRIGEMINAL SOMATOSENSATION IN THE CALIFORNIA SEA LION

Pinnipeds (seals, sea lions, and walruses) have the largest vibrissae of all animals (Ling, 1977; Todd, 1852). Examination of the whisker follicles show that seals and sea lions have more sensory axons per follicle than in any other group of animals (McGovern et al., 2014; Wohlert et al., 2015). Pinnipeds are trigeminal specialists, yet little is known about the neural structures that support their abilities.

California sea lions hunt for fish during dives that average 80 meters deep and 3 minutes long but can be as deep as 274 meters and as long as 10 minutes (Feldkamp et al., 1989). During these dives they may use their well-developed whisker array to detect changes in water flow that suggest the movement of prey in water. Behavioral tests show that California sea lions can use their whiskers to follow hydrodynamic trails created to mimic the wake of a fish. They can do this even while blindfolded, auditory signals are blocked, and the fish have a five-second head start (Glaser et al., 2011). Above water, they can be trained to use their whiskers to discriminate between objects of different shapes and sizes. For example, they perceive a difference of as small as 0.33 cm in the diameters of circular disks (Dehnhardt, 1990; Dehnhardt, 1994). While engaged in these active touch tasks, sea lions keep their whiskers fully extended forward and move their entire head to bring different whiskers in contact

with the object (Dehnhardt, 1994). However, when balancing a ball on their nose, sea lions move their whiskers in conjunction with their neck (Milne and Grant, 2014). Clearly they have a different strategy for active vibrissal touch compared the rostrocaudal whisking that laboratory rodents employ. In addition, California sea lions have been observed to use their whiskers in social displays by extending the tips forward to touch the face of a conspecific (Peterson, 1967).

The majority of research on pinnipeds is limited to behavioral studies like those mentioned above. As marine mammals, they enjoy special protections under the Marine Mammal Protections Act of 1972. This act carefully regulates the collection of pinnipeds. Thus, most of what is known of pinniped neuroanatomy is limited to historical specimens in museum collections, or more recently, to studies using magnetic resonance imaging that can be done on both live animals and specimens that are not ideally preserved (Montie et al., 2009; Montie, 2010).

The challenges to investigating pinniped neuroanatomy with histological methods are difficult but not insurmountable. First, getting fresh, well-preserved specimens from animals that died from natural causes requires special circumstances. Second, the brains are large, and few labs are equipped to handle tissues of this magnitude. These challenges were overcome, and some of the results from these efforts are reported in Chapter II. In that chapter I describe the anatomy of the somatosensory areas in brainstem, thalamus, and cortex of the California sea lion. So little is known about pinnipeds neuroanatomy that there are many questions left to investigate with this tissue resource.

TRIGEMINAL SOMATOSENSATION IN THE STAR-NOSED MOLE

This star-nosed mole contrasts with the other animals investigated here in that, rather than the vibrissae being the most prominent trigeminal sensory structures, the chief organ for facial touch in the this species is an elaboration of the glabrous nose. The mole's nose has 22 finger-like nasal appendages or rays that are actively brought into contact with the environment in a sequences of touching, withdrawing, and reorienting motions that can be repeated as fast as 13 times per second (Catania and Remple, 2004). These moles have small eyes and instead rely primarily on the tactile star to explore their underground wetland habitat (Hamilton, 1931). The rays are completely covered in by small somatosensory domes known as Eimer's organs (Eimer, 1871). Externally, these receptors appear as 40-50 μm diameter domes. Internally, they each house a Merkel cell-neurite complex, a

laminated corpuscle, and two classes of free nerve endings (Catania, 1996; Marasco et al., 2006). Up to 28,000 Eimer's organs cover the star surface (Catania and Kaas, 1997).

Previous explorations of the trigeminal somatosensory system in the star-nosed mole revealed an anatomically visible representation of the star in the somatosensory cortex of the star-nosed mole (Catania and Kaas, 1995). When the cortex is stained for markers of metabolic activity, the sensitive rays are represented in dark stripes that indicate high activity in those area (Catania and Kaas, 1995). The dark stripes are separated from other rays by lightly stained septa. All together, these form a pattern of 11 darkly stained stripes radiating out from a central point, one stripe representing each ray. More recently, a similar star pattern was found in the principal sensory nucleus of the brainstem (Catania et al., 2011). Together, the cortical and brainstem representations are analogous to the cortical barrels and one of the three barrelette patterns expected in the brainstem.

A notable feature of the star cortex is that the representation of the particular ray with the least sensory surface area, the most medial ventral ray, covers 25% of the total star representation in primary somatosensory cortex (Catania, 1995). Similar distorted body representations are seen in the "homunculus" of the somatosensory cortex in other animals, such as in the large representations of hands and lips in humans or the large representation of teeth in naked mole rats (Catania and Remple, 2002; Penfield, 1937). There is an intuitive sense that the amount of cortical space devoted to body regions is related to the importance of that area in somatosensory behaviors. A popular proximal explanation for this magnification is that the size of a representation in primary sensory areas of the central nervous system is directly proportional to the number of sensory afferents from that region (Hudspeth et al., 2013). This explanation is supported in mice by the directly proportional relationship between the area of cortical barrels and the number of myelinated fibers that innervate their respective vibrissae follicle (Welker and Van der Loos, 1986). However, this does not appear to be the case in the star-nosed mole.

The cortical overrepresentation of the medial ventral ray persists if the number of Eimer's organs on that ray or the number of myelinated fibers from that ray are considered (Catania and Kaas, 1997; Catania et al., 2011; Catania and Remple, 2004). The brainstem representation of the medial ventral ray is also larger than would be expected by these figures, but here it only comprises 14% of the representation instead of 25% of the representation as in cortex (Catania et al., 2011). This leads to the questions of how, and why, these star maps differ, and what is leading to this overrepresentation of the medial ventral ray? In Chapter III I begin to address these questions by reporting on the remaining two star maps in the brainstem of the star-nosed mole. In this chapter I comparing the

proportions of a star representation in the spinal trigeminal nucleus to the proportion of neural tissue devoted to each ray in the other stations of the somatosensory pathway. By measure as many of the star representations as possible I aimed to identify what part of this pathway contributed to the magnification seen in cortex.

TRIGEMINAL SOMATOSENSATION IN PROSIMIAN PRIMATES

Primates, as a group, have relatively short and indistinct facial tactile hairs that have been considered to be lacking relative to those of other mammals (Jones, 1929; Pocock, 1914). Indeed humans are one of very few mammals that lack them all together (Muchlinski, 2010). Nevertheless, facial touch is important to primates, as demonstrated by behavior, neurobiology, and pathology. Behaviorally, touch to the face is important for non-verbal communication in primates (Burgoon, 1991). In addition, the face is the site of important sensory motor activities including as verbal communication and ingestion behaviors (Sherwood, 2005). Neurobiologically, the human face is overrepresented in our cortical somatosensory representation (Penfield, 1937). This overrepresentation is likely related to the small size of single unit receptive fields, as measured in peripheral nerves. The size of tactile receptive fields on the face is similar to those found for the human hand (Johansson et al., 1988; Vallbo and Johansson, 1984). These small receptive fields likely support the values for psychophysical two-point discrimination tests that are reported in human hands and faces; using their ring finger, humans can discriminate a sensation as two objects and rather then experiencing them as one if they are as close as 2 mm apart, with their chin they must be at least 10 mm apart, while with the back of the neck the distance must be at least 55 mm apart (Gellis and Pool, 1977; Nolan, 1985). Lastly, disorders of facial touch carry severe consequences. Loss of sensation to the face results in difficulties in eating and communicating (Smith and Cutrer, 2011), whereas pathological activation of pain pathways, can lead to trigeminal neuralgia, a condition of intractable facial pain that is so distressing that historically it has also been known as “the suicide disease” (Prasad and Galetta, 2009).

In seeking to investigate facial touch in primates I choose to focus on the prosimian galago. Galagos, or bushbabies, are nocturnal arboreal primates native to Africa. There are 19 species of galagos (family: Galigadae), here we consider the northern greater galago (*Otolemur garnetti)* (Wilson and Reeder, 2005*)*. These animals have a tapered face, large forward facing eyes, and thin vibrissae. Unlike most other primates, the vibrissal follicles have muscle attachments, although galagos have not been observed to actively move their whiskers when investigating their surroundings (Muchlinski et al., 2013). The tactile hairs on their face consist of eight or nine comparatively

long mystacial vibrissae, 39-51 short maxillary vibrissae, and 35-37 short mandibular vibrissae. The unremarkable appearance of their facial tactile hairs suggests that these structures are not important sensory arrays. This is particularly true for the small number of thin mystacial vibrissae. It is likely that galagos acquire information about the objects around their head through vision or through tactile exploration with their dexterous hands and feet, rather than the mystacial vibrissae.

Galagos, with their undistinguished whiskers, do not look like champion animals for facial touch. However, the same could be said for humans. As basal primates with unimpressive whiskers they are well-suited to bridge the gap between the wealth of information on rodent trigeminal systems and growing knowledge the neurobiology of this pathway in primates. In Chapter IV I investigate the trigeminal somatosensory system in galagos and find robust similarities with that from rodents.

LITERATURE REVIEW OF THE SOMATOSENSORY BRAINSTEM NUCLEI

In Chapter V, I review what is known about the anatomy of the trigeminal brainstem nuclei across mammals. This chapter includes a presentation of many brainstems sections that is unique in its breadth across the class Mammalia.

The brainstem varies little across mammals and thus is rarely the focus of interesting comparisons. But seen another way, it is remarkable that a structure with such little anatomically-visible variability in its general design can serve the diverse sensory requirements of whales, monkeys and shrews, while other parts of the nervous system of these animals have changed to a greater extent. If this literature review is appreciated only as a summary of research in the field, then it is useful, if perhaps also dense. However, it is also an exercise to see if the brainstem is a particularly informative structure for comparisons across broad ranges of mammals precisely for the reason it is often neglected: it has changed so little that any changes there are are likely to be important.

As part of my training I have had access to an unusual variety of mammalian brains. While examining these samples I noticed that the anatomy of the brainstem was consistently identifiable even in mammals that were only distantly related, whereas a thalamus or cortex from a novel animal was more difficult to instantly identify. The qualitative pattern I saw was that change seemed to progress fastest in the cortex, followed by the thalamus, and was slowest in the brainstem.

Another biological level where different components have different rates is of change is the sequences of nucleotides and amino acids that make up genes and proteins, respectively. For genes and proteins, those that support functions that are crucial to life can change over generations, but do so more slowly than something of the same class that is non-essential (Alberts, 2015). That concept helps to explain some of the differences in the rate of sequence change for different genes and proteins. For sequence information, the differing rates of change can be used to extract information over different time scales. Sequences that evolve quickly are most useful for comparisons between closely related samples, whereas slowly evolving sequences are useful for reaching further back in time.

A fast rate of change for the cortex, slower for the thalamus, and slowest for the brainstem matched with the broad understanding of the consequences to perturbations to the function of these areas. Damage to the cortex is less devastating to life than similar events in the thalamus. Even more deleterious are alterations in brainstem functioning, which are often devastating and lethal. I wondered if a similar logic used for gene and protein evolution would be useful for understanding how brains change over generations. If so, then studying the very slowly evolving brainstem may be best for comparing animals that are distantly related, such as for a review of mammals. I anticipated that I would find some traits that commonly changed, which would represent normal ways that brains change over time or even in development. I also thought I might find a few drastic changes to the overall plan, and these would represent unusual events in brain evolution that might be particularly important to understanding significant changes in brain structures. Chapter V is the result of this exercise.

CONCLUSION

Finally, in Chapter VI, I summarize the major conclusions about the organization of the trigeminal somatosensory system of sea lions, star-nosed moles, and galagos, and suggest directions future research on these animals could investigate. I will also review the major trends delineated in the literature review in Chapter V. Lastly, I will summarize how the findings here relate back to the anatomically distinct topographic maps seen in the whisker-to-barrel pathway in laboratory rodents.

REFERENCES

Ahl, A. S. (1986). The role of vibrissae in behavior: a status review. *Vet Res Commun* **10**, 245-68.

Alberts, B. (2015). Molecular biology of the cell. New York, NY: Garland Science, Taylor and Francis Group.

Alfred, J. and Baldwin, I. T. (2015). New opportunities at the wild frontier. *Elife* **4**.

Berg, R. W. and Kleinfeld, D. (2003). Rhythmic whisking by rat: retraction as well as protraction of the vibrissae is under active muscular control. *J Neurophysiol* **89**, 104-117.

Bier, E. and McGinnis, W. (2004). Model organisms in the study of development and disease. *Oxford Monographs On Medical Genetics* **49**, 25-45.

Brecht, M., Preilowski, B. and Merzenich, M. M. (1997). Functional architecture of the mystacial vibrissae. *Behav Brain Res* **84**, 81-97.

Burgoon, J. K. (1991). Relational message interpretations of touch, conversational distance, and posture. *Journal of Nonverbal behavior* **15**, 233-259.

Capecchi, M. R. (1989). The new mouse genetics: altering the genome by gene targeting. *Trends Genet* **5**, 70-6.

Carvell, G. E. and Simons, D. J. (1990). Biometric analyses of vibrissal tactile discrimination in the rat. *J Neurosci* **10**, 2638-48.

Catania, K. C. (1995). Magnified cortex in star-nosed moles. *Nature* **375**, 453-4.

Catania, K. C. (1996). Ultrastructure of the Eimer's organ of the star-nosed mole. *J Comp Neurol* **365**, 343-54.

Catania, K. C. and Kaas, J. H. (1995). Organization of the somatosensory cortex of the star-nosed mole. *J Comp Neurol* **351**, 549-67.

Catania, K. C. and Kaas, J. H. (1997). Somatosensory fovea in the star-nosed mole: behavioral use of the star in relation to innervation patterns and cortical representation. *J Comp Neurol* **387**, 215-33.

Catania, K. C., Leitch, D. B. and Gauthier, D. (2011). A star in the brainstem reveals the first step of cortical magnification. *PLoS One* **6**, e22406.

Catania, K. C. and Remple, F. E. (2004). Tactile foveation in the star-nosed mole. *Brain Behav Evol* **63**, 1-12.

Catania, K. C. and Remple, M. S. (2002). Somatosensory cortex dominated by the representation of teeth in the naked mole-rat brain. *Proc Natl Acad Sci U S A* **99**, 5692-7.

Clarke, W. and Bowsher, D. (1962). Terminal distribution of primary afferent trigeminal fibers in the rat. *Exp Neurol* **6**, 372-383.

Cong, L., Ran, F. A., Cox, D., Lin, S., Barretto, R., Habib, N., Hsu, P. D., Wu, X., Jiang, W. and Marraffini, L. A. (2013). Multiplex genome engineering using CRISPR/Cas systems. *Science* **339**, 819-823.

Dehnhardt, G. (1990). Preliminary results from psychophysical studies on the tactile sensitivity in marine mammals. In *Sensory abilities of cetaceans*, pp. 435-446: Springer.

Dehnhardt, G. (1994). Tactile size discrimination by a California sea lion (Zalophus californianus) using its mystacial vibrissae. *J Comp Physiol A* **175**, 791-800.

Doudna, J. A. and Charpentier, E. (2014). Genome editing. The new frontier of genome engineering with CRISPR-Cas9. *Science* **346**, 1258096.

Ebner, F. T. and Kaas, J. H. (2015). Somatosensory System. In *The Rat Nervous System* pp. 675-701 San Diego: Academic Press.

Eimer, T. (1871). Die Schnauze des Maulwurfes als Tastwerkzeug. *Arch. Mikr. Anat.* **7**, 181–191.

Feldkamp, S. D., DeLong, R. L. and Antonelis, G. A. (1989). Diving patterns of California sea lions, Zalophus californianus. *Canadian Journal of Zoology* **67**, 872-883.

Fox, K. (2008). Barrel Cortex. New York: Cambridge University Press.

Gellis, M. and Pool, R. (1977). Two-point discrimination distances in the normal hand and forearm: application to various methods of fingertip reconstruction. *Plast Reconstr Surg* **59**, 57-63.

Glaser, N., Wieskotten, S., Otter, C., Dehnhardt, G. and Hanke, W. (2011). Hydrodynamic trail following in a California sea lion (Zalophus californianus). *J Comp Physiol A Neuroethol Sens Neural Behav Physiol* **197**, 141-51.

Grant, R. A., Itskov, P. M., Towal, R. B. and Prescott, T. J. (2014). Active touch sensing: finger tips, whiskers, and antennae. *Front Behav Neurosci* **8**, 50.

Guić-Robles, E., Valdivieso, C. and Guajardo, G. (1989). Rats can learn a roughness discrimination using only their vibrissal system. *Behav Brain Res* **31**, 285-289.

Hamilton, W. B. (1931). Habits of the Star-Nosed Mole, Condylura cristata. *Journal of Mammalogy* **12**, 345-355.

Heiligenberg, W. (1991). The neural basis of behavior: a neuroethological view. *Annu Rev Neurosci* **14**, 247-267.

Hill, D. N., Bermejo, R., Zeigler, H. P. and Kleinfeld, D. (2008). Biomechanics of the vibrissa motor plant in rat: rhythmic whisking consists of triphasic neuromuscular activity. *The Journal of Neuroscience* **28**, 3438-3455.

Hudspeth, A. J., Jessell, T. M., Kandel, E. R., Schwartz, J. H. and Siegelbaum, S. A. (2013). Principles of neural science.

Johansson, R. S., Trulsson, M., Olsson, K. A. and Westberg, K. G. (1988). Mechanoreceptor activity from the human face and oral mucosa. *Exp Brain Res* **72**, 204-8.

Jones, F. W. (1929). Man's place among the mammals. New York,
London,: Longmans E. Arnold & co.

Karr, T. L. and Alberts, B. M. (1986). Organization of the cytoskeleton in early Drosophila embryos. *J Cell Biol* **102**, 1494-509.

Konishi, M. (1986). Centrally synthesized maps of sensory space. *Trends Neurosci* **9**, 163-168.

Krebs, H. A. (1975). The August Krogh Principle:"For many problems there is an animal on which it can be most conveniently studied". *Journal of Experimental Zoology* **194**, 221-226.

Krieger, P. and Groh, A. (2015). Sensorimotor integration in the whisker system. New York: Springer.

Krogh, A. (1929). The progress of physiology. *American Journal of Physiology--Legacy Content* **90**, 243-251.

Lawson, N. D. and Wolfe, S. A. (2011). Forward and reverse genetic approaches for the analysis of vertebrate development in the zebrafish. *Dev Cell* **21**, 48-64.

Ling, J. K. (1977). Vibrissae of marine mammals. *Functional anatomy of marine mammals* **3**, 387-415.

Ma, P. M. (1991). The barrelettes--architectonic vibrissal representations in the brainstem trigeminal complex of the mouse. I. Normal structural organization. *J Comp Neurol* **309**, 161-99.

Marasco, P. D., Tsuruda, P. R., Bautista, D. M., Julius, D. and Catania, K. C. (2006). Neuroanatomical evidence for segregation of nerve fibers conveying light touch and pain sensation in Eimer's organ of the mole. *Proc Natl Acad Sci U S A* **103**, 9339-44.

McGovern, K. A., Marshall, C. D. and Davis, R. W. (2014). Are Vibrissae Viable Sensory Structures for Prey Capture in Northern Elephant Seals, Mirounga angustirostris? *Anat Rec (Hoboken)*.

Milne, A. O. and Grant, R. A. (2014). Characterisation of whisker control in the California sea lion (Zalophus californianus) during a complex, dynamic sensorimotor task. *J Comp Physiol A Neuroethol Sens Neural Behav Physiol* **200**, 871-9.

Montie, E. W., Pussini, N., Schneider, G. E., Battey, T. W., Dennison, S., Barakos, J. and Gulland, F. (2009). Neuroanatomy and volumes of brain structures of a live California sea lion (Zalophus californianus) from magnetic resonance images. *Anat Rec (Hoboken)* **292**, 1523-47.

Montie, E. W. W., E.; Pussini, N.; Battey, T.W.K.; Barakos, J.; Dennison, S.; Colegrove, K.; Gulland, F. (2010). Magnetic resonance imaging quality and volumes of brain structures from live and postmortem imaging of California sea lions with clinical signs of domoic acid toxicosis. *Dis Aquat Organ* **91**, 243-256.

Morgan, T. H. (1910). Sex Limited Inheritance in Drosophila. *Science* **32**, 120-2.

Muchlinski, M. N. (2010). A comparative analysis of vibrissa count and infraorbital foramen area in primates and other mammals. *J Hum Evol* **58**, 447-73.

Muchlinski, M. N., Durham, E. L., Smith, T. D. and Burrows, A. M. (2013). Comparative histomorphology of intrinsic vibrissa musculature among primates: implications for the evolution of sensory ecology and "face touch". *Am J Phys Anthropol* **150**, 301-12.

Nolan, M. F. (1985). Quantitative measure of cutaneous sensation. Two-point discrimination values for the face and trunk. *Phys Ther* **65**, 181-5.

Penfield, W. B., E. (1937). Somatic motor and sensorv representation in the cerebral cortex of man as studied by electrical stimulation. *Brain* **60**, 389-443.

Peterson, R. S. B., G. A. (1967). The natural history and behaviour of the California sea lion. Stillwater, OK, USA: American Society of Mammalogists.

Pocock, R. I. (1914). On the Facial Vibrissæ of Mammalia. *Proceedings of the Zoological Society of London* **84**, 889–912.

Prasad, S. and Galetta, S. (2009). Trigeminal neuralgia: historical notes and current concepts. *Neurologist* **15**, 87-94.

Preuss, T. M. (1995). Do rats have prefrontal cortex? The Rose-Woolsey-Akert program reconsidered. *Cognitive Neuroscience, Journal of* **7**, 1-24.

Prigg, T., Goldreich, D., Carvell, G. E. and Simons, D. J. (2002). Texture discrimination and unit recordings in the rat whisker/barrel system. *Physiol Behav* **77**, 671-5.

Sawyer, E. K., Turner, E. C. and Kaas, J. H. (2016). Somatosensory brainstem, thalamus, and cortex of the California sea lion (Zalophus californianus). *J Comp Neurol* **524**, 1957-75.

Sherwood, C. C. (2005). Comparative anatomy of the facial motor nucleus in mammals, with an analysis of neuron numbers in primates. *Anat Rec A Discov Mol Cell Evol Biol* **287**, 1067-79.

Smith, J. H. and Cutrer, F. M. (2011). Numbness matters: a clinical review of trigeminal neuropathy. *Cephalalgia* **31**, 1131-44.

Smith, R. L. (1973). The ascending fiber projections from the principal sensory trigeminal nucleus in the rat. *Journal of Comparative Neurology* **148**, 423-445.

Striedter, G. F., Belgard, T. G., Chen, C.-C., Davis, F. P., Finlay, B. L., Güntürkün, O., Hale, M. E., Harris, J. A., Hecht, E. E. and Hof, P. R. (2014). NSF workshop report: discovering general principles of nervous system organization by comparing brain maps across species. *Brain Behav Evol* **83**, 1-8.

Todd, R. B. (1852). The cyclopaedia of anatomy and physiology: Sherwood.

Torvik, A. (1956). Afferent connections to the sensory trigeminal nuclei, the nucleus of the solitary tract and adjacent structures. An experimental study in the rat. *Journal of Comparative Neurology* **106**, 51-141.

Vallbo, A. B. and Johansson, R. S. (1984). Properties of cutaneous mechanoreceptors in the human hand related to touch sensation. *Hum Neurobiol* **3**, 3-14.

Van der Loos, H. (1976). Barreloids in mouse somatosensory thalamus. *Neurosci Lett* **2**, 1-6.

van der Weyden, L., White, J. K., Adams, D. J. and Logan, D. W. (2011). The mouse genetics toolkit: revealing function and mechanism. *Genome Biol* **12**, 224.

Veinante, P., Jacquin, M. F. and Deschênes, M. (2000). Thalamic projections from the whisker-sensitive regions of the spinal trigeminal complex in the rat. *Journal of Comparative Neurology* **420**, 233-243.

Vincent, S. B. (1912). The functions of the vibrissae in the behavior of the white rat: University of Chicago.

Welker, E. and Van der Loos, H. (1986). Quantitative correlation between barrel-field size and the sensory innervation of the whiskerpad: a comparative study in six strains of mice bred for different patterns of mystacial vibrissae. *J Neurosci* **6**, 3355-73.

Wilson, D. E. and Reeder, D. M. (2005). Mammal species of the world : a taxonomic and geographic reference. Baltimore: Johns Hopkins University Press.

Wohlert, D., Kroger, J., Witt, M., Schmitt, O., Wree, A., Czech-Damal, N., Siebert, U., Folkow, L. and Hanke, F. D. (2015). A Comparative Morphometric Analysis of Three Cranial Nerves in Two Phocids: The Hooded Seal (Cystophora Cristata) and the Harbor Seal (Phoca Vitulina). *Anat Rec (Hoboken)* **299**, 370–378.

Woolsey, T. A. and Van der Loos, H. (1970). The structural organization of layer IV in the somatosensory region (SI) of mouse cerebral cortex. The description of a cortical field composed of discrete cytoarchitectonic units. *Brain Res* **17**, 205-42.

CHAPTER II

The somatosensory brainstem, thalamus, and cortex of the California sea lion (*Zalophus californianus)*

This chapter is reproduced with permission from the published work by Sawyer, E. K., Turner, E. C. and Kaas, J. H. (2016). Somatosensory brainstem, thalamus, and cortex of the California sea lion (Zalophus californianus). *Journal of Comparative Neurology* 524, 1957-75. It is unaltered in content.

ABSTRACT

Pinnipeds (sea lions, seals and walruses) are notable for many reasons, including their ape-sized brains, their adaptation to a coastal niche that combines mastery of the sea with strong ties to land, and the remarkable abilities of their trigeminal whisker system. Yet, little is known about the central nervous system of pinnipeds. Here we report on the somatosensory areas of the nervous system of the California sea lion (*Zalophus californianus)*. Using stains for Nissl, cytochrome oxidase, and vesicular glutamate transporters, we investigated the primary somatosensory areas in the brainstem, thalamus and cortex in one sea lion pup, and the external anatomy of the brain in a second pup. We find that the sea lion's impressive array of whiskers is matched by a large trigeminal representation in the brainstem with well-defined parcellation that resembles the barrelettes found in rodents, but scaled up in size. The dorsal column nuclei are large and distinct. The ventral posterior nucleus of the thalamus has divisions, with a large area for the presumptive head representation. Primary somatosensory cortex is located in the neocortex just anterior to the main vertical fissure, and precisely locating it as we do here is useful for comparing the highly gyrified pinniped cortex to other carnivores. To our knowledge this work is the first comprehensive report on the central nervous system areas for any sensory system in a pinniped. The results may be useful in both the veterinary setting and for comparative studies related to brain evolution.

INTRODUCTION

California sea lions (*Zalophus californianus*) are members of the order Carnivora, but despite their close phylogenetic relationship to bears, weasels, dogs, and cats, their lifestyle is drastically different (Agnarsson et al.,

2010; Song et al., 2012). As members of the otariid (eared seal) clade within pinnipeds, they are semi-aquatic animals that are voracious predators in the water, but are obligatory tied to land for parturition and weaning their young (Peterson, 1967). From the wild shorelines of the Pacific to zoos and aquariums worldwide, California sea lions are charismatic animals that are appreciated by humans for their unique behavioral repertoire and extremes of mammalian adaptations.

California sea lions' bodies are built to function both on land and in water, presenting unusual constraints on their musculoskeletal system, sensory systems, and other major organ systems. Independently from the primate lineage they have evolved a brain similar in mass to chimpanzees' (Berta and Sumich, 1999; Bininda-Emonds, 2000; Herndon et al., 1999). They are readily trainable, remarkably agile in water, and are both vocal and social animals (Friedman and Leftwich, 2014; Peterson, 1967; Robards, 1979). As is true for other pinnipeds, sea lions have substantial mystacial vibrissae that are part of a sophisticated touch system we are only beginning to fully appreciate (Dehnhardt, 2008). In the wild, sea lions appear to use their whiskers in social settings by bringing their whiskers in contact with the snout of conspecifics, as if in greeting (Peterson, 1967). It is thought they may also use their whiskers to detect water disturbances caused by potential prey items (Dehnhardt et al., 1998). Sea lion diets show that they are capable of locating fish and squid during dives that average about 80 m in depth, but these dives can be extend much deeper (274 m) (Feldkamp et al., 1989; Fiscus and Baines, 1966).

In experimental settings, California sea lions are able to use their whiskers to follow the hydrodynamic trail made by a remote controlled submarine creating a wake which mimics that of a fish. California sea lions can still complete this task while blindfolded but not when their vibrissae are blocked by a muzzle (Glaser et al., 2011). California sea lions can also use their whiskers to differentiate the size and shape of objects upon direct contact (Dehnhardt, 1994), and they can manipulate their whiskers to complete complicated sensorimotor tasks (Milne and Grant, 2014).

Despite our knowledge of pinniped behavior and our anthropomorphic interest in the evolution of large brains, little is known about the brains of sea lions. What is known includes a recent report on 1.5 T magnetic resonance imaging of a live California sea lion (Montie et al., 2009) and a body of research on the effect of the toxin domoic acid on the central nervous system of California sea lions, a significant health threat to marine mammals that can mimic symptoms of temporal lobe epilepsy and cause deficits in spatial memory (Buckmaster et al., 2014; Cook et al., 2015; Goldstein et al., 2008; Montie, 2010; Scholin et al., 2000). Meanwhile, other basic questions, such as

Fig. 1: The California sea lion. **A**: An adult female rests on a rock, displaying the full body of a sea lion. **B**: The whisker pad on a sea lion. **C**: Two sea lions move their whiskers towards the other in greeting. **D**: The long forelimbs of the sea lion is nearly completely webbed. The forelimbs are used for propulsion when swimming. **E**: The hind limb and tail of the sea lion. The hindlimb is webbed but has 5 distinct digits at the distal end of the limb. Hindlimbs are used during swimming for directional corrections, and can be rotated forward for walking or sitting when on land. **F**: A sea lion displaying its long flexible neck.

the anatomy and organization of the major primary sensory areas of the brainstem, thalamus and cortex have remained understudied.

One area of particular interest is the somatosensory system of pinnipeds. First, the highly specialized mystacial whiskers of pinnipeds share many superficial features with the well-studied whisker system in rodents. In rats and mice, the whisker follicles are represented by anatomically distinct modules in the brainstem, thalamus and cortex (Ma, 1991; Van der Loos, 1976; Woolsey and Van der Loos, 1970). As a result, this pathway has become an exemplar of somatotopic mapping in the central nervous system (Fox, 2008). These modules are found in the brainstem in the principal sensory nucleus (PrV), the spinal trigeminal subnucleus interpolaris (SpVi) and the spinal trigeminal subnucleus caudalis (SpVc); in the ventral posterior nucleus (VP) of the thalamus; and in primary somatosensory cortex. It is unknown how the whisker representation is organized in the central nervous system of any pinniped, which all have brains considerably larger than any rodent. It is not obvious that the ~2 g brain of an adult rat should contain the same organizational features as the ~375 g brain of an adult sea lion, especially in light of metabolic and geometric constraints that arise with such extreme scaling of the brain.

Beyond the organization of the representation of the vibrissae follicles, the sea lion has webbed forelimbs, a trait that is rare in mammals. From the digits of primates to raccoons, breaks in skin surfaces are often represented by cell-sparse septa in somatosensory areas of the central nervous system (Qi et al., 2011; Rasmusson, 1988; Strata et al., 2003; Welker and Johnson, 1965). The forelimb/flipper of the sea lion is a limb at the opposite extreme; it is behaviorally important in locomotion but externally the digits are barely recognizable. It is unknown how the forelimb is represented in the sea lion nervous system.

To explore these and other unknown architectonic features, we used various histological stains to investigate the anatomy of the trigeminal nerve, somatosensory brainstem, thalamus and cortex in the California sea lion.

METHODS

ANIMALS

Images of live animals in Figure 1 were taken at the Central Park Zoo (New York City, NY). Tissue samples were collected from two California sea lion (*Zalophus californianus*) pups (both female, age estimated at 10 months) that were stranded on the California coast during the "unusual mortality event" in the spring of 2015

(Healy, 2015). They were transported to The Marine Mammal Center (Sausalito, CA) for care, where staff veterinarians determined that they had poor clinical prognoses and that euthanasia was the appropriate medical treatment. Veterinary staff euthanized the animals with a barbiturate overdose. The small sample size was dictated by the rare and valuable nature of this tissue. Samples were collected by The Marine Mammal Center under a Marine Mammal Protection Act permit from the National Marine Fisheries Service (no: 18786).

TISSUE PRESERVATION

The bodies of two sea lion pups were given to after the veterinary staff had declared the animals dead. The bodies were immediately decapitated and flexible rubber tubes were inserted into both carotid arteries and held in place with an adjustable plastic band. The head was then perfused through the carotid arteries via a gravity perfusion with four liters of 0.01 M phosphate buffered saline (PBS), followed by four liters of 4 % paraformaldehyde (PFA) in phosphate buffer (pH 7.5) for a total time of 20 minutes. For both animals no more than 15 minuets passed between the declaration and the beginning of the perfusion. After perfusion, the brain was removed and cranial nerves were sampled bilaterally and stored in 10% formaldehyde. The brains were post-fixed in 4% PFA for 36 hours. One brain was then blocked into 6 pieces; the brainstem, the cerebellum, and the left and right anterior and posterior cortex. Brain tissue blocks were then placed into 30% sucrose (in PB) for at least 3 days for cryo-protection before sectioning. The other brain was kept whole for examination of the external anatomy.

TISSUE PROCESSING

Segments of cranial nerve V were cut close to the brainstem and post-fixed in 2.5% glutaraldehyde solution in PBS for at least 48 hours. They were then transferred to osmium tetroxide, dehydrated in a graded ethanol series, placed into propylene oxide, and embedded in resin. They were then cut at 1 μm, mounted onto a glass slide and stained with 1% toluidine blue.

Both sides of each animal's head were photographed so that the whisker patterns could be compared. From one animal, a section of skin was removed from the whisker pad area. This section was stored in 10% formaldehyde, embedded in paraffin, cut at 5 μm and then stained for hematoxylin and eosin.

After cryo-protection, the brainstem and the right anterior cortex were cut in coronal sections, while the left anterior cortex was cut in the horizontal plane. The blocks of brain tissue were sectioned at 50 μm using a freezing

sliding microtome. The sections were divided into eight series and some series were stained for cytochrome oxidase (CO) (Wong-Riley, 1979), Nissl substance with thionin or vesicular glutamate transporter 1 or 2 protein (VGLUT1, VGLUT2). Nissl preparations were used to identify cell bodies, while the CO preparations revealed areas of elevated metabolic activity. Vesicular glutamate transporters are found in the synaptic vesicles in the terminals of glutamatergic neurons, and thus stains for these proteins label areas of dense terminations of excitatory, glutamatergic axons. Immunohistochemical methods have been previously described elsewhere (Balaram et al., 2013). Stained sections were mounted onto glass slides and coverslipped.

ANTIBODY CHARACTERIZATION

Please see table 1 for a list of antibodies used. Rabbit anti-VGLUT1 from Synaptic Systems (Goettingen, Germany) is generated against Strep-Tag® fusion protein of rat VGLUT1 (amino acids 456–560). Preabsorption with the immunogen resulted in negative immunolabeling (Zhou et al., 2007). No staining was observed in VGLUT1 -/- mice (Wojcik et al., 2004). This antibody has been used to label vesicular glutamate transporter 1 in rodents (Dondzillo et al., 2010) and primates (Balaram et al., 2013).

Mouse anti-VGLUT2 from Millipore (USA) is generated against a recombinant rat protein. In Western blots of primate cortex the antibody recognizes a 56-kDa band, which is the known molecular weight of VGLUT2 (Baldwin et al., 2013). This antibody has been used to label vesicular glutamate transporter 2 in rodents (Dondzillo et al., 2010), shrews (Balaram et al., 2013), and primates (Balaram et al., 2013).

In rodents and primates VGLUT1 and VGLUT2 have characteristic expression patterns. Some of these patterns include VGLUT2 being strongly expressed in layer IV of primary sensory areas in mice (Liguz-Lecznar and Skangiel-Kramska, 2007), primates (Balaram et al., 2013), and ferrets (Nahmani and Erisir, 2005), whereas VGLUT1 is strongly expressed throughout the neocortex in layers I-III (mice: (Kaneko and Fujiyama, 2002), primates: (Balaram et al., 2013)). In mice the thalamus has a nearly uniform distribution of VGLUT1, but much more discrete distributions of VGLUT2 (Kaneko and Fujiyama, 2002). In addition, in mice immunoreactivity for VGLUT2 is limited to the granular cell layer of the hippocampus, whereas immunoreactivity for VGLUT1 is more distributed throughout the hippocampal layers. The immunostaining we saw for our VGLUT1 and VGLUT2 antibodies in the sea lion tissue matched these previously reported distribution patterns.

Antigen	**Description of Immunogen**	**Source, Host Species, Cat. #, Clone or Lot#, RRID**	**Concentration (µg/ml)**
Vesicular glutamate transporter 1 (VGLUT1)	Recombinantprotein from rat (aa 456–560)	Synaptic Systems, rabbit polyclonal, 135 303, AB_887876	0.2
Vesicular glutamate transporter 2 (VGLUT2)	Recombinant protein from rat VGLUT2	Millipore, mouse monoclonal, MAB5504, AB_2187552	0.2
Biotinylated horse anti-mouse IgG	Mouse IgG	Vector, mouse polyclonal, BA-2000, AB_2313581	3
Biotinylated goat anti-rabbit IgG	Rabbit IgG	Vector, rabbit polyclonal, BA-1000, AB_2313606	3

Table 1: Commercially available antibodies used in this study.

Stains for VGLUT1 have also been used to reveal barrelette patterns in the brainstem of mice and other animals (rodents: (Kaneko et al., 2002; Sakurai et al., 2013), primates: (Sawyer et al., 2015)). Stains for VGLUT2 have been used to reveal anatomical patterns in the thalamus of mice and other animals (rodents: (Graziano et al., 2008; Louderback et al., 2006), primates: (Qi et al., 2011; Sawyer et al., 2015)).

IMAGE ACQUISITION AND ANALYSIS

High-resolution images of the processed tissue were obtained using a SCN400 Slide Scanner (Leica, Germany) or Imager M2 microscope with a mounted AxioCam Mrc (Zeiss, Germany). The images were imported into Adobe Photoshop (Adobe Systems, CA, USA), where they were manipulated only for brightness and contrast.

For the trigeminal nerve counts, 60x images of entire semi-thin sections were imported into Adobe Illustrator (Adobe Systems, CA, USA). We counted every nerve present at two levels of the nerve. A marker was placed on every myelinated fiber. An image of just the markers was imported into ImageJ (Schneider et al., 2012), and counted using the "analyze particles" function. Every nerve in a single section was counted for both the left and right trigeminal nerves. The diameters of a random sample of 1096 nerve fibers were measured to reveal the distribution of the sizes.

For the cortical reconstruction, sections stained for CO, VGLUT2 and Nissl were examined. Primary somatosensory cortex was identified as a region with a well-developed layer 4 defined by small cells in Nissl stained sections, and a darkly stained band in the location of layer 4 in CO and VGLUT2 preparations. Sections stained for CO were scanned and the images were imported into Adobe Illustrator. Every 400 μm a cortical section was traced and the regions with a dark CO band were marked. The traces were aligned and major sulci identified. The boundaries of the presumptive somatosensory cortex were identified and the area was plotted on a drawing from a photograph of the juvenile California sea lion brain.

ANATOMICAL DESIGNATIONS

Anatomical designations for nuclei and sulci were made with reference to earlier reports in sea lions (Montie et al., 2009; Murie, 1874), their fellow otariid fur seals (Fish, 1898; Ladygina et al., 1985), more distantly related phocid seals (Rioch, 1937; Turner and Miller, 1880), as well as reports on the brains of other carnivores

(polar bear [*Urus maritimus*]: (Kappers et al., 1936), raccoon [*Procyon lotor*] (Rasmusson, 1982; Welker and Seidenstein, 1959), dog [*Canis familiaris]* (Singer, 1962), cat [*Felis domesticus]* (Snider and Niemer, 1961)).

RESULTS

PERIPHERAL NERVOUS SYSTEM

EXTERNAL ANATOMY OF THE SEA LION: Some of the features of the sea lion body form that are relevant to the organization of their somatosensory representation in the central nervous system are displayed in Figure 1. Sea lions have sleek, cylindrically-shaped bodies with a long flexible neck and webbed limbs (Fig. 1a, d, e, f). Their forelimbs are broad and powerful (Fig. 1a, d, f). The digits are almost completely webbed, and there are no visible nails. The hindlimbs are short compared to its body and can be rotated forward during terrestrial locomotion or can trail behind the body during swimming (Fig. 1a, e). The digits of the hindlimb are webbed but the distal tips are separate, and the middle three digits of the hindlimb have nails. Between their hindlimbs, they also have a short, stout tail.

Sea lions have an array of facial vibrissae, with hairs that are long, thick, and straight and found on both their mystacial pad and above their eyes (Fig. 1a,b and 2a). They can extend their mystacial whiskers forward, as visible in Figure 1C, or lay them back flat against their face. In these specimens some whiskers were blunt at the end, suggestive of recent damage to the array. Of the undamaged whiskers, the shortest mystical whiskers were near the nares (0.3 cm) and the longest were at the ventral caudal extent of the whisker pad (11.5 cm). The average whisker length was 3.0 cm (n= 139). The distribution of the vibrissae was identical on both sides of the face in the two specimens examined such that there were two supraorbital whiskers and the mystacial pad was arranged in six rows with a total of 38 vibrissae (Fig. 2b). Row A had four vibrissae, row B had six, rows C-D had eight each, and row F had four. Routine hematoxylin and eosin staining of a single whisker follicle revealed blood cells in the cavernous sinus (Fig. 2c), which is a distinguishing feature of vibrissa follicles as opposed to the hair follicles for pelage. The staining also revealed where the deep vibrissal nerve penetrates the dermal capsule.

TRIGEMINAL NERVE: The trigeminal nerve was noticeably large compared to the other cranial nerves. The presumptive motor root was distinctive as a separate bundle of fibers that ran adjacent to the thick trigeminal sensory root. Two classes of myelinated fibers were present: those with thick myelin sheaths and those with thin

sheaths (see examples in Figure 2D). The class of fibers with thin sheaths was 2.58 ± 0.64 um in diameter (n= 452), while the class of fibers with thick sheaths was larger (8.62 ± 2.65 um in diameter (n= 643)). The diameter of myelinated axons in the sensory root appeared to segregate into a biomodal distribution with a peak for the thickly myelinated axons (Fig. 2g bottom) and another for the thinly myelinated axons (Fig. 2g top). There were 118,603 (±1,834) myelinated fibers in the sensory root and 3,534 (±1,90) myelinated fibers in the motor root. In the sensory root there were 57,248
(±1,197) thinly myelinated fibers and 61,355 (±3,031) thickly myelinated fibers axons. In the motor root there were 626 (±141) thinly myelinated fibers and 2,909 (±49) thickly myelinated fibers axons.

CENTRAL NERVOUS SYSTEM

The ascending somatosensory pathway in mammals has relays in the brainstem, thalamus and cortex. A basic schematic of the connections between the areas that will be discussed in this section is shown in Figure 3.

BRAINSTEM: In the SpVc, SpVi, and PrV there was distinct parcellation of the tissue (Fig. 4 a-d, Fig. 4 e-h, and Fig. 4 i-l, respectively). The Nissl preparations (Fig. 4 a, e, i) revealed clusters of cells, the CO preparations (Fig. 4 b, f, j) contained marked modules of high metabolic activity, and the VGLUT1 immunohistochemistry (Fig. 4 c, g, k) revealed dense termination of nerve afferents. These modules were separated by septa with lower cell density which stained sparsely for CO and VGLUT1 protein. The pattern was similar to the distribution of the whiskers across the surface of the face, though in no single tissue section was there a perfect one-to-one correspondence. In the SpVc, the pattern was visible over 4.2 mm on the rostrocaudal axis (from section 49 to 133), and the average cross-sectional area of the modules was 66,800 (±28,000) μm^2. In the SpVi, the pattern was visible over 5 mm on the same axis (from section 157 to 257), and the average cross-sectional area of the modules was 34,000 (±16,200) μm^2. In the PrV the pattern was visible over 3.8 mm (from section 393 to 469), and the average cross-sectional area of the modules was 28,900 (±13,700) μm^2.

The Dorsal Column Nuclei (DCN) were present in the dorsomedial medulla as a group of cells with large neuronal cell bodies (Fig. 5 E, F). These nuclei stained darkly for cytochrome oxidase and VGLUT1 protein (Fig. 5G-J), and there were many cell-sparse septa in this nuclear group. The DCN were present from the first sections cut

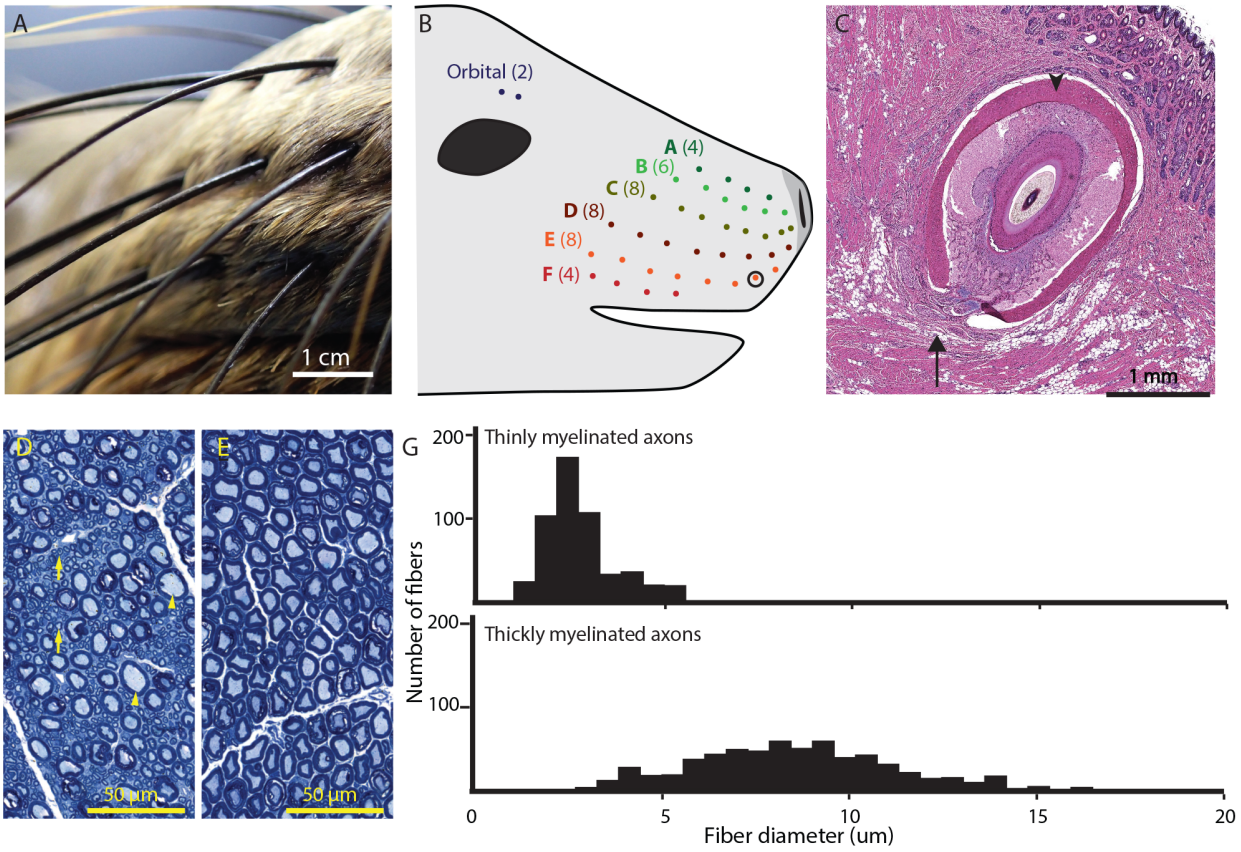

Fig. 2: The peripheral trigeminal somatosensory system of the California sea lion. **A**: A photo of the mystacial vibrissae. **B**: A diagram of the location of the vibrissae on the head of the sea lion. **C**: A longitudinal section of the whisker follicle circled in B that has been stained for hematoxylin and eosin. The arrow points to the deep vibrissal nerve that innervated the base of the follicle. The arrowhead indicates the location of blood cells in the cavernous sinus, a feature of whisker follicles. **D**: A photomicrograph of the sensory root of the trigeminal nerve stained with toluidine blue. Arrowheads point to examples of large fibers, and arrows point to examples of small fibers. **E**: A photomicrograph of the motor root of the trigeminal nerve stained with toluidine blue. **F**: Histograms of the bimodal distribution of axon diameters in the sensory root of the trigeminal nerve of thinly myelinated (top) and thickly myelinated (bottom) fibers.

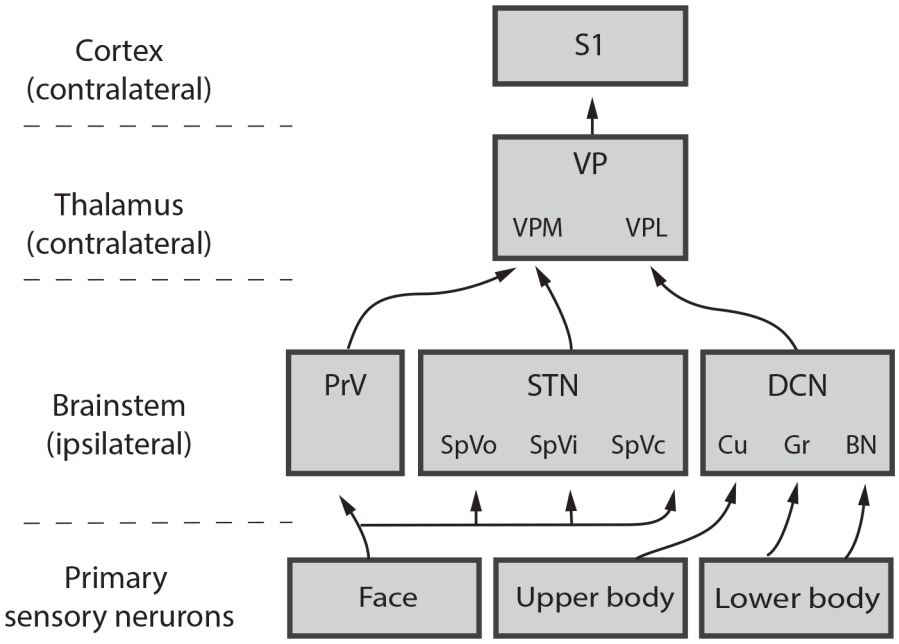

Fig. 3: A basic schematic of the lemniscal somatosensory pathway. Abbreviations: BN= Bischoff's nucleus, Cu= cuneate, DCN= dorsal column nucleus, Gr= gracile nucleus, PrV= principal sensory nucleus, S1= primary somatosensory cortex; STN= spinal trigeminal nucleus, SpVc= spinal trigeminal subnucleus caudalis, SpVi= spinal trigeminal subnucleus interpolaris, SpVo= spinal trigeminal subnucleus oralis, VP= ventroposterior nucleus, VPL= ventroposterior lateral subnucleus, VPM= ventroposterior medial subnucleus.

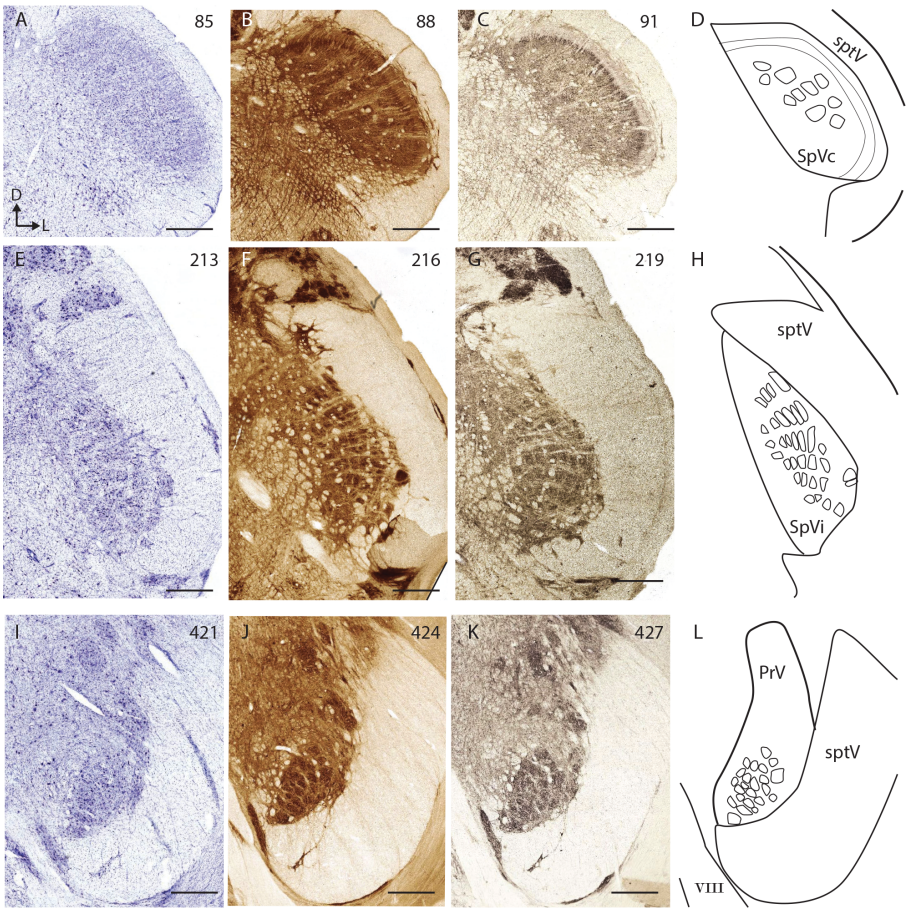

Fig. 4: The trigeminal brainstem of the California sea lion. **A, B: and C**: Photomicrographs of sections of the spinal trigeminal subnucleus caudalis stained for Nissl substance, cytochrome oxidase (CO) and vesicular glutamate transporter 1 (VGLUT1), respectively. **D**: A sketch indicating the location of modules in B. **E, F and G**: Photomicrographs of sections of the spinal trigeminal subnucleus interpolaris, stained as in A, B, and C. **H** A sketch indicating the location of modules in F. **I, J and K**: Photomicrographs of sections of the principal sensory nucleus, stained as in A, B, and C. **L:** A sketch indicating the location of modules in I. In all parts of the figure the number of the section is indicated in the upper right and dorsal is up whereas lateral is to the right. Scale bar = 1 mm. All sections are oriented as shown in A. Abbreviations: VIII= 8TH cranial nerve, D= dorsal, L= lateral, PrV= principal sensory nucleus, SpVc= spinal trigeminal subnucleus caudalis, SpVi= spinal trigeminal subnucleus interpolaris, SpVt= spinal trigeminal tract.

at the level of the caudal SpVc and terminated 10.4 mm rostral to that at the level of the caudal SpVi (sections 1 to 209) (Fig. 5 k). At the posterior extent of the DCN, a cluster of neurons is distinctly dorsal to the rest of the DCN and is located within the gracile fasciculus (Fig. 5E, G, I). However, in sections that are more anterior, this cell group becomes continuous with the gracile nucleus (Fig. 5 F, J, K). It is unclear if this cell group is best interpreted as Bischoff's nucleus or as a mediodorsal extreme of the gracile nucleus. Here we label it as Bischoff's nucleus and indicate it as distinct from the gracile. The boundaries of the cuneate, gracile, and presumptive Bischoff's nucleus are indicated in Figure 5. Finally, within the individual nuclei of the DCN, distinct septa are sometimes present.

THALAMUS: In the coronal (Fig. 6A-D) and horizontal (Fig. 6F-L) sections the VP stains darkly for cytochrome oxidase and VGLUT2 protein. In Nissl-stained sections, the neuronal cell bodies in the VP are larger than those in the surrounding tissue. In the coronal sections, the major subdivision between ventroposterior lateral nucleus (VPL), ventroposterior medial nucleus (VPM) and the ventroposterior inferior nucleus (VPI) could be identified, as shown in the dashed lines in Figure 6B-D. Figure 6E illustrates the shifting boundaries of the VPM and VPL throughout the rostrocaudal extent of the VP. A large portion of the VP consists of the VPM, the face representation.

In the horizontal sections the VP nucleus also has a parcellated appearance, which is created by the septa that run through the nucleus. These septa are most visible in the sections stained for VGLUT2 protein, where they can be seen as lightly-stained strips bordered by darkly-stained regions (Fig. 6 I, L). Septa are also present but less obvious in sections stained for CO and Nissl (Fig. 6J, K). Some example septa are marked with arrows in Figure 6I-K. These septa could mark boundaries separating the representation of major body regions, but no clearly defined anatomically visible somatotopic map was obvious in the coronal or horizontal planes. The VP was rostrocaudally present over 5 mm in the sections cut in the coronal plane (sections 641 to 745), and dorsoventrally over 6.8 mm in the sections cut in the horizontal plane (sections 529 to 665).

CORTEX: The external anatomy of one intact juvenile California sea lion brain was examined. The brain was wider in the parietal/occipital regions than in the frontal regions. It was 6.0 cm wide in the anterior portion, 10.1 cm wide at the widest part of the brain near the posterior end, and 10.2 cm long. The weight after perfusion and immersion fixation was 288.4 g.

The sea lion neocortex has many features typical of carnivorans, but it was notable in the large number of sulci and gyri that are absent in terrestrial members. Distinctive sulci bordering the presumptive somatosensory area are marked in the line drawings in Figure 7. The location of the sulci on the two hemispheres was not identical though they were roughly similar (Fig. 7A, B). The large cerebellum is found under the occipital lobe. The pseudosylvian sulcus and coronal sulcus are oriented nearly vertically (Fig. 7). The anterior portion of the suprasylvian sulcus is not well visible from the external surface but is found on the anterior wall of the convolution labeled as the pseudosylvian sulcus.

The cortex was processed for CO, VGLUT2 protein and Nissl. Some regions of cortex had a distinctive dark band in the sections stained for CO and VGLUT2 protein (Fig. 8). This densely-stained band corresponds to layer 4 in the adjacent Nissl-stained sections (Fig. 8E-G). In these regions, layer 4 was cell dense, layer 5 was cell sparse, and layer 6 was thick and cell dense (Fig. 8F). Together, all these features suggest a primary sensory region of cortex, which in this case appears to be (due to its anterior location) somatosensory cortex.

A series of cortical sections were examined in order to reconstruct the location of the primary somatosensory cortex (S1). The lateral edges of cortical sections 225 to section 681 (spanning 2.23 cm on the rostrocaudal axis) had regions containing the layer 4 band-like features of primary sensory cortex (Fig. 9C). At the anterior extent of S1 this band was present dorsolaterally, absent in a mid-lateral segment, and then was again present ventrolaterally. These two segments of S1 united near section 553, and the suprasylvian sulcus served as a ventral boundary. In the horizontal sections, S1 was visible from section 89 to section 805 (spanning 3.58 cm on the dorsoventral axis) (Fig. 9D). Most dorsally, S1 was present just anterior to the coronal sulcus. By section 193, S1 extends from the coronal sulcus to the suprasylvian sulcus (which is found within the pseudosylvian fissure), and this pattern is maintained to the ventral extent of the area. The extent of S1 is indicated in Figure 9A and B.

DISCUSSION

We present a histological investigation of the primary somatosensory areas in the brainstem, thalamus and cortex of the California sea lion. To our knowledge, this is the first such investigation in any member of the clade Pinnipedia. In light of unusual circumstances affording uncommon access to juvenile sea lions, we were able to preserve the nervous system tissue unusually thoroughly, allowing the histology for markers of metabolism and for specific proteins.

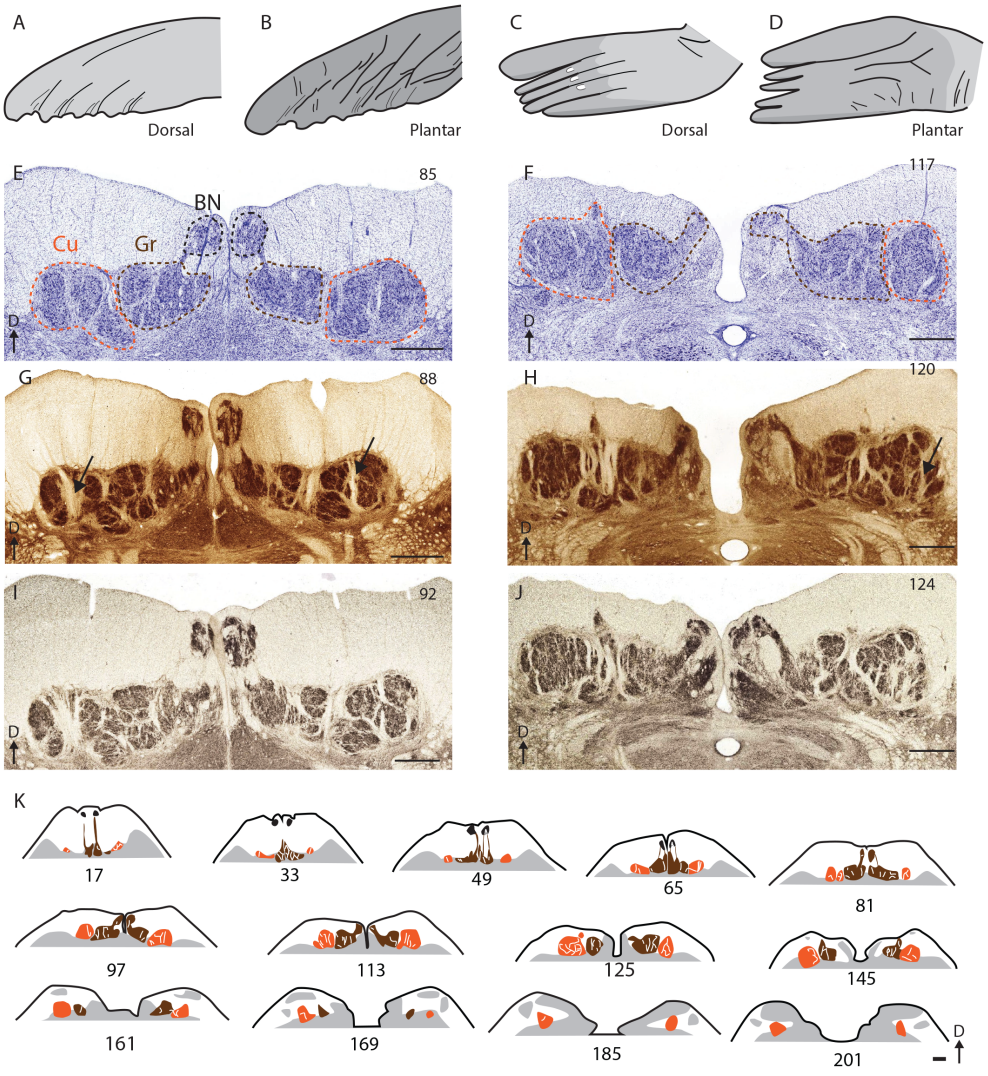

Fig. 5: The dorsal column nuclei (DCN) of the California sea lion. **A and B**: Sketch of the forelimb of a sea lion. C and D: Sketch of the hindlimb of a sea lion. **E and F**: Photomicrographs of the DCN stained for Nissl substance. The number of the section is indicated in the upper right. The cuneate, gracile, and Bischoff's nucleus is outlined in dotted lines of orange, brown and black, respectively. **G and H**: Photomicrographs of the cuneate-gracile complex stained for cytochrome oxidase, labeled as in A and B. **I and J**: Photomicrographs of the cuneate-gracile complex stained for vesicular glutamate transporter 1, labeled as in A and B. **K**: Sketches of the cuneate-gracile complex showing the throughout its rostral caudal extent, from section 17 (most caudal) to 201 (most rostral). The cuneate, gracile, and Bischoff's nucleus are colored orange, brown and black, respectively. Scale bar = 1 mm. Abbreviations: BN= Bischoff's nucleus, Cu= cuneate nucleus, D= dorsal, Gr= gracile nucleus.

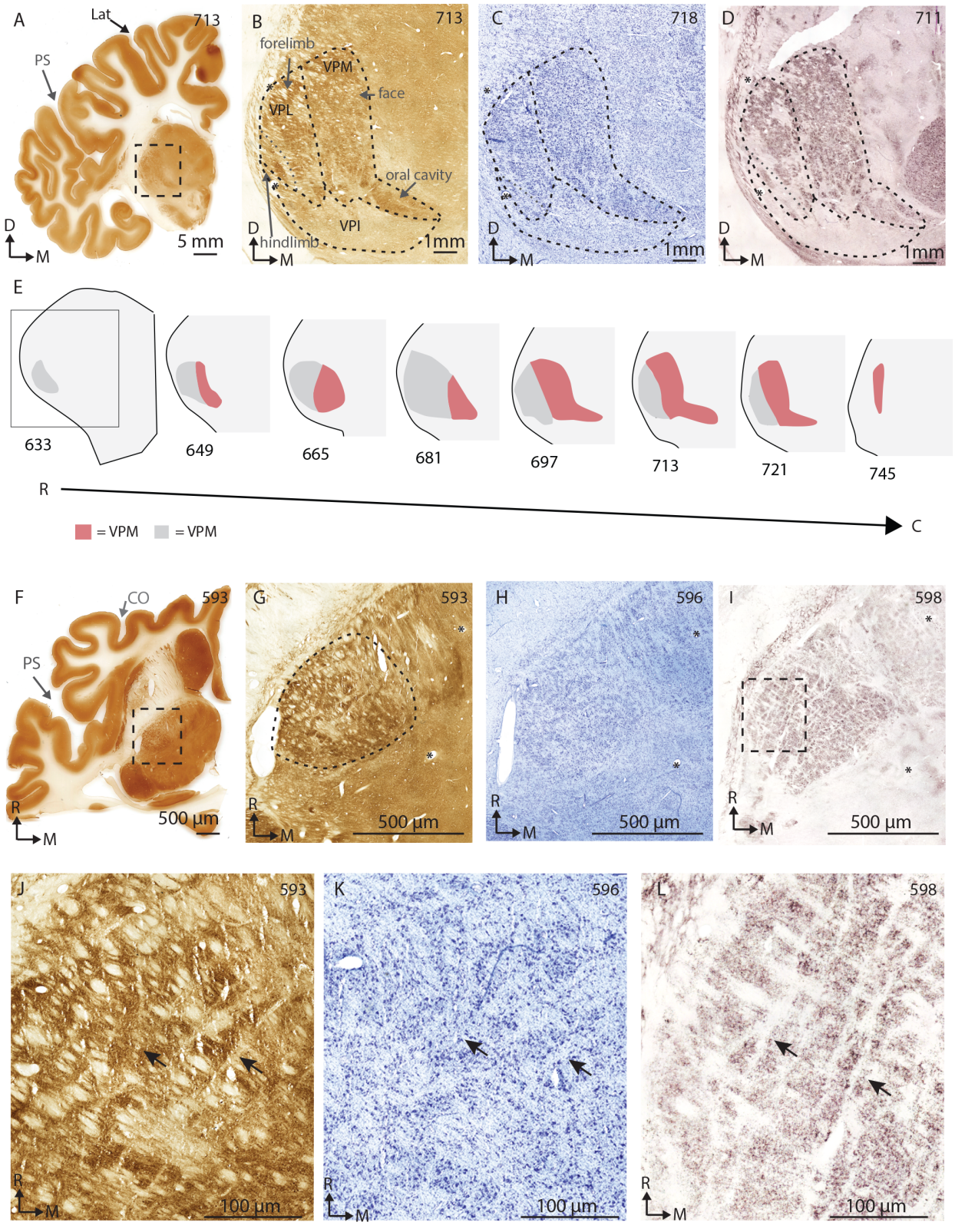
A
Lat
713
PS
D
M
5 mm
B
713
forelimb
VPM
face
VPL
oral cavity
VPI
hindlimb
1mm
C
718
1mm
D
711
1mm
E
633
649
665
681
697
713
721
745
R
C
= VPM
= VPM
F
CO
593
PS
500 µm
G
593
500 µm
H
596
500 µm
I
598
500 µm
J
593
100 µm
K
596
100 µm
L
598
100 µm

Fig. 6: The somatosensory thalamus of the California sea lion. **A**: A photomicrograph of a coronal section of the anterior cortex, stained for cytochrome oxidase. The area outlined by the dashed line is seen in B, C and D. **B, C and D**: Photomicrographs of matched sections of the thalamus that have been cut in the coronal plane and stained for cytochrome oxidase, Nissl and vesicular glutamate transporter 2 (VGLUT2), respectively. The areas outlined by the dotted lines are the ventroposterior medial subnucleus (VPM), the ventroposterior lateral subnucleus (VPL) and the ventral posterior inferior nucleus (VPI). Asterix mark matching blood vessels. **E:** Traces of the ventroposterior nucleus in a series of coronal sections, showing the relative contributions of the VPM and VPL across the rostral-caudal axis. The VPM, the area representing the head region, is shaded red while the VPL is shaded in grey. **F**: A photomicrograph of a horizontal section of the anterior cortex, stained for cytochrome oxidase. The area outlined by the dashed line is seen in F, G and H. **G**, **H** and **I**: A photomicrograph of matched sections of the thalamus that have been cut in the horizontal plane and stained for cytochrome oxidase, Nissl, and VGLUT2. Asterix mark matching blood vessels. The area outlined by the dotted line in F is the VP. The area outlined by the dashed line in I is seen in J, K, and l. **J, K and L**: matched images of a central region of the ventroposterior nucleus, as seen in F-H but at a higher magnification. Arrows indicate septa. In all parts of the figure the number of the section is indicated in the upper right. Abbreviations: C= caudal, Co= coronal sulcus, D= dorsal, Lat= lateral sulcus, M= medial, Ps= pseudosylvian sulcus, R= rostral.

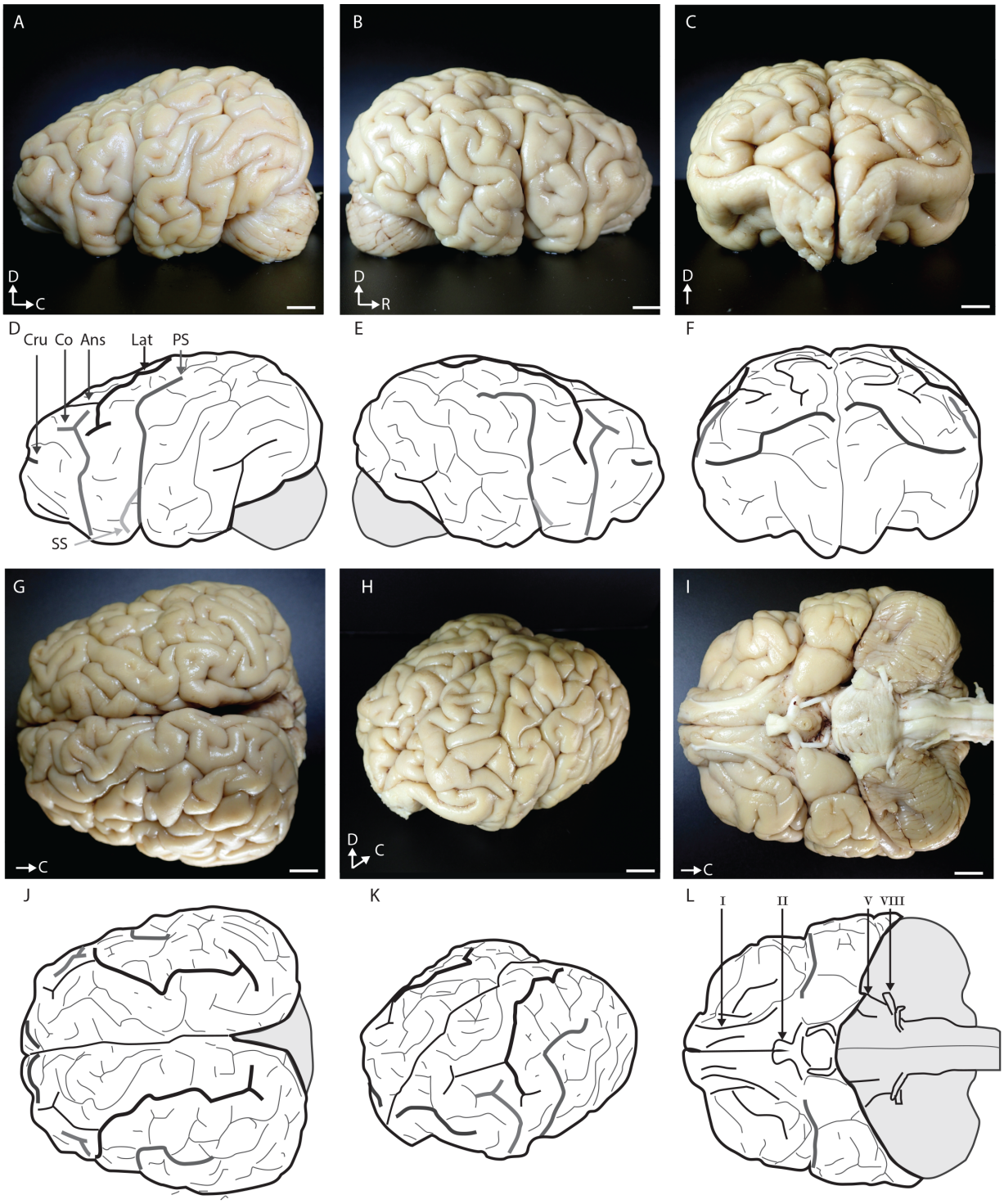
A
D
C
B
D
R
C
D
D
Cru Co Ans Lat PS
SS
E
F
G
C
H
D
C
I
C
J
K
L
I
II
V VIII

Fig. 7: The external anatomy of the brain of the California sea lion. A, B: and C: A left lateral, right lateral, and frontal view, respectively. (**D**), (**E**), and (**F**): A drawing of A, B and C, with 4 major sulci labeled. (**G**), (**H**) and (**I**): A dorsal, isometric, and ventral view, respectively. (**J**), (**K**) and (**L**): A drawing of G, H and I with the same major sulci highlighted as in D, E and F. In addition, the sensory cranial nerves are labeled in L. Scale bar = 1 cm. Abbreviations: Ans= ansate sulcus, C= caudal, Co= coronal sulcus, Cru= cruciate sulcus, D= dorsal, Lat= lateral sulcus, Ps= pseudosylvian sulcus, R= rostral, SS= suprasylvian sulcus.

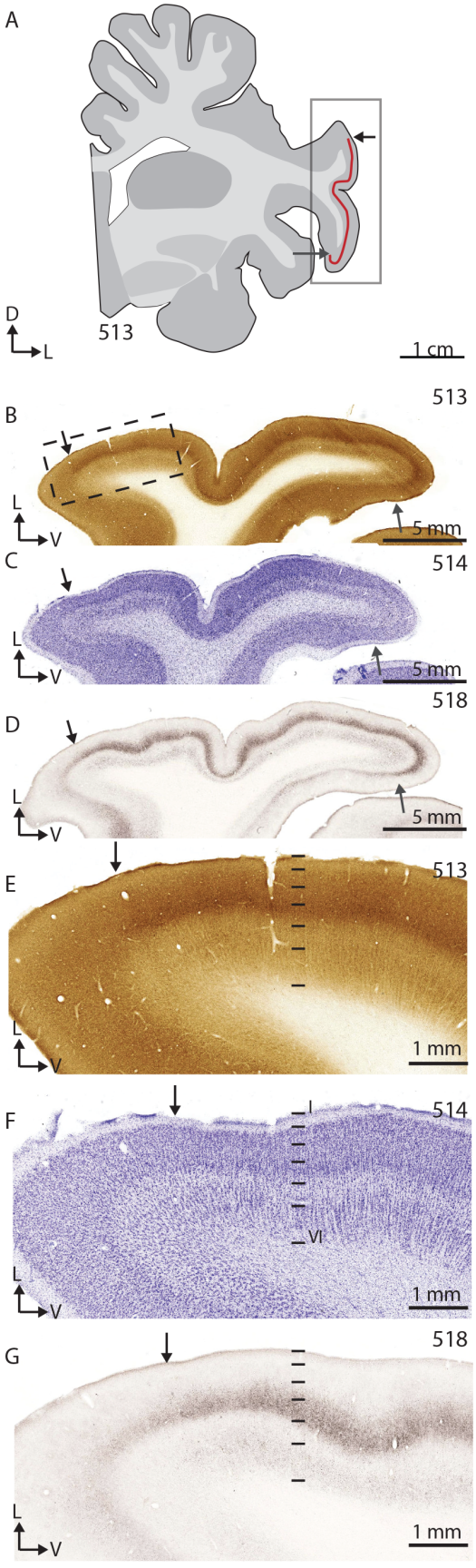
A
D
L
513
1 cm
513
B
L
V
5 mm
C
514
L
V
5 mm
518
D
L
V
5 mm
E
513
L
V
1 mm
F
514
I
VI
L
V
1 mm
518
G
L
V
1 mm

Fig. 8: Example histology on coronal sections of the anterior sea lion cortex. **A:** A schematic of sections 513-518. The red line is the area where the presumptive primary somatosensory cortex is, as defined in sections stained for cytochrome oxidase (CO), Nissl, and vesicular glutamate transporter 2 protein (VGLUT2). The grey line indicates the area enlarged in B, C, and D. Arrows point to the borders of the histologically defined area. **B**: Section 513, stained for cytochrome oxidase, showing a dark brown stripe in layer 4. The dashed line indicates the area enlarged in E, F and G. **C**: Section 514, stained for Nissl substance, showing a neuron dense layer 4 and 6 and a neuron sparse layer 5. **D:** Section 518, stained for VGLUT2, showing dense labeling corresponding to layer 4, and more sparse labeling corresponding to layer 6. **E, F and G:** Enlarged sections of B, C, and D. Black horizontal lines indicate the boundaries of the layers as defined by cytoarchitecture in F. Abbreviations: D= dorsal, L= lateral, V= ventral.

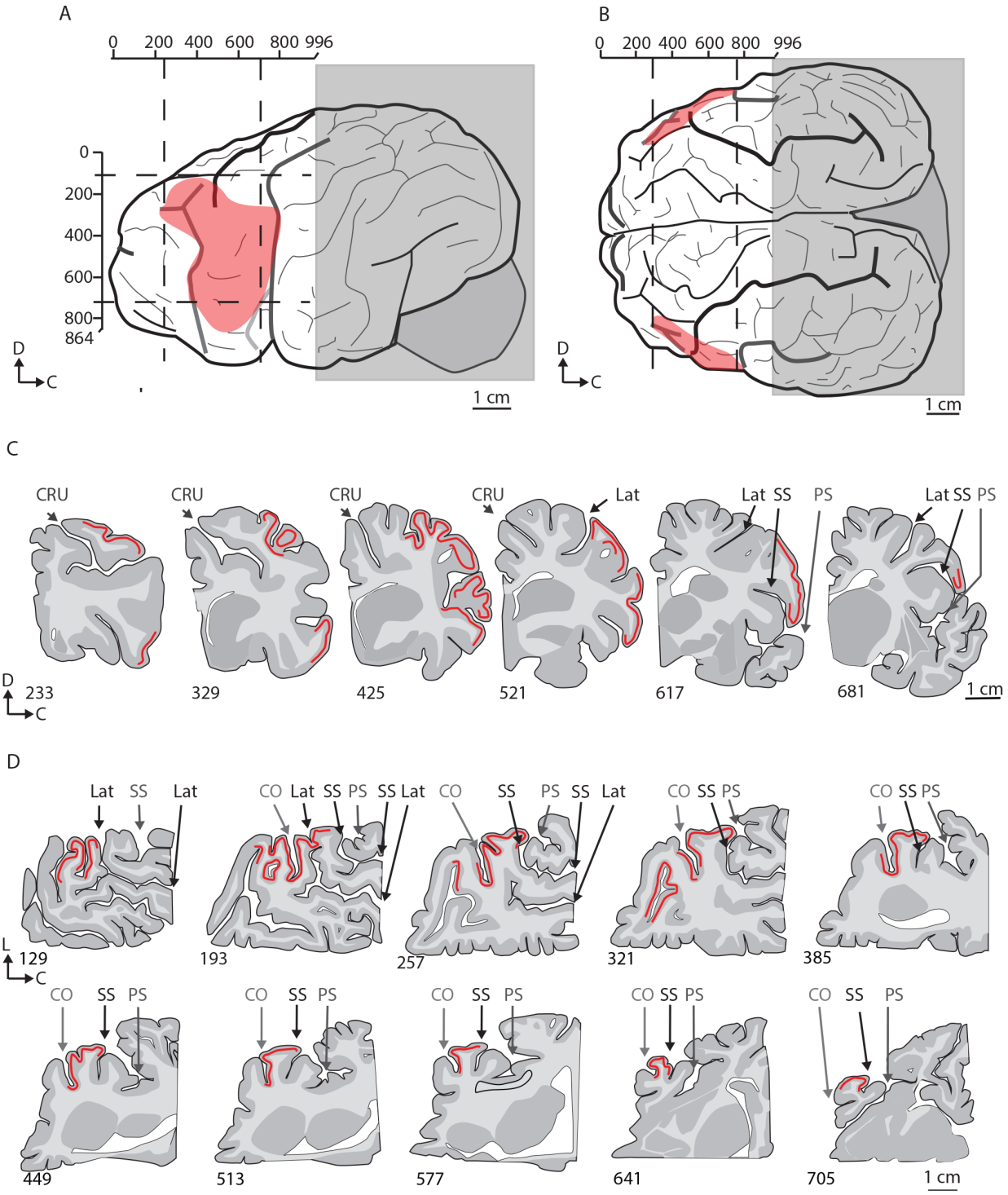
A
0 200 400 600 800 996
0
200
400
600
800
864
D
C
1 cm
B
0 200 400 600 800 996
D
C
1 cm
C
CRU
CRU
CRU
CRU
Lat
Lat SS
PS
Lat SS PS
D
233
329
425
521
617
681
1 cm
D
Lat SS Lat
CO Lat SS PS SS Lat
CO SS PS SS Lat
CO SS PS
CO SS PS
L
129
193
257
321
385
CO SS PS
CO SS PS
CO SS PS
CO SS PS
CO SS PS
449
513
577
641
705
1 cm

Fig. 9: The location of the presumptive somatosensory cortex. **A and B**: Sketches of a lateral view and dorsal view of the cortex of a California sea lion. One hemisphere was cut in the coronal plane, and one in the horizontal plane. The area shaded in grey was not examined in this study. The numbered bars on the margins of the sketches indicate the numbering of the 50 μm sections that comprise the area that was examined. The red overlay indicates the area that where histological and cytoarchitectural markers of primary sensory cortex were revealed (as shown in Figure 9). Note that there are some variations in the sulcal pattern between individuals and between hemispheres in the same individual. **C and D**: Schematic of coronal sections C and horizontal sections D, with the area where there were histological and cytoarchitectural markers of primary sensory cortex marked with a red stripe. The number of the section is indicated at the lower left. Arrows point to major sulci. Abbreviations: C= caudal; Co= coronal sulcus, Cru= cruciate sulcus, D= dorsal, L= lateral, Lat= lateral suclus, Ps= pseudosylvian, SS= suprasylvian sulcus.

SEA LION WHISKERS AND THE TRIGEMINAL SOMATOSENSORY PATHWAY

Our examination of the anatomy of the sea lion whiskers is largely consistent with previous reports (Dehnhardt, 1994; Stephens et al., 1973). Dernhardt reported that the California sea lions has 38 whiskers in 6 rows, which we also observe, though we find that whiskers are distributed differently within those rows (Dehnhardt, 1994). We found that the 6 rows, from dorsal to ventral, had 4, 6, 8, 8, 8 and 4 whiskers, while Dehnhardt found they had 5, 7, 7, 7, 8 and 4. This could be a real difference in the animals we studied but could also be the result of the row designation for the short and thin whiskers near the nares, as these are slightly ambiguous.

Our quantification of the myelinated fibers in the trigeminal sensory and motor roots of the sea lion are comparable to a recent study measuring the number of axons in the trigeminal nerve of related Phocid hooded seals (*Cystophora cristata*) and harbor seals (*Phoca vitulina*) (Wohlert et al., 2015). That study reported 166,700 (± 900) myelinated fibers in the sensory root of the trigeminal nerve in the hooded seal and 129,000 (±3,600) axons in the same location in the harbor seal. The motor roots for the hooded and harbor seals had 7,600 (±2,200) and 7,800 (±1,100), respectively. Those estimates for the seal are similar in magnitude to the direct counts of the myelinated fibers in the trigeminal nerve of the California sea lion completed in this study (sensory root= 118,602 (±1834), motor root = 3534 (±190)). The larger number of fibers in the trigeminal sensory root of the seals may reflect more refined sensory abilities of the whiskers of seals than of sea lions (ex. (Dehnhardt et al., 2001; Glaser et al., 2011; Murphy, 2013)). However, other factors, such as the size of the animal and the innervation of the rest of the head, are also expected to contribute to those estimates. For example, the number of myelinated fibers in the trigeminal sensory root of a human, which lack a specialized mystacial whisker system, has been estimated at 170,000, with 7,700 axons in the motor root (Pennisi et al., 1991), numbers that are comparable with axons counts reported for pinnipeds. In the future, it may be interesting to investigate the special properties of trigeminal somatosensation in pinnipeds by counting the number of fibers in the maxillary branches of the trigeminal nerve, as this would be a more direct measurement of the innervation of the mystacial vibrissae than counts of the entire trigeminal nerve.

Though not directly comparable in methodology, other researchers have estimated the number of myelinated fibers innervating the whisker pads of other pinnipeds. Based on counting the fibers innervating selected vibrissae and multiplying that by the number of vibrissae the animal has, a single mystacial pad of ringed seals and northern elephant seals are both estimated to have about 160,000 myelinated fibers (Hyvarinen et al., 2009; McGovern et al., 2015), and bearded seals nearly 321,000 (Marshall et al., 2006).

Whiskers have a special place in neuroanatomy, as their representations in the central nervous system provide some of the most stunning examples of somatotopic maps. The best examples come from rodents, where the punctate distributions of vibrissal follicles on the face are replicated in a one-to-one manner in cellular columns in the brainstem, thalamus and cortex. These modules have been termed "barrelettes," "barreloids," and "barrels," respectively (Belford and Killackey, 1979a; Ma, 1991; Van der Loos, 1976; Woolsey and Van der Loos, 1970). Here we found a similar pattern of modules in the trigeminal somatosensory nuclei of the brainstem. In the SpVi we found modules that were organized in 6 rows, similar to the 6 rows of whiskers on the sea lion mystacial pad. However, a 6-row organization was less clear in the PrV and SpVc, and in no area did we find 38 modules in the same section. Given the limitations of the material available, this is not surprising. With more samples at the optimal stage of the animal's development and with tissue sectioned in optimal angles/orientations, it is likely that some sections of the PrV and the SpVi would clearly show 6 rows with a total of 38 modules.

More generally, another remarkable feature of the sea lion brain is its absolute size. The brainstem is interesting in that, though large, the general architecture is still well recognizable compared to smaller mammalian model organisms, such as rats (Fig. 10). To illustrate these gross similarities, Figure 10 shows a comparison between the brainstem of a California sea lion and that of an adult rat. While bigger brainstems are expected in larger animals, larger modules representing the whiskers are not a foregone conclusion. A larger brain must overcome the challenge of needing progressively thicker and longer connections to link areas that are farther apart (Striedter, 2005), and this wiring challenge continues with increasing brain size. One way to solve the problem is to add more, small, functional regions, a solution seen in the cortex of primates (Kaas, 2000). It has been suggested that some cortical modules (e.g., barrels in primary somatosensory cortex, blobs in primary visual cortex, entorhinal clusters, and modules in the dolphin insular cortex) all have a similar cross-sectional area despite the range of overall brain sizes these in which these modules are found (Manger et al., 1998). However, the barrelette-like structures in the sea lion SpVc, SpVi and PrV are 11, 6, and 10 times larger in cross-sectional area than those found in a mouse (Ma, 1991). The presence of such large barrelettes in the sea lion brainstem does not fit the pattern suggested for a limit on the size of modules found in the cortex, and may indicate that the brainstem and cortex evolved under different constraints.

SEA LION LIMBS AND THE ASCENDING BODY REPRESENTATION

BRAINSTEM: The dorsal column nuclei are the site of the first central nervous system synapse for primary somatosensory neurons in the dorsal column-medial lemniscal pathway. These nuclei receive somatosensory input from the neck, forelimb, trunk and hindlimbs. From lateral to medial, the dorsal column nuclei are the cuneate, with sensory input from the upper body; the gracile, with sensory input from the trunk and the hindlimb; and the sometimes-present Bischoff's nucleus, with sensory input from the tail.

The body plan of the sea lion is specialized for its semi-aquatic environment in many ways. The forelimbs of the otariids are unique in marine mammals; unlike dolphins, whales, phocid seals and otters, sea lions and fur seals create thrust for swimming by forcefully bringing their forelimbs together in front of their body (Friedman and Leftwich, 2014; Robards, 1979). Sea lions will also use both their forelimbs and hindlimbs for stability and turning (Robards, 1979). Otariid pinnipeds are also distinct from phocid seals in that they retain the ability to use their forelimbs in terrestrial locomotion.

Here, we report a robust DCN with many cell-sparse septa in the cuneate-gracile complex. It is possible these septa represent a feature of the forelimb/flipper anatomy that is not visible from a gross external inspection but would be apparent if the distribution of somatosensory receptors on the flipper were analyzed more closely. We also report a distinct dorsal-medial cell group at the caudal extent of the gracile nucleus that may be an example of Bischoff's nucleus. Bischoff's nucleus is a DCN found in some animals, and is often associated with the representation of the tail (Johnson et al., 1968; Ostapoff and Johnson, 1988; Sarko et al., 2007). However, sea lions have diminutive tails, so it is surprising to find such a distinct cell group. Without experimental evidence we do not know if this cell group in the expected location of Bischoff's nucleus represents the tail or another body part.

Bischoff's nucleus has been found in other mammals that have independently evolved aquatic lifestyles, such as manatees and whales (Sarko et al., 2007; Wilson, 1933) . It is possible that the presence of this distinct cell group is related to a characteristic sensation of swimming that all of these animals experience, perhaps sensing water movements at the caudal end of the body. This could be tested by examining the tail and hind flippers to see if a strong sensory role is likely based on their anatomy, which could be done by looking for high innervation density of, or specialized somatosensory receptors on, these surfaces. It is also possible that the nucleus is related to a reduction in hindlimbs that is seen in marine mammals. Sea lions and fur seals have maintained the ability to use their hind limbs to walk on land, but these hind limbs are reduced compared to their more terrestrial relatives. It would be

interesting to look for this brainstem nucleus in the phocidae, members of the pinniped clade that have lost the terrestrial function of their hindlimbs, and which have hind limbs that are more fluke-like. If this nucleus is related to a lost of individuality of the hind limbs we might expect this nucleus to be more pronounced in the phocidae than in the sea lion.

THALAMUS: The VP is the main somatosensory nucleus in the thalamus. In mammals, the representation of the head area is more medial in the VPM, and the representation of the body is more lateral in the VPL.

The sea lion VP had lightly stained and cell-poor septa separating more densely stained and cell-dense modules (Fig. 6D, H, K). Similar septa are apparent in the VP in other mammalian species. In monkeys and prosimian primates there is a distinct septum separating the hand and face representation, another separating the hand and leg representation, and there are even septa that divide the representations of the digits (Le Gros Clark, 1932; Qi et al., 2011; Sawyer et al., 2015). In the sea lion, the coronal sections have septa that likely represent the forelimb/face border. Based on these septa, the presumptive face representation in the thalamus is large. This result is consistent with the behavioral importance of the whiskers (Dehnhardt, 1994; Glaser et al., 2011; Milne and Grant, 2014), the large trigeminal nerve, the size of the trigeminal representation in the brainstem, and previous electrophysiological mapping in pinniped cortex that reported a large face representation (Ladygina et al., 1985).

With further investigation and additional techniques it should be possible to further divide the sea lion VP complex. In other species, a more cell-dense portion of the VP complex, the ventroposterior superior nucleus, receives proprioceptive input (primates: (Kaas et al., 1984), raccoons: (Wiener et al., 1987) cats: (Dykes et al., 1986)). This division is probably present in the superior portion of the VP complex in sea lions as well. In addition, near the medial extent of the oral cavity representation there should be a parvocellular division of the VPM, an area which has been implicated in taste processing in primates (Iyengar et al., 2007). This would be an interesting area for future work as pinnipeds have non-functional copies of taste receptors involved in the perception of umami and sweet flavors (Jiang et al., 2012; Sato and Wolsan, 2012), which might be reflected in the anatomy of this nucleus.

In addition, in many rodents thalamic barreloids represent the vibrissal follicles (Van der Loos, 1976) and similar whisker-related segmentation has been reported in prosimian primates (Sawyer et al., 2015). However, many of these patterns are best visualized in non-traditional cutting planes that usually require trial-and-error to perfect (Haidarliu and Ahissar, 2001). In the sea lion thalamus, we hypothesize that there are modules that represent

the whiskers follicles. However, this investigation is limited to histology of the brain of one animal, and the tissue was cut at traditional coronal and horizontal angles. Thus, the lack of clear whisker-related modules is unsurprising, as it is unlikely we cut the tissue in the optimal angle or orientation for visualization of the VP. It is possible that, within the areas of the VPM with a mottled appearance, such modules would be revealed with further investigation in additional specimens.

CORTEX: There have been efforts to describe the external anatomy of sea lion brains (Montie et al., 2009; Murie, 1874), but the many sulci in pinnipeds present a challenge when attempting to identify which cortical landmarks are likely to be homologous to those in other carnivores and which are unique to pinnipeds. Previous anatomical reports in sea lions (Montie et al., 2009; Murie, 1874), fur seals (Ladygina et al., 1985), phocid seals (Rioch, 1937), and other carnivorans(bears (Kappers et al., 1936), raccoons (Rasmusson, 1982; Welker and Seidenstein, 1959), dogs (Singer, 1962), cats (Snider and Niemer, 1961)) were used as references, but in some cases the labeling schemes were in conflict. For example, the location of the ansate sulcus in the otariids (eared seals) is either a branch off the anterior end of the lateral sulcus that does not make contact with the suprasylvian (Ladygina et al. 1986), a short connection between the medial suprasylvian sulcus and the lateral sulcus (Fish, 1898) or it is not labeled (Murie, 1874). Similarly, the coronal sulcus is either a long vertically oriented sulcus that is continuous with the suprasylvian sulcus (Fish, 1898; Ladygina et al., 1985), a diagonally oriented short sulcus that does not come into contact with other sulci (Rioch, 1937), or is not labeled (Murie, 1874). Given these and other conflicts, the labeling of the major sulci was undertaken with caution and limited to those near the presumptive somatosensory cortex.

The sulci patterns for the sea lion and closely related carnivorans are shown in Figure 11. The location of S1 is also shown in cats, dogs and raccoons (Bromiley et al., 1956; Dykes et al., 1980; Felleman et al., 1983; Rasmusson, 1982; Welker and Seidenstein, 1959). The species most closely related to pinnipeds for which there is electrophysiological mapping of the somatosensory cortex are the raccoon and domestic dog. In raccoons and dogs, S1 extends between the ansate sulcus dorsally, the coronal sulcus rostrally and the suprasylvian sulcus caudally (Bromiley et al., 1956). In the external examination of the sea lion cortex, S1 appears to extend more caudally compared to other carnivores, stretching all the way to the pseudosylvian sulcus. However, in sections we found that the suprasylvian sulcus is hidden along the rostral bank of the pseudosylvian fissure, and that S1 terminates in that

rostral bank. In cats, S1 is more restricted and does not extend to the suprasylvian sulcus. Our finding that S1 in sea lions is roughly bordered by the same sulci as in other carnivoran species lends support to the sulci naming scheme offered here.

Electrophysiological mapping in any pinniped is rare. The most relevant to this study is a multi-unit mapping experiment in a somatosensory area in fur seals (Ladygina et al., 1985). They reported an area that contained an inverted representation of the body so that the tail was represented dorsal and just anterior to the coronal sulcus, the tip of the face was represented just anterior to the pseudosylvian sulcus and the rest of the body was represented in a somatotopic layout in between. Within this map, the mystacial vibrissae had a large representation that was located just anterior to the pseudosylvian sulcus. This placement is roughly consistent with another investigation in the harbor seal which used surface electrodes to locate a region of cortex that was responsive to taps on the upper lip or mystacial pad (Alderson et al., 1960). Given the phylogenetic distance between sea lions, fur seals, and harbor seals, both of these studies are remarkably consistent with the results reported here. The biggest difference is that Ladygina and colleagues continued to report somatosensory responses to a point slightly more anterior to the coronal sulcus than we have labeled as a primary somatosensory area (Ladygina et al., 1985). This could be the result of using stimuli that would activate proprioceptive afferents, as they are represented in dysgranular area 3a, which is just anterior to S1 in cats (Dykes et al., 1980).

CONCLUSIONS

To our knowledge this work represents the most comprehensive examination of the central nervous system representation of a sensory system in any pinniped to date, a group of mammals with unique sensory specializations and large brains. We described the somatosensory regions in the brainstem, thalamus, and cortex. The trigeminal somatosensory system is interesting in a comparative sense to the well-studied rodent trigeminal system, and particularly fascinating in pinnipeds for the remarkable hydrodynamic trail following abilities it facilitates. We show that the face region has a large and distinct representation in the brainstem and thalamus. Our well-defined S1 region in the sea lion helps clarify sulcal homologies between the gyrified brains of pinnipeds and terrestrial carnivores. Here we show that despite the great phenotypic differences between mice and California sea lions, many fundamental aspects of central nervous system organization are shared.

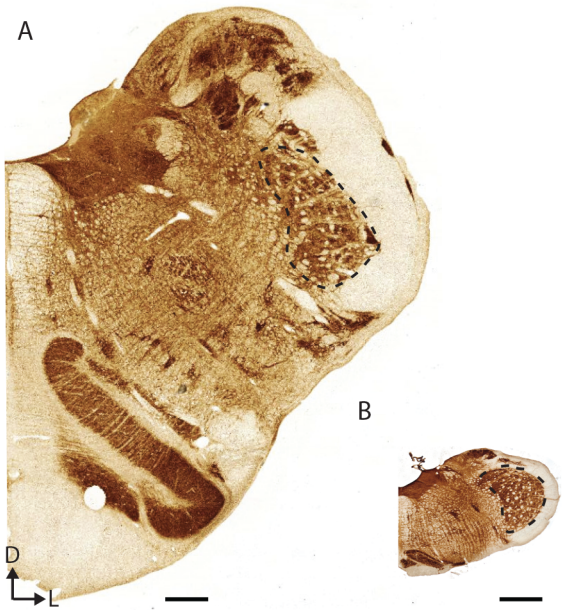

Fig. 10: The size of a sea lion and a rat brainstem. **A**: A section of a sea lion brainstem at the level of the caudal SpVi. **B**: A section of an adult rat brainstem at the same level. Scale bar = 1 mm. Abbreviations: D= dorsal, L= lateral.

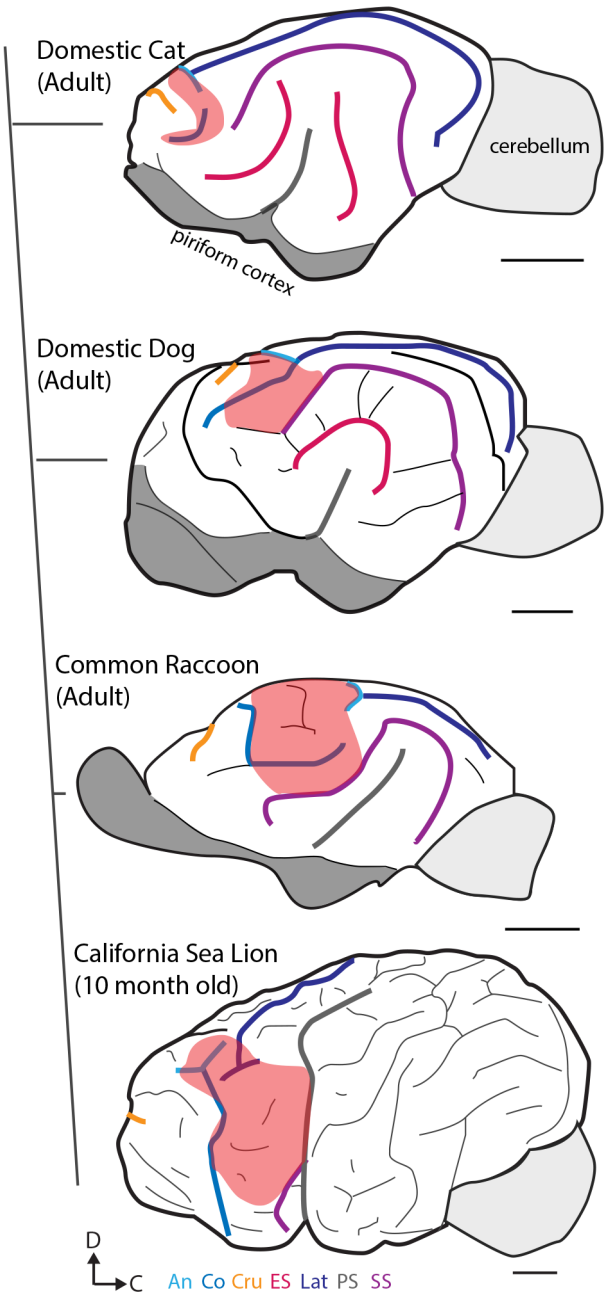
Domestic Cat
(Adult)
cerebellum
piriform cortex
Domestic Dog
(Adult)
Common Raccoon
(Adult)
California Sea Lion
(10 month old)
D
C
An Co Cru ES Lat PS SS

Fig. 11: Sketches of the lateral view of several carnivore brains, organized with a caldogram . The branched line to the left of the figure is based on Agnarsson et al. (2010). The branching pattern indicates clades, but the branch length does not indicate phylogenetic distance. The sulcal pattern shifts across species but the sulci bordering S1 are consistent. The sulcal pattern of the cat, dog and raccoon brains are based off of Snider and Niemer (1961), Singer (1962), Welker and Seidenstein (1959) and Rasmusson (1982). In the cat, dog and raccoon, S1 (as defined by electrophysiological mapping) is shaded in red. The area for S1 in the cat comes from Dykes et al. 1980 and Felleman et al. 1983, S1 in the dog from Bromiley et al. 1956, and S1 in the raccoon is from Welker and Seidenstein (1959) and Rasmusson (1982). S1 in the sea lion is from the results of this study. Note that the suprasylvian sulcus (SS) in the sea lion is found folded within the psuedosylvian fissure. Scale bar = 1 cm. Abbreviations: Ans= ansate sulcus C= caudal; Co= coronal sulcus, Cru= cruciate sulcus; D= dorsal, ES= ectosylvian sulcus, Lat= lateral sulcus, Ps= pseudosylvian sulcus.

ACKNOWLEDGMENTS

This work could not have taken place without the assistance of the research staff and veterinarians at The Marine Mammal Center and we thank them for their assistance and flexibility. The EM samples were prepared in part through the use of the Vanderbilt University Medical Center Cell Imaging Shared Resource. In addition, the histology of the whisker follicle was prepared by Vanderbilt University Medical Center's Translational Pathology Shared Resource, and some images were visualized using the Digital Histology Shared Resource. We thank Lauren Trice for her significant and dedicated assistance with the histology for this large brain. We thank Duncan Leitch and Nina Patzke for their intellectual contributions and technical assistance. This work was funded by NIH grant NS016446 to JHK and NIH grant NS084706 to EKS, and a dissertation enhancement grant from the Vanderbilt University Graduate School to EKS.

REFERENCES

Agnarsson, I., Kuntner, M. and May-Collado, L. J. (2010). Dogs, cats, and kin: a molecular species-level phylogeny of Carnivora. *Mol Phylogenet Evol* **54**, 726-45.

Alderson, A. M., Diamantopoulos, E. and Downman, C. B. (1960). Auditory cortex of the seal (Phoca vitulina). *J Anat* **94**, 506-11.

Balaram, P., Hackett, T. A. and Kaas, J. H. (2013). Differential expression of vesicular glutamate transporters 1 and 2 may identify distinct modes of glutamatergic transmission in the macaque visual system. *J Chem Neuroanat* **50-51**, 21-38.

Baldwin, M. K., Balaram, P. and Kaas, J. H. (2013). Projections of the superior colliculus to the pulvinar in prosimian galagos (Otolemur garnettii) and VGLUT2 staining of the visual pulvinar. *J Comp Neurol* **521**, 1664-82.

Belford, G. R. and Killackey, H. P. (1979). The development of vibrissae representation in subcortical trigeminal centers of the neonatal rat. *J Comp Neurol* **188**, 63-74.

Berta, A. and Sumich, J. L. (1999). Integumentary and sensory systems. In *Marine mammals : evolutionary biology*, pp. xiii, 494 p. San Diego: Academic Press.

Bininda-Emonds, O. R. P. (2000). Pinniped brain sizes. *Marine Mammal Science* **16**, 469-481.

Bromiley, R. B., Pinto Hamuy, T. and Woolsey, C. N. (1956). Somatic afferent areas I and II of dog's cerebral cortex. *J Neurophysiol* **19**, 485-99.

Buckmaster, P. S., Wen, X., Toyoda, I., Gulland, F. M. and Van Bonn, W. (2014). Hippocampal neuropathology of domoic acid-induced epilepsy in California sea lions (Zalophus californianus). *J Comp Neurol* **522**, 1691-706.

Cook, P. F., Reichmuth, C., Rouse, A. A., Libby, L. A., Dennison, S. E., Carmichael, O. T., Kruse-Elliott, K. T., Bloom, J., Singh, B., Fravel, V. A. et al. (2015). Algal toxin impairs sea lion memory and hippocampal connectivity, with implications for strandings. *Science* **350**, 1545-7.

Dehnhardt, G. (1994). Tactile size discrimination by a California sea lion (Zalophus californianus) using its mystacial vibrissae. *J Comp Physiol A* **175**, 791-800.

Dehnhardt, G., Mauck, B. and Bleckmann, H. (1998). Seal whiskers detect water movements. *Nature* **394**, 235-236.

Dehnhardt, G., Mauck, B., Hanke, W. and Bleckmann, H. (2001). Hydrodynamic trail-following in harbor seals (Phoca vitulina). *Science* **293**, 102-4.

Dehnhardt, G. M., B. (2008). Mechanoreception in secondarily aquatic vertebrates. *Sensory Evolution on the Threshold: Adaptations in Secondarily Aquatic Vertebrates*, 295-314.

Dondzillo, A., Satzler, K., Horstmann, H., Altrock, W. D., Gundelfinger, E. D. and Kuner, T. (2010). Targeted three-dimensional immunohistochemistry reveals localization of presynaptic proteins Bassoon and Piccolo in the rat calyx of Held before and after the onset of hearing. *J Comp Neurol* **518**, 1008-29.

Dykes, R. W., Herron, P. and Lin, C. S. (1986). Ventroposterior thalamic regions projecting to cytoarchitectonic areas 3a and 3b in the cat. *J Neurophysiol* **56**, 1521-41.

Dykes, R. W., Rasmusson, D. D. and Hoeltzell, P. B. (1980). Organization of primary somatosensory cortex in the cat. *J Neurophysiol* **43**, 1527-46.

Feldkamp, S. D., DeLong, R. L. and Antonelis, G. A. (1989). Diving patterns of California sea lions, Zalophus californianus. *Canadian Journal of Zoology* **67**, 872-883.

Felleman, D. J., Wall, J. T., Cusick, C. G. and Kaas, J. H. (1983). The representation of the body surface in S-I of cats. *J Neurosci* **3**, 1648-69.

Fiscus, C. H. and Baines, G. A. (1966). Food and Feeding Behavior of Steller and California Sea Lions. *Journal of Mammalogy* **47**, 195-200.

Fish, P. A. (1898). The brain of the fur seal, callorhinus ursinus; with a comparative description of those of zalophus californianus, phoca vitulina, ursus americanus and monachus tropicalis. *Journal of Comparative Neurology* **8**, 57-91.

Fox, K. (2008). Barrel Cortex. New York: Cambridge University Press.

Friedman, C. and Leftwich, M. C. (2014). The kinematics of the California sea lion foreflipper during forward swimming. *Bioinspir Biomim* **9**, 046010.

Glaser, N., Wieskotten, S., Otter, C., Dehnhardt, G. and Hanke, W. (2011). Hydrodynamic trail following in a California sea lion (Zalophus californianus). *J Comp Physiol A Neuroethol Sens Neural Behav Physiol* **197**, 141-51.

Goldstein, T., Mazet, J. A., Zabka, T. S., Langlois, G., Colegrove, K. M., Silver, M., Bargu, S., Van Dolah, F., Leighfield, T., Conrad, P. A. et al. (2008). Novel symptomatology and changing epidemiology of domoic acid toxicosis in California sea lions (Zalophus californianus): an increasing risk to marine mammal health. *Proc Biol Sci* **275**, 267-76.

Graziano, A., Liu, X. B., Murray, K. D. and Jones, E. G. (2008). Vesicular glutamate transporters define two sets of glutamatergic afferents to the somatosensory thalamus and two thalamocortical projections in the mouse. *J Comp Neurol* **507**, 1258-76.

Haidarliu, S. and Ahissar, E. (2001). Size gradients of barreloids in the rat thalamus. *J Comp Neurol* **429**, 372-87.

Healy, J. (2015). Starving Sea Lions Washing Ashore by the Hundreds in California. In *The New York Times*, pp. A12. New York: The New York Times Company.

Herndon, J. G., Tigges, J., Anderson, D. C., Klumpp, S. A. and McClure, H. M. (1999). Brain weight throughout the life span of the chimpanzee. *J Comp Neurol* **409**, 567-72.

Hyvarinen, H., Palviainen, A., Strandberg, U. and Holopainen, I. J. (2009). Aquatic environment and differentiation of vibrissae: comparison of sinus hair systems of ringed seal, otter and pole cat. *Brain Behav Evol* **74**, 268-79.

Iyengar, S., Qi, H. X., Jain, N. and Kaas, J. H. (2007). Cortical and thalamic connections of the representations of the teeth and tongue in somatosensory cortex of new world monkeys. *J Comp Neurol* **501**, 95-120.

Jiang, P., Josue, J., Li, X., Glaser, D., Li, W., Brand, J. G., Margolskee, R. F., Reed, D. R. and Beauchamp, G. K. (2012). Major taste loss in carnivorous mammals. *Proc Natl Acad Sci U S A* **109**, 4956-61.

Johnson, J. I., Jr., Welker, W. I. and Pubols, B. H., Jr. (1968). Somatotopic organization of raccoon dorsal column nuclei. *J Comp Neurol* **132**, 1-43.

Kaas, J. H. (2000). Why is Brain Size so Important:Design Problems and Solutions as Neocortex Gets Biggeror Smaller. *Brain and Mind* **1**, 7-23.

Kaas, J. H., Nelson, R. J., Sur, M., Dykes, R. W. and Merzenich, M. M. (1984). The somatotopic organization of the ventroposterior thalamus of the squirrel monkey, Saimiri sciureus. *J Comp Neurol* **226**, 111-40.

Kaneko, T. and Fujiyama, F. (2002). Complementary distribution of vesicular glutamate transporters in the central nervous system. *Neurosci Res* **42**, 243-50.

Kaneko, T., Fujiyama, F. and Hioki, H. (2002). Immunohistochemical localization of candidates for vesicular glutamate transporters in the rat brain. *J Comp Neurol* **444**, 39-62.

Kappers, C. U. A., Huber, G. C. and Crosby, E. C. (1936). The comparative anatomy of the nervous system of vertebrates, including man. New York,: Macmillan.

Ladygina, T. F., Popov, V. V. and Supin, A. Y. (1985). Topical organization of somatic projections in the fur seal cerebral cortex. *Neurophysiology* **17**, 246-252.

Le Gros Clark, W. E. (1932). The struture and funciton of the thalamus. *Brain* **55**, 406-470.

Liguz-Lecznar, M. and Skangiel-Kramska, J. (2007). Vesicular glutamate transporters VGLUT1 and VGLUT2 in the developing mouse barrel cortex. *Int J Dev Neurosci* **25**, 107-14.

Louderback, K. M., Glass, C. S., Shamalla-Hannah, L., Erickson, S. L. and Land, P. W. (2006). Subbarrel patterns of thalamocortical innervation in rat somatosensory cortical barrels: Organization and postnatal development. *J Comp Neurol* **497**, 32-41.

Ma, P. M. (1991). The barrelettes--architectonic vibrissal representations in the brainstem trigeminal complex of the mouse. I. Normal structural organization. *J Comp Neurol* **309**, 161-99.

Manger, P., Sum, M., Szymanski, M., Ridgway, S. H. and Krubitzer, L. (1998). Modular subdivisions of dolphin insular cortex: does evolutionary history repeat itself? *J Cogn Neurosci* **10**, 153-66.

Marshall, C. D., Amin, H., Kovacs, K. M. and Lydersen, C. (2006). Microstructure and innervation of the mystacial vibrissal follicle-sinus complex in bearded seals, Erignathus barbatus (Pinnipedia: Phocidae). *Anat Rec A Discov Mol Cell Evol Biol* **288**, 13-25.

McGovern, K. A., Marshall, C. D. and Davis, R. W. (2015). Are vibrissae viable sensory structures for prey capture in northern elephant seals, Mirounga angustirostris? *Anat Rec (Hoboken)* **298**, 750-60.

Milne, A. O. and Grant, R. A. (2014). Characterisation of whisker control in the California sea lion (Zalophus californianus) during a complex, dynamic sensorimotor task. *J Comp Physiol A Neuroethol Sens Neural Behav Physiol* **200**, 871-9.

Montie, E. W., Pussini, N., Schneider, G. E., Battey, T. W., Dennison, S., Barakos, J. and Gulland, F. (2009). Neuroanatomy and volumes of brain structures of a live California sea lion (Zalophus californianus) from magnetic resonance images. *Anat Rec (Hoboken)* **292**, 1523-47.

Montie, E. W. W., E.; Pussini, N.; Battey, T.W.K.; Barakos, J.; Dennison, S.; Colegrove, K.; Gulland, F. (2010). Magnetic resonance imaging quality and volumes of brain structures from live and postmortem imaging of California sea lions with clinical signs of domoic acid toxicosis. *Dis Aquat Organ* **91**, 243-256.

Murie, J. (1874). Researches upon the Anatomy of the Pinnipedia.—Part III. Descriptive Anatomy of the Sea-lion (Otaria jubata). *The Transactions of the Zoological Society of London* **8**, 501-582.

Murphy, C. T. (2013). Structure and Function of Pinniped Vibrissae.

Nahmani, M. and Erisir, A. (2005). VGLUT2 immunochemistry identifies thalamocortical terminals in layer 4 of adult and developing visual cortex. *J Comp Neurol* **484**, 458-73.

Ostapoff, E. M. and Johnson, J. I. (1988). Distribution of cells projecting to thalamus vs. those projecting to cerebellum in subdivisions of the dorsal column nuclei in raccoons. *J Comp Neurol* **267**, 211-30.

Pennisi, E., Cruccu, G., Manfredi, M. and Palladini, G. (1991). Histometric study of myelinated fibers in the human trigeminal nerve. *J Neurol Sci* **105**, 22-8.

Peterson, R. S. B., G. A. (1967). The natural history and behaviour of the California sea lion. Stillwater, OK, USA: American Society of Mammalogists.

Qi, H. X., Gharbawie, O. A., Wong, P. and Kaas, J. H. (2011). Cell-poor septa separate representations of digits in the ventroposterior nucleus of the thalamus in monkeys and prosimian galagos. *J Comp Neurol* **519**, 738-58.

Rasmusson, D. D. (1982). Reorganization of raccoon somatosensory cortex following removal of the fifth digit. *J Comp Neurol* **205**, 313-26.

Rasmusson, D. D. (1988). Projections of digit afferents to the cuneate nucleus in the raccoon before and after partial deafferentation. *J Comp Neurol* **277**, 549-56.

Rioch, D. M. (1937). A physiological and histological study of the frontal cortex of the seal (Phoca vitulina). *The Biological Bulletin* **73**, 591-602.

Robards, M. J. (1979). Somatic neurons in the brainstem and neocortex projecting to the external nucleus of the inferior colliculus: an anatomical study in the opossum. *J Comp Neurol* **184**, 547-65.

Sakurai, K., Akiyama, M., Cai, B., Scott, A., Han, B. X., Takatoh, J., Sigrist, M., Arber, S. and Wang, F. (2013). The organization of submodality-specific touch afferent inputs in the vibrissa column. *Cell Rep* **5**, 87-98.

Sarko, D. K., Johnson, J. I., Switzer, R. C., 3rd, Welker, W. I. and Reep, R. L. (2007). Somatosensory nuclei of the manatee brainstem and thalamus. *Anat Rec (Hoboken)* **290**, 1138-65.

Sato, J. J. and Wolsan, M. (2012). Loss or major reduction of umami taste sensation in pinnipeds. *Naturwissenschaften* **99**, 655-9.

Sawyer, E. K., Liao, C. C., Qi, H. X., Balaram, P., Matrov, D. and Kaas, J. H. (2015). Subcortical barrelette-like and barreloid-like structures in the prosimian galago (Otolemur garnetti). *Proc Natl Acad Sci U S A* **112**, 7079-84.

Schneider, C. A., Rasband, W. S. and Eliceiri, K. W. (2012). NIH Image to ImageJ: 25 years of image analysis. *Nat Methods* **9**, 671-5.

Scholin, C. A., Gulland, F., Doucette, G. J., Benson, S., Busman, M., Chavez, F. P., Cordaro, J., DeLong, R., De Vogelaere, A., Harvey, J. et al. (2000). Mortality of sea lions along the central California coast linked to a toxic diatom bloom. *Nature* **403**, 80-4.

Singer, M. (1962). The brain of the dog in section. Philadelphia,: Saunders.

Snider, R. S. and Niemer, W. T. (1961). A stereotaxic atlas of the cat brain. Chicago: University of Chicago Press.

Song, S., Liu, L., Edwards, S. V. and Wu, S. (2012). Resolving conflict in eutherian mammal phylogeny using phylogenomics and the multispecies coalescent model. *Proc Natl Acad Sci U S A* **109**, 14942-7.

Stephens, R. J., Beebe, I. J. and Poulter, T. C. (1973). Innervation of the vibrissae of the California sea lion, Zalophus californianus. *Anat Rec* **176**, 421-41.

Strata, F., Coq, J. O. and Kaas, J. H. (2003). The chemo- and somatotopic architecture of the Galago cuneate and gracile nuclei. *Neuroscience* **116**, 831-50.

Striedter, G. F. (2005). Principles of brain evolution. Sunderland, Mass.: Sinauer Associates.

Turner, W. and Miller, W. C. S. (1880). Report on the seals collected during the voyage of H. M. S. Challenger in the years 1873-76. Edinburgh.

Van der Loos, H. (1976). Barreloids in mouse somatosensory thalamus. *Neurosci Lett* **2**, 1-6.

Welker, W. I. and Johnson, J. I. (1965). Correlation between Nuclear Morphology and Somatotopic Organization in Ventro-Basal Complex of the Raccoon's Thalamus. *J Anat* **99**, 761–790.

Welker, W. I. and Seidenstein, S. (1959). Somatic sensory representation in the cerebral cortex of the racoon (Procyon lotor). *J Comp Neurol* **111**, 469-501.

Wiener, S. I., Johnson, J. I. and Ostapoff, E. M. (1987). Organization of postcranial kinesthetic projections to the ventrobasal thalamus in raccoons. *J Comp Neurol* **258**, 496-508.

Wilson, R. B. (1933). The anatomy of the brain of the whale (Balaenoptera sulfurea). *J Comp Neurol* **58**, 419-480.

Wohlert, D., Kroger, J., Witt, M., Schmitt, O., Wree, A., Czech-Damal, N., Siebert, U., Folkow, L. and Hanke, F. D. (2015). A Comparative Morphometric Analysis of Three Cranial Nerves in Two Phocids: The Hooded Seal (Cystophora Cristata) and the Harbor Seal (Phoca Vitulina). *Anat Rec (Hoboken)* **299**, 370–378.

Wojcik, S. M., Rhee, J. S., Herzog, E., Sigler, A., Jahn, R., Takamori, S., Brose, N. and Rosenmund, C. (2004). An essential role for vesicular glutamate transporter 1 (VGLUT1) in postnatal development and control of quantal size. *Proc Natl Acad Sci U S A* **101**, 7158-63.

Wong-Riley, M. (1979). Changes in the visual system of monocularly sutured or enucleated cats demonstrable with cytochrome oxidase histochemistry. *Brain Res* **171**, 11-28.

Woolsey, T. A. and Van der Loos, H. (1970). The structural organization of layer IV in the somatosensory region (SI) of mouse cerebral cortex. The description of a cortical field composed of discrete cytoarchitectonic units. *Brain Res* **17**, 205-42.

Zhou, J., Nannapaneni, N. and Shore, S. (2007). Vessicular glutamate transporters 1 and 2 are differentially associated with auditory nerve and spinal trigeminal inputs to the cochlear nucleus. *J Comp Neurol* **500**, 777-87.

CHAPTER III

Organization of the Spinal Trigeminal Nucleus in Star-Nosed Moles (*Condylura cristata*)

This chapter is reproduced with permission from the published work by Sawyer E. K., Leitch D. B. L., Catania K. C. 2014. Organization of the spinal trigeminal nucleus in Star-nosed moles. *Journal of Comparative Neurology*. 52(14) 3335-3350. It is unaltered in content.

ABSTRACT

Somatosensory inputs from the face project to multiple regions of the trigeminal nuclear complex in the brainstem. In mice and rats three subdivisions contain visible representations of the *mystacial vibrissae*: the principal sensory nucleus, the spinal trigeminal subnucleus interpolaris and subnucleus caudalis. These regions are considered important for touch with high spatial acuity, active touch, and pain and temperature sensation, respectively. Like mice and rats, the star-nosed mole (*Condylura cristata*) is a somatosensory specialist. Given the visible star pattern in preparations of the star-nosed mole cortex and the principal sensory nucleus, we hypothesized there were star patterns in the spinal trigeminal nucleus subnuclei interpolaris and caudalis. In sections processed for cytochrome oxidase we found star-like segmentation consisting of lightly stained septa separating darkly stained patches in subnucleus interpolaris (juvenile tissue) and subnucleus caudalis (juvenile and adult tissue). Subnucleus caudalis represented the face in a three-dimensional map with the most anterior part of the face represented more rostrally than posterior parts of the face. Multi-unit electrophysiological mapping was used to map the ipsilateral face. Ray-specific receptive fields in adults matched the CO-segmentation. The mean areas of multiunit receptive fields in subnucleus interpolaris and caudalis were larger than previously mapped receptive fields in the mole's principal sensory nucleus. The proportion of tissue devoted to each ray's representation differed between subnucleus interpolaris and the principal sensory nucleus. Our finding that different trigeminal brainstem maps can exaggerate different parts of the face could provide new insights for the roles of these different somatosensory stations.

INTRODUCTION

The trigeminal sensory complex in the brainstem is the first relay in the central nervous system for facial somatosensation. Upon entering the brainstem, sensory neurons branch to send inputs to four different somatosensory regions (Bosman et al., 2011; Diamond et al., 2008). This anatomical segregation suggests facilitation of parallel processing and raises the possibility that these regions are specialized for different submodalities of somatosensation.

The main trigeminal somatosensory nuclei in the brainstem are the principal sensory nucleus (PrV) and the spinal trigeminal nucleus (STN). The STN is divided into three subnuclei, subnuclei oralis (SpVo), interpolaris (SpVi) and caudalis (SpVc) (Fig. 1) (Olszewski, 1950). The PrV is found most rostrally, followed caudally by the SpVo, SpVi, and SpVc. The SpVi is further divided into a rostral and caudal component (Phelan and Falls, 1989). Primary somatosensory axons from the face project to both the STN and PrV. Thick axons, which are presumably from mechanoreceptor afferents, project to the PrV and to all subnuclei in the STN, whereas thin axons that are presumably nociceptive and/or thermoceptive project only to the STN (Anstrom, 1953; Gerard, 1923; Jacquin et al., 1986a; Jacquin et al., 1986b; Ramon y Cajal, 1896). Four parallel somatosensory pathways arise from the four trigeminal somatosensory (sub)nuclei suggesting that each pathway channels information for different facets of touch (Diamond et al., 2008; Henderson, 1995). The PrV is thought to be important for mediating discriminative touch (with high spatial acuity), the SpVi for accounting for sensation from movement initiated by the animal, and the SpVc for pain and temperature sensation (Diamond et al., 2008). The role of SpVo is more elusive but is thought to be involved in oral and perioral reflexes and nociception (Devoize et al., 2010; Nash et al., 2009). The functions of the PrV and each subnuclei of the STN have primarily been studied in the context of whisking behavior in rodents.

Rats and mice are useful for studying trigeminal somatosensation because their *mystacial vibrissae have large, anatomically visible representations,* with each facial whisker follicle visible as a distinct unit. In the brainstem, thalamus, and cortex, the arrays of patches representing mystacial vibrissae are known respectively as barrelettes (visible in PrV, caudal SpVi, and SpVc)(Belford and Killackey, 1979b; Erzurumlu et al., 2010), barreloids (visible in the ventral posterior medial nucleus of the thalamus) (Van der Loos, 1976), and barrels (visible in the primary somatosensory cortex) (Woolsey and Van der Loos, 1970).

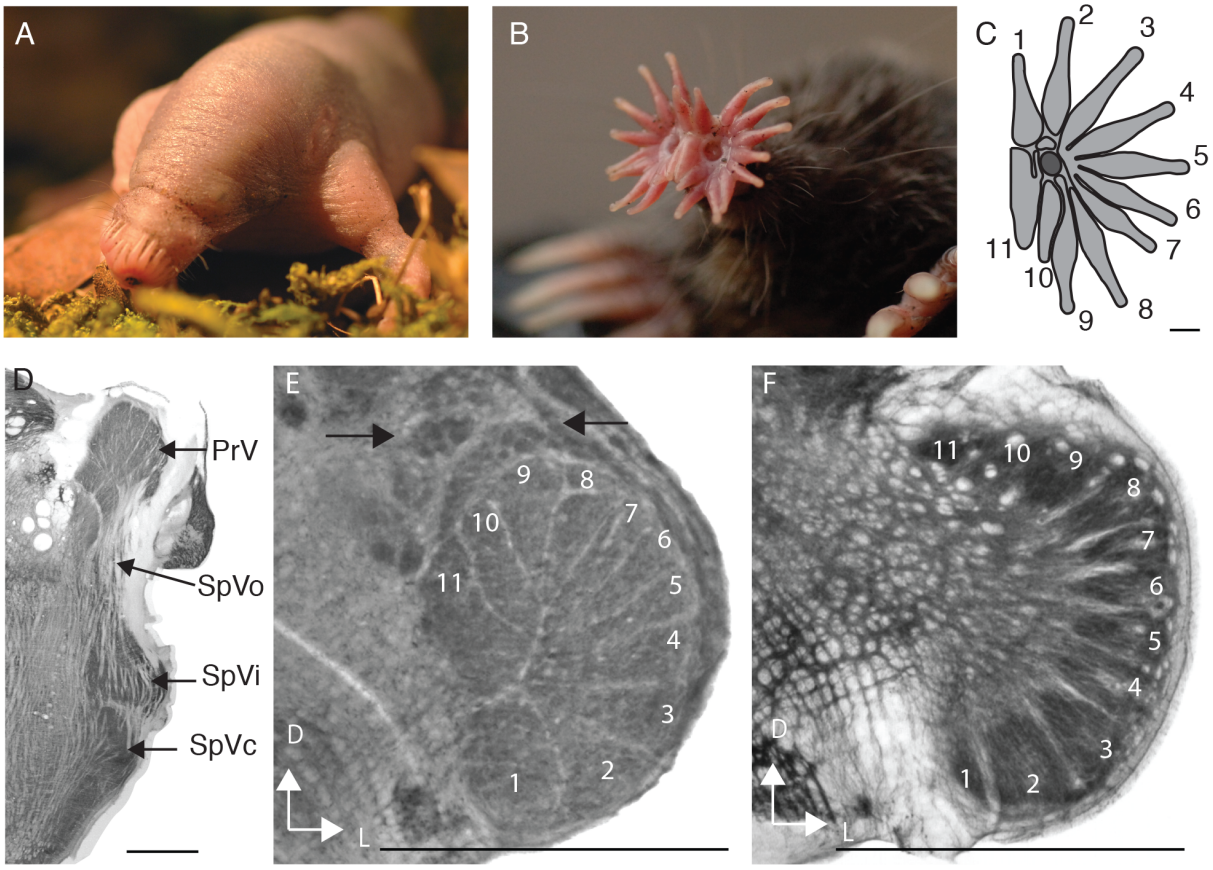

Fig. 1: The star and somatosensory brainstem of the star-nosed mole. **A**: A juvenile star-nosed mole, postnatal day 7, exhibiting nasal rays that have not yet detached from the snout. **B**: An adult star-nosed mole exhibits the mature morphology of the star. **C**: A diagram of half of a star with rays that are numbered following Catania and Kaas (1995) **D:** A representative horizontal section of the brainstem of a and star-nosed mole processed for cytochrome oxidase (CO) with labeled subdivisions of the trigeminal nuclear complex. **E:** A representative coronal section processed for CO from a juvenile star-nosed mole (16.4 g) illustrating the star representation of the spinal trigeminal subnucleus interpolaris (SpVi). Black arrows point out barrelette-like dark patches. **F:** A representative coronal section processed for cytochrome oxidase from an adult star-nosed mole illustrating the star representation in spinal trigeminal subnucleus caudalis (SpVc). Both micrographs display light septa separating 11 dark segments corresponding to each of the 11 rays. PrV = principal trigeminal nucleus, SpVo = spinal trigeminal nucleus oralis, D = dorsal, L = lateral. Scale bars= 1 mm

The star-nosed mole (*Condylura cristata*) has sensitive, finger-like nasal appendages that are used for exploring their environment (Fig. 1 A-C). They have reduced eyes and instead rely primarily on the tactile star to explore the underground wetland areas of their habitat (Hamilton, 1931). The star consists of 22 fleshy rays (Fig. 1A-C) completely covered with a mosaic of touch receptors known as Eimer's organs. Externally, these receptors appear as 40-50 μm diameter domes. Internally, they each house a Merkel cell-neurite complex, a laminated corpuscle, and two classes of free nerve endings (Catania, 1996; Marasco et al., 2006). Up to 28,000 Eimer's organs cover the star surface (Catania and Kaas, 1997). The small, closely packed Eimer's organs suggest that the star is a somatosensory surface optimized for high resolution touch and behavioral tests demonstrate that by rapidly repeating sequences of touching, withdrawing, and reorienting motions, moles can locate and quickly eat prey items that are as small as 1 mm^2 (Catania and Kaas, 1997). Star-nosed moles preferentially use ray 11, their "somatosensory fovea," for this task (Catania and Kaas, 1997).

Central nervous system representations of the star have been investigated at the level of the somatosensory cortex (Catania and Kaas, 1995) and in PrV of the brainstem (Catania et al., 2011b). In both areas a visible star pattern with individual representations of each nasal ray were found, similar to the barrels and barrelettes found for whiskers in mice and rats. The proportions of the cytochrome oxidase (CO) stained-segments in the star pattern are different in the cortex compared to PrV. For example, ray 11 has only 7% of the Eimer's organs on the star, yet accounts for 13% of the star representation in the PrV and 25% of the star representation in the primary somatosensory cortex (Catania and Kaas, 1997; Catania et al., 2011b), which may be related to preferential use of ray 11 in fine discrimination tasks.

In the present study, we investigated whether the star representation was present in the SpVi and SpVc in a manner analogous to the barrelettes found in rats and mice. Using histological analyses and multi-unit electrophysiological mapping, we examined the organization and receptive field size of these subnuclei. We hypothesized that the different functional roles of the two areas might be represented anatomically in star representations that accentuated different regions of the star surface. To test this we measured the volume of the ray representations in SpVi and compared it to the ray representations in the PrV to see if the areas had same pattern of afferent magnification.

METHODS

ANIMALS

Eleven adult and six juvenile star-nosed moles were used in this study. The adults were used for electrophysiology and histology; the juveniles were used for only histology. The adult star-nosed moles were collected in Potter County, Pennsylvania (under permit # 112-2011). The juvenile star-nosed moles were obtained from the litters of wild-caught pregnant moles that gave birth and raised young while in laboratory housing. The juveniles used were 3.0, 10.5, 12.9, 13.8, 17.9 and 23.2 g (approximately postnatal days 0, 4, 5, 6, 9, and 15, respectively). Ages were estimated from similar anatomical stages in rodents and by tracking development from the time the juveniles were first observed in the nest. These were estimates because birth was not directly observed in the underground nest. The mass of the juveniles is reported when describing different juvenile cases. All procedures conformed to the National Institutes of Health standards concerning the use and welfare of experimental animals and were approved by the Vanderbilt University Animal Care and Use Committee (Animal Welfare Assurance Number A-3227-01).

ELECTROPHYSIOLOGY AND RECEPTIVE FIELD MAPPING

Moles were initially anesthetized with 15% urethane (1.0 g/kg) and 10% ketamine (10 mg/ kg). They were given supplemental injections to maintain a surgical plane of anesthesia as needed. The animal's head was fixed, and a craniotomy was made over one or both of the cerebellar hemispheres. The angle of the micromanipulator varied between experiments to allow access to different areas of the brainstem. Recordings were made with low-impedance tungsten electrodes (1.0–1.5 M Ω at 1000 Hz) with a tip diameter of 1 μm . Responses were amplified and monitored with a Powerlab 4/30 data acquisition unit using a speaker and a computer running LabChart software (ADinstruments). Electrode penetrations were made through the cerebellum into the brainstem nuclei. When responses to the face and star were obtained, receptive fields were defined using a fine wooden probe, and the extent of the receptive field for each recording site was drawn on a schematic of the mole's nose. Receptive fields were found exclusively on the ipsilateral face. Receptive fields were noted at 100 μm intervals until responses were no longer obtained. After recording receptive fields, the electrode was returned to a site along that penetration, the receptive field was remapped, and the site was marked with a single electrolytic microlesion at 10 microamps for 5-10 seconds. For selected tracks a continuous lesion was made by withdrawing the electrode at 25 μm/sec while the electrode was supplied with 10 microamps of current.

After recordings, moles were euthanized with an overdose of sodium pentobarbital (120 mg/kg) and transcardially perfused with phosphate buffered saline (PBS) (pH 7.3) followed by 4% paraformaldehyde. Rodents used for histology were euthanized using identical procedures.

HISTOCHEMISTRY

The brainstem was removed and cryoprotected overnight in 30% sucrose in PBS. The ventral surface of the brainstem was considered to be a horizontal plane. Brainstems were cut coronally at a thickness of 40 μm. The sections were stained for Nissl substance with thionin, processed for cytochrome oxidase (Carroll and Wong-Riley, 1984) or myelin (Gallyas, 1979).

Sections were photographed with a Zeiss AxioCam HRc digital camera (Zeiss, Jena, Germany) mounted onto a Zeiss Axioskop microscope using Zeiss Axiovision 4.5 software (Carl Zeiss Microimaging, Thornwood, NY, USA). Images were imported into Adobe Photoshop CS5 and adjusted for optimal contrast and brightness but were otherwise unaltered.

SIZE OF RECEPTIVE FIELDS

Lesions and electrode tracts were used to determine the location of each recording site and receptive field. Receptive field drawings were digitized and their areas were measured in ImageJ (Schneider et al., 2012). Additionally, the areas of receptive fields in PrV were measured from records from a previous study that used the same anesthesia protocol but for which receptive field size was recorded but not analyzed for area (Catania et al., 2011b).

RECONSTRUCTION OF STAR REPRESENTATIONS

The 3-dimensional organization of the subnuclei was investigated by volumetric reconstruction. Photomicrographs of serial sections were imported into *Reconstruct* software version 1.1.0 (Synapse Web Reconstruct, RRID:nif-0000-23420) (Fiala, 2005). Sections were aligned by matching anatomical landmarks and using the "rigid alignment" function.

The volume of each ray representation in SpVi was measured by tracing the pale septa that marked the boundary of each CO-segment. This was done in all sections in which the septa were present. A total of 6 complete

representations were reconstructed from the 4 juvenile animals (body masses of 10.5g, 12.9g, 13.8g, 16.4g). In two animals, both sides of the brainstem had representations that were complete; in the other two animals, tears in the tissue precluded one side from being measured. The total volume of the ray representations was calculated using the following formula: volume = (area of each section) x (thickness of section) x (number of sections), which is consistent with similar studies (Ashwell et al., 2006; Catania et al., 2011b).

Larger animals had larger SpVi's, but the proportions of the star did not systematically differ with animal size (none of the 11 linear regressions revealed a significant effect of the animal's mass on the proportion of the nucleus devoted to that ray). Therefore, the percentage of the star devoted to each ray, and not the absolute volume of the ray representation, was used for the remaining statistical analyses. All statistical analyses were done in SPSS version 21.

RESULTS

ANATOMY OF SUBNUCLEUS INTERPOLARIS

A star representation was observed in sections from caudal SpVi stained for CO in juvenile star-nosed moles (Fig. 1E). Lightly-stained septa divided the nucleus into 11 densely stained patches which together formed a characteristic star pattern similar to that observed in PrV, S1, and S2 of the star-nosed mole (Catania and Kaas, 1995; Catania et al., 2011b). Densely stained barrelette-like patches were dorsal to the star representation (Fig. 1E, arrows). The star pattern was observed in animals that were approximately 4 to 9 days old (10.5 g to 17.9 g, respectively) but was not obvious in younger or older animals (3.0 g and 23.2 g, respectively). The 3.0 g animal (postnatal day 0) lacked septa in SpVi. The SpVi of the 23.2 g animal (approximately postnatal day 15) was similar to that of an adult star-nosed mole in lacking clear septa (Fig. 2A).

The topography of the representation of the star in SpVi was determined through multiunit electrophysiological recordings while stimulating the ipsilateral face and body. As the electrode was lowered ventrally through the nucleus, receptive fields systematically progressed from the forelimb (when the electrode was in the adjacent cuneate nucleus), to the mystacial vibrissae (when it was in the dorsal SpVi), to the more ventral rays (e.g., ray 11) followed by more dorsal rays (e.g., ray 1) (Fig. 2). This produced an inverted representation such that dorsal rays were represented ventrally in the nucleus, and the ventral rays were represented dorsally.

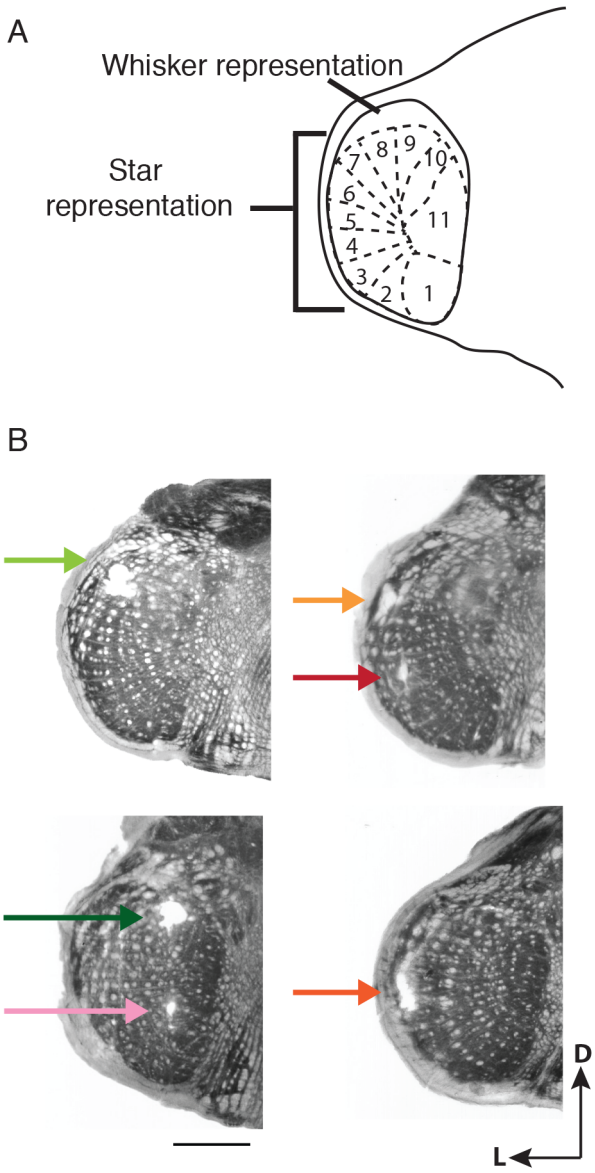
A
Whisker representation
Star
representation
1
2
3
4
5
6
7
8
9
10
11
B
D
L
C
1
2
3
4
5
6
7
8
9
10
11

Fig. 2: Electrophysiology of the spinal trigeminal subnucleus interpolaris (SpVi). **A**: A schematic of SpVi in an adult. The star representation is not visible in a cytochrome oxidase (CO)- stained adult SpVi. The pattern from a CO stained juvenile section is traced in dotted lines over the adult nucleus. **B**: Microlesions in vibrissae and star-responsive areas in SpVi. The shade of the arrows matches the receptive fields drawn in part C. The receptive field on the nose included both the whiskers and the hairy skin between the whiskers. Scale bar = 500 μm. **C**: Left: The approximate locations of the lesions mapped onto the schematic of SpVi. Right: The locations of the receptive fields that correspond to the lesions in part B. Abbreviations: D = dorsal, L = lateral.

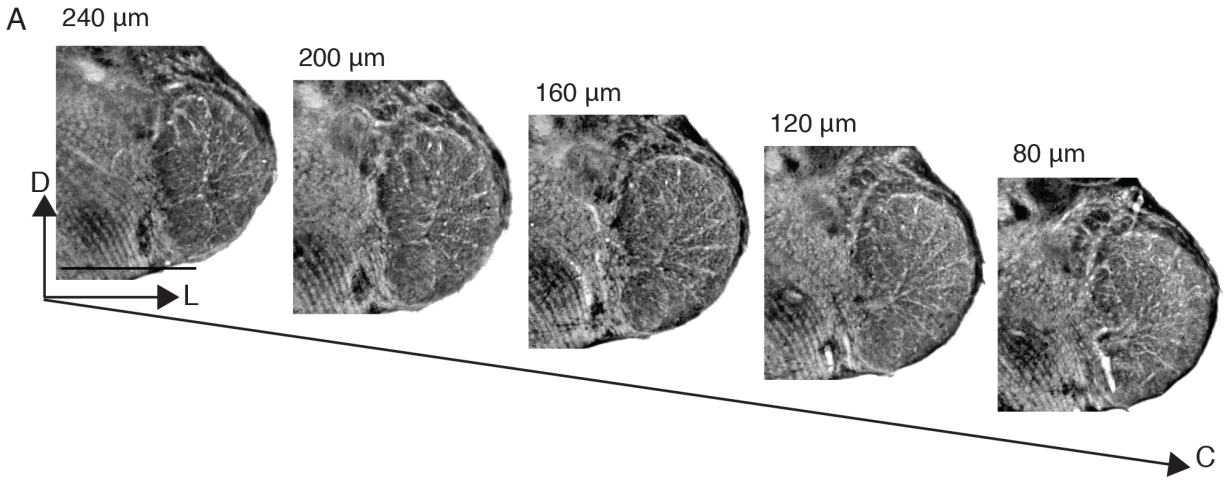
A
240 µm
200 µm
160 µm
120 µm
80 µm
D
L
C

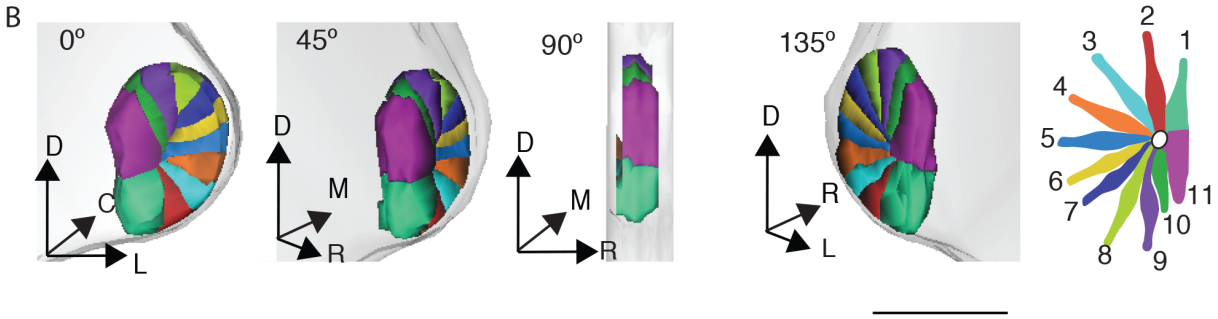
B
0°
45°
90°
135°
D
C
L
M
R
1
2
3
4
5
6
7
8
9
10
11

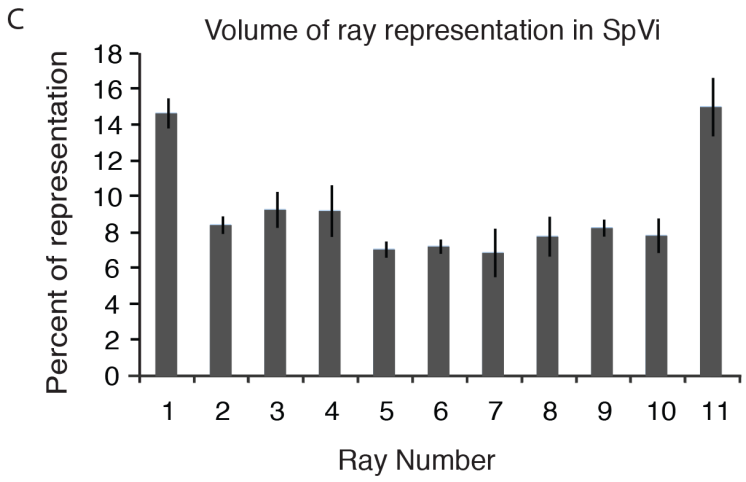
C
Volume of ray representation in SpVi
Percent of representation
0
2
4
6
8
10
12
14
16
18
1
2
3
4
5
6
7
8
9
10
11
Ray Number

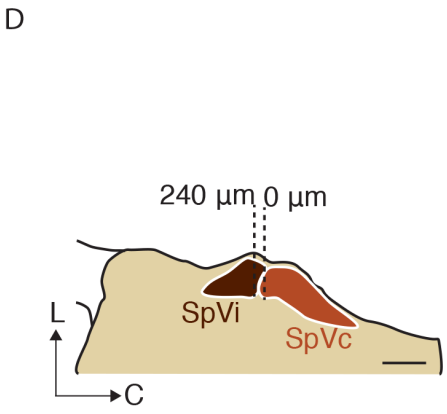
D
240 µm
0 µm
SpVi
SpVc
L
C

Fig. 3: Reconstruction of the ray representations in the spinal trigeminal subnucleus interpolaris (SpVi). **A:** Consecutive coronal sections of SpVi processed for cytochrome oxidase from a 13.8 g juvenile mole. The number above each section is the distance in μm rostral to the SpVi SpVc border, where the most rostral section with SpVc is set to zero. **B:** The 3-dimensional reconstruction of the ray representations in a variety of orientations and a key for the coloration of the reconstruction. **C:** Quantification of the volumes of the ray representations as measured by percent of star representation ((Volume of ray/volume of all rays) x 100). The representations of rays 1 and 11 were significantly larger than the other rays ($p<0.01$). Error bars represent 95% confidence interval. **D:** A schematic of a horizontal section of the brainstem illustrating the extent of caudal SpVi from which sections in part B are depicted. Abbreviations: C = caudal, D = dorsal, L = lateral, M = medial, R = rostral, SpVc= Spinal trigeminal nucleus caudalis. Scale bars= 1 mm.

The volume of each ray representation was reconstructed from six juvenile samples processed for CO (Fig. 3). The star pattern was present at the caudal extent of SpVi with consecutive coronal sections revealing nearly identical segmentation patterns (Fig. 3A, B). The proportion of total SpVi volume devoted to each ray's representation was not equal (ANOVA, $F(10,55) = 59.744$, $p < 0.01$). Tukey's HSD test revealed that rays 1 and 11 had volumes that were not significantly different from each other, but were larger than the volumes of any other ray (Fig. 3C).

Previous studies have reported the number of Eimer's organs on the star, the number of myelinated fibers dedicated to each ray, the volume of each ray representation in the PrV, and the area of the ray representation in S1 (Catania and Kaas, 1997; Catania et al., 2011b). From that data we calculated the percent of neural tissue devoted to each ray at these various stations along the somatosensory pathway. This allowed us to compare the results in SpVi to previous work (Fig. 4). We then asked if the proportion of neural tissue devoted to each of the rays was equal at different stations. Rays that had a larger proportion of neural tissue in one station were overrepresented, and rays with a smaller proportion were underrepresented. These terms were used instead of magnification, as in cortical magnification, because that specific phenomenon is sometimes explained as a linear reflection of receptor density, which we are not suggesting here. It should be noted that, though the graph in Figure 4 is organized to show the general progression from the periphery to the neocortex, the PrV and SpVi are parts of parallel somatosensory pathways.

The proportion of neural tissue devoted to each ray differed between stations in the somatosensory pathway. A two-factor ANOVA, with the factors of ray number and somatosensory station, showed a significant main effect for ray ($F(54,10) = 139.954$, $p < 0.01$) and an interaction effect for ray and somatosensory station ($F(54, 40) = 36.445$, $p < 0.01$). The ray effect reflected that the sizes of the ray representations are not identical. The interaction effect showed that the proportion of neural tissue devoted to each ray is different at each level of the somatosensory pathway. One-factor ANOVAs of each of the rays revealed that all rays had a significant area effect ($p < 0.01$ in all cases). Within each ray a Tukey's HSD test was used to determine how somatosensory station affected the percentage of neural tissue devoted to that ray. The effects can be summarized in that the majority of appendages, rays 2 through 9, were underrepresented in the central nervous system (i.e., S1, PrV, and SpVi) compared to the peripheral nervous system (i.e., Eimer's organs and myelinated afferents from each ray). Three rays - rays 1, 10 and 11 - did not fit this pattern. Rays 10 and 11 had a pattern opposite to rays 2 through 9 in that

they were overrepresented in the central nervous system compared to the periphery. Finally, ray 1 was unlike all the rest. Ray 1 had the greatest percentage of neural tissue in the SpVi, and in descending order of proportion compared to the rest of the star, PrV, Eimer's organs, myelinated fibers from the ray, and S1 area (Fig. 4). Thus, SpVi differed from all other stations analyzed in that ray 1 was most overrepresented there.

ANATOMY OF SUBNUCLEUS CAUDALIS

The SpVc is a laminated structure that resembles the dorsal horn of the spinal cord. We identified a series of lamina including a thin substantia marginalis along the lateral edge (consistent with Rexed lamina I), a thicker horseshoe shaped substantia gelatinosa (consistent with Rexed laminae II and III), and an innermost substantia magnocellularis (consistent with Rexed lamina VI) (nomenclature follows (Olszewski, 1950)). The layers of the SpVc can be delimitated on the basis of cell distributions visible in a Nissl-stained preparation, with the thin substantia marginalis characterized by 2-3 rows of sparse large neurons, the substantia gelatinosa being densely packed with small cells, and the substantia magnocellularis composed of both small and large neurons that are less densely packed (Olszewski, 1950). The substantia gelatinosa and substantia magnocellularis can also be distinguished by the denser network of fibers present in the magnocellular layer compared to the gelatinosa layer (Torvik, 1956a) (Fig. 5 A-D).

The organization of SpVc varied along the rostral-caudal axis (Fig. 6). We found that measuring the rostral-caudal location of a section was best done in our study by designating the most rostral section in which caudalis was present (the SpVi/SpVc border) as our zero point.

Subnucleus caudalis in star-nosed moles had prominent septa that segmented the middle laminae of the nucleus into 11 regions, visible in CO-processed sections (Fig. 1F). Ray septa were observed consistently across adjacent sections, beginning approximately 400 μm caudal to the SpVi/SpVc border and continuing caudally for approximately 300 μm. The septa for ray 11 were consistently faint in CO stains.

Approximately 600 μm caudal to the SpVi/SpVc border, a distinct area with barrelette-like patches was found in the medial and dorsal part of the nucleus (Fig. 6B). Based on comparisons between the sections stained for Nissl substance, myelin and CO these barrelette-like patches appeared to be located in the substania magnocellularis. Further caudally the star pattern in the substantia gelatinosa layer diminished until it was no longer present at 700

μm from the SpVi/SpVc border. Juvenile animals displayed the same pattern as adults but were scaled in the rostral-caudal axis to match the smaller brainstem (Fig. 6C).

In the dorsal/ventral plane, the orientation of the star representation was the same as that seen in SpVi such that ray 11 was represented dorsomedially, ray 1 was represented ventromedially, and the intervening rays were represented in sequence between those two. As the recording electrode was advanced ventrally through the nucleus, the receptive fields reliably shifted from more ventral rays (e.g., ray 11) to more dorsal rays (e.g., 1). Ray-responsive units were found in both the gelatinosa (Fig. 7A) and the magnocellularis division (Fig. 7B). The data suggest that receptive fields might be larger in the gelatinosa layer than in the magnocellular layer, but the sample size of recording locations definitively isolated to specific laminae precludes more strict assessment of this hypothesis. Some lesions appeared in locations rostral to the most distinct septa.

It was not possible to determine the rostral-caudal organization of the rays' representation in SpVc by comparing the location of lesions to the corresponding receptive fields on the star. However, lesions in areas of SpVc responsive to vibrissae were clearly caudal to the star representation (Fig. 6A).

SIZE OF RECEPTIVE FIELDS

Neurons in the PrV had the smallest receptive fields of the nuclei tested (Fig. 8). There was no statistical difference between the size of the receptive field in neurons in the SpVi and SpVc. The mean receptive field size for neurons in PrV was 0.69 mm^2 (SD = 0.45, n = 68), for the SpVi was 1.98 mm^2 (SD = 0.41, n = 28), and for the SpVc was 1.79 mm^2 (SD = 0.96, n = 62). The size of the receptive fields was different between PrV and SpVi or SpVc (Kruskal-Wallis $p< 0.01$), reflecting smaller receptive fields in PrV than in SpVi (T-test with equal variances not assumed, t (31.3) = -6.26, $p<0.01$) or SpVc (T-test with equal variances not assumed, t (82.8) = -8.16, $p<0.01$). If all receptive fields on ray 11, the fovea, are removed from the analysis the statistical significance of the results is unchanged.

DISCUSSION

We identified representations of the star in the interpolaris (SpVi) and caudalis (SpVc) subnuclei of the spinal trigeminal nucleus of the star-nosed mole. Subnucleus oralis (SpVo) lacked CO-segments corresponding to

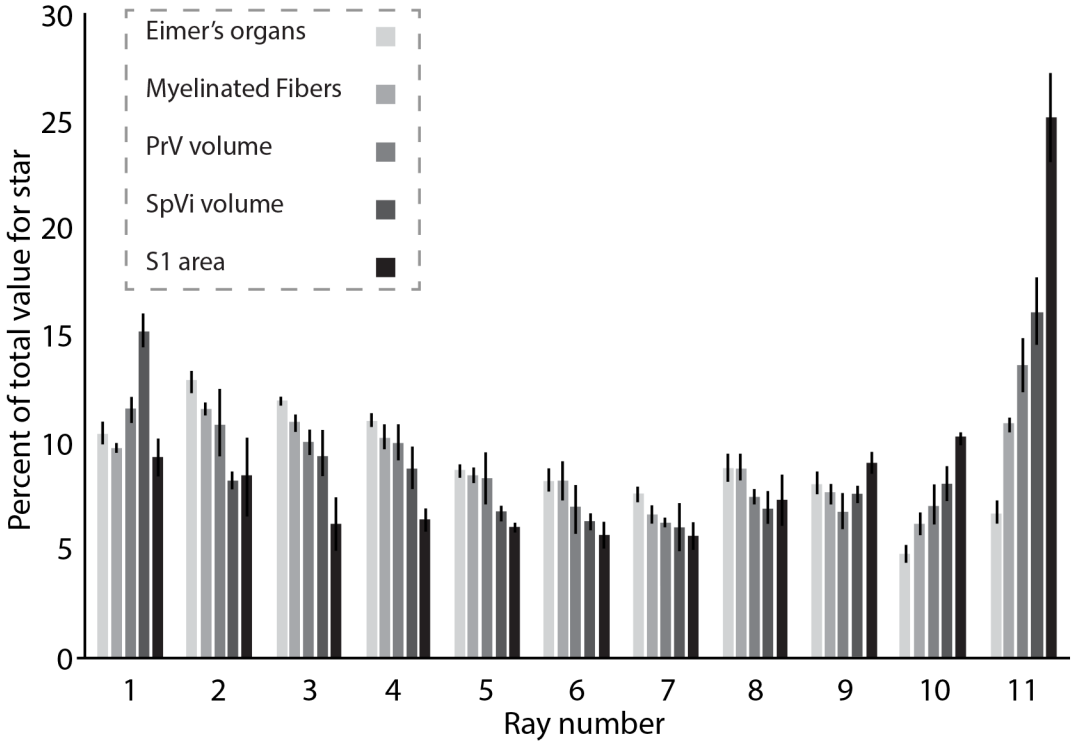

Fig. 4: Percentage of tissue in the star pathway devoted to each ray, from the periphery to the cortex. The displayed measurements are the percentage of Eimer's organs on each ray (Catania and Kaas, 1997), the percentage of myelinated fibers devoted to each ray (Catania and Kaas, 1997), the percentage of PrV volume devoted to each ray representation (PrV; analyzed using coronal sections processed for cytochrome oxidase- CO) (Catania et al., 2011b), the percentage of SpVi volume devoted to each ray representation (for the star pattern) (SpVi; analyzed using coronal sections processed for CO), and the percentage of primary somatosensory cortex devoted to each ray representation for the star pattern (analyzed using flattened cortex sections processed for CO)(Catania and Kaas, 1995). Within each ray grouping along the X-axis, the bars represent the more peripheral measurements on the left to the more central measurements to the right. Error bars represent 95% the confidence interval.

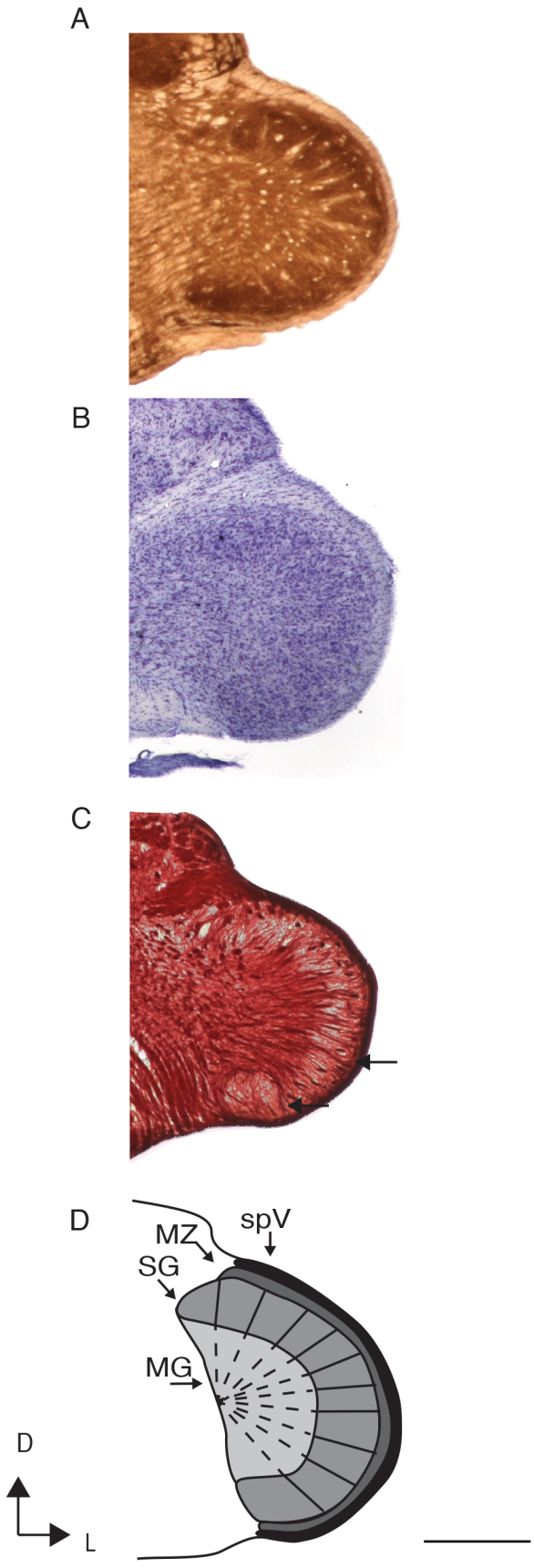
A
B
C
D
spV
MZ
SG
MG
D
L

Fig. 5: Laminae in the spinal trigeminal subnucleus caudalis (SpVc). **A:** A coronal section of the SpVc processed for cytochrome oxidase showing the septa dividing the nucleus into 11 darkly stained CO-segments. **B:** A coronal section stained for Nissl substance, showing the laminated structure of the SpVc. **C:** A coronal section stained for myelin and further illustrating laminar differentiation and fibers traversing the substantia gelatinosa (arrows). **D**: Schematic of the laminae and the septa marking the rays. Abbreviations: MG= substantia magnocellularis, MZ = substantia marginalis; SG= substantia gelatinosa; spV= spinal trigeminal tract. Scale bar = 500 μm.

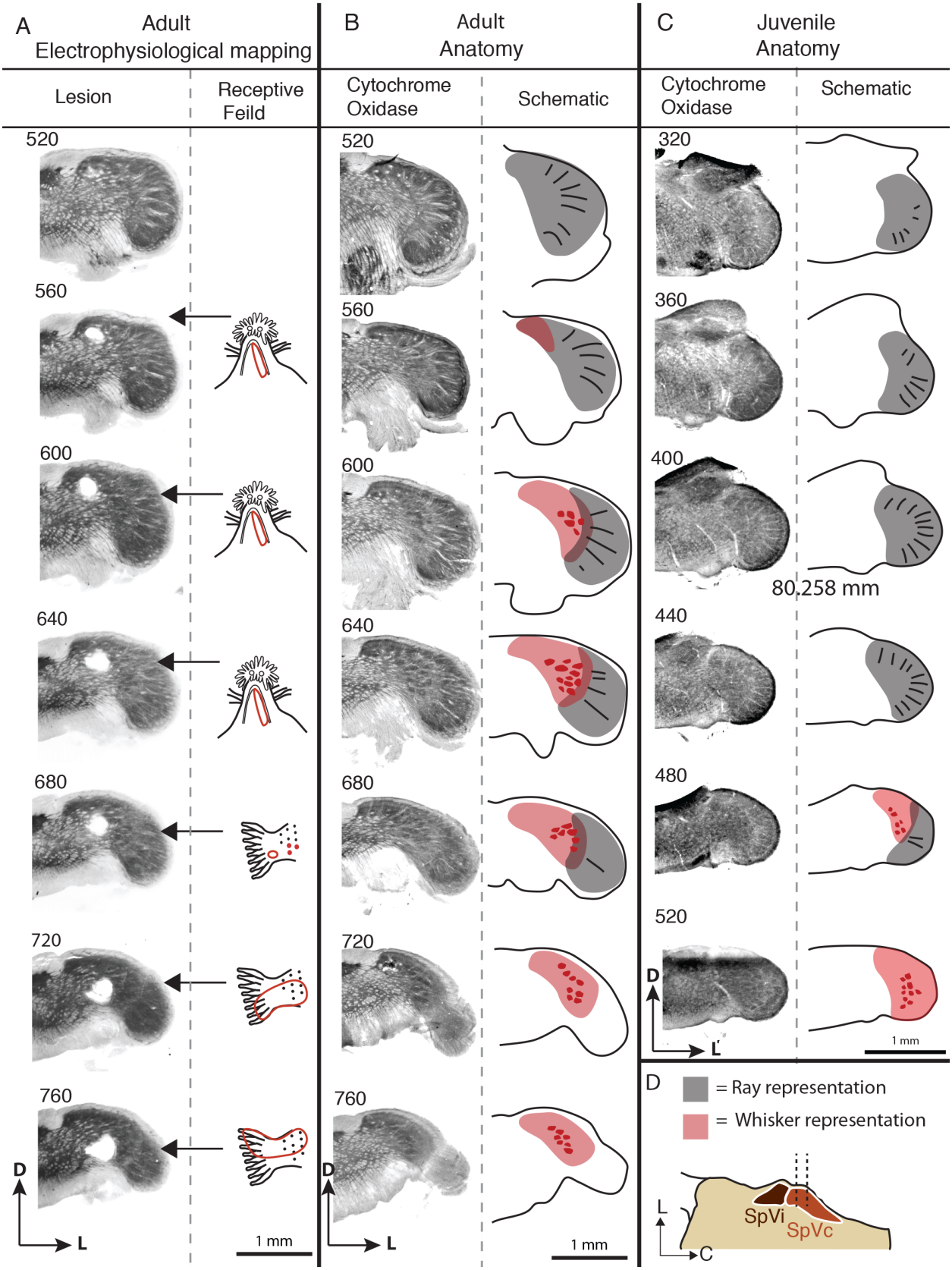
A
Adult
Electrophysiological mapping
Lesion
Receptive Feild
B
Adult
Anatomy
Cytochrome Oxidase
Schematic
C
Juvenile
Anatomy
Cytochrome Oxidase
Schematic
520
560
600
640
680
720
760
320
360
400
440
480
520
80.258 mm
D
L
1 mm
D
= Ray representation
= Whisker representation
SpVi
SpVc
L
C

Fig. 6: The transition from the star representation to the vibrissae representation in spinal trigeminal subnucleus caudalis (SpVc). **A:** Left column: Consecutive cytochrome oxidase (CO) processed sections in an adult. The number in the upper left of each photomicrograph is the distance caudal to the spinal trigeminal subnucleus interpolaris (SpVi)/SpVc border in μm. Sections 560-760 illustrate a lesion made along the entire electrode tract. Right column: Receptive fields on the skin on the face and the vibrissae that correspond with the lesion on the left. **B and C:** Left: Consecutive CO stained sections in SpVc in an adult and juvenile, respectively. Right: a schematic of the segmentation visible in the section with black lines representing ray septa and red circles representing barrelette-like CO-patches . **D:** Top: coloring scheme for schematics in B and C. Bottom: a schematic of a horizontal section of the brainstem, showing where along the rostrocaudal axis the sections in part A-C are located. Abbreviations: C = Caudal, D = dorsal, L = lateral. Scale bars for micrographs = 1 mm

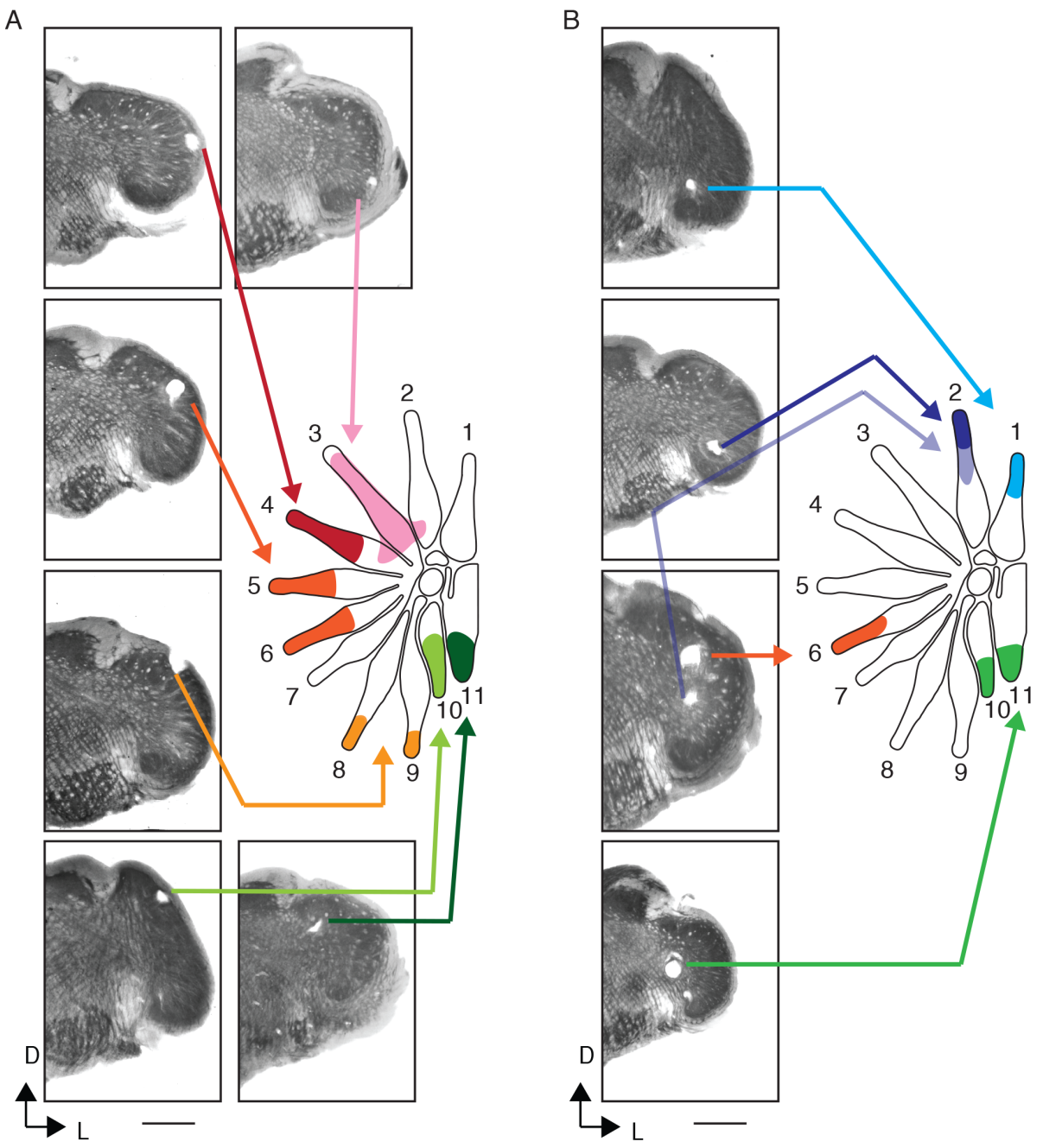

Fig. 7: Microlesions in the spinal trigeminal nucleus caudalis (SpVc) and corresponding receptive fields. **A** Sections with lesions in the substantia gelatinosa layer. **B:** Sections with lesions in the substantia magnocellularis layer. Abbreviations: D = dorsal, L = lateral Scale bar for micrographs = 500 µm.

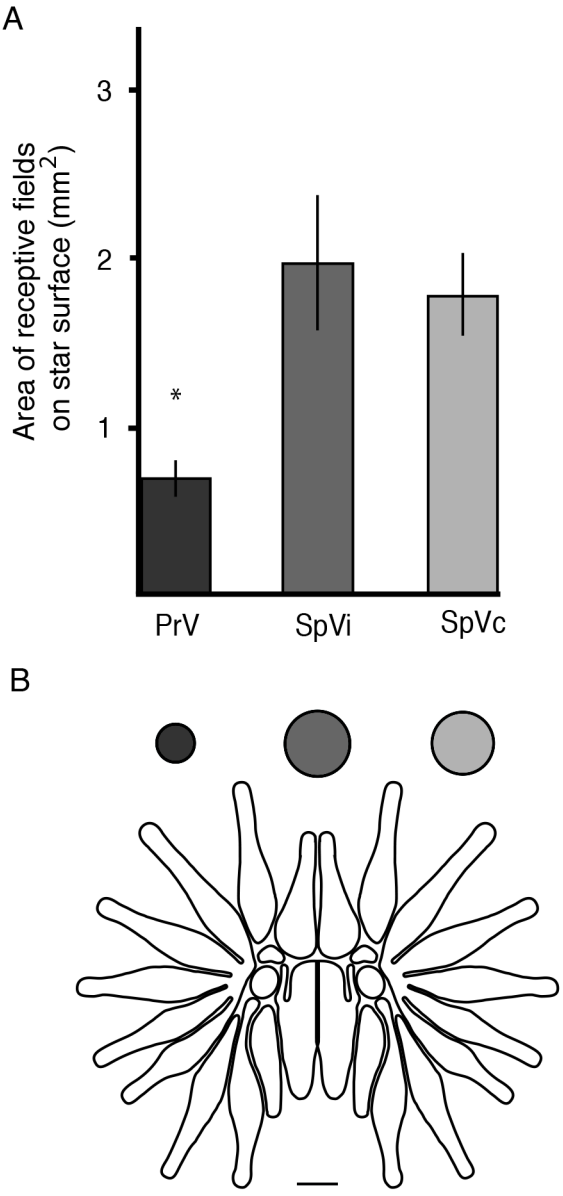

Fig. 8: Size of receptive fields in the principle sensory nucleus (PrV), spinal trigeminal subnucleus interpolaris (SpVi) and spinal trigeminal subnucleus caudalis (SpVc). **A:** Graph of the average size of the multiunit receptive fields recorded in the PrV, SpVi and SpVc in dark grey, grey and light grey, respectively. Receptive fields in PrV are smaller than in the other two areas ($p < 0.01$). Error bars represent 95% confidence interval. In PrV n= 68, in SpVi n= 28 In SpVc n=62. **B:** Schematic of half of a star with the size of the receptive fields displayed to scale. Scale bar = 1 mm

the receptor arrays of star-nosed moles, consistent with the absence of barrelettes in this subnucleus in rats and mice. For SpVi and SpVc, segmentation was visible in coronal sections processed for CO and these segments were matched to the rays of the nose through multiunit electrophysiological recordings. The representation of the mole's face in SpVi was broadly similar to that found in rats and mice. The anatomy of SpVc suggests the anterior part of the face is represented in the rostral part of the nucleus, and the posterior part of the face is represented more caudally (Fig. 9 H, K).

In addition to mapping the nuclei, we measured the volume of the ray representations in SpVi. The relatively small ray 11 had a large representation in SpVi. A large representation for ray 11 has also been observed in the PrV and the somatosensory cortex (Catania and Kaas, 1997; Catania et al., 2011b). However, SpVi differed from the other somatosensory stations in that ray 1 also had a disproportionately large representation. Lastly, we found that the mean areas of multiunit receptive fields in SpVi and SpVc were larger than in PrV.

ANATOMY OF THE SENSORY STAR

Initial patterning of the trigeminal nuclei was observed in the star-nosed mole as early as postnatal day 5. In 0-7 day-old moles the star appendages are folded back onto the snout (Fig. 1A) forming strips of sensory tissue parallel to the rostral-caudal body axis, with the tips of the rays most caudal on the animal and the bases most rostral. These strips are on the same rostral-caudal plane as whisker follicles. The rays become free at about one week of age (Catania, 2001), at which point the anatomy of the star is like that of an adult mole (Fig. 1 B). The mobile rays in adults can be in a plane perpendicular to the rostral-caudal body axis or swept forward so that the tips of the rays are more rostral than the bases.

ANATOMY OF SUBNUCLEUS INTERPOLARIS

In the star-nosed mole, the glabrous skin of the nose dominates the map in caudal SpVi, and the mole's presumptive barrelettes are found in a small area dorsal to the star representation. As is the case for the barrelettes of rats and mice, the star pattern was only seen in the caudal part of SpVi. Different areas of the face are accentuated in moles and compared to rodents, so that in the mole the representation of the nose is large and the representation of the whiskers is small, but in mice and rats the reverse is true (Fig. 9 C-F). In moles, the large representation of the nose and the relatively small vibrissal representation are consistent with the behavioral importance of the star and

also with the large size of the star representation found in the neocortex and PrV (Catania and Kaas, 1995; Catania et al., 2011b).

In moles the representation is inverted dorsoventrally so that the dorsal rays on the face are represented ventrally in the subnucleus, and the ventral receptors are represented dorsally in the subnucleus. The midline rays on the star are represented medially in the nucleus, and the lateral rays of the star are represented laterally in the nucleus.

The patterning along the medial-lateral axis of the nucleus is thus similar in rodents and star-nosed moles; in both animals the receptors nearest the midline are represented most medially, and those farther from the midline are represented more laterally. This interpretation is consistent for both juvenile moles, with the rays back, and adult moles with the rays detached. When the rays lay back on the snout, as when the brainstem patterning is first observed, then rays 1 and 11 are closer to the midline at the most anterior tip of the animal than the tips of lateral rays (eg., ray 5). This situation mimics the progression from high to low numbered whiskers in a mouse. When the rays are free from the snout in adults, the same progression would be from the midline rays toward the more lateral parts of the star. This overall topography is consistent with the clear map of the nose in primary somatosensory cortex in star-nosed moles and pigs (Catania and Kaas, 1995; Craner and Ray 1991). This organizational scheme is also consistent with that seen in the brainstem of other species including pigeons (Silver and Witkovsky, 1973), cats (Hayashi et al., 1984), and shrews (Catania et al., 2013).

The neural tissue devoted to each ray can be measured at many points from the periphery to the neocortex (Catania and Kaas, 1997; Catania et al., 2011b). The anatomical parameters measured for the star to date include the number of Eimer's organs on each ray, the number of myelinated fibers innervating each ray, the volume of the ray representations in PrV, and the area of the ray representations in primary somatosensory cortex. This report adds the volume of ray representations in SpVi to that data set. The measurements in SpVi were limited to juvenile animals. The measurements were taken from animals at different developmental stages and the absolute volumes of the subnuclei increased with increasing age. As a result, data were analyzed as the percent of neural tissue devoted to each ray across the different cases.

In general, ray 11 monopolized an increasing percentage of the star representation at higher stations (Fig. 4). Ray 10 showed a more modest increase in proportional representation at higher stations, whereas the other rays

showed a general decrease in proportional representation. The only exception to this trend was ray 1 in SpVi, which had a comparatively large representation.

The anatomical differences between the PrV and the SpVi is particularly interesting given that barrelettes in PrV and SpVi have similar relative sizes in rodents (Belford and Killackey, 1979b; Ma, 1991). It is possible that the overrepresentation of rays 1 and 11 in SpVi, which are both medial in the nucleus, is due to a structural limitation in how areas can be mapped in medial SpVi. However, the fact that the most medial SpVi barrelettes in rats and mice have the smallest cross-sectional area suggests this is not the case (Fig. 9C-D). The anatomical difference between the representations of the rays in the PrV and SpVi is consistent with specialization of these processing areas.

The PrV is usually considered the relay for touch with high-spatial acuity. It has been suggested that the SpVi maybe important in active, or generative, touch, (for review: Bosman et al., 2011; Diamond et al., 2008). If the SpVi has a special role in generative touch, then the large representations of rays 1 and 11 could be related to their special role in movement of the star. Ray 11 is the focus of ballistic reorienting movements of the star that reliably bring ray 11 into contact with a potential food item (Catania and Kaas, 1997). The movement of ray 1 is unique in that this ray often points forward while the rest of the star is flared back (Catania and Remple, 2004). Oriented this way, ray 1 is the first ray to contact a substrate. It is possible that the tactile information of first contact between ray 1 and a substrate could be useful in optimizing the force with which the rest of the star touches the ground. Given the speed of star movements, with 13 independent touches occurring within one second (Catania and Kaas, 1997), a sensorimotor loop mediating such optimization would need to be fast.

The brainstem tactile sensorimotor loop is an excitatory reflex arc in which deflection of a whisker can lead to a motor response with a short latency component of 5 to 10 ms (Nguyen and Kleinfeld, 2005)–fast enough to be involved in optimizing the force of a star touch. Nguyen and Kleinfeld, who studied this loop in rats, speculate that the trigeminal sensorimotor loop may be important for holding sensors against a surface and in controlling the force imparted on the sensors (2005). The same could be true in the star-nosed mole. This loop is likely mediated by direct projections from the trigeminal nuclei to the facial motor nucleus (Nguyen and Kleinfeld, 2005). Which subdivisions of the spinal trigeminal nucleus are involved is not known, but in rats both the SpVi and SpVc have direct projections to the facial nucleus (Hattox et al., 2002). It is possible that the large representations of ray 1 and 11 in SpVi are related to the trigeminal sensormotor loop.

It is also possible that the representations of ray 1 and 11 SpVi are related to other aspects of star movement. It has been observed that during whisking in awake rats, inhibitory signals from the SpVi suppress neurons in the PrV (Furuta et al., 2008; Lee et al., 2008). This raises the possibility that movement-induced suppression by SpVi projections plays a role in selecting which of the inputs are relayed through the PrV and further along the lemniscal pathway. Actively touching materials with such a variety of physical properties likely places many further demands on the star-nosed mole somatosensory system. As part of a foraging excursion a star-nosed mole might burrow through mud, traverse rocks at the edge of the water, dive in, and then use its star to trap air bubbles as it locates invertebrates via underwater olfaction.

Regardless of SpVi's role in somatosensation, the difference in the star representation in the PrV and SpVi shows that the somatotopic maps in the PrV and the SpVi can develop to exaggerate different areas of the periphery, which suggests that the PrV and SpVi are anatomically specialized for different functions.

ANATOMY OF SUBNUCLEUS CAUDALIS

There is an inverted star representation in the rostral portion of subnucleus caudalis and a vibrissae representation in more caudal areas. The somatotopic organization of mole SpVc along the rostral-caudal axis is consistent with the organization of SpVc reported in other mammals, including humans (DaSilva et al., 2002; Dejerine, 1985), cats (Panneton and Burton, 1981; Shigenaga et al., 1986; Yokota and Nishikawa, 1980) and rats (Arvidsson, 1982; Jacquin et al., 1983; Rustioni et al., 1971). This organization of caudalis was nicknamed the onion-skin model in recognition of the way the concentric circles of innervation around the mouth mimic the anatomy of an onion (Dejerine, 1985). The representation of the star in SpVc is spread along the rostral-caudal axis such that no single 2-dimensional plane contains the whisker representation and all 11 rays. Instead, the map is contained within a 3-dimensional tube with the most anterior areas of the face represented in the most rostral part of the nucleus and more posterior elements of the face represented caudally in sequence. This is best demonstrated in this study by the star-responsive areas that are more rostral to whisker-responsive areas. Though we were unable to resolve shifts in receptive field locations on a single ray in the rostral-caudal axis for caudalis, we hypothesize that the base of each ray is represented rostrally within the nucleus, and the tip is represented more caudally. This organization is suggested by the progression from absent or faint septa rostrally in the nucleus to distinct septa more

caudally. This pattern would be expected if the continuous sensory surface near the nostrils and the base of the rays was represented rostrally and the discontinuous surface at the tips of the rays was represented caudally.

It was difficult to resolve the receptive field shifts along a ray in this experiment because the microlesions we used to mark out rostral-caudal location were visible in at least 4 consecutive sections, which did not give us the resolution needed to map along the rostral-caudal axis. We did not attempt to reconstruct the volume of the ray representations in SpVc because we were not confident in the rostral boundary of the ray representations (the presumptive base representation). Thus, although the area of the representations of ray's 1 and 11 appear smallest in coronal cuts (Fig. 1F), additional studies will be required to investigate this question in detail.

SpVc is a laminated structure, consisting of three cell layers (Olszewski, 1950). The innermost layer, the magnocellular division, is the site of barrelettes in rodents (Ma, 1991). Other investigations have found that neurons in this layer can be induced to fire in anesthetized animals by lightly touching the face (Amano et al., 1986; Hu et al., 1981; Price et al., 1976). The middle layer, the substantia gelatinosa, does not have a visible whisker representation and is silent in many *in vivo* recordings that use gentle stimulation similar to the stimuli in this study (Amano et al., 1986; Hu et al., 1981; Price et al., 1976). Instead of processing light touch sensations, the substantia gelatinosa is thought to house interneurons that are critical to pain and temperature sensation (Davies and North, 2009).

Our results in the SpVc differ from work done in other animals in two ways. First, the star septa for the representation are in the substantia gelatinosa, not the substantia magnocellularis. The ray septa contain thick bundles of axons that course through the substantia gelatinosa to the substantia magnocellularis. Such collaterals are seen in SpVc of rats and mice (Ma, 1991; Price et al., 1976) but the regular divisions of the substantia gelatinosa into segments that correspond to trigeminal anatomy is not previously reported. In rats a bundle of collateral axons tend to send their projections to just one barrelette-like cluster (Ma, 1991). Perhaps the 11 subdivisions observed in the star-nosed mole are the result of the afferents from the same ray grouping together. The absence of an obviously visible star pattern in the magnocellular layer of SpVc is noteworthy given the presence of the barrelette-like representation in that layer at more caudal levels. It is possible that a visible star representation would be found in the magnocellular layer by analyzing more cases, but that seems unlikely given the lack of any clear septa despite sectioning the nucleus at many angles and in many developmental stages.

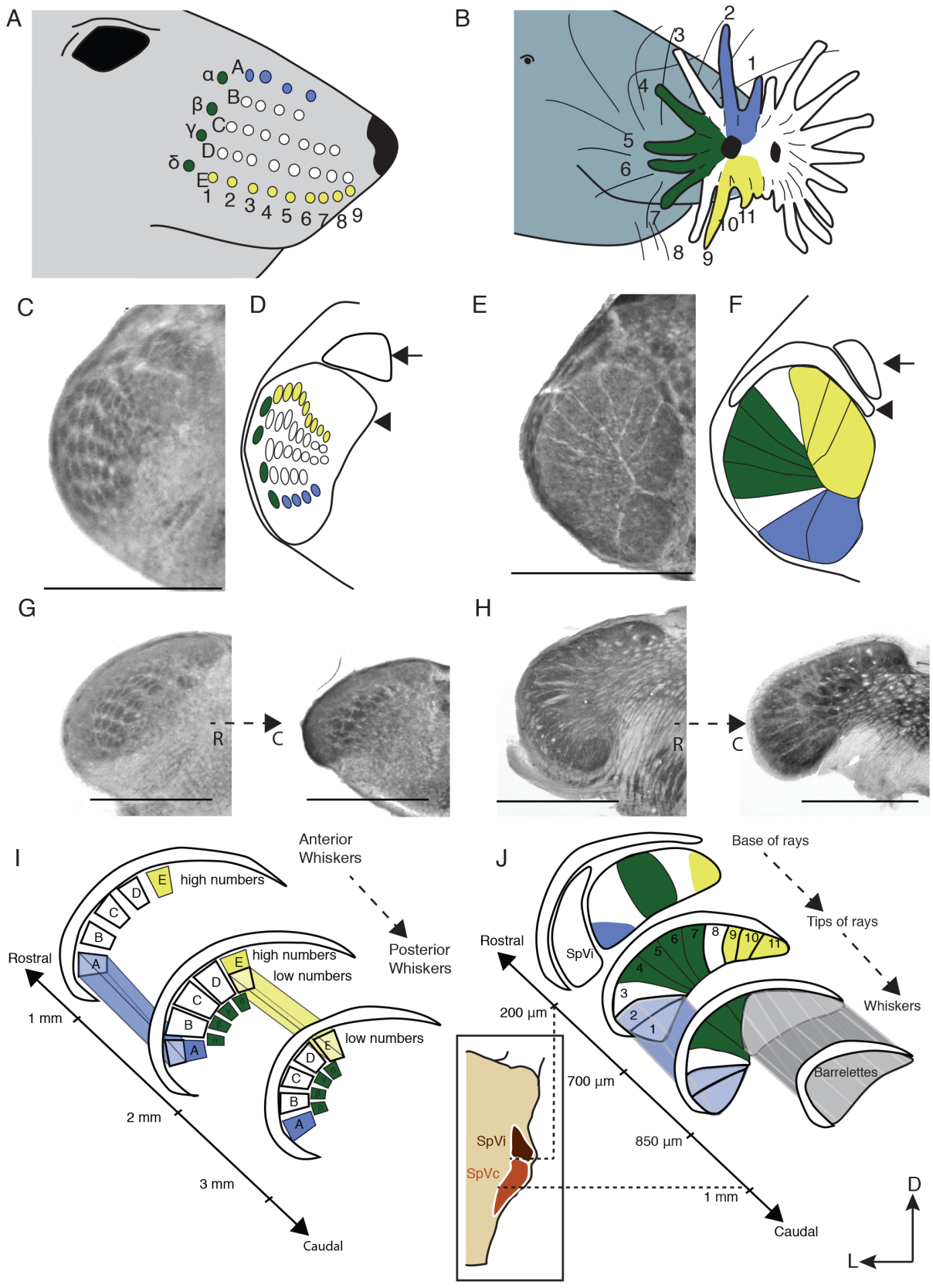
A
α
β
γ
δ
A
B
C
D
E
1 2 3 4 5 6 7 8 9
B
1
2
3
4
5
6
7
8
9
10
11
C
D
E
F
G
R
C
H
R
C
I
Anterior Whiskers
Posterior Whiskers
high numbers
high numbers
low numbers
low numbers
Rostral
1 mm
2 mm
3 mm
Caudal
J
Base of rays
Tips of rays
Rostral
SpVi
Whiskers
Barrelettes
200 µm
700 µm
850 µm
1 mm
SpVi
SpVc
Caudal
D
L

Fig. 9: A comparison between peripheral sensory surfaces and corresponding brainstem representations (subnuclei interpolaris (SpVi) and caudalis (SpVc)) in rats and star-nosed moles. All sections in this figure are in the coronal plane and stained for cytochrome oxidase. **A:** A schematic of the *mystacial vibrissae* of a rat and **B:** A schematic of the star, mystacial, and mandibular vibrissae of a star-nosed mole. **C:** A section of SpVi from a juvenile rat. **D**: A schematic of C. **E**: A section of SpVi from a juvenile star-nosed mole. **F**: A schematic of E. **G** and **H**: Sections of the SpVc from a juvenile rat and star-nosed mole, respectively. In each pair the section on the right is more rostral in the nucleus than the section on the left, showing how the pattern changes along rostral-caudal axis. **I and J**: Spaced, schematized coronal sections of SpVc in rats and star-nosed moles illustrating the rostrocaudal organization of the nucleus. High-numbered whiskers in rats and the base of the rays in moles are more rostral in the nucleus. Lower-numbered whiskers in rats and all mystacial vibrissae in moles are more caudal. The rostrocaudal scale is the approximate distance caudal from obex, which was selected in this diagram to match the metrics in Arvidsson (1982). **I** is modified from in Arvidsson (1982) Fig. 6. The insert in **J** is a drawing of a horizontal section of the brainstem to give the approximate rostrocaudal location of the diagram.

The second distinctive finding was that light mechanical stimulation of the star was a sufficient stimulus for neuronal responses in the substantia gelatinosa. In other animals, such stimulation was usually not sufficient for activation in this layer (Amano et al., 1986; Hu et al., 1981; Price et al., 1976). Our findings in caudalis could reflect an adaptation of the mole as a light touch specialist and may relate to what has been seen as a de-emphasis of pain receptors in favor of touch receptors in the star (Gerhold et al., 2013).

SIZE OF RECEPTIVE FIELDS

Star-nosed moles can use their stars to locate prey less than a millimeter in diameter (Catania and Kaas, 1997). Consistent with this ability, neurophysiological cortical recordings find receptive field sizes that average 0.71 mm^2. These receptive fields of cortical neurons are among the smallest reported for representations of glabrous skin, including for the highest acuity areas of the primate hand (DiCarlo et al., 1998; Pons et al., 1987; Sur et al., 1980; Vega-Bermudez and Johnson, 1999; Xerri et al., 1998). Because these cortical responses must be transmitted from subcortical structures, we measured the sizes of multiunit receptive fields in SpVi and SpVc and compared these to receptive fields in PrV from a previous study. Although receptive field size can be affected by depth of anesthesia (Friedberg et al., 1999) the same procedure was used in all studies. We found that within the PrV receptive fields were 0.69 mm^2, which is very similar to the size of receptive fields found in the cortex. In SpVi and SpVc the receptive fields were more than twice as large (though still extraordinarily small) (DiCarlo et al., 1998; Pons et al., 1987; Sur et al., 1980; Vega-Bermudez and Johnson, 1999; Xerri et al., 1998). This finding that the PrV had smaller receptive fields than the SpVi and SpVc is consistent with the PrV having a special role in high-acuity touch. It is also consistent with findings in rats that neurons in the PrV have receptive fields that encompass fewer whiskers than neurons in the SpVi (Timofeeva et al. 2004).

The segmentation of the SpVi and the SpVc is similar in many ways to the segmented organization observed for the whisker representation in rodent brainstem. The CO-segments that represent the nasal rays in moles are analogous to the barrelettes found in rodents and suggest that similar underlying developmental mechanisms are acting across diverse species and sensory systems to pattern the central nervous system. Despite these general similarities across species, the organization of star-nosed mole brainstem also reveals a number of specializations that relate to the mole's particular sensory surface (the star) and behavior (tactile foveation). For example the different nasal rays are differentially proportioned (in contrast to rodent whiskers) at various stations

and have differently sized receptive fields. These findings may ultimately provide further insights into the functions of the distinct trigeminal subnuclei and into how representations of important sensory surface develop at different CNS stations.

ACKNOWLEDGMENTS

We thank Diana Bautista, Kristin Gerhold, Lucy Sawyer, and Pamela Tsuruda for assistance collecting the star-nosed moles used in this study, and Elizabeth Catania for help collecting the moles and technical assistance. We also thank Diana Sarko, Barbara O'Brien for advice editing this manuscript. We thank the Vanderbilt University Department of Animal Care for providing excellent animal care.

REFERENCES

Amano, N., Hu, J. W. and Sessle, B. J. (1986). Responses of neurons in feline trigeminal subnucleus caudalis (medullary dorsal horn) to cutaneous, intraoral, and muscle afferent stimuli. *J Neurophysiol* **55**, 227-43.

Anstrom, K. E. (1953). On the central course of afferent fibres in the trigeminal, facial, glossopharyngeal, and vagal nerves and their nuclei in the mouse. *Acta physiol. scand. Suppl.* **106**, 209-320.

Arvidsson, J. (1982). Somatotopic organization of vibrissae afferents in the trigeminal sensory nuclei of the rat studied by transganglionic transport of HRP. *J Comp Neurol* **211**, 84-92.

Ashwell, K. W., Hardman, C. D. and Paxinos, G. (2006). Cyto- and chemoarchitecture of the sensory trigeminal nuclei of the echidna, platypus and rat. *J Chem Neuroanat* **31**, 81-107.

Belford, G. R. and Killackey, H. P. (1979). Vibrissae representation in subcortical trigeminal centers of the neonatal rat. *J Comp Neurol* **183**, 305-21.

Bosman, L. W., Houweling, A. R., Owens, C. B., Tanke, N., Shevchouk, O. T., Rahmati, N., Teunissen, W. H., Ju, C., Gong, W., Koekkoek, S. K. et al. (2011). Anatomical pathways involved in generating and sensing rhythmic whisker movements. *Front Integr Neurosci* **5**, 53.

Carroll, E. W. and Wong-Riley, M. T. (1984). Quantitative light and electron microscopic analysis of cytochrome oxidase-rich zones in the striate cortex of the squirrel monkey. *J Comp Neurol* **222**, 1-17.

Catania, K. C. (1996). Ultrastructure of the Eimer's organ of the star-nosed mole. *J Comp Neurol* **365**, 343-54.

Catania, K. C. (2001). Early development of a somatosensory fovea: a head start in the cortical space race? *Nat Neurosci* **4**, 353-4.

Catania, K. C., Catania, E. H., Sawyer, E. K. and Leitch, D. B. (2013). Barrelettes without barrels in the American water shrew. *PLoS One* **8**, e65975.

Catania, K. C. and Kaas, J. H. (1995). Organization of the somatosensory cortex of the star-nosed mole. *J Comp Neurol* **351**, 549-67.

Catania, K. C. and Kaas, J. H. (1997). Somatosensory fovea in the star-nosed mole: behavioral use of the star in relation to innervation patterns and cortical representation. *J Comp Neurol* **387**, 215-33.

Catania, K. C., Leitch, D. B. and Gauthier, D. (2011). A Star in the Brainstem Reveals the First Step of Cortical Magnification. *Plos One* **6**.

DaSilva, A. F., Becerra, L., Makris, N., Strassman, A. M., Gonzalez, R. G., Geatrakis, N. and Borsook, D. (2002). Somatotopic activation in the human trigeminal pain pathway. *J Neurosci* **22**, 8183-92.

Davies, A. J. and North, R. A. (2009). Electrophysiological and morphological properties of neurons in the substantia gelatinosa of the mouse trigeminal subnucleus caudalis. *Pain* **146**, 214-21.

Dejerine, J. (1985). Classics in Neurology - Intermittent Claudication of the Spinal-Cord (Reprinted from Semiologie Des Affections Du Systeme Nerveux, P9 267-269, 1914). *Neurology* **35**, 860-860.

Devoize, L., Domejean, S., Melin, C., Raboisson, P., Artola, A. and Dallel, R. (2010). Organization of projections from the spinal trigeminal subnucleus oralis to the spinal cord in the rat: a neuroanatomical substrate for reciprocal orofacial-cervical interactions. *Brain Res* **1343**, 75-82.

Diamond, M. E., von Heimendahl, M., Knutsen, P. M., Kleinfeld, D. and Ahissar, E. (2008). 'Where' and 'what' in the whisker sensorimotor system. *Nat Rev Neurosci* **9**, 601-12.

DiCarlo, J. J., Johnson, K. O. and Hsiao, S. S. (1998). Structure of receptive fields in area 3b of primary somatosensory cortex in the alert monkey. *J Neurosci* **18**, 2626-45.

Erzurumlu, R. S., Murakami, Y. and Rijli, F. M. (2010). Mapping the face in the somatosensory brainstem. *Nat Rev Neurosci* **11**, 252-63.

Fiala, J. C. (2005). Reconstruct: a free editor for serial section microscopy. *J Microsc* **218**, 52-61.

Friedberg, M. H., Lee, S. M. and Ebner, F. F. (1999). Modulation of receptive field properties of thalamic somatosensory neurons by the depth of anesthesia. *J Neurophysiol* **81**, 2243-52.

Furuta, T., Timofeeva, E., Nakamura, K., Okamoto-Furuta, K., Togo, M., Kaneko, T. and Deschenes, M. (2008). Inhibitory gating of vibrissal inputs in the brainstem. *J Neurosci* **28**, 1789-97.

Gallyas, F. (1979). Silver staining of myelin by means of physical development. *Neurol Res* **1**, 203-9.

Gerard, M. W. (1923). Afferent impulses of the trigeminal nerve. *A.M.A. Arch. Neurol. Psychiat.* **9**, 306–338.

Gerhold, K. A., Pellegrino, M., Tsunozaki, M., Morita, T., Leitch, D. B., Tsuruda, P. R., Brem, R. B., Catania, K. C. and Bautista, D. M. (2013). The star-nosed mole reveals clues to the molecular basis of mammalian touch. *PLoS One* **8**, e55001.

Hamilton, W. B. (1931). Habits of the Star-Nosed Mole, Condylura cristata. *Journal of Mammalogy* **12**, 345-355.

Hattox, A. M., Priest, C. A. and Keller, A. (2002). Functional circuitry involved in the regulation of whisker movements. *J Comp Neurol* **442**, 266-76.

Hayashi, H., Sumino, R. and Sessle, B. J. (1984). Functional organization of trigeminal subnucleus interpolaris: nociceptive and innocuous afferent inputs, projections to thalamus, cerebellum, and spinal cord, and descending modulation from periaqueductal gray. *J Neurophysiol* **51**, 890-905.

Henderson, T. A. J., M. F. (1995). What makes subcortical barrels? In *Cerebral Cortex, the Barrel Cortex in Rodents*, vol. 11 (ed. J. E. G. D. I. T.), pp. 123-178. New York: Plenum.

Hu, J. W., Dostrovsky, J. O. and Sessle, B. J. (1981). Functional properties of neurons in cat trigeminal subnucleus caudalis (medullary dorsal horn). I. Responses to oral-facial noxious and nonnoxious stimuli and projections to thalamus and subnucleus oralis. *J Neurophysiol* **45**, 173-92.

Jacquin, M. F., Renehan, W. E., Mooney, R. D. and Rhoades, R. W. (1986a). Structure-function relationships in rat medullary and cervical dorsal horns. I. Trigeminal primary afferents. *J Neurophysiol* **55**, 1153-86.

Jacquin, M. F., Semba, K., Egger, M. D. and Rhoades, R. W. (1983). Organization of HRP-labeled trigeminal mandibular primary afferent neurons in the rat. *J Comp Neurol* **215**, 397-420.

Jacquin, M. F., Woerner, D., Szczepanik, A. M., Riecker, V., Mooney, R. D. and Rhoades, R. W. (1986b). Structure-function relationships in rat brainstem subnucleus interpolaris. I. Vibrissa primary afferents. *J Comp Neurol* **243**, 266-79.

Lee, S., Carvell, G. E. and Simons, D. J. (2008). Motor modulation of afferent somatosensory circuits. *Nat Neurosci* **11**, 1430-8.

Ma, P. M. (1991). The barrelettes--architectonic vibrissal representations in the brainstem trigeminal complex of the mouse. I. Normal structural organization. *J Comp Neurol* **309**, 161-99.

Marasco, P. D., Tsuruda, P. R., Bautista, D. M., Julius, D. and Catania, K. C. (2006). Neuroanatomical evidence for segregation of nerve fibers conveying light touch and pain sensation in Eimer's organ of the mole. *Proc Natl Acad Sci U S A* **103**, 9339-44.

Nash, P. G., Macefield, V. G., Klineberg, I. J., Murray, G. M. and Henderson, L. A. (2009). Differential activation of the human trigeminal nuclear complex by noxious and non-noxious orofacial stimulation. *Hum Brain Mapp* **30**, 3772-82.

Nguyen, Q. T. and Kleinfeld, D. (2005). Positive feedback in a brainstem tactile sensorimotor loop. *Neuron* **45**, 447-57.

Olszewski, J. (1950). On the anatomical and functional organization of the spinal trigeminal nucleus. *J Comp Neurol* **92**, 401-13.

Panneton, W. M. and Burton, H. (1981). Corneal and periocular representation within the trigeminal sensory complex in the cat studied with transganglionic transport of horseradish peroxidase. *J Comp Neurol* **199**, 327-44.

Pons, T. P., Wall, J. T., Garraghty, P. E., Cusick, C. G. and Kaas, J. H. (1987). Consistent features of the representation of the hand in area 3b of macaque monkeys. *Somatosens Res* **4**, 309-31.

Price, D. D., Dubner, R. and Hu, J. W. (1976). Trigeminothalamic neurons in nucleus caudalis responsive to tactile, thermal, and nociceptive stimulation of monkey's face. *J Neurophysiol* **39**, 936-53.

Ramon y Cajal, S. (1896). Beitrag zum Studium der Medulla oblongata, des Kleinhirns uud des Ursprungs der Gehirnnerven. Leipzig: J. A. Barth.

Rustioni, A., Sanyal, S. and Kuypers, H. G. (1971). A histochemical study of the distribution of the trigeminal divisions in the substantia gelatinosa of the rat. *Brain Res* **32**, 45-52.

Schneider, C. A., Rasband, W. S. and Eliceiri, K. W. (2012). NIH Image to ImageJ: 25 years of image analysis. *Nat Methods* **9**, 671-5.

Shigenaga, Y., Chen, I. C., Suemune, S., Nishimori, T., Nasution, I. D., Yoshida, A., Sato, H., Okamoto, T., Sera, M. and Hosoi, M. (1986). Oral and facial representation within the medullary and upper cervical dorsal horns in the cat. *J Comp Neurol* **243**, 388-408.

Silver, R. and Witkovsky, P. (1973). Functional characteristics of single units in the spinal trigeminal nucleus of the pigeon. *Brain Behav Evol* **8**, 287-303.

Sur, M., Merzenich, M. M. and Kaas, J. H. (1980). Magnification, receptive-field area, and "hypercolumn" size in areas 3b and 1 of somatosensory cortex in owl monkeys. *J Neurophysiol* **44**, 295-311.

Torvik, A. (1956). Afferent connections to the sensory trigeminal nuclei, the nucleus of the solitary tract and adjacent structures; an experimental study in the rat. *J Comp Neurol* **106**, 51-141.

Van der Loos, H. (1976). Barreloids in mouse somatosensory thalamus. *Neurosci Lett* **2**, 1-6.

Vega-Bermudez, F. and Johnson, K. O. (1999). SA1 and RA receptive fields, response variability, and population responses mapped with a probe array. *J Neurophysiol* **81**, 2701-10.

Woolsey, T. A. and Van der Loos, H. (1970). The structural organization of layer IV in the somatosensory region (SI) of mouse cerebral cortex. The description of a cortical field composed of discrete cytoarchitectonic units. *Brain Res* **17**, 205-42.

Xerri, C., Merzenich, M. M., Peterson, B. E. and Jenkins, W. (1998). Plasticity of primary somatosensory cortex paralleling sensorimotor skill recovery from stroke in adult monkeys. *J Neurophysiol* **79**, 2119-48.

Yokota, T. and Nishikawa, N. (1980). Reappraisal of somatotopic tactile representation within trigeminal subnucleus caudalis. *J Neurophysiol* **43**, 700-12.

CHAPTER III

Subcortical Barrelette-Like and Barreloid-Like Structures in the Prosimian Galago (*Otolemur garnetti)*

This chapter is reproduced with permission from the published work by Sawyer E. K., Liao C.-C., Qi H., Balaram P., Matrov D., and Kaas J. H. 2015. Barreloid-like structures in the ventroposterior medial subnucleus of the somatosensory thalamus in prosimian galagos. *Proceedings of the National Academy of Sciences* 12 (22) 7079-7084 Some additional content has been added.

ABSTRACT

Galagos are prosimian primates that resemble ancestral primates more than most other extant primates. As in many other mammals, the facial vibrissae of galagos are distributed across the upper and lower jaws and above the eye. In rats and mice, the mystacial macrovibrissae are represented throughout the ascending trigeminal pathways as arrays of cytoarchitecturally distinct modules, with each module having a nearly one-to-one relationship with a specific facial whisker. The macrovibrissal representations are termed barrelettes in the trigeminal somatosensory brainstem, barreloids in the ventroposterior medial subnucleus of the thalamus, and barrels in primary somatosensory cortex. Despite the presence of facial whiskers in all non-human primates, barrel-like structures have not been reported in primates. By staining for cytochrome oxidase, Nissl, and vesicular glutamate transporter proteins, we show a distinct array of barrelette-like and barreloid-like modules in the principal sensory nucleus, the spinal trigeminal nucleus, and the ventroposterior medial subnucleus of the galago, *Otolemur garnetti*. Labeled terminals of primary sensory neurons in the brainstem and cell bodies of thalamocortically projecting neurons demonstrate that barrelette-like and barreloid-like modules are located in areas of these somatosensory nuclei that are topographically consistent with their role in facial touch. Serendipitously, the plane of section that best displays the barreloid-like modules reveals a remarkably distinct homunculus-like patterning which, we believe, is one of the clearest somatotopic maps of an entire body surface yet found.

INTRODUCTION

Nearly all mammals use facial vibrissae as a sensory organ to transduce distant touch. In some species, but most famously in rats and mice, individual whiskers have been shown to be represented as distinct modules in the ascending lemniscal and paralemniscal somatosensory pathways (Bosman et al., 2011). These modules have been termed barrelettes, barreloids, and barrels in the brainstem, thalamus, and cortex, respectively (Belford and Killackey, 1979a; Ma, 1991; Van der Loos, 1976; Woolsey and Van der Loos, 1970). The discovery of the barrel pathway has allowed researchers to visualize how somatosensory inputs are anatomically organized in the brain. The barrel pattern provides clear anatomical landmarks that enable further research on the development, connection, functional organization, and plasticity of the somatosensory system: many investigators have embraced this system in their research programs (for review see (Ebner and Kaas, 2015; Fox, 2008)). Beyond the experimental convenience of the system, the nearly perfect correspondence of one whisker to one barrel invokes questions about the development and evolution of nervous systems in general, such as if development of the organization of sensory systems is largely controlled by properties intrinsic to the central nervous system or largely dictated by the arrangement of peripheral receptors (Kaas and Catania, 2002; Van der Loos, 1978). In addition, do whisker-modules have a function, or are they just a spandrel (Gould and Lewontin, 1979; Purves et al., 1992) that tells us more about the morphology of the periphery and brain development than sensory processing? (Horton and Adams, 2005)

Despite the plethora of work examining the function and organization of barrel structures, mostly in mice and rats, similar structures have yet to be identified in primates. Evidence for barrel-like structures in primates would provide a concrete anatomical link between primates and the body of work on rodent somatosensory systems.

Prosimian galagos (Fig. 1A) were selected because galagos have an array of whiskers on the face with muscular and nerve attachments at the base of the whisker follicles (Muchlinski et al., 2013), suggesting they have some whisking function. In addition, galagos are a member of the most basal clade of primates, one that retained the nocturnal and arboreal lifestyle of early primates (Martin, 1990). We hypothesized the somatosensory system of galagos could resemble that of the common ancestor of primates.

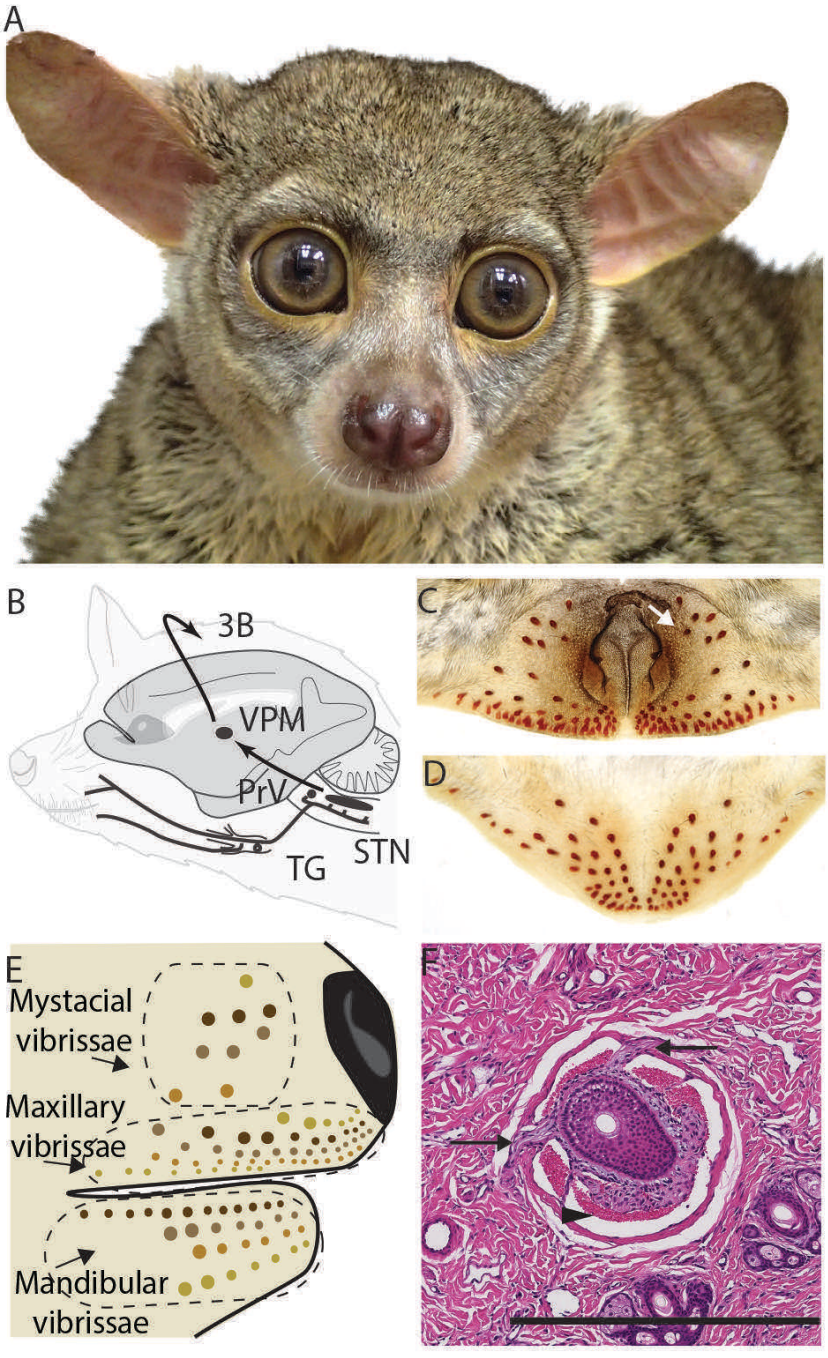
A
B
3B
VPM
PrV
TG
STN
C
D
E
Mystacial
vibrissae
Maxillary
vibrissae
Mandibular
vibrissae
F

Fig. 1. **A:** An adult galago (*Otolemur garnetti)*. **B:** A simplified diagram of the trigeminal somatosensory lemniscal pathway. **C-D:** Cleared skin samples of the upper C and lower D face reveal the blood sinuses of vibrissae. The white arrow in C points to an asymmetrically present blood sinus. **E:** Schematic of one side of a galago face indicating the mystacial and vibrissae. **F**: A transverse section of the flattened skin of the face stained for Hematoxylin and eosin showing the blood sinuses and innervation of a vibrissae follicle. The arrowhead indicates a blood sinus; arrows indicate nerves innervating the follicle. Scale bar = 500 μm. Abbreviations: 3b= primate primary somatosensory cortex. VPM= ventroposterior medial subnucleus of the thalamus, PrV= principle sensory nucleus, STN = spinal trigeminal nucleus, TG= trigeminal ganglion.

Antigen	**Description of Immunogen**	**Source, Host Species, Cat. #, Clone or Lot#, RRID**	**Concentration (μg/ml)**
Vesicular glutamate transporter 1 (VGLUT1)	Recombinantprotein from rat (aa 456–560)	Synaptic Systems, rabbit polyclonal, 135 303, AB_887876	0.2
Vesicular glutamate transporter 2 (VGLUT2)	Recombinant protein from rat VGLUT2	Millipore, mouse monoclonal, MAB5504, AB_2187552	0.2
Biotinylated horse anti-mouse IgG	Mouse IgG	Vector, mouse polyclonal, BA-2000, AB_2313581	3
Biotinylated goat anti-rabbit IgG	Rabbit IgG	Vector, rabbit polyclonal, BA-1000, AB_2313606	3

Table 1: Commercially available antibodies used in this study.

The trigeminal lemniscal pathway in galagos, the main pathway leading to the barrels in the mouse and rat cortex, is illustrated in Figure 1B. Our research systematically examined central nervous system nuclei within this pathway. First, we examined the whisker pattern on the face of galagos (Fig. 1C, D). Then we used histology and neural tracers to investigate the anatomy and connections of the principal sensory nucleus (PrV) and the spinal trigeminal nucleus subnucelus interpolaris (SpVi), the two divisions of the somatosensory brainstem that have distinct barrelette patterns in rodents. We then used the same techniques to investigate the anatomy of the ventroposterior medial subnucleus (VPM), the site of barreloids in the rodent thalamus. Additionally we related the cortical histology to dense electrophysiolgical multiunit recording in the face representation in contralateral primary somatosensory area 3b, which receives projections from barreloid structures in VPM.

METHODS

The PrV, SpVi, VPM and cortex were examined in nine prosimian galagos (*Otolemur garnetti*). Four were used for neural tracers and histology (two male; all adult) and five were used for histology only (two male; one juvenile, four adults). All research was conducted in compliance with the guidelines established by the National Institutes of Health and were approved by the Animal Care and Use Committee of Vanderbilt University.

Thalamic tracer experiments were completed in five hemispheres from four animals. Animals were anesthetized with a mixture of ketamine hydrochloride (10–25 mg/kg) and isoflurane (1–2% isoflurane in oxygen). Area 3b of cortex was exposed and microelectrode multiunit recordings (1 MΩ at 1 kHz) were used to map receptive fields under ketamine and xylazine anesthesia. Small amounts (0.02 µL) of the neural tracer cholera toxin subunit B (1% CTB, Sigma, St. Louis, MO) in sterile distilled water were injected into selected cortical regions at depths of 600–1000 µm. Additionally, 10 µL of CTB-HRP (cholera toxin B subunit linked to horseradish peroxidase) was injected into the whisker follicles on the face of one animal. The opening was closed and the animal was monitored in recovery. Prophylactic antibiotics and analgesics were administered postoperatively. After three to five days the animals were anesthetized as described above, and cortical mapping was resumed until a dense map of the face region of area 3B was obtained. All galagos were euthanized with sodium pentobarbital and perfused transcardially with phosphate buffered (PB) saline followed by 2–3% paraformaldehyde (phosphate bufferin PB, (pH 7.5). The brain from each animal was removed, blocked, and cryoprotected in 30% sucrose overnight. Each block was cut on a freezing sliding

microtome into 40-µm sections. Cortical blocks were flattened and cut tangential to the pia surface. Brainstem blocks were cut coronally, and thalamic blocks were cut 15 degrees off of horizontal as illustrated in Figure 3E. All brains were processed so that alternate sections highlighted different features. Tetramethylbenzidine (TMB) immunohistochemistry was used to visualize CTB-HRP. Architectural boundaries were defined with stains for cytochrome oxidase (CO), Nissl substance, or for vesicular glutamate transporter 1 or 2 protein (VGLUT1, VGLUT2). The specificity of the VGLUT antibodies has been confirmed in primates (Balaram et al., 2013; Baldwin et al., 2013). Details of the reagents used for the immunohistocemisty can be found in supplemental table 1. The skin of the face was removed from four animals, of which three were cleared with xylene in order to remove skin pigmentation while leaving blood sinuses visible (Haidarliu and Ahissar, 1997) . One was stored in 10% formaldehyde and then processed for Hematoxylin and Eosin.

High-resolution images of the processed tissue were obtained using a SCN400 Slide Scanner (Leica, Wetzlar, Germany) or a Nikon DXM1200 camera mounted on the microscope Nikon E800 microscope (Nikon, Melville, NY). The images were manipulated only for brightness and contrast using Adobe Photoshop (Adobe Systems, San Jose, CA). Distributions of labeled cells and terminals were plotted on the images, which were then overlaid on to adjacent sections stained for architectural features.

RESULTS

VIBRISSAE

In galagos, the mysticial vibrissae are as thin as the other facial vibrissae, similar in length to some of the caudal vibrissae just above the mouth and on the chin, and are not obviously whisked. Since the prefix "macro" and "micro" is ambiguous in this situation, we refer to galago vibrissae as mystacial, mandibular, and maxillary vibrissae (Fig. 1E).

Galagos have 8 or 9 mystacial vibrissae just caudal to the nose and numerous vibrissae near the mouth on both the upper and lower jaws (Fig. 1. C-E). The number and distribution of the mystacial vibrissae varied between animals and sometimes between sides of the face on the same animal (Fig. 1C). In the 3 animals investigated, the 4 mystacial vibrissae rows, from dorsal to ventral, contained 1, 3, 2-3, and 2 vibrissae each. The vibrissae above and below the mouth were abundant. The number of maxillary vibrissae ranged from 39 to 51 and the number of

mandibular vibrissae ranged from 35-37. All tactile hairs were thin hairs, with hair shafts measuring about 60 μm in diameter at the base. Mystacial vibrissae were 0.5 to 1.1 mm long; both the maxillary and mandibular vibrissae were mostly under 0.2 mm in length, though in both sets the most caudal vibrissae measured 0.7 to 0.8 mm.

SOMATOSENSORY BRAINSTEM

Barrelette-like modules are present in the in the PrV and caudal SpVi (Fig. 2). In SpVi the modules are apparent as densely stained circles in sections processed for CO and VGLUT1, but were not observed in Nissl stained sections (Fig. 2E-H). In the PrV the modules were less clear but still visible as densely stained areas in CO and VGLUT1 stained sections. Similar PrV structures appeared as disorganized groups of cells separated by lightly stained septa in Nissl preparations(Fig. 2 A-D). The VGLUT2 and CO dense modules were 50 to 60 μm in diameter in SpVi and 50-90 μm in the PrV.

In both the PrV and the SpVi there are two separate clusters of the barrelette-like modules, one dorsomedial in the nucleus and one ventrolateral in the nucleus. In both nuclei an injection of CTB-HRP in the vibrissae follicles of the upper-jaw labeled terminals in the ventrolateral region (Fig. 2J-O, and an injection in the lower-jaw labeled terminals in the dorsomedial region (Fig. 2P-U). The two distinct patches of label in the PrV following the upper-chin injection (Fig. 2Q) may be indicative of label filling two distinct barreloid-like modules. In both the SpVi and the PrV there are too few barrelette-like structures in any one section for a one-to-one relationship between the vibrissae and the brainstem modules.

SOMATOSENSORY THALAMUS

The best plane for visualizing barreloid-like modules in the VPM is 15 degrees off the horizontal plane as illustrated in (Fig. 3H). This angle was found based on extrapolating from the rod-like anatomy visible in coronal sections of the VPM and with limited trial and error. In that favorable plane, there are distinct barreloid-like structures that are most apparent in VGLUT2 stained sections (Fig. 3A, B). These darkly stained areas reflect the density of VGLUT2 protein in the presynaptic terminals. The barreloid-like structures are also visible in the patchy distribution of cell bodies sections stained for Nissl substance, yet are barely detectable as darkly stained CO modules (Fig. 3C, D, F, G). The VGLUT2 dense patches were 65 to 140 μm in diameter and were visible over multiple adjacent sections, spanning about 200 μm. The densely stained modules organized into two distinct

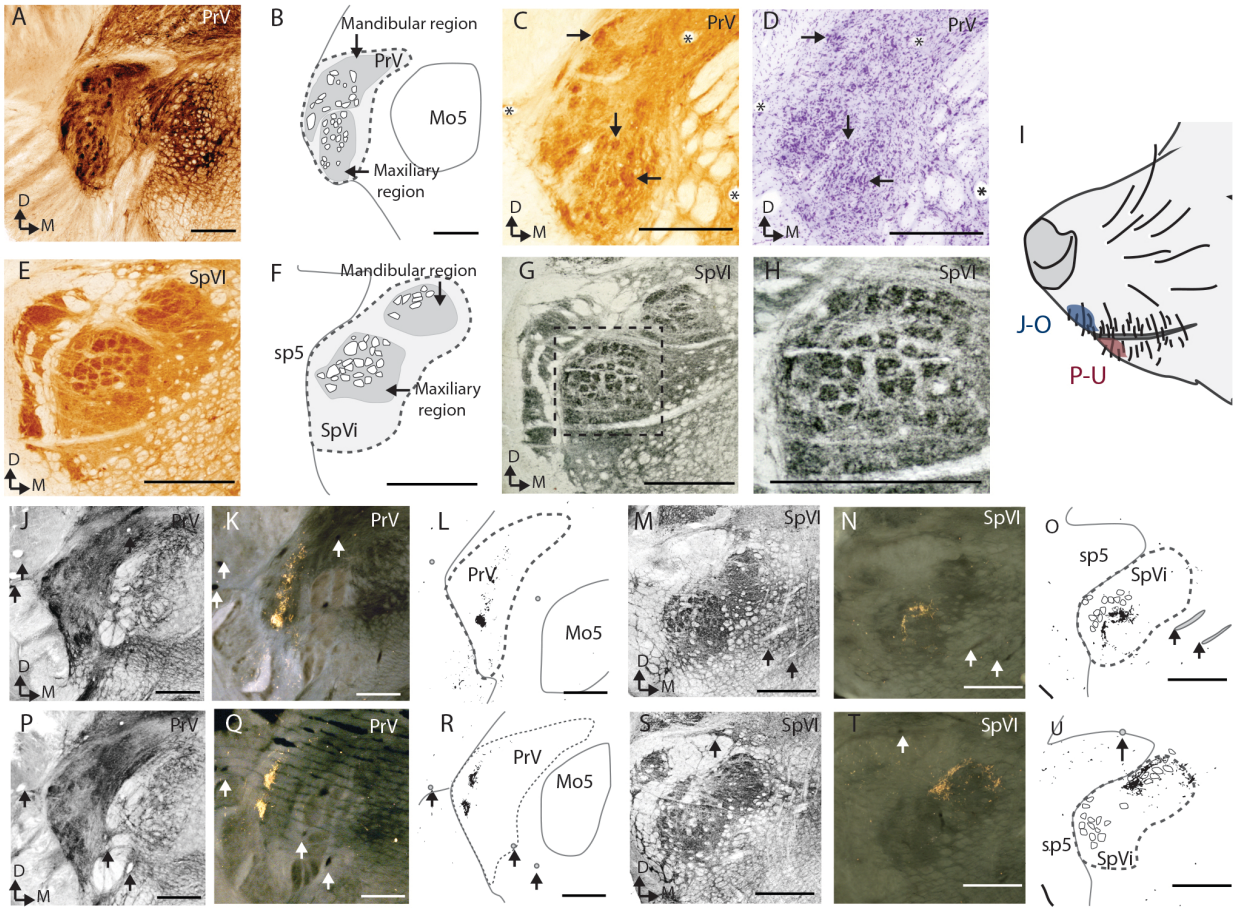

Fig. 2. A-D: Histology of the principal sensory nucleus (PrV). **A:** A coronal section stained for cytochrome oxidase (CO) showing densely stained modules. **B:** A schematic of the anatomy in A. **C and D:** Adjacent sections stained for CO and Nissl substance showing the CO dense modules and disorganized clumps of cell bodies. Asterisks mark the same blood vessels and arrows mark barrelette-like modules. **E-H**: Histology of spinal trigeminal nucleus interpolaris (SpVi). **E**: A coronal section stained for CO showing densely stained modules. **F**: A schematic of the anatomy in E. **G and H**: Two magnifications of a section adjacent to E, stained for vesicular glutamate transporter 1 (VGLUT1) in which modules are visible. **I**: The location of the injections of the tracer (cholera toxin subunit B conjugated to horseradish peroxidase). **J-O**: The results from the tracer injection into the tip of the upper jaw; a section stained for VGLUT1 (SpVi: **J**, PrV: **M**), an adjacent section stained for the HRP conjugate of the tracer (SpVi: **K**, PrV: **N**), and an overlay schematic (SpVi: **L**, PrV:**O**). **P-U**: The results from the tracer injection into the tip of the upper jaw organized the same way as J-O. Abbreviations: Mo5= Motor nucleus of the 5th nerve., sp5= spinal tract of the 5th nerve. Scale bar= 500 um.

groups, one was more caudal and lateral than the other. As in PrV and SpVi, there are not enough barrelette-like structures for a one-to-one relationship between vibrissae and thalamic modules.

In addition to the barreloid-like modules, there was an area with five larger segments in the posteromedial region of the VPM. These measured between 50 and 100 um in diameter. Cell bodies in this area were labeled after tracer was injected into the tooth representation in area 3b.

Serendipitously, this best plane of cut for the barreloid-like modules also resulted in a galago-specific somatotopic pattern in the ventral posterior lateral subnucleus as well (Fig. 3E). The likely hand/face border, septa between digits, and a border between the palm of the forelimb and hindlimb were readily visible in all stained sections.

Microelectrode recordings were used to identify injection sites in S1 (area 3b), whose neurons responded to touch on various locations of the face and body. At selected locations CTB tracer was injected to examine the thalamo-cortical connections. The results from the injection of tracers in area 3b indicate that thalamo-cortical projections are somatotopically arranged in the VPM (Individual cases: Fig.4-8, summary of all cases: Fig. 9). The somatotopy following tracer injections matches the somatotopy suggested by the pattern of septa. Injections into the face representation in cortex (two in the lower jaw, two in the upper jaw, and one in the teeth representations) resulted in labeled cell bodies overlapping the barreloid-like structures in the thalamus. Locations of labeled neurons resulting from the separate injections in the arm, digits of the forelimb, and hindlimb representations confirmed the orientation of the thalamic representation and were consistent with the interpretation of the other major septa between the hand and face, the digits, and the hand and hind limb within VPM.

PRIMARY SENSORY CORTEX

Dense mapping of the face region of 3b revealed that most of the area devoted to the face representation was responsive to the vibrissae of the upper and lower jaw, whereas only a small region had receptive fields corresponding to the mystacial vibrissae. The results individual cases are presented in Figures 4-8, and a summary of all cases is shown in Figure 9. In the five hemispheres mapped, 387 electrode penetrations had tactile receptive fields on the head, 152 had receptive fields on the vibrissae of the upper lip, 76 on the vibrissae of the lower lip, and only 16 on the mystacial region. We were unable to find barrel-like structures in our histology of sections of the

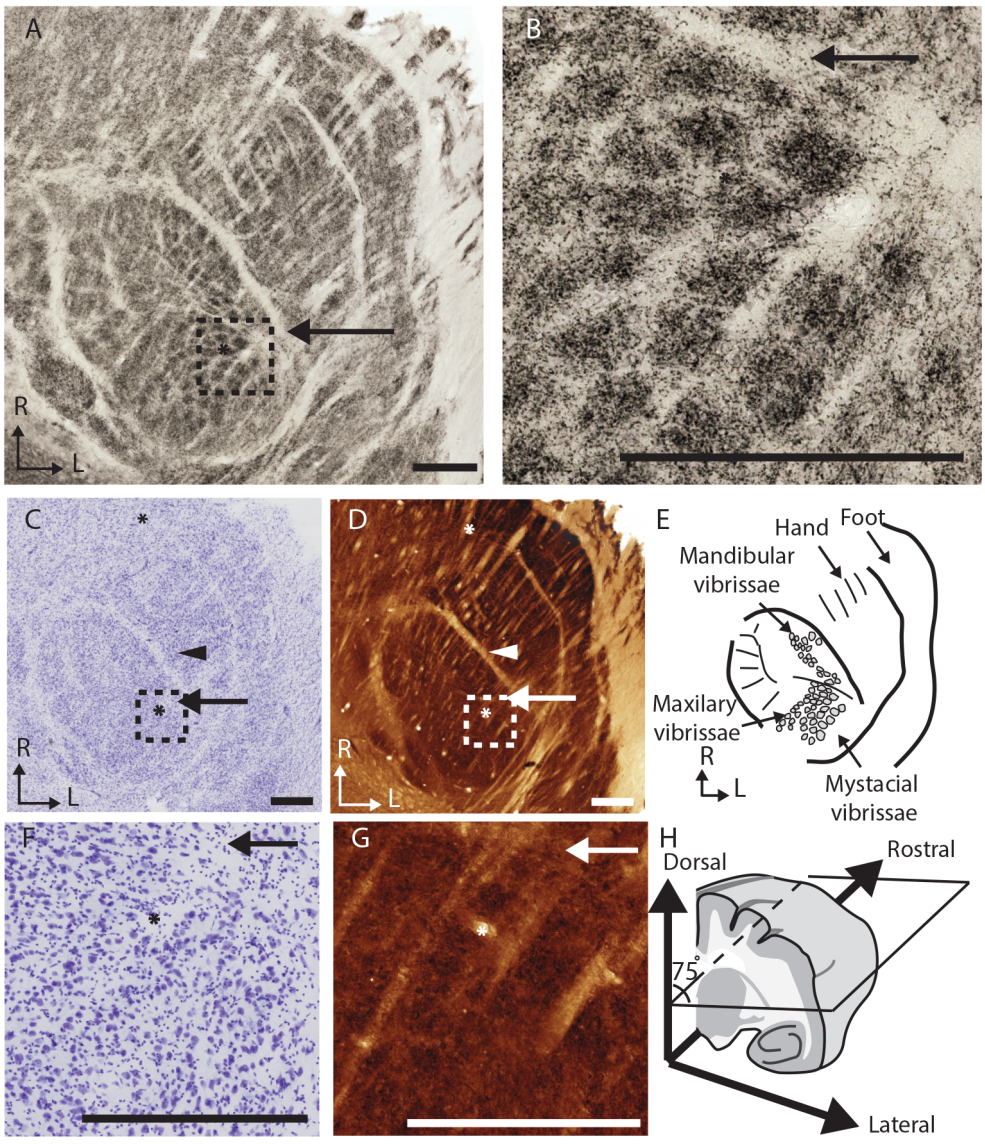
A
R
L
B
C
R
L
D
R
L
E
Hand
Foot
Mandibular vibrissae
Maxilary vibrissae
R
L
Mystacial vibrissae
F
G
H
Dorsal
Rostral
75°
Lateral

Fig. 3. A Photomicrographs of a section of the ventroposterior nucleus in a galago stained for vesicular glutamate transporter 2 (VGLUT2) showing distinct septa between representations of different body regions, including the barreloid-like structures on the face representation and the septa for the digits of the hand. The dotted line in A displays the perimeter of B. **B:** Enlarged selections of A showing barreloid-like clumping of VGLUT2 positive terminals. C:, **D:** Adjacent sections stained for Nissl C and cytochrome oxidase (D). **E**: Diagram of the septa seen in A, C and D showing the "galagounculus". **F and G**: Enlarged selections of C, D showing patchy neuron distribution, and subtle areas of CO dense staining. **H**: Schematic of the angle of cut for the sections in A-B, C-D, and F-G. **I-K**: Coronal sections through the VPM of stained for Nissl substance (I), cytochrome oxidase (J) and VGLUT2 (K). The dotted line in K marks the angle of cut used to achieve sections with circular barreloid-like representations. Arrows point to the hand/face border. Asterisks mark the same selected blood vessels in all sections. Arrowheads point to the Arrowheads point to the septa between the barreloid-like modules. Scale bar= 500 μm.

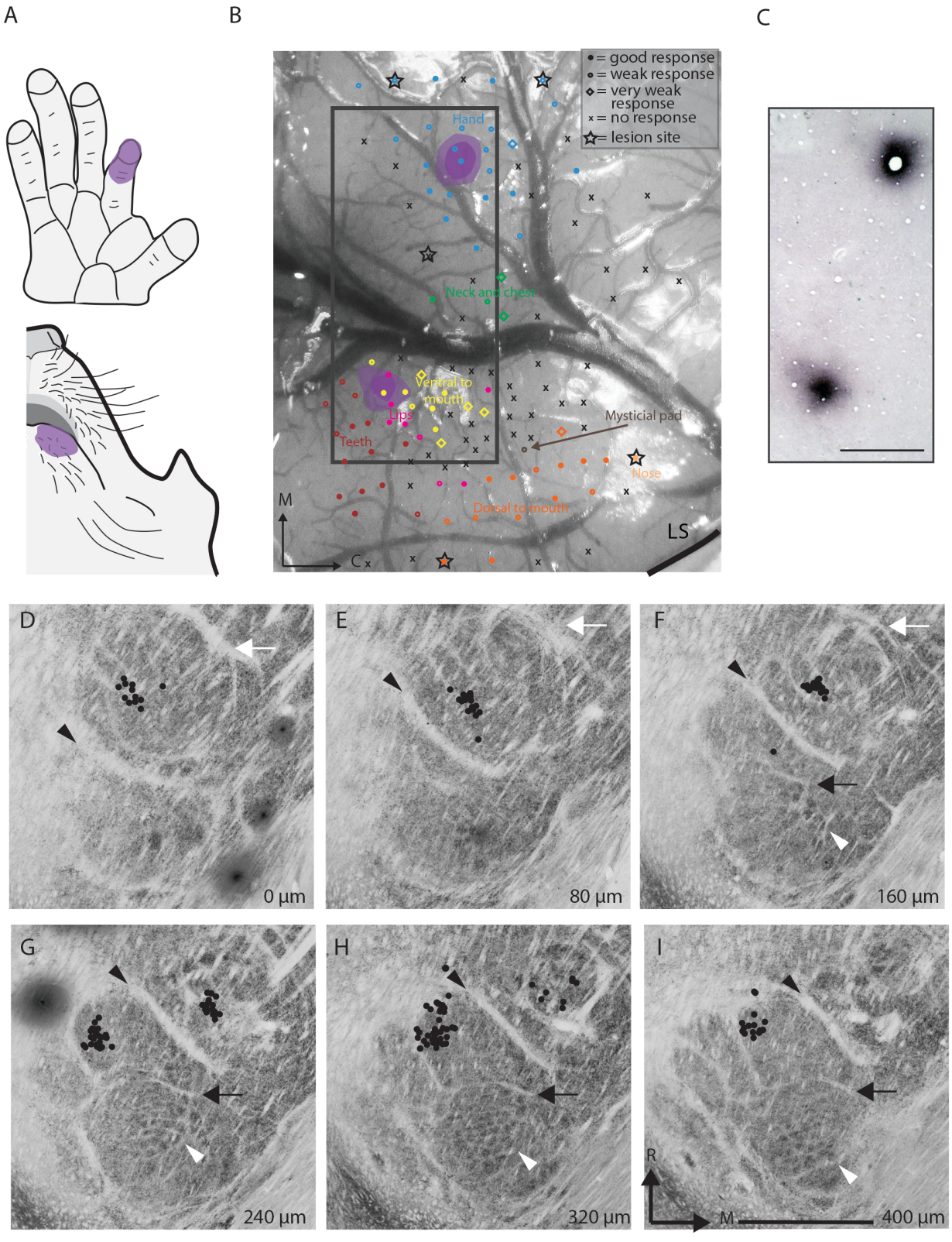
A
B
C
= good response
= weak response
= very weak response
= no response
= lesion site
Hand
Neck and chest
Ventral to mouth
Lips
Teeth
Mysticial pad
Nose
Dorsal to mouth
M
C
LS
D
0 µm
E
80 µm
F
160 µm
G
240 µm
H
320 µm
I
R
M
400 µm

Fig. 4. A Electrophysiologically defined receptive fields of cortical injection sites. **B:** Photomicrograph of the explored region in somatosensory area 3b of galago case 14–09, which shows the locations of microelectrode penetrations (dots, diamonds and x's) and the electrolytic lesions (stars). Filled circles mark good responses; open circles mark weak responses; diamonds mark very weak responses; x's mark microelectrode penetrations with no responses. The focus and halo of the cholera toxin subunit B (CTB) injections are marked in purple. The grey square corresponds to the tissue section in C. **C**: A section of flattened cortex processed for CTB showing the injection sites. **D-I**: Sections from the ipsilateral thalamus, processed for VGLUT2. The location of CTB stained cell bodies in the adjacent sections are marked with black dots. The most dorsal section in which labeled cells were present is labeled as 0 um (D) and the most ventral section with labeled cells is 400 um (I) . All thalamic sections have orientation and scale shown in I. Black arrowheads= hand/face border; black arrow= oral fissure border; white arrowhead= barreloid-like VGLUT2 clusters; white arrows= hand/foot border. Scale bar= 1 mm

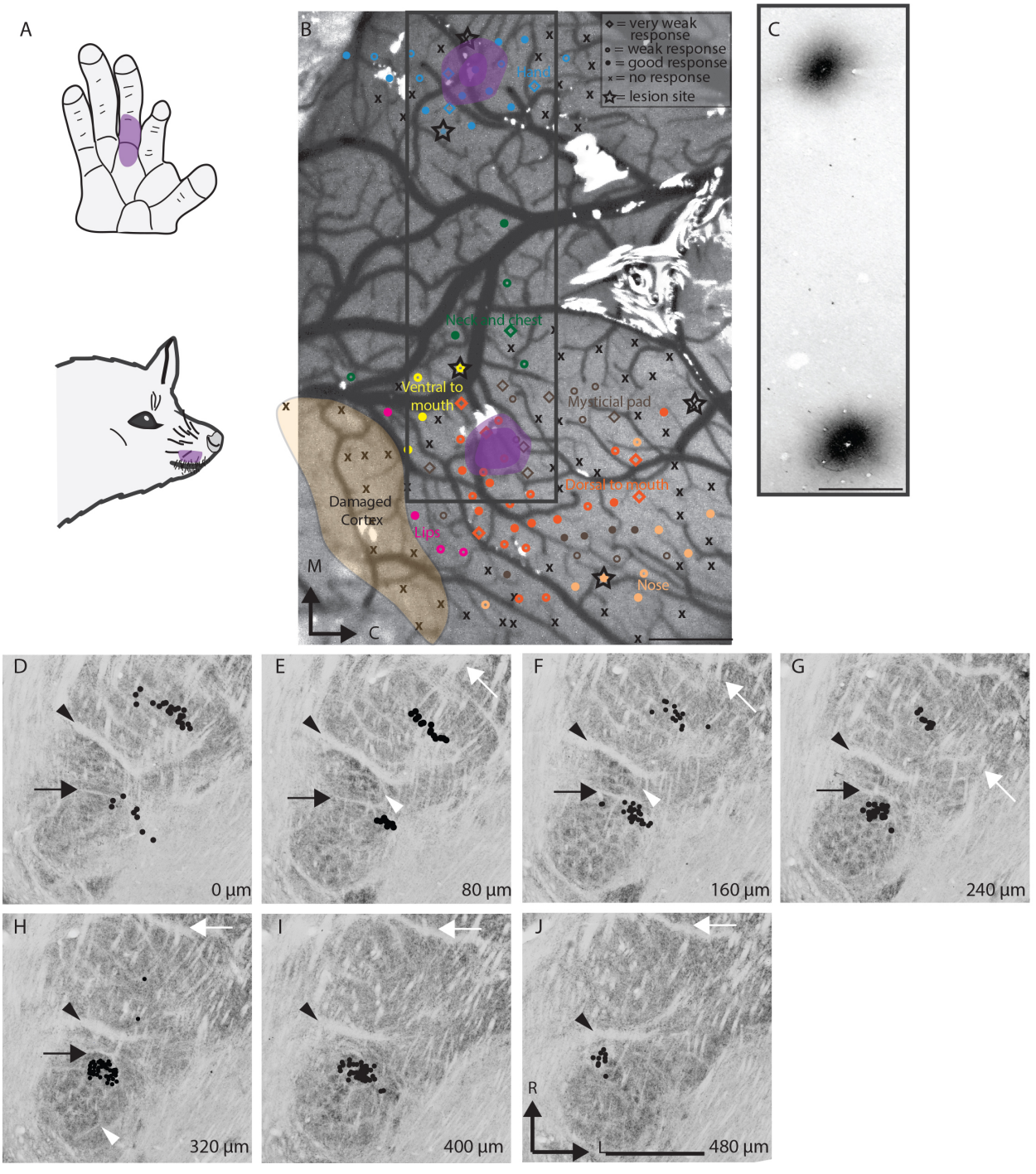
A
B
C
◇= very weak response
○ = weak response
● = good response
× = no response
☆= lesion site
Hand
Neck and chest
Ventral to mouth
Mystacial pad
Dorsal to mouth
Damaged Cortex
Lips
Nose
M
C
D
0 µm
E
80 µm
F
160 µm
G
240 µm
H
320 µm
I
400 µm
J
R
L
480 µm

Fig. 5 A Electrophysiologically defined receptive fields of cortical injection sites. **B:** Photomicrograph of the explored region in somatosensory area 3b of galago case 14–13, which shows the locations of microelectrode penetrations (dots, diamonds and x's) and the electrolytic lesions (stars). Filled circles mark good responses; open circles mark weak responses; diamonds mark very weak responses; x's mark microelectrode penetrations with no responses. The focus and halo of the cholera toxin subunit B (CTB) injections are marked in purple. The grey square corresponds to the tissue section in C. **C**: A section of flattened cortex processed for CTB showing the injection sites. **D-J**: Sections from the ipsilateral thalamus, processed for VGLUT2. The location of CTB stained cell bodies in the adjacent sections are marked with black dots. The most dorsal section in which labeled cells were present is labeled as 0 um (D) and the most ventral section with labeled cells is 480 um (J) . All thalamic sections have orientation and scale shown in I. Black arrowheads= hand/face border; black arrow= oral fissure border; white arrowhead= barreloid-like VGLUT2 clusters; white arrows= hand/foot border. Scale bar= 1 mm

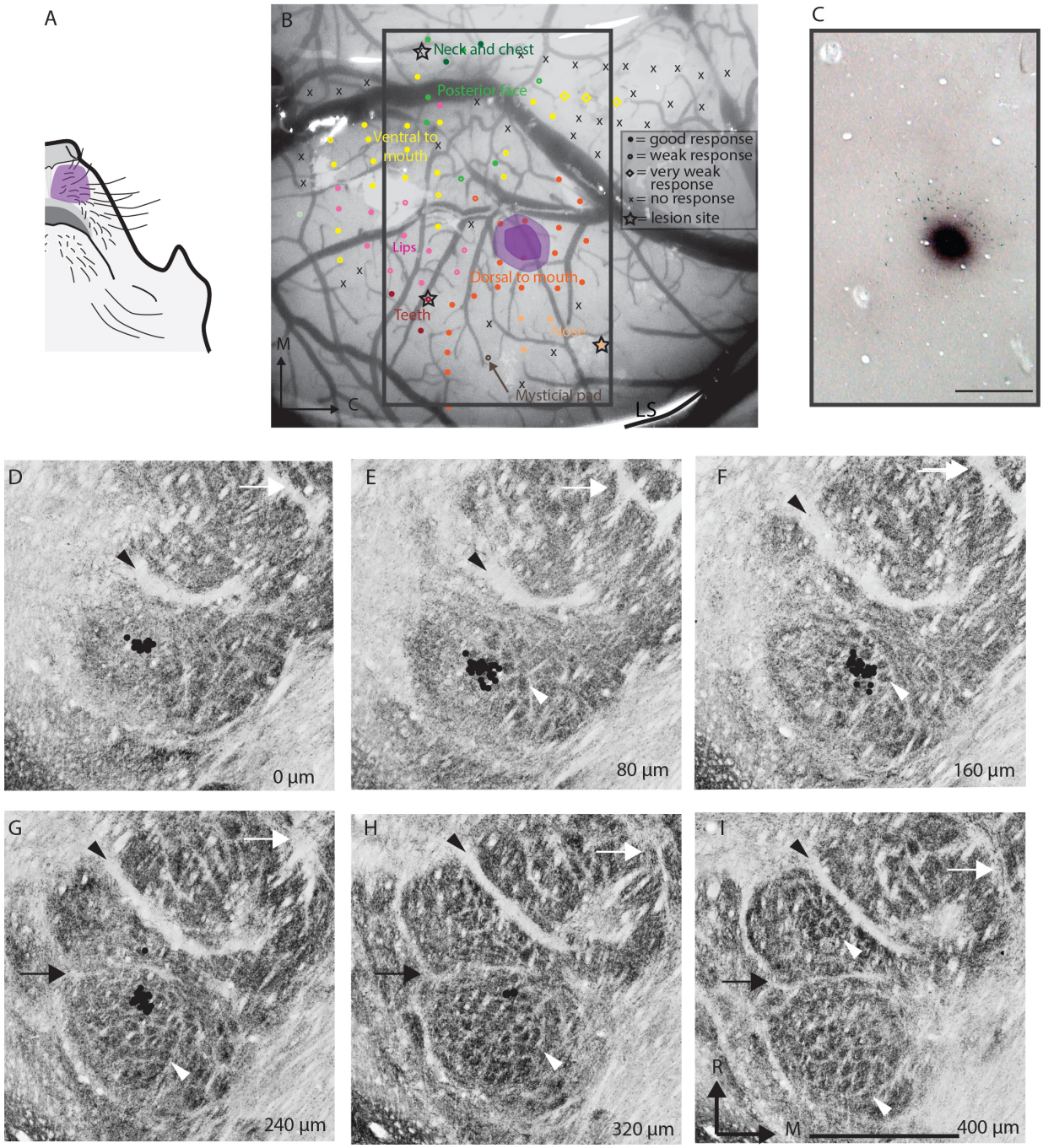
A
B
Neck and chest
Posterior face
Ventral to mouth
Lips
Dorsal to mouth
Teeth
Nose
Mystacial pad
= good response
= weak response
= very weak response
= no response
= lesion site
M
C
LS
C
D
0 µm
E
80 µm
F
160 µm
G
240 µm
H
320 µm
I
R
M
400 µm

Fig. 6 A Electrophysiologically defined receptive fields of cortical injection site. **B:** Photomicrograph of the explored region in somatosensory area 3b of galago case 14–16, which shows the locations of microelectrode penetrations (dots, diamonds and x's) and the electrolytic lesions (stars). Filled circles mark good responses; open circles mark weak responses; diamonds mark very weak responses; x's mark microelectrode penetrations with no responses. The focus and halo of the cholera toxin subunit B (CTB) injections are marked in purple. The grey square corresponds to the tissue section in **C**: C. A section of flattened cortex processed for CTB showing the injection site. **D-I**: Sections from the ipsilateral thalamus, processed for VGLUT2. The location of CTB stained cell bodies in the adjacent sections are marked with black dots. The most dorsal section in which labeled cells were present is labeled as 0 um (D) and the most ventral section with labeled cells is 400 um (I) . All thalamic sections have orientation and scale shown in I. Black arrowheads= hand/face border; black arrow= oral fissure border; white arrowhead= barreloid-like VGLUT2 clusters; white arrows= hand/foot border. Scale bar= 1 mm

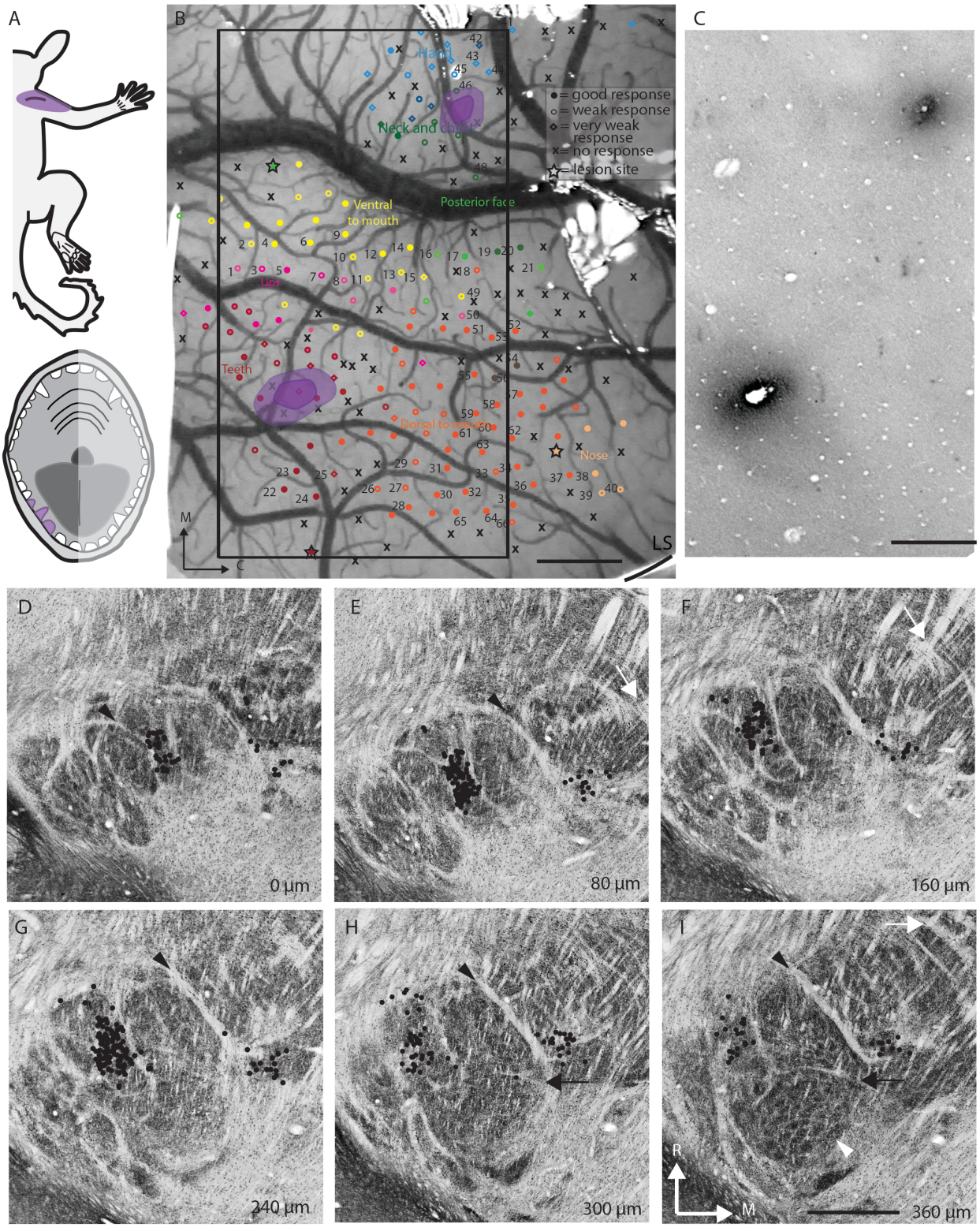
A
B
C
Hand
Neck and chest
Ventral to mouth
Posterior face
Lips
Teeth
Dorsal to lips
Nose
● = good response
○ = weak response
◇ = very weak response
x = no response
☆ = lesion site
M
C
LS
D
0 µm
E
80 µm
F
160 µm
G
240 µm
H
300 µm
I
R
M
360 µm

Fig. 7 A Electrophysiologically defined receptive fields of cortical injection sites. **B:** Photomicrograph of the explored region in somatosensory area 3b of galago case 14–31 (left), which shows the locations of microelectrode penetrations (dots, diamonds and x's) and the electrolytic lesions (stars). Filled circles mark good responses; open circles mark weak responses; diamonds mark very weak responses; x's mark microelectrode penetrations with no responses. The focus and halo of the cholera toxin subunit B (CTB) injections are marked in purple. The grey square corresponds to the tissue section in C. **C**: A section of flattened cortex processed for CTB showing the injection sites. **D-I**: Sections from the ipsilateral thalamus, processed for VGLUT2. The location of CTB stained cell bodies in the adjacent sections are marked with black dots. The most dorsal section in which labeled cells were present is labeled as 0 um (D) and the most ventral section with labeled cells is 460 um (I) . All thalamic sections have orientation and scale shown in I. Black arrowheads= hand/face border; black arrow= oral fissure border; white arrowhead= barreloid-like VGLUT2 clusters; white arrows= hand/foot border. Scale bar= 1 mm

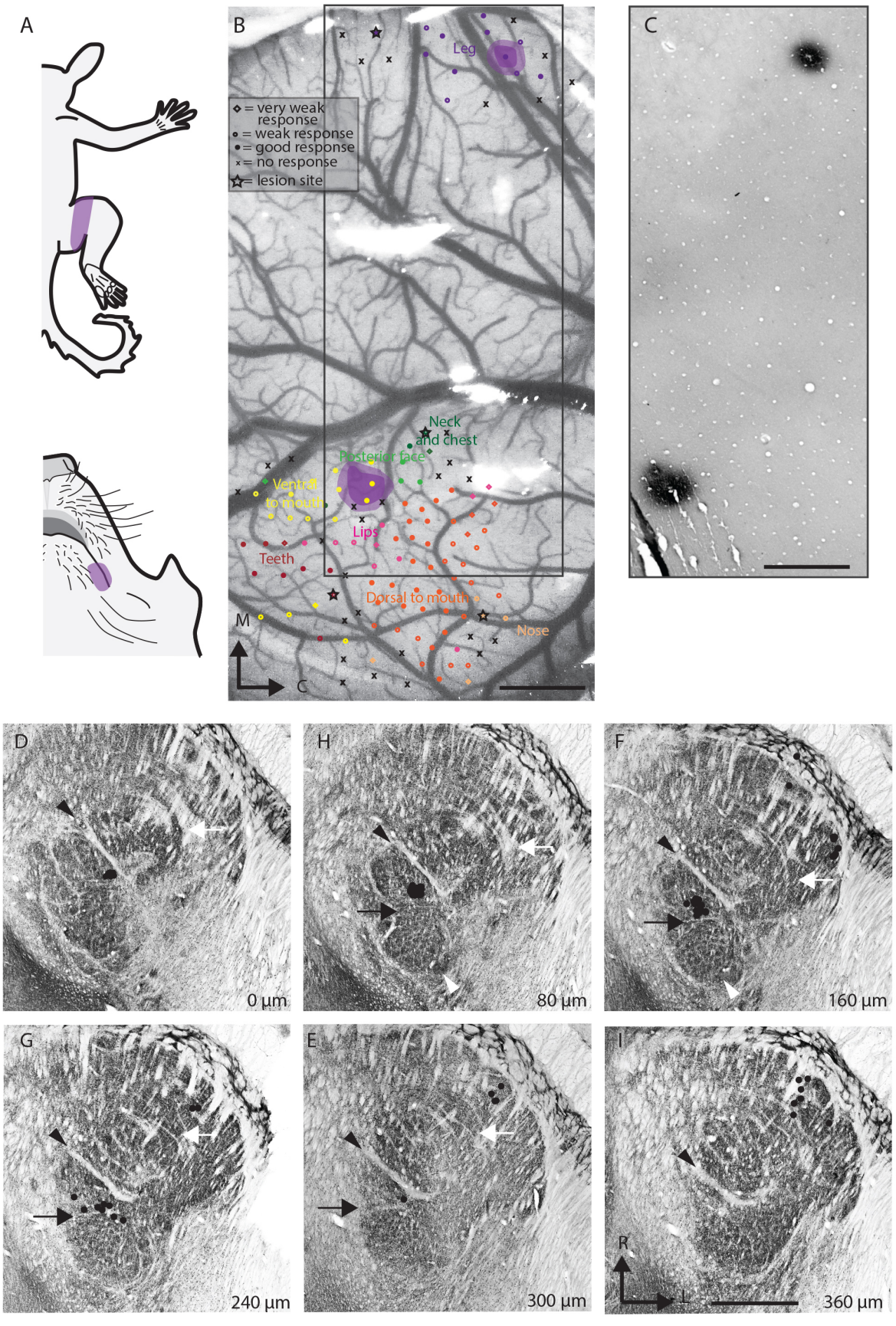
A
B
C
Leg
◇ = very weak response
◦ = weak response
● = good response
× = no response
☆ = lesion site
Neck and chest
Posterior face
Ventral to mouth
Lips
Teeth
Dorsal to mouth
Nose
M
C
D
0 µm
H
80 µm
F
160 µm
G
240 µm
E
300 µm
I
R
L
360 µm

Fig. 8 A Electrophysiologically defined receptive fields of cortical injection sites. **B:** Photomicrograph of the explored region in somatosensory area 3b of galago case 14–31 (right), which shows the locations of microelectrode penetrations (dots, diamonds and x's) and the electrolytic lesions (stars). Filled circles mark good responses; open circles mark weak responses; diamonds mark very weak responses; x's mark microelectrode penetrations with no responses. The focus and halo of the cholera toxin subunit B (CTB) injections are marked in purple. The grey square corresponds to the tissue section in **C**: C. A section of flattened cortex processed for CTB showing the injection siteS. **D-I**: Sections from the ipsilateral thalamus, processed for VGLUT2. The location of CTB stained cell bodies in the adjacent sections are marked with black dots. The most dorsal section in which labeled cells were present is labeled as 0 um (D) and the most ventral section with labeled cells is 360 um (I) . All thalamic sections have orientation and scale shown in I. Black arrowheads= hand/face border; black arrow= oral fissure border; white arrowhead= barreloid-like VGLUT2 clusters; white arrows= hand/foot border. Scale bar= 1 mm

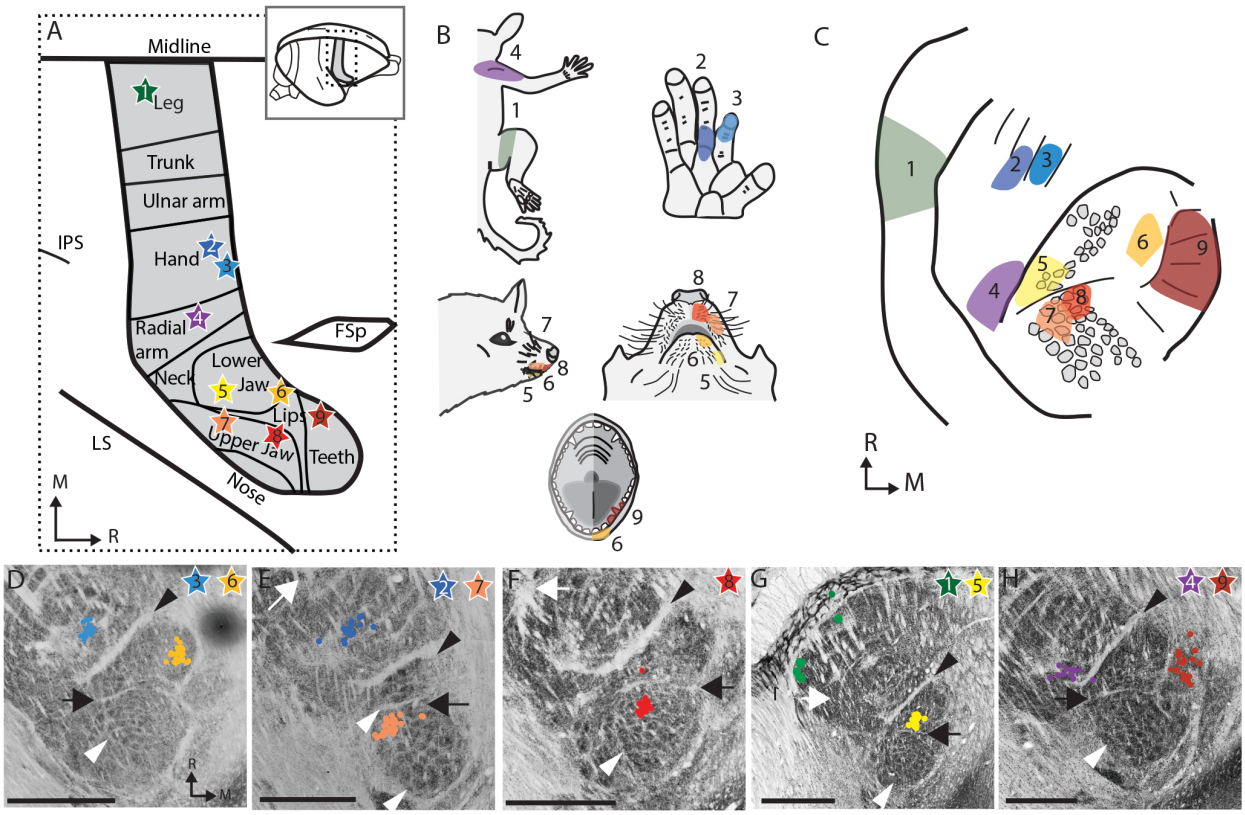

Fig 9. Somatotopy of the connections from the ventroposterior nucleus of the thalamus to cortical area 3b. **A:** Summary schematic of the nine cortical injection sites (stars)for the tracer cholera toxin subunit B (CTB) in the 5 hemispheres investigated (4 animals). The placement of the injection sites were defined experimentally with 100 to 300 points in each cortex as well as reference to Wu and Kaas, 2003. The stars are numbered and colored to match the rest of the figure. FSp = posterior frontal suclus, IPS = Intraparietal sulcus, LS = lateral sulcus. **B:** The multiunit receptive field recorded at the tracer injection sites. **C**: A summary schematic of the locations of CTB stained cell bodies. **D-H**: The location of CTB stained cell bodies (colored dots) mapped onto the adjacent section stained for vesicular glutamate transporter 2 (VGLUT2). Panels D through H are all from different hemispheres. Black arrowheads = hand/face border; black arrow = oral fissure border; white arrowhead = barreloid-like VGLUT2 clusters; white arrows = hand/foot border. Scale bar = 1 mm

cortex in cytochrome oxidase, Nissl, VGLUT2, parvalbumin, and myelin stains of adult and juvenile tissue (both coronal sections and sections cut tangenital to the surface of area 3b).

DISSCUSSION

Using histology and labeled connections we found barrelette- and barreloid-like modules in the brainstem and thalamus of prosimian galagos. As anatomically distinct segments of the central nervous system that represent tactile hairs, they are similar in appearance to the barrel structures seen in rodents. However, there are differences between the modules found in this study and those seen in other animal groups. Regardless, the overarching theme of modular representation of discrete sensory organs is consistent. This is the first time such clear whisker-related modules have been reported in primates, making this an important link between work on the rodent barrel system and primate sensory processing.

VIBRISSAE

Our findings on the morphology of the mystacial vibrissae are in agreement with Muchlinski et al.'s recent comparative study (Muchlinski et al., 2013), where galagos were found to have discrete rows of mystacial vibrissal with well-developed intrinsic musculature. Our study differed from theirs in that we examined the vibrissae distribution on both sides of the face in three galagos, as opposed to one animal, and also examined the maxillary and mandibular vibrissae. It is unclear if our unique finding of supernumerary whiskers is biologically significant. If variation in vibrissal arrays applies broadly to this species, then it could be indicative of relaxed selection on a non-vital sensory array. However, animals investigated here all originated in the same research-breeding colony, so the trait could be a specific of this population. Vibrissae number is known to vary in between different strains of mice (Van der Loos et al., 1984).

Another extensive comparative study counted whiskers on the upper jaw of 527 species, including *Otolemur garnetti* (Muchlinski, 2010). They found that galagos had 22 macrovibrissa and 12 mandibular vibrissae. Even allowing for different definitions of a macro and a microvibrissa, this is less than we counted. The difference is likely due to a difference in methodology; while Muchlinski (2010) counted hairs and rete ridge collars visible by external examination of the snout with a dissection microscope, we used a pigment-clearing method to visualize and

count blood sinuses innervating individual vibrissae. It is possible that there are more hair follicles with blood sinuses than externally visible rete ridge collars.

SOMATOSENSORY BRAINSTEM

Barrelettes were first defined as a cell-free hollow surrounded by a cell-dense perimeter separated from other barrelettes by a cell-sparse septa, all features that were visible in Nissl stained sections of mouse brainstem (Ma, 1991). These barrelettes also stain darkly for CO, succinic dehydrogenase and VGLUT1 (Belford and Killackey, 1979a; Sakurai et al., 2013) in rats and mice. Such clear nuclear organization was not observed in galagos, but densely stained CO and VGLUT1 fields were identified. As in rats, the barrelette pattern was more easily delineated in SpVi than in the PrV (Belford and Killackey, 1979a). It is possible that the PrV barrelette pattern could be better visualized in sections cut at slightly different angle, which facilitated the visualization of the PrV somatotopic map in other species (Catania et al., 2011a).

In many species, the individual barrels are larger in the SpVi than in the PrV (Belford and Killackey, 1979a; Catania et al., 2013). In mice, barrelettes in the SpVi have a cross sectional diameter of about 140 to 170 μm and 75 to 105 μm in the PrV (Ma, 1991). The comparatively large SpVi follicle representations are intriguing, given that the smaller representations in the PrV are the main conduit for driving impulses to the large cortical representation. However, it has been hypothesized that the SpVi is important for monitoring sensations from self-generated movement - something that would be important for whisking species (Diamond et al., 2008). In galagos, the cross-sectional diameter of the modules was much more similar in the SpVi and PrV. It is possible that similar sized modules in the SpVi compared to the PrV is related to the minor role of vibrissal movement in galago tactile behavior.

The densely stained CO region in SpVi of galagos has distinct dorsal and ventral regions separated by a lightly stained septum. This lima-bean shape differs from the SpVi in mice and rats but looks remarkably similar to the SpVi in wallabies (Waite et al., 1994). Based on the location of the tracer-stained terminals in the tracer study, we hypothesize that the dorsal region corresponds to the mandibular region and the ventral portion to the maxillary region. The lima-bean shape probably comes from devoting a similar sized volume of tissue to the representation of both the upper and the lower jaws, instead of the nucleus being dominated by the representation of the upper jaw. The inverted representation is consistent with that found in other animals, including rodents (Arvidsson, 1982;

Erzurumlu et al., 2010), cats (Hayashi et al., 1984), moles (Sawyer et al., 2014), and pigeons (Silver and Witkovsky, 1973).

Previously, macaques and squirrel monkeys have been shown to have a parcellated organization in the PrV and an unparcellated SpVi in CO stained sections(Noriega and Wall, 1991). Our results differ from those in that in galagos the most distinct organization was seen within the SpVi and both nuclei had more distinct modules overall.

THALAMUS

The VP nucleus of the thalamus in primates has architectural features that reflect its somatotopic organization (Jones, 2007; Kaas, 2008; Welker, 1973). For example, a distinct cell-poor septum, the arcuate lamella, marks the border between the hand and face representations. Other septa delineate the representations of the digits, and a more lateral septum separates the hand representation from the foot (Qi et al., 2011). In the VPM of macaques, there are rod-like segmentations that correspond to facial and oral regions such as the hard palate and regions of the posterior oral cavity (Rausell and Jones, 1991). Our study adds to those findings by locating barreloid-like modules for facial vibrissae in the VPM of prosimian galagos.

Van der Loos defined mouse barreloids as rod shaped domains roughly 70 μm in diameter (Van der Loos, 1976), similar to the size of the structures in galagos. In mice the barreloids have a cell-poor core surrounded by a cell dense perimeter 3 to 4 cells thick (Van der Loos, 1976). Later investigations have been able to visualize the barreloids as areas of dense staining for a variety of other reaction products, such as succinic dehydrogenase, CO, and VGLUT2 (Belford and Killackey, 1979a; Louderback et al., 2006). Our procedures did not reveal clear cell-hollow cylinders and only faintly labeled CO clusters; however, we found clear VGLUT2 dense clusters. It is interesting that these modules were delineated so strongly by the localization of VGLUT2 protein but not by more traditional stains. In rats VGLUT2 is expressed in the synaptic terminations from the PrV (Ge et al., 2010; Graziano et al., 2008), and an intact PrV is necessary for barreloid formation (Ding et al., 2003; Killackey and Fleming, 1985). The patterning of the VGLUT2 clusters in the VPM of galagos suggests that PrV also sends VGLUT2-expressing projections to the VPM in primates.

In addition to the barreloid-like segmentation, we located another region within the VPM with larger segments. Based on the location of these segments between the hypothesized lower and upper jaw representations, and considering the location of the label resulting from an injection into the cortical representation of a tooth (Fig.

4), we believe these segments are relevant to the representation of the teeth and mouth. It is possible that these segments are similar to the VPM rods found in macaques (Jones et al., 1986).

The serendipitous finding of a plane of section resulting in a visible representation of the thalamic galago somatosensory map is, we believe, one of the clearest somatotopic maps of an entire skin surface of a mammal yet found. While the presence of a neural representation of the body surface in the somatosensory thalamus is of no great surprise, such a clear visualization reveals the somatosensory order of the representation with an unparalleled precision.

CORTEX

The topographic representation of the galago body surface in S1 (area 3b) has been established previously (Wu and Kaas, 2003), but the details of the face representation had not been thoroughly investigated. In doing so, we found that the cortical area devoted to the mystacial vibrissae was small compared to the area devoted to the maxillary and mandibular vibrissae. The relative size of the representations of body areas in primary somatosensory cortex (S1) is loosely related to how important that body area is to the animal's sensory biology. For example, the large representations of lips and hands in humans illustrate how important these regions are to us (Penfield, 1937). More specifically, the size of each representation is often related to the sensitivity and acuity of touch for that body area (Catania and Remple, 2004; Sur et al., 1980). The small size of the mystacial vibrissae representation suggests that these vibrissae are not highly important sensory organs to galagos. Based on the cortical representations, galagos are more invested in the tactile information from the small vibrissae on its chin and lips than the mystacial vibrissae.

Experiments in rats and mice suggest that microvibrissae of the chin and lips are important in object recognition, while the longer macrovibrissae are more important for gauging distances of near objects (Brecht et al., 1997). Visual observations of galagos during regular feedings revealed no distinct whisking behavior related to the mystacial vibrissae. Actively foraging galagos were most often observed to reach for food items with their hands and then bring the grasped item to their faces, they infrequently grabbed for food directly with their mouth. It is possible that having grasping hands and improved visual acuity reduces the importance of macrovibrissae.

Our failure to find barrels in the cortex does not guarantee they are not present because the use of other histological markers or sections from an earlier timepoint in galago development could also reveal them. However,

our group has performed research on galagos for decades and we have access to a collection of brain sections from these studies. Despite surveying cortex sections from more than 20 cases from previous studies that were processed for various stains (cytochrome oxidase, Nissl, VGLUT2, parvalbumin and myelin stains), cut at various angles (flattened preparations, coronal and horizontal sections) and in animals of ages 1 day to mature adults, we found no evidence of barrel-like structures. These additional negative results support the conclusion that barrel-like structures are not present in area 3b of galagos.

The presence of subcortical whisker modules in species ranging from marsupial wallabies to primates suggests that mammals share many features of subcortical somatosensory processing. The absence of cortical whisker modules in many species suggests that the cortex may be the most likely site for species-specific changes.

CONCLUSION

Sensory vibrissae are a part of the tactile sensory system that is present in some form in nearly all species of mammals (excluding monotremes, anteaters, and humans) (Muchlinski, 2010; Pocock, 1914). The phylogenetic distribution of barrel-like modules in the central nervous system is more disparate but is still well distributed among mammals. Here we demonstrate these modules in the trigeminal somatosensory nuclei of the thalamus and brainstem in a primate. The wide distribution of discrete units in the trigeminal lemniscal pathway suggest that the units form due to a basal and shared trait related to the sensory possessing of the whisker array. The answer to "what is a barrel for?" needs to account for their presence in such a wide range of animals. Progress on this question might be made by investigating difference in sensory processing in an animal with prominent whiskers but without whisker-related modules. Though only mammals possess whiskers, some non-mammals have sensory arrays that, like whiskers, have punctate distributions (eg. the integumentary sensory organs on crocodilians (Leitch and Catania, 2012) and barbels on fish and turtles (Fox, 1999). It would be interesting to see if these too are represented by modular units in the brainstem, as such a result would suggest broad commonalities in how the brain organizes sensory input across an even wider range of life.

ACKNOWLEDGMENTS

We thank Laura Trice for help with histological procedures, Mary Feurtado, Daniel Miller, Jamie Reed, Emily Rockoff and Iwona Stepniewaska for surgical assistance. This work was funded by NIH grant NS016446 to JHK and NIH grant NS084706-02 to EKS.

REFERENCES

Arvidsson, J. (1982). Somatotopic organization of vibrissae afferents in the trigeminal sensory nuclei of the rat studied by transganglionic transport of HRP. *J Comp Neurol* **211**, 84-92.

Balaram, P., Hackett, T. A. and Kaas, J. H. (2013). Differential expression of vesicular glutamate transporters 1 and 2 may identify distinct modes of glutamatergic transmission in the macaque visual system. *J Chem Neuroanat* **50-51**, 21-38.

Baldwin, M. K., Balaram, P. and Kaas, J. H. (2013). Projections of the superior colliculus to the pulvinar in prosimian galagos (Otolemur garnettii) and VGLUT2 staining of the visual pulvinar. *J Comp Neurol* **521**, 1664-82.

Belford, G. R. and Killackey, H. P. (1979). The development of vibrissae representation in subcortical trigeminal centers of the neonatal rat. *J Comp Neurol* **188**, 63-74.

Bosman, L. W., Houweling, A. R., Owens, C. B., Tanke, N., Shevchouk, O. T., Rahmati, N., Teunissen, W. H., Ju, C., Gong, W., Koekkoek, S. K. et al. (2011). Anatomical pathways involved in generating and sensing rhythmic whisker movements. *Front Integr Neurosci* **5**, 53.

Brecht, M., Preilowski, B. and Merzenich, M. M. (1997). Functional architecture of the mystacial vibrissae. *Behav Brain Res* **84**, 81-97.

Catania, K. C., Catania, E. H., Sawyer, E. K. and Leitch, D. B. (2013). Barrelettes without barrels in the American water shrew. *PLoS One* **8**, e65975.

Catania, K. C., Leitch, D. B. and Gauthier, D. (2011). A star in the brainstem reveals the first step of cortical magnification. *PLoS One* **6**, e22406.

Catania, K. C. and Remple, F. E. (2004). Tactile foveation in the star-nosed mole. *Brain Behav Evol* **63**, 1-12.

Diamond, M. E., von Heimendahl, M., Knutsen, P. M., Kleinfeld, D. and Ahissar, E. (2008). 'Where' and 'what' in the whisker sensorimotor system. *Nat Rev Neurosci* **9**, 601-12.

Ding, Y. Q., Yin, J., Xu, H. M., Jacquin, M. F. and Chen, Z. F. (2003). Formation of whisker-related principal sensory nucleus-based lemniscal pathway requires a paired homeodomain transcription factor, Drg11. *J Neurosci* **23**, 7246-54.

Ebner, F. T. and Kaas, J. H. (2015). Somatosensory System. In *The Rat Nervous System* pp. 675-701 San Diego: Academic Press.

Erzurumlu, R. S., Murakami, Y. and Rijli, F. M. (2010). Mapping the face in the somatosensory brainstem. *Nat Rev Neurosci* **11**, 252-63.

Fox, H. (1999). Barbels and barbel-like tentacular structures in sub-mammalian vertebrates: a review. *Hydrobiologia* **403**, 153-193.

Fox, K. (2008). Barrel Cortex. New York: Cambridge University Press.

Ge, S. N., Ma, Y. F., Hioki, H., Wei, Y. Y., Kaneko, T., Mizuno, N., Gao, G. D. and Li, J. L. (2010). Coexpression of VGLUT1 and VGLUT2 in trigeminothalamic projection neurons in the principal sensory trigeminal nucleus of the rat. *J Comp Neurol* **518**, 3149-68.

Gould, S. J. and Lewontin, R. C. (1979). The spandrels of San Marco and the Panglossian paradigm: a critique of the adaptationist programme. *Proc R Soc Lond B Biol Sci* **205**, 581-98.

Graziano, A., Liu, X. B., Murray, K. D. and Jones, E. G. (2008). Vesicular glutamate transporters define two sets of glutamatergic afferents to the somatosensory thalamus and two thalamocortical projections in the mouse. *J Comp Neurol* **507**, 1258-76.

Haidarliu, S. and Ahissar, E. (1997). Spatial organization of facial vibrissae and cortical barrels in the guinea pig and golden hamster. *J Comp Neurol* **385**, 515-27.

Hayashi, H., Sumino, R. and Sessle, B. J. (1984). Functional organization of trigeminal subnucleus interpolaris: nociceptive and innocuous afferent inputs, projections to thalamus, cerebellum, and spinal cord, and descending modulation from periaqueductal gray. *J Neurophysiol* **51**, 890-905.

Horton, J. C. and Adams, D. L. (2005). The cortical column: a structure without a function. *Philos Trans R Soc Lond B Biol Sci* **360**, 837-62.

Jones, E. G. (2007). The thalamus. New York: Cambridge University Press.

Jones, E. G., Hendry, S. H. and Brandon, C. (1986). Cytochrome oxidase staining reveals functional organization of monkey somatosensory thalamus. *Exp Brain Res* **62**, 438-42.

Kaas, J. H. (2008). The somatosensory thalamus and associated pathways. In *The senses: a comprehensive reference*, (ed. A. I. K. Basebaum, A.; Shepherd, G.M.; Westheimer, G.; Gardner, E.; Kaas, J.H.), pp. 117–141. San Diego: Academic Press.

Kaas, J. H. and Catania, K. C. (2002). How do features of sensory representations develop? *Bioessays* **24**, 334–343.

Killackey, H. P. and Fleming, K. (1985). The role of the principal sensory nucleus in central trigeminal pattern formation. *Brain Res* **354**, 141-5.

Leamey, C. A., Marotte, L. R. and Waite, P. M. (1996). Timecourse of development of the wallaby trigeminal pathway. II. Brainstem to thalamus and the emergence of cellular aggregations. *J Comp Neurol* **364**, 494-514.

Leitch, D. B. and Catania, K. C. (2012). Structure, innervation and response properties of integumentary sensory organs in crocodilians. *J Exp Biol* **215**, 4217-30.

Louderback, K. M., Glass, C. S., Shamalla-Hannah, L., Erickson, S. L. and Land, P. W. (2006). Subbarrel patterns of thalamocortical innervation in rat somatosensory cortical barrels: Organization and postnatal development. *J Comp Neurol* **497**, 32-41.

Ma, P. M. (1991). The barrelettes--architectonic vibrissal representations in the brainstem trigeminal complex of the mouse. I. Normal structural organization. *J Comp Neurol* **309**, 161-99.

Martin, R. D. (1990). Primate origins and evolution. . LondonChapman and Hall.: Chapman and Hall.

Muchlinski, M. N. (2010). A comparative analysis of vibrissa count and infraorbital foramen area in primates and other mammals. *J Hum Evol* **58**, 447-73.

Muchlinski, M. N., Durham, E. L., Smith, T. D. and Burrows, A. M. (2013). Comparative histomorphology of intrinsic vibrissa musculature among primates: implications for the evolution of sensory ecology and "face touch". *Am J Phys Anthropol* **150**, 301-12.

Noriega, A. L. and Wall, J. T. (1991). Parcellated organization in the trigeminal and dorsal column nuclei of primates. *Brain Res* **565**, 188-94.

Penfield, W. B., E. (1937). Somatic motor and sensorv representation in the cerebral cortex of man as studied by electrical stimulation. *Brain* **60**, 389-443.

Pocock, R. I. (1914). On the Facial Vibrissæ of Mammalia. *Proceedings of the Zoological Society of London* **84**, 889–912.

Purves, D., Riddle, D. R. and LaMantia, A. S. (1992). Iterated patterns of brain circuitry (or how the cortex gets its spots). *Trends Neurosci* **15**, 362-8.

Qi, H. X., Gharbawie, O. A., Wong, P. and Kaas, J. H. (2011). Cell-poor septa separate representations of digits in the ventroposterior nucleus of the thalamus in monkeys and prosimian galagos. *J Comp Neurol* **519**, 738-58.

Rausell, E. and Jones, E. G. (1991). Histochemical and immunocytochemical compartments of the thalamic VPM nucleus in monkeys and their relationship to the representational map. *J Neurosci* **11**, 210-25.

Sakurai, K., Akiyama, M., Cai, B., Scott, A., Han, B. X., Takatoh, J., Sigrist, M., Arber, S. and Wang, F. (2013). The organization of submodality-specific touch afferent inputs in the vibrissa column. *Cell Rep* **5**, 87-98.

Sawyer, E. K., Leitch, D. B. and Catania, K. C. (2014). Organization of the spinal trigeminal nucleus in star-nosed moles. *J Comp Neurol* **522**, 3335-50.

Silver, R. and Witkovsky, P. (1973). Functional characteristics of single units in the spinal trigeminal nucleus of the pigeon. *Brain Behav Evol* **8**, 287-303.

Sur, M., Merzenich, M. M. and Kaas, J. H. (1980). Magnification, receptive-field area, and "hypercolumn" size in areas 3b and 1 of somatosensory cortex in owl monkeys. *J Neurophysiol* **44**, 295-311.

Van der Loos, H. (1976). Barreloids in mouse somatosensory thalamus. *Neurosci Lett* **2**, 1-6.

Van der Loos, H., Dorfl, J. and Welker, E. (1984). Variation in pattern of mystacial vibrissae in mice. A quantitative study of ICR stock and several inbred strains. *J Hered* **75**, 326-36.

Van der Loos, H. D., J. (1978). Does the skin tell the somatosensory cortex how to construct a map of the periphery? *Neurosci Lett* **7**, 23-30.

Waite, P. M., Marotte, L. R. and Leamey, C. A. (1994). Timecourse of development of the wallaby trigeminal pathway. I. Periphery to brainstem. *J Comp Neurol* **350**, 75-95.

Waite, P. M., Marotte, L. R. and Mark, R. F. (1991). Development of whisker representation in the cortex of the tammar wallaby Macropus eugenii. *Brain Res Dev Brain Res* **58**, 35-41.

Welker, W. I. (1973). Principles of organization of the ventrobasal complex in mammals. *Brain Behav Evol* **7**, 253-336.

Woolsey, T. A. and Van der Loos, H. (1970). The structural organization of layer IV in the somatosensory region (SI) of mouse cerebral cortex. The description of a cortical field composed of discrete cytoarchitectonic units. *Brain Res* **17**, 205-42.

Wu, C. W. and Kaas, J. H. (2003). Somatosensory cortex of prosimian Galagos: physiological recording, cytoarchitecture, and corticocortical connections of anterior parietal cortex and cortex of the lateral sulcus. *J Comp Neurol* **457**, 263-92.

CHAPTER V

Literature Review of the Anatomy of the Brainstem Somatosensory Nuclei in Mammals

This chapter is modified from the submitted chapter: Sawyer, E. K., and Sarko, D. K. Evolution of the somatosensory brainstem in mammals. In Kaas, J. H. and Herculano-Houzel, S., *Evolution of the Nervous System*. Submitted. New York, NY: Elsevier.

ABSTRACT

The anatomy of the somatosensory nuclei of the brainstem changes little between even distantly related mammals, which allows for useful comparisons over broad evolutionary distances. Below we summarize what is known about the neuroanatomy of the trigeminal, cuneate, and gracile nuclei in mammals. These comparisons show repeated patterns in mammalian evolution, such as expansion of these nuclei in species with somatosensory specializations. It also highlights more rare innovations, such as the appearance of novel nuclei or a change in the orientation of the somatotopic map.

INTRODUCTION

Compared to the mammalian neocortex, the brainstem is evolutionarily more stable, making it well-suited for comparisons between distantly related species. Because the basic organization of the brainstem is so stable, anatomical comparisons are more translatable across species than such comparisons would be in the more variable higher cortical areas. Using anatomy also allows greater inclusivity of mammalian species in a neuroanatomical survey than has been involved in functional and physiological experiments. Here we will ask what kinds of morphological variations in the neuroantomy of the somatosensory brainstem are common in evolution (i.e., part of the generalizable mammalian plan), and which are rare exceptions?

In this review of comparative neuroanatomy of the somatosensory brainstem nuclei, we first describe the basic structure of the principal somatosensory pathway, which is a critical foundation for understanding how features of this pathway may vary. Second, we review what is known about the brainstem somatosensory nuclei in several mammalian orders. We devote extra attention to mammals with notable elaborations of the somatosensory

surface (e.g., the prominent facial whiskers of pinnipeds or the specialized glabrous hands of primates). Finally, we discuss what overarching trends emerge and describe areas for future research.

SOMATOSENSORY PATHWAYS

The somatosensory pathways convey the sensations of pain, temperature, proprioception, and discriminative touch. They can be divided into the spinal cord pathway for sensory inputs from the neck, limbs, and trunk, and the trigeminal pathway for the head (see Fig. 1 for a simplified schematic of these pathways)(reviews: (Ashwell, 2013; Ebner and Kaas, 2015)). The nuclei highlighted in red are the focus of this review. The components that are shaded in grey - including those areas involved in proprioception, pain, and temperature from the body, and the primary somatosensory areas of the thalamus and cortex - are beyond the focus of the present review.

Primary sensory neurons that convey discriminative touch from the body have nerve endings in the cutaneous periphery, with cell bodies in the dorsal root ganglion and axons that enter the spinal cord at the appropriate rostral-caudal level for their origin of inputs. These axons then project rostrally in white matter tracts along the mediodorsal aspect of the spinal cord, terminating in the dorsal column nuclei of the caudal medulla. The rostral body surface (neck, rostral trunk, and forelimb) is represented laterally in the cuneate nucleus, whereas the caudal body surface (caudal trunk and hindlimb) is represented in the gracile nucleus. In addition, the representation of the tail is sometimes identified as a distinct nucleus known as Bischoff's nucleus and located medially at the caudal-most extent of the gracile nucleus (Johnson et al., 1968; Ostapoff and Johnson, 1988). However, this nucleus is indistinct or unidentified in many mammals, and for the purpose of this chapter will be included with the cuneate-gracile complex. Most neurons in the cuneate-gracile complex send axons to the lateral division of the principal somatosensory nucleus in the thalamus, the ventroposterior nucleus (VPL). Neurons in the ventral posterior nucleus of the thalamus project to the primary somatosensory cortex.

Somatosensory inputs from the head follow a distinct pathway. The trigeminal nerve (CN V) carries the majority of the somatosensory information from the head (the glossophyaryngeal and vagal nerves also convey tactile information for limited regions of the head including parts of the internal mouth and parts of the pinnae). These sensory neurons that innervate the cutaneous periphery have cell bodies that are located in in the trigeminal ganglion with axons extending into the brainstem. As these axons enter the brainstem they either: 1) bifurcate and

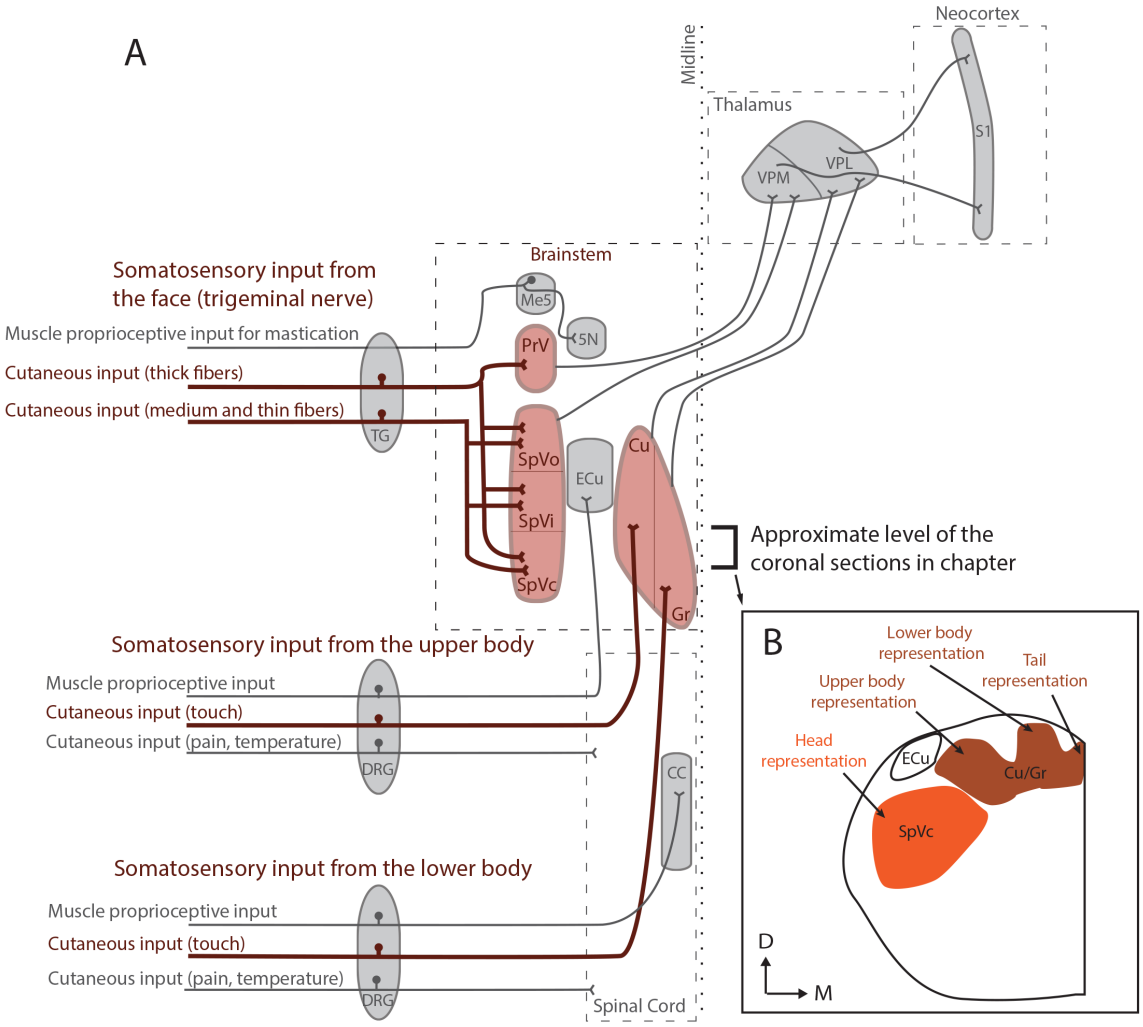
A
Neocortex
Midline
Thalamus
S1
VPM
VPL
Brainstem
Somatosensory input from
the face (trigeminal nerve)
Me5
5N
Muscle proprioceptive input for mastication
PrV
Cutaneous input (thick fibers)
Cutaneous input (medium and thin fibers)
TG
SpVo
ECu
Cu
SpVi
SpVc
Gr
Approximate level of the
coronal sections in chapter
Somatosensory input from the upper body
Muscle proprioceptive input
Cutaneous input (touch)
Cutaneous input (pain, temperature)
DRG
CC
Somatosensory input from the lower body
Muscle proprioceptive input
Cutaneous input (touch)
Cutaneous input (pain, temperature)
DRG
Spinal Cord
B
Lower body
representation
Tail
representation
Upper body
representation
Head
representation
ECu
Cu/Gr
SpVc
D
M

Fig. 1: Schematic of the ascending tactile somatosensory pathways in a mammal (adapted from Ashwell 2013 fig 9.1 and 9.2). **A:** A simplified diagram of the ascending somatosensory pathways for the face and body. Sensory information is conveyed along pseudounipolar primary sensory neurons, through ganglia, to various stations in the brainstem. The brainstem nuclei that are the focus of this chapter are highlighted in red and include: the principal sensory nucleus (PrV), the spinal trigeminal nucleus (SpV), and the cuneate-gracile complex (Cu and Gr). These nuclei send projections to the ventral posterior nucleus of the thalamus, which in turn sends projections to the primary somatosensory cortex (S1). Other labeled nuclei in the brainstem are involved in the processing of proprioceptive, pain, and temperature signals from the body or face but will not be discussed in this chapter. **B:** A schematic of the tissue sections in Figures 3 and 5-9. The representative plane of section is from the level of the brainstem where the spinal trigeminal nucleus (orange) and the Cu-Gr complex (red) are present, approximately at the level of the obex, as delineated in A. The coloring of the nuclei will be consistent throughout the figures in this chapter. Abbreviations: 5N= motor trigeminal nucleus, CC= Clark's column, Cu = cuneate nucleus, DRG= dorsal root ganglion, ECu= external cuneate nucleus, Gr = gracile nucleus, Me5= mesencephalic nucleus of 5, PrV = principal sensory trigeminal nucleus, S1 = primary somatosensory cortex, SpVc= spinal trigeminal subnucleus caudalis, SpVo= spinal trigeminal subnucleus oralis, SpVi= spinal trigeminal subnucleus interpolaris, TG= trigeminal ganglion, VPL = ventral posterior lateral nucleus of the thalamus, VPM = ventral posterior medial nucleus of the thalamus. D = dorsal, M = Medial.

A

Laboratory rat (*Rattus norvegicus*)
Spinal trigeminal subnucleus interpolaris
cytochrome oxidase

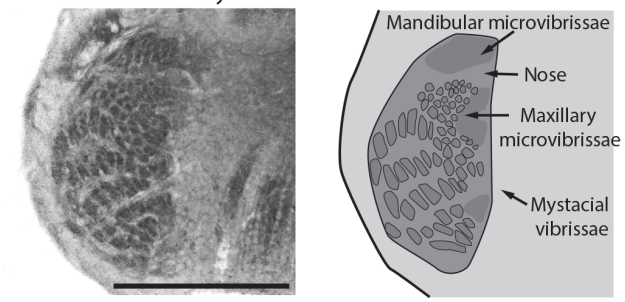

B

Harbor seal (*Phoca vitulina*)
Spinal trigeminal subnucleus interpolaris
Nissl

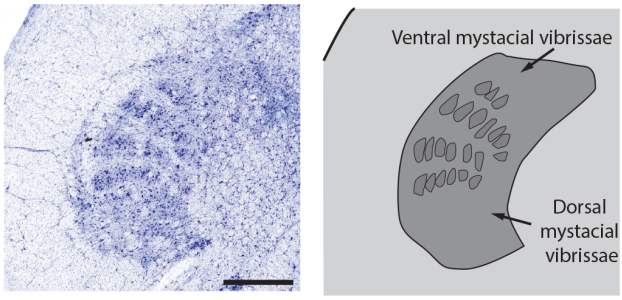

C

Common raccoon (*Procyon lotor*)
Cuneate nucleus
Nissl

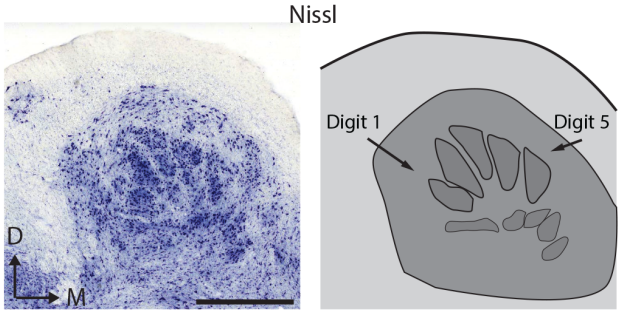

Fig 2: Anatomically visible somatotopic maps in the brainstem somatosensory nuclei. A photomicrograph of the stained section (left column), matched with a labeled schematic (right column). **A:** The spinal trigeminal subnucleus interpolaris in a laboratory rat (post-natal day 7), processed for CO, which shows modules that represent the whisker follicles. **B**: The spinal trigeminal subnucleus interpolaris in a harbor seal, stained for Nissl, showing cell-dense modules which likely represent the whisker follicles. **C**: The cuneate nucleus in a common raccoon, stained for Nissl, and showing cell-dense modules that represent the digits on the hand (Johnson et al., 1968). Orientation is the same for all sections. D = dorsal, M = Medial. Scale bars = 1 mm

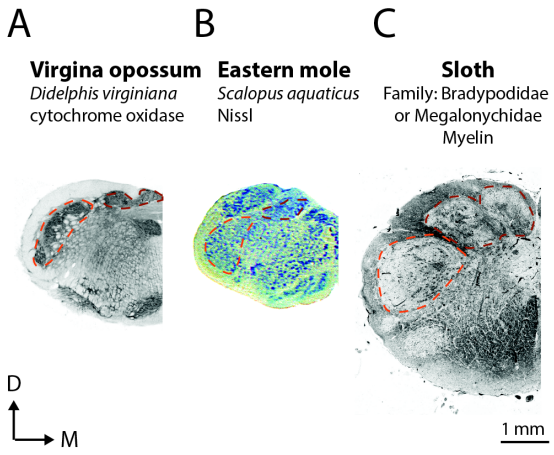

Fig 3: Example stains used in this chapter. In each, the spinal trigeminal subnucleus caudalis is outlined in orange, and the cuneate-gracile complex is outlined in red (the same convention is preserved throughout Figures 5-9). **A:** A photomicrograph of a coronal section of a brainstem of a Virginia opossum processed for cytochrome oxidase. **B:** A matching section from an Eastern mole stained for Nissl substance. **C**: A matching section from a sloth (unknown genus) stained for myelin. Scale bar is 1 mm, and matches Figures 5-9. D = dorsal, M = medial.

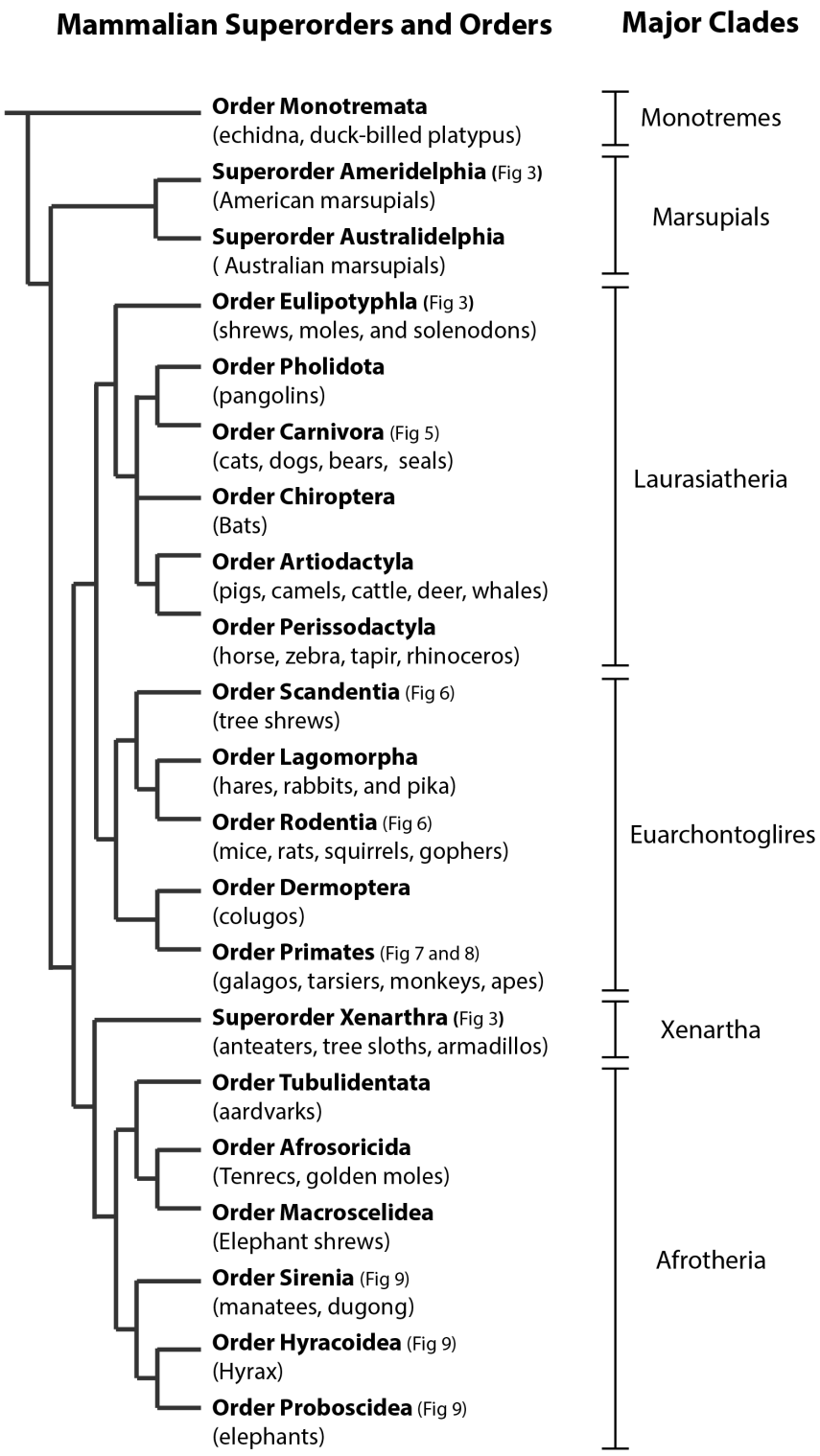

Fig 4. A cladogram of the orders of mammals, based off of Meredith et al. 2011. Orders that are represented in the figures in this chapter are marked accordingly.

send one branch rostrally to the principal sensory nucleus (PrV) and a second branch caudally to the spinal trigeminal nucleus (SpV), or 2) only project to SpV (Astrom, 1953; Cajal, 1896; Shigenaga et al., 1990) (but see (Windle, 1926) who reports axons projecting only to the PrV).

The PrV is vital to the sense of discriminative touch on the face. Its main projection is to the medial division of the principal somatosensory nucleus in the thalamus, the ventral posterior nucleus (VPM). Olszewski used cytoarchitectural analysis to divide the SpV of primates into 3 subregions (Olszewski, 1950), and these delineations have been applied across mammals. From rostral to caudal, the subnuclei of the SpV are subnucleus oralis (SpVo), subnucleus interpolaris (SpVi), and subnucleus caudalis (SpVc). The functional roles of each of these subnuclei in somatosensation are debated (Bosman et al., 2011; Diamond et al., 2008; Moore et al., 2015). There is strong support for the view that an intact SpVc is important for pain and temperature sensation in the face (Bereiter et al., 2000; Dubner and Bennett, 1983). In rodents, there is ongoing research evaluating the hypothesis that SpVi is involved in filtering out sensory inputs induced by self-initiated movements - such as those in afferents that are excited when a rodent sweeps its whiskers forward in air – in order to emphasize stimulus-driven responses (Moore et al., 2015; Yu et al., 2006). The role of the SpVo remains unclear.

In some animals with prominent whiskers, there are anatomically distinct modules in the trigeminal brainstem nuclei that functionally represent the vibrissae follicles in a one-to-one manner. These were termed "barrelettes" in mice and rats, and will be discussed in more detail later in this chapter. The visible barrelettes are present in three complete maps of the whisker pad in the brainstem, one in each the PrV, SpVi, and SpVc (Belford and Killackey, 1979; Arvidsson, 1982; Ma and Woolsey, 1984). There are no barrelettes in the SpVo (Nomura and Mizuno, 1986).

Barrelettes are one example of anatomically visible somatotopic mapping in the brainstem nuclei of some animals. Brainstem somatotopic maps are most obvious in animals that have a highly innervated and segmented somatosensory periphery, such as the digits of raccoons or primates, the rays of the star-nosed mole, or the punctate distribution of whiskers on mice and rats (Belford and Killackey, 1979b; Catania et al., 2011a; Florence et al., 1988; Florence et al., 1989; Johnson et al., 1968; Ma and Woolsey, 1984; Sawyer et al., 2014). Figure 2 demonstrates several examples of brainstem somatotopic subdivisions with darkly stained modules representing parts of the body with a high density of receptors separated by lightly stained border zones.

Altogether, the brainstem nuclei involved in touch are somatotopically arranged such that in coronal sections the dorsomedial-to-ventrolateral progression begins with the hindlimb, followed by the forelimb, and ultimately the head representation. The head representation is oriented such that the top of the head is represented ventrally and the tip of the nose is facing toward the midline. A pervasive assumption is that the size of each somatosensory nucleus/subnucleus is related to the innervation density of the area represented. This assumption likely holds some truth, although there is little empirical evidence for a constant scaling factor (discussed in chapter 5 of (Striedter, 2005)).

For this chapter, we have collected a wide variety of mammalian brainstems in order to demonstrate not only the diversity of specializations, but the commonality of pervasive organizing principles. Representative brainstem sections were chosen from the laboratory collections of Jon Kaas and Roger Reep. Although it was not possible to display every section with the same histological stain, we limited the stains to those for Nissl substance, cytochrome oxidase (CO), and myelin (Figure 3). In the Nissl sections cell bodies are blue. In the sections processed for CO, regions with high concentrations of mitochondria, reflecting high metabolic activity such as would be present at nerve terminals, are darker than areas with low metabolic activity. In the sections stained for myelin, the bundles of myelinated axons are a dark grey. We have selected sections at approximately the same level of the brainstem, a goal that is tempered by the limitations posed by sample availability. All sections are cut in the coronal plane at a level where spinal trigeminal subnucleus caudalis (outlined in orange) and the cuneate-gracile complex (outlined in red) are visible (Figure 1B, Figure 3). All photomicrograph figures are similarly scaled to emphasize overall size differences. Because nuclei are three-dimensional structures and the area of a nucleus in one section is only a suggestion of the volume of that structure. Therefore the figures should not be interpreted as reliable indications of the relative sizes of the nuclei, but rather seen as a starting place for comparisons and discussions.

ANATOMICAL REVIEW

Below I review the somatosensory brainstem nuclei of members of major divisions of the mammalian radiation. We have organized them as such (Monotremes, Marsupials, Laurasiatheria, Euarchontoglires, Xenartheria, Afrotheria) and according to the phylogenetic relationships put forth by Meredith (2011) (Fig. 1). These nuclei are also found in non-mammalian vertebrates but the focus of the present chapter is restricted to mammals.

Because there is a paucity of research on several orders of mammals some orders are not covered in the following review. I know of no research on the somatosensory brainstems in the orders Demoptera (colugos) or the Tublidentata (for which the only extant species is the aardvark, *Orycteropus afer*). Similarly, there was little research appropriate for this chapter on Lagomorphs (hares and rabbits), Perissodactyls (horses, rhinos, tapirs, ect.), Macroscelidea (elephant shrews), or Scandentia (tree shrews, though see in Figure 7), Afrosoricida (but see (Stephan et al., 2012). To our knowledge, the only references to the somatosensory brainstem in the Pholidota (pangolins) briefly notes that a specimen had a large dorsomedial component of the cuneate-gracile complex (ex. Figure 5 in Chang, 1944)(Chang, 1944; Chang, 1947). This order is composed of 8 species of pangolins, or "scaly anteaters", and some of these species have strong prehensile tails that they use when climbing trees. It is possible that this enlargement represented the tail.

MAJOR CLADE MONOTREMES, SUPER ORDER MONOTREMES

The extant monotremes are found in Australia and New Guinea and include the duck-billed platypus and four species of echidna (Griffiths, 1978). The monotreme clade is the mammalian group that is most distantly related to all other mammals, which makes them of particular interest. Monotremes lack tactile hairs, but do have specialized somatosensory rostrums (Ashwell, 2013).

TRIGEMINAL NUCLEI: Echidna *(*Family *Tachiglossidae):* Echidnas are terrestrial animals that have a thin pointy nose with a high density of mechanoreceptors and putative electroreceptors on the distal tip. Echidnas are speculated to use their nose to probe the leaf litter and soil for small prey items (Ashwell, 2013). Despite this specialized functionality, the trigeminal brainstem of the echidna is unremarkable in size, and similar to the structure of the laboratory rat (Ashwell et al., 2006). The chemoarchitecture of the SpVc differs from other mammals in that there is a punctate distribution of C-fiber terminals in the gelatinous layer of SpVc, instead of the continuous distribution seen in rodents (Ashwell et al., 2006). To date, the functional implications of this difference remain unknown.

Platypus *(Ornithorhynchus anatinus):* The bill of the semi-aquatic platypus is a specialized sensory structure used to locate motile prey underwater and/or to search for prey items in the mud (Taylor et al. 1992, Paullo and Macmillian 2004). The broad, leathery bill is densely covered with longitudinal mechanosensory "push-rod" complexes, and two kinds of electroreceptive organs (Manger and Pettigrew, 1996). In the primary somatosensory

cortex the bill is represented by alternating bands that stain darkly or lightly for CO. Electrophysiological mapping suggests that the dark bands receive mechanosensory inputs whereas the light bands receive electroreceptive inputs (Krubitzer et al., 1995).

The PrV, SpVi, and SpVo are large when compared to an echidna or a rat and are also large when compared to other nuclei within the platypus brainstem (Ashwell et al., 2006). These nuclei are also more neuron-dense than the same nuclei in rats. The SpVc is unremarkable in size (Ashwell et al., 2006; Hines, 1929). Specific stripes corresponding to the stripes of receptors on the bill, or in the bands in the cortex, were not seen in any of the trigeminal somatosensory nuclei in the platypus.

CUNEATE-GRACILE COMPLEX: The cuneate-gracile complex in monotremes has been described as appearing large, but these statements are limited to qualitative descriptions by various authors (Abbie, 1934; Ashwell, 2013; Hines, 1929; Pettigrew et al., 1998).

MAJOR CLADE MARSUPIALS, SUPERORDER MARSUPIALS

This clade consists of the marsupials of Australia and the Americas, the superorders Australidelphia and Ameridelphia, respectively. Though less specious than eutherian mammals, marsupials comprise the other major adaptive radiation in mammals, and as such they are valuable for the study of mammalian brain evolution (Ashwell, 2010) (Figure 4). The smallest marsupial is the long-tailed planigale (*Planigale ingrami*) (body weight of approximately 4.2 g), and the largest is the red kangaroo (*Macropus rufus*) (body weight of approximately 75 kg) (Van Dyck and Strahan, 2008). In addition, marsupials are altricial and continue their development in an external pouch. The accessibility of the immature animals makes them a particularly good study group for the study of development.

TRIGEMINAL NUCLEI: In the Australian Tamir wallaby (*Macropus eugenii*) the PrV and SpVc are described as large, while the SpVi and SpVo are "less clearly seen" (Waite et al., 1994). Brainstem patches that resemble the barrelettes are seen in the PrV, SpVi and SpVc, but are less clear than in rats and mice (Waite et al., 1994). However, whisker-

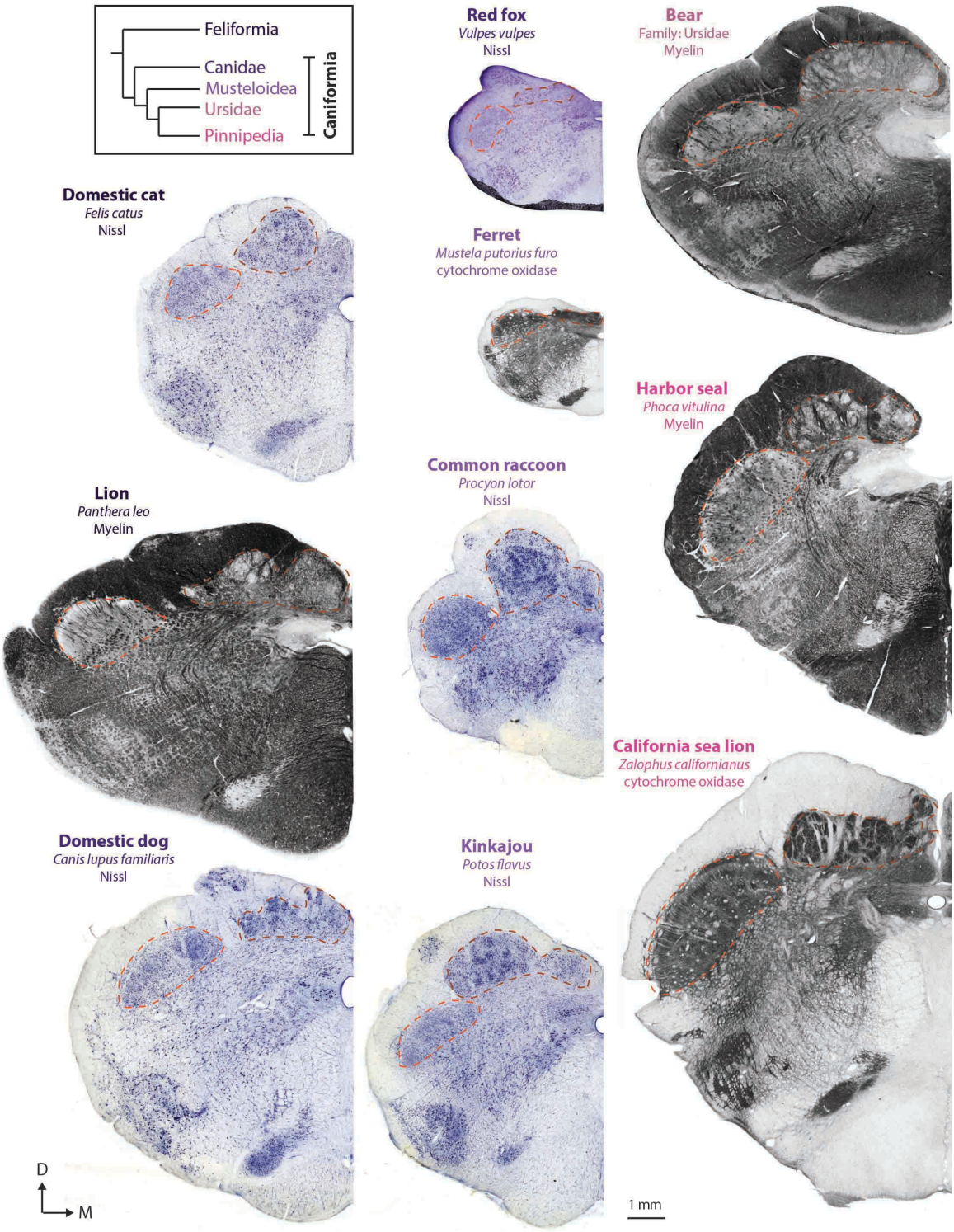
Feliformia
Canidae
Musteloidea
Ursidae
Pinnipedia
Caniformia
Red fox
Vulpes vulpes
Nissl
Bear
Family: Ursidae
Myelin
Domestic cat
Felis catus
Nissl
Ferret
Mustela putorius furo
cytochrome oxidase
Harbor seal
Phoca vitulina
Myelin
Common raccoon
Procyon lotor
Nissl
Lion
Panthera leo
Myelin
California sea lion
Zalophus californianus
cytochrome oxidase
Domestic dog
Canis lupus familiaris
Nissl
Kinkajou
Potos flavus
Nissl
D
M
1 mm

Fig. 5: A cladogram showing relationships between groups within the order Carnivora with brainstem sections from a selection of carnivores. The most species-specific identifier available for the section is given above the photomicrograph, along with the stain shown. Sections stained for myelin and cytochrome oxidase are shown in black and white while sections stained for nissl are shown in color. The shade of the section name matches the groups shown in the cladogram. The spinal trigeminal subnucleus caudalis is outlined in orange, and the cuneate-gracile complex is outlined in red. Note the large parcellated cuneate nucleus in the raccoon and the kinkaju and the large spinal trigeminal nucleus the sea lion and harbor seal. Scale bar is 1 mm, and matches Figures 3, and 6-9. D = dorsal, M = medial.

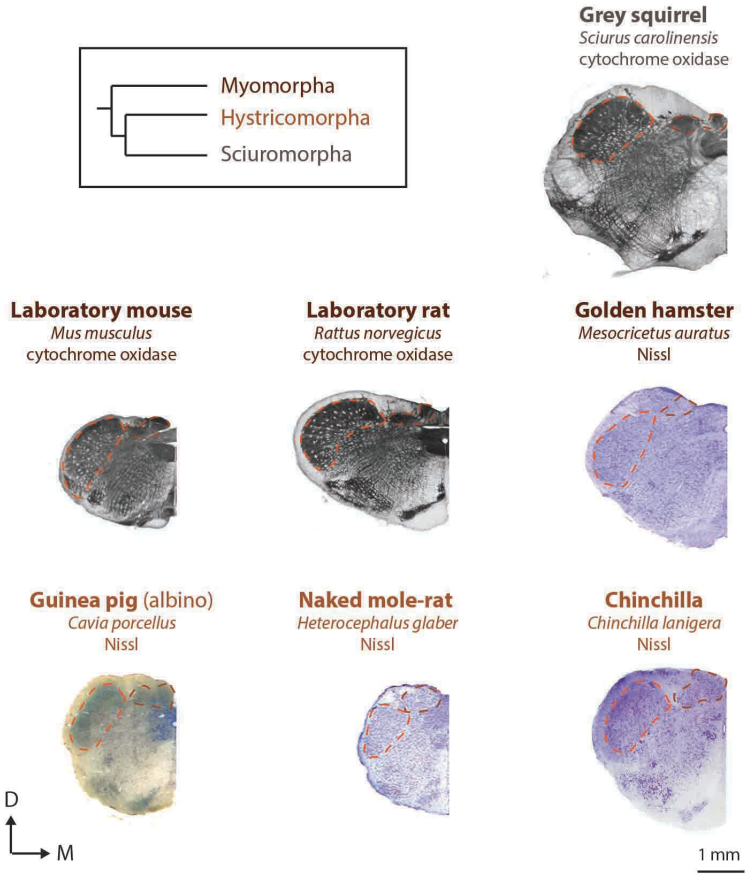

Fig. 6: A cladogram showing relationships between groups within the order Rodentia with brainstem sections from a selection of rodents. The most species-specific identifier available for the section is given above the photomicrograph, along with the stain shown. Sections stained for myelin and cytochrome oxidase are shown in black and white while sections stained for nissl are shown in color. The coloring of the section name matches the groups shown in the cladogram. The spinal trigeminal subnucleus caudalis is outlined in orange, and the cuneate-gracile complex is outlined in red. The spinal trigeminal nucleus in the laboratory mouse and rat appear large compared to other rodents. In all rodents shown the cuneate-gracile complex appears small.Scale bar is 1 mm, and matches Figures 3, 5, and 7-8. D = dorsal, M = medial.

related barrel structures are seen in the cortex (Waite et al., 1991). Cortical barrels have also been described in other Australian marsupials (Huffman et al., 1999; Weller, 1993) but never in an American marsupial. This is surprising as American opossums engage in whisking behavior and have distinctive mystacial whiskers (Grant et al., 2013; Ramamurthy and Krubitzer, 2016), but since neither of these factors definitively correlates with the presence of cortical barrels, the lack of barrels is not extraordinarily unusual (Woolsey et al., 1975). It is unknown if there are barrelettes at the level of the trigeminal somatosensory system in American marsupials. Barrelettes were not detectable in our material (Figure 3A).

CUNEATE-GRACILE COMPLEX: References to the cuneate-gracile complex in marsupials suggest that the complex is somatotopically organized and similar in appearance to other mammals (Culberson, 1987; Hamilton and Johnson, 1973).

MAJOR CLADE LAURASIATHERIA, ORDER EULIPOTYPHLA

The order Eulipotyphla has been recently proposed and consists of some of them members of the former order Insectivora. It contains hedgehogs, shrews, moles, and solenodons. The smallest mammal by mass, the Etruscan shrew (*Suncus etruscus*) (body weight of approximately 1.8 g), is in this group (Jurgens, 2002). The largest member is the group may be the European hedgehog, which can reach to about 1600 g in body weight (Reeve, 1994). Some of the distinctive features of the central nervous system of this clade include the gross resemblance to the central nervous system of the earliest mammals. For example, the Eulipotyphla tend to have a large paleocortex and small neocortex. However, members of this group also show distinctive somatosensory specializations, such as the well-developed whiskers of the North American water shrew (*Sorex palustris*), the somatosensory star of the star-nosed mole (*Condylura cristata*), and the large, powerful forepaws of the fossorial moles (e.g., *Scalopus aquaticus*). Of these, the brainstems of several shrews and moles have been best investigated.

TRIGEMINAL NUCLEI: Star-nosed mole (*Condylura cristrata*): The somatosensory star on the nose of the star-nosed mole is a special example of elaboration of trigeminal somatosensation. The star is an elaborate glabrous structure with 22 rays that are covered by thousands of somatosensory receptor complexes known as Eimer's organs. The mole uses this nasal array to tap along the muddy substrate to locate potential food items. The representation of this

star-structure has been studied at the level of the brainstem and cortex (Catania and Kaas, 1995; Catania et al., 2011a; Sawyer et al., 2014). In the brainstem, the PrV is large. The absolute volume of the ray representation in the PrV of a 55 g star-nosed mole has a volume of 0.71 mm^3, which is larger than the 0.57 mm^3 volume of the PrV in a 274g rat (Ashwell et al., 2006; Catania et al., 2011a). When the PrV, SpVi, and SpVc of the star nosed mole are qualitatively compared to other moles species they also appears large (Catania et al., 2011a), though volume measurements for the other mole species are not available. In the PrV, SpVi, and SpVc there is an anatomically visible representation of the star, much like the barrelettes in rodents (Catania et al., 2011a; Sawyer et al., 2014).

A special feature of the somatosensory system of the star-nosed mole is that the two medial ventral rays, though small in peripheral surface area compared to the other rays on the face, have a comparatively large representation in the cortex (Catania, 1995). This over-representation of the medial-ventral ray is thought to be related to its behavioral importance as a "tactile fovea" and perhaps associated with the greater innervation density of that ray (Catania and Kaas, 1997). Thus, it is surprising that the representation of these rays in the brainstem nuclei is not as dramatically overrepresented as in the cortex. This suggests that the over-representation of the foveal ray in the cortex is due partly to a process that occurs beyond the brainstem relay.

North American water shrew *(Sorex palustris*): Water shrews are one of the smallest diving mammals. They have an elaborate set of whiskers that they can use to find prey on land and in the water (Catania et al., 2008) and a large trigeminal nerve for their size (Leitch et al., 2014). One study used CO to find strikingly clear barrelettes in the PrV, SpVi, and SpVc of juvenile water shrews (Catania et al., 2013). The barrelettes were less clear but still present in the adult animals. The PrV and all components of the spinal trigeminal track appear large in coronal sections (Catania et al., 2013).

CUNEATE-GRACILE COMPLEX: Moles have large, muscular forelimbs that are used to excavate tunnels with a powerful breaststroke-like motion (Christian, 1950). The skeletal anatomy of the forelimbs is significantly modified in order to produce the force needed to dig through soil. The limb is rotated in such a way that the 1st digit points ventrally, and their 5^{th} digit points dorsally (Edwards, 1937). When brain size is taken into account, the cuneate-gracile complex is larger in the fossorial moles (Figure 3B) (Talpidae) than in the shrews (Soricidae) (Stephan, 2012).

MAJOR CLADE LAURASIATHERIA, ORDER CARNIVORA

Carnivores are a diverse group of animals including cats, dogs, weasels, raccoons, bears, seals, and sea lions. This group represents a range in brain size that rivals the primate order, from the diminutive least weasel (*Mustela nivalis*) (with a wide range for body mass of 25g to 250g) (Nowak and Walker, 1991) to the southern elephant seal (*Mirounga leonine*) (adult male body mass of approximately of 3510 kg with a brain mass of approximately 1400 g, which is approximately the mass of the human brain)(Bininda-Emonds, 2000; Haight, 1988). Photomicrographs of brainstem sections from this group are shown in Figure 5. Here we discuss select examples that illustrate some of the diversity of this group.

TRIGEMINAL NUCLEI: California Sea Lions *(Zalophus californianus):* Sea lions have long, thick facial whiskers that are one of the most innervated mystacial pads in vertebrates (McGovern et al., 2015; Sawyer et al., 2016; Wohlert et al., 2015). They can use their whiskers to follow hydrodynamic trails (or wakes), which may be used when foraging underwater (Glaser et al., 2011). They also use their whiskers in social displays by extending the tips forward to touch the face of a conspecific (Peterson, 1967). Both the spinal trigeminal nucleus and the principle sensory nucleus appear large, though measurements of the volume of these nuclei are not available. A collection of cell-dense modules that stain darkly for CO can be seen in the PrV, SpVi, and SpVc in an arrangement that is similar to the barrelettes seen in mice and rats (Figure 5). A seemingly similar arrangement is visible in the harbor seals (*Phoca vitulina*) (Figure 5). It is likely that these modules indicate the representations of the whiskers in the brainstem.

CUNEATE-GRACILE COMPLEX: Raccoon *(Procyon locor*): Raccoons have well-innervated and dexterous glabrous forepaws (Iwaniuk and Whishaw, 1999; Turnbull and Rasmusson, 1987). The cuneate of the raccoon is hypertrophied and has distinct cell dense modules that are separated by cell sparse septa (Johnson et al., 1968). These modules represent the pads of the raccoon's forepaw, with 5 elongated strips representing the digits. Within the cuneate nucleus the representation of the extremities is organized such that the distal glabrous surface of the digits is represented dorsal to the proximal surface, which in turn is dorsal to the palm representation (Johnson et al., 1968) (Figures 2, 5, and 10F). Data from the small hind limb representation are limited but appear to show the

opposite arrangement, with the distal ends of the digits represented more ventrally than proximal regions (Johnson et al., 1968).

California Sea Lions: Among marine mammals, sea lions have a unique mode of swimming. While other marine mammals undulate their spine and tail, sea lions create forward force by extending their flippers to their sides like wings, then forcefully clapping their arms together in front of their body (Friedman and Leftwich, 2014; Godfrey, 1985), a movement that appears to shares some traits with the flapping wings of a flying animal. The brainstem of the California sea-lion has a well-developed cuneate-gracile complex with distinctive septa, as seen in tissue sections stained for Nissl, CO and vesicular glutamate transporter 1 (Sawyer et. al., 2016). As the sea lion's flipper is a sturdy, webbed limb lacking obvious breaks in the sensory surface, it is not clear which breaks in the body surfaces these septa might represent.

MAJOR CLADE LAURASIATHERIA, ORDER CHIROPTERA

Bats are the only mammals with true flight. They are a specious group, with the largest bat being the giant golden-crowned flying fox (*Acerodon jubatus*) (body weight of approximately 1.2 kg) and the smallest being Kitti's hog-nosed bat (*Craseonycteris thonglongyai*) (body weight of approximately 2 g)(Nowak and Walker, 1991). The somatosensory system of bats is outstanding in at least two ways: the wing-forelimbs that are found in all species of Chiroptera and are unique to this group, and the infrared sensory system that is limited in mammals to the three extant species of vampire bats (Kürten, 1982).

TRIGEMINAL NUCLEI: Three species of bats, the vampire bats, have an infrared (IR) sense that they can use to find the warm-blooded mammals that are the source of the bat's blood meals. The IR receptors are located on "leaf pits" near the nares (Kürten, 1984). Ion channels that mediate the reception of the heat signal are modified from the heat-sensitive TrpV1 channel, and the impulses travel along the trigeminal nerve (Gracheva et al., 2011), strongly suggesting that the IR system was modified from the facial somatosensory system. The central nervous system representation of the IR sense is almost completely unstudied. In a single anatomical study the brainstem of one species of vampire bat (*Desmodus rotundus*) was compared to the brainstem of three bats that lack the IR sense, and a histologically distinct nucleus was noted in the vampire bat. This putative IR nucleus was located lateral to the descending spinal trigeminal tract, at about the level of the SpVo and SpVc (Kishida et al., 1984).

CUNEATE-GRACILE COMPLEX: The skeletal arrangement of bat wings follow the typical mammalian forelimb plan, but with digits 2 to 5 elongated. The wing surface consists of webbing between the digits (except for digit 1, which is free) and between the digits and the body. When flying, the limb is positioned such that digit 1 points anteriorly and the remaining digits extend posteriorly. The primary somatosensory nerve endings are most dense along the leading edge and the lateral tip of the wing (Chadha et al., 2011). In addition, the wings of microchiropteran bats have regular arrays of raised hair-domes associated with Merkel endings on the dorsal and ventral wing surfaces (Zook and Fowler, 1986). These hair-domes are thought to detect air flow and assist with critical flight maneuvers and navigation (Sterbing-D'Angelo et al., 2011).

Not only is the wing of the bat special, but the orientation of the limb representation in the primary somatosensory cortex is unlike other mammals. Bats are the only known group of mammals in which the primary somatosensory cortex orientation of the limb is reversed. In all other mammals studied, the distal tips of the digits point toward anterior cortex (Kaas, 1983), but in bats the distal tips point toward posterior cortex (Calford et al., 1985; Chadha et al., 2011; Krubitzer and Calford, 1992; Wise et al., 1986). It has been suggested that this reversal is related to the position of the wing in flight, which suggests a connection between the somatotopic organization of sensory areas and "extrapersonal space" (Calford et al., 1985; Manger et al., 2001).

A single multiunit mapping study has investigated the cuneate nucleus in *Pteropus scapulatus* (little red flying fox)(Martin, 1993). Unexpectedly, no evidence supporting a clear topography of the wing was found; instead, the map of the body appeared to be disorganized. A later study employing both electrophysiological recordings and neural tract tracers investigated the somatosensory nuclei of the somatosensory thalamus (Manger et al., 2001). The orientation of the representation of the bat's wing in the ventral posterior nucleus of the thalamus matched the orientation in the cortex, suggesting that the bat-specific-orientation of the limb representation emerged between the level of the cuneate and the thalamus. However, further work is needed to clarify the organization of the bat cuneate.

MAJOR CLADE LAURASIATHERIA, ORDER ARTIODACTYLA

The artiodactyls are the even-toed ungulates, which include the hippopotamus, deer, giraffes, llamas, camels, pigs, cows, sheep, and goats, among others. Modern phylogenies also put cetaceans in this order (Graur,

1994; Meredith et al., 2011; Murphy et al., 2001). Some texts consider the land members of the artiodactyls and the marine members separately due to the great phenotypic divergence that has taken place. Here we consider them together because it more clearly documents an independent lineage's evolution with adaptions to a broad range of environments. The smallest member of this clade is the lesser mouse-deer (body weight of approximately 2 kg), and the largest is the blue whale (body weight of approximately 115,000 kg body weight), which is also the largest mammal (Matsubayashi, 2003; Small, 1971).

The land artiodactyls include many commonly known animals, but despite this, little research has been done to characterize their neuroanatomy. For the majority of species studied, the external anatomy suggests that there is little emphasis placed on the representation of the hindlimbs and more emphasis on the face. A small cuneate-gracile complex and relatively large trigeminal nuclei have been noted in the giraffe (Badlangana et al., 2007) and sheep (Woudenberg, 1970). Electrophysiological mapping of the neocortex also found a large representation of the mouth and lips in sheep (Johnson et al., 1974). The external anatomy of the face of some species suggests that there may be important tactile regions, such as the oral regions of the hippopotamus, which is studded with prominent tactile hairs, or the large glabrous snout of the pig. Unfortunately, descriptions of the brainstem neuroanatomical correlates of these body surfaces are lacking.

During the evolution from a terrestrial ungulate-like mammal to a marine mammal, cetaceans lost functional hindlimbs, greatly elaborated their tail, and transformed their forelimbs from legs into flippers. In addition, some whales and dolphins have specialized hairs and some dolphins have pits on their head region; both of these structures are presumed to be sensory adaptations. In humpback whales (*Megaptera novaeangliae*), the base of the hair has developed into a visible, knob-like swelling called a tubercle. These tubercles are highly innervated (Yablokov, 1974). Their function maybe related to feeling the density of plankton while feeding, detecting low frequency sound, perceiving water movement, or sensing a yet unknown stimuli (Mercado III, 2014). It has been proposed that the pit structures in the Guiana dolphin (*Sotalia guianensis*) might be electrosensory (Czech-Damal et al., 2012). Another unusual feature in cetaceans is the tusk of narwhals (*Monodon monoceros*) which is highly innervated by dentinal tubules projecting to the trigeminal nerve. If this is an important sensory apparatus, as some have suggested (Nweeia et al., 2014), it should have a significant representation in the trigeminal somatosensory brainstem.

Very little research has investigated the central nervous system representation of any aspect of the somatosensory system in cetaceans. However, it has been descriptively noted that cuneate-gracile complex is proportionally reduced in size compared to other mammals (this has been noted in a short beaked common dolphin (*Delphinus delphis*) (Hatschek, 1902), a bottle nosed-dolphin (genus: *Tursiops*) (Wilson, 1933), and a baleen whale (genus: *Balaenoptera)* (Norris and Sciences, 1966)). The SpV and the PrV also appear reduced in size compared to other mammals but not as much as the dorsal column nuclei (Hatschek, 1902; Norris and Sciences, 1966; Wilson, 1933). The size of the trigeminal nucleus in the baleen whales may be related to the large size of their head (about 1/3 of the body) (Norris and Sciences, 1966). No mention of any special representation of the tubercles, pits, or tusk could be found.

MAJOR CLADE EUARCHONTOGLIRES, ORDER RODENTIA

The Rodentia is the most specious order of mammals. It contains the well-studied lab mouse and lab rat, but also more exotic species such as semi-aquatic beavers, fossorial naked mole-rats, and arboreal flying squirrels (Wilson and Reeder, 2005). The smallest rodent is the Baluchistan pygmy jerboa (*Salpingotulus michaelis*) (approximately 3.75g), and the largest is the capybara (*Hydrochoerus hydrochaeris*) (approximately 50kg) (Herrera, 1993; Roberts, 2005). The great diversity of habitats that rodents have evolved to exploit, complemented by the extensive body of work in laboratory mice and rats, makes rodents an excellent order for comparative studies. Photomicrographs of brainstem sections from this group are shown in Figure 6.

TRIGEMINAL NUCLEI: The Laboratory Mouse and Rat (*Mus musculus* and *Rattus norvegicus*): Rats, mice, and many other rodents have large, moveable mystacial vibrissae which they actively whisk when exploring the world around them (Vincent, 1912). The whisker somatosensory pathway in rats and mice is one of the most thoroughly investigated somatosensory systems (Fox, 2008).

Mice and rats have a well-developed trigeminal system in which barrelettes - the anatomically distinct subunits in the brainstem that functionally represent whisker follicles - were first described (Belford and Killackey, 1979b; Ma and Woolsey, 1984). Barrelettes are present in the PrV, SpVi, and SpVc of the mouse and rat. They are often visualized using stains for cytochrome oxidase, succinic dehydrogenase, Nissl substance, or vesicular glutamate transporter 1 and are best distinguished during early development (Belford and Killackey, 1980; Sakurai

et al., 2013). Since their initial discovery, barrelettes have been detected in other rodent species, including the hamster (Jacquin et al., 1993) and guinea pig (Sikich et al., 1986).

The whisker-related patterns in the thalamus (barreloids) and cortex (barrels) are dependent on the proper development of the PrV but not SpV (Killackey and Fleming, 1985). Despite this, the SpVi barrelette representation is more distinctive than the PrV's in many respects: the volume of the SpVi is greater, the average cross-sectional area of the barrelettes is larger, and the overall pattern of barrels is generally clearer in the SpVi (Ashwell et al., 2006; Ma, 1991).

Naked mole-rat (Heterocephalus glaber): Naked mole-rats are fossorial, herbivorous rodents that inhabit subterranean tunnel systems in east central Africa. As their name suggests, naked mole-rats do not have fur, but instead have an array of sparsely-distributed, vibrissae-like hairs on their body that serve tactile and orientation functions (Crish et al., 2003; Park et al., 2003). Naked mole-rat incisors may represent the most specialized dentition known to date. The incisors exhibit an enlarged representation in primary somatosensory cortex, occupying 30% of primary somatosensory cortex compared to just 7% in rats (Catania and Remple, 2002; Henry et al., 2006; Remple et al., 2003).

Although somewhat indistinct barrels are present in the neocortex of naked mole-rats (Henry et al., 2006), no barrelettes were reported in a study of the brainstem (Henry et al., 2008). The trigeminal nuclei are relatively large, and inputs from the behaviorally important incisors project extensively to all trigeminal nucleus subdivisions (Henry et al., 2008).

CUNEATE-GRACILE COMPLEX: The Laboratory Mouse and Rat: The cuneate-gracile complex in laboratory rats and mice has an organization similar to that of other mammals. The paw representation is large compared to that of the rest of the body, but the entire complex is small overall compared to other animals (Maslany et al., 1991). The termination patterns of axons labeled by the injection of a neural tracer into the skin indicate that the representation of the paws in the cuneate is oriented such that the digits are dorsal and the palmar pads are ventral (Maslany et al., 1991).

Naked mole-rat: Although not specifically examined in a study by Henry et al., cytochrome oxidase-processed sections of the naked mole-rat brainstem also revealed relatively large - although not parcellated - cuneate

and gracile nuclei, indicating no visibly evident subdivisions representing tactile body hairs or clear functional subdivisions for body regions (Henry et al., 2008) (see also Figure 6)

MAJOR CLADE EUARCHONTOGLIRES, ORDER PRIMATES

The primate order consists of the Strepsirrhini primates (the galagos, potos, lemurs, and lorises), and the Haplorhini primates (the tarsiers, the New-Xorld monkeys, the Old-World monkeys, and the apes). Their phylogenetic relationships are shown in Figures 7 and 8. The smallest known primate is the Berthe's mouse lemur (*Microcebus berthae*) (body weight of approximately 30 g) (Dammhahn, 2005) and the largest is the western gorilla (*Gorilla gorilla*) (body weight of approximately 105 kg). Even though humans are not the largest ape our brain is more than twice the mass of the gorilla brain, more than three times the mass of the other great apes, and more than 13 times the mass of the gibbon (Stephan et al., 1981; Tobias, 1971). As suggested by the similar sizes across brainstem sections in Figure 8, the large human brain was not the result of a uniform increase in the entire brain, but mosaic evolution that selectively increased the size of the neocortex relative to the brainstem (Stephan et al., 1981; Striedter, 2005).

The sensitive hands of primates are one of the most distinctive features of the primate somatosensory system. An additional distinctive feature is the tactile pad on the prehensile tail of new-world primates in the family Atelidae (which includes the spider monkey, woolly monkey, and howler monkey) (Fleagle, 2013). In the trigeminal system, primates appear to be less reliant on tactile hairs on the face, instead compensating with their hands and acute vision. Humans are one of the very few mammals that lack tactile facial hairs. Lastly, the bipedalism of humans is rare in mammals and may also be reflected in the somatosensory brainstem.

TRIGEMINAL NUCLEI: The trigeminal nuclei appear small in primates (Figures 7 and 8). In proportion to their brainstem, the trigeminal nucleus in primates is on average smaller in volume than in the Scandentia or Afrosoricida, which may reflect a shift away from the reliance on facial whiskers (Stephan et al., 1981). In galagos there are barrelette-like structures in the PrV and SpVi (Sawyer et al., 2015), and modules have also been reported in the PrV of macaques and squirrel monkeys as well (Noriega and Wall, 1991). In humans the somatosensory brainstem nuclei representing the face may be more involved in representing the oral cavity and related to our uniquely well-

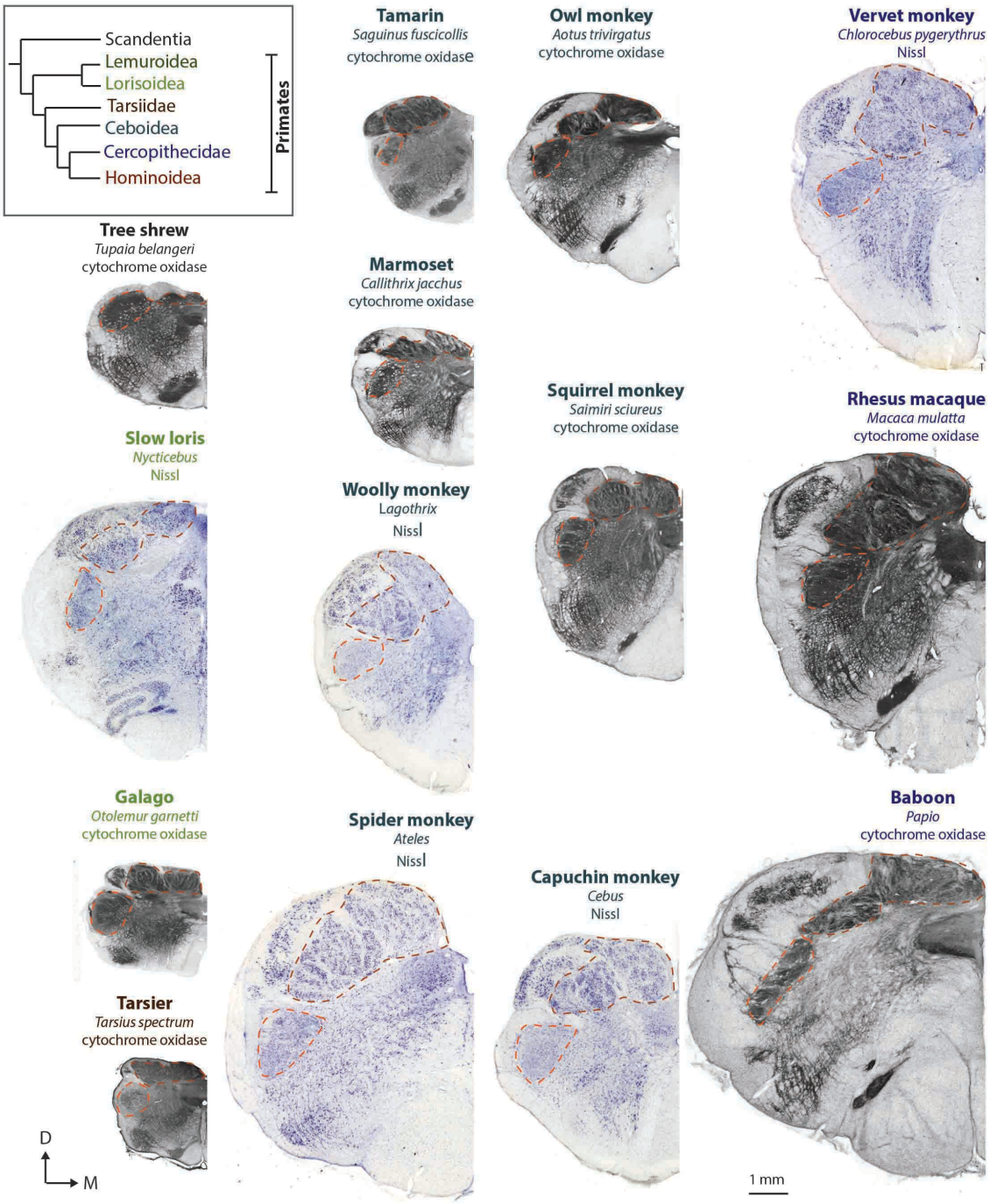
Scandentia
Lemuroidea
Lorisoidea
Tarsiidae
Ceboidea
Cercopithecidae
Hominoidea
Primates
Tree shrew
Tupaia belangeri
cytochrome oxidase
Slow loris
Nycticebus
Nissl
Galago
Otolemur garnetti
cytochrome oxidase
Tarsier
Tarsius spectrum
cytochrome oxidase
D
M
Tamarin
Saguinus fuscicollis
cytochrome oxidase
Marmoset
Callithrix jacchus
cytochrome oxidase
Woolly monkey
Lagothrix
Nissl
Spider monkey
Ateles
Nissl
Owl monkey
Aotus trivirgatus
cytochrome oxidase
Squirrel monkey
Saimiri sciureus
cytochrome oxidase
Capuchin monkey
Cebus
Nissl
Vervet monkey
Chlorocebus pygerythrus
Nissl
Rhesus macaque
Macaca mulatta
cytochrome oxidase
Baboon
Papio
cytochrome oxidase
1 mm

Fig. 7: A cladogram showing relationships between groups within the order Primates with brainstem sections from a selection of primates. The most species-specific identifier available for the section is given above the photomicrograph, along with the stain shown. Sections stained for myelin and cytochrome oxidase are shown in black and white while sections stained for nissl are shown in color. The shade of the section name matches the groups shown in the cladogram. The spinal trigeminal subnucleus caudalis is outlined in orange, and the cuneate-gracile complex is outlined in red. Compared to Figures 5, and 6, the cuneate-gracile nucleus appears large and parcellated in all primates, while the trigeminal nucleus appears to be small. Scale bar is 1 mm, and matches Figures 3, 5-6, and 8-9. D = dorsal, M = medial.

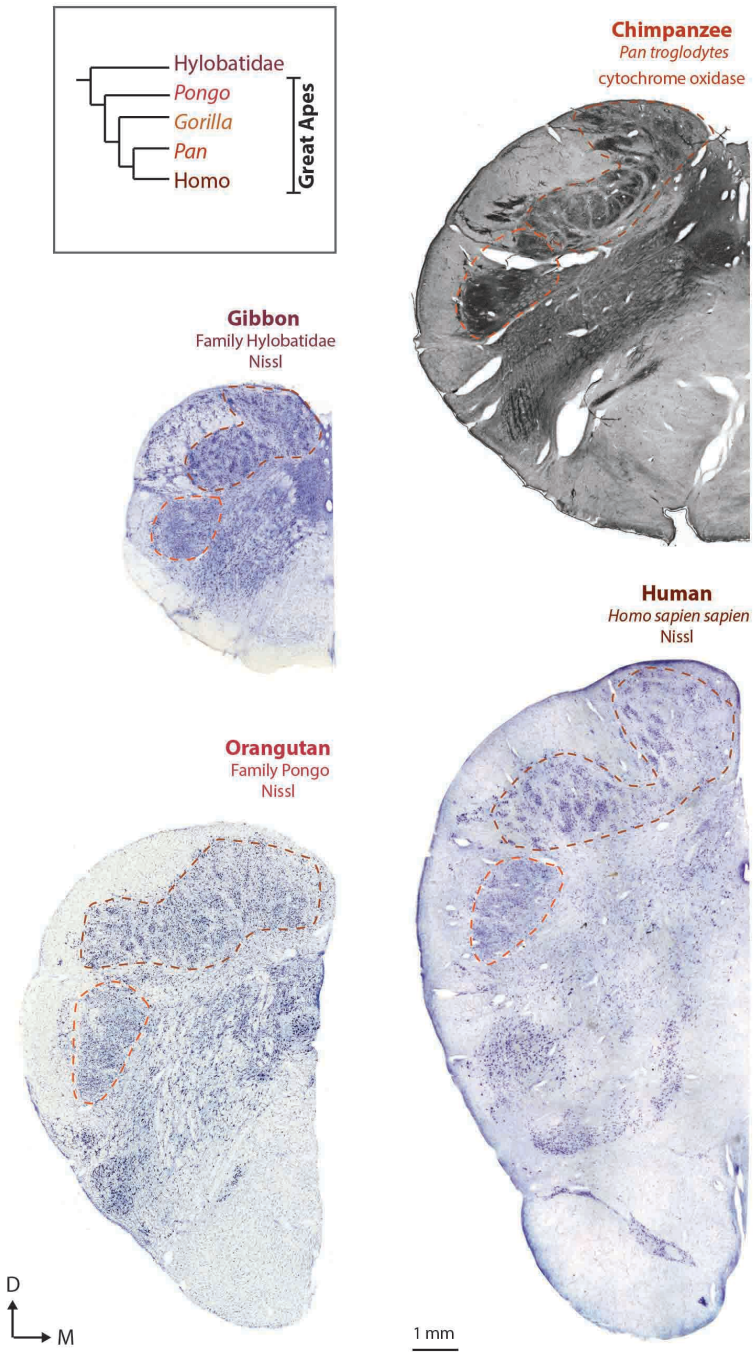
Hylobatidae
Pongo
Gorilla
Pan
Homo
Great Apes
Chimpanzee
Pan troglodytes
cytochrome oxidase
Gibbon
Family Hylobatidae
Nissl
Human
Homo sapien sapien
Nissl
Orangutan
Family Pongo
Nissl
D
M
1 mm

Fig. 8: A cladogram showing relationships between groups within the superfamily Hominoidea (Apes) with brainstem sections from a selection of apes. The most species-specific identifier available for the section is given above the photomicrograph, along with the stain shown. Sections stained for myelin and cytochrome oxidase are shown in black and white while sections stained for nissl are shown in color. The shade of the section name matches the groups shown in the cladogram. The spinal trigeminal subnucleus caudalis is outlined in orange, and the cuneate-gracile complex is outlined in red. The sections shown resemble the other primate sections in Figure 7 in that the cuneate-gracile complex is large and well divided and the trigeminal nucleus is small. In the chimpanzee section, there are five distinct modules in the cuneate nucleus that could represent the digits of the hand. Scale bar is 1 mm, and matches Figures 3, 5-7, and 9. D = dorsal, M = medial.

developed speech capabilities, but the comparative aspect of this remains understudied (but see (Usunoff et al., 1997)).

CUNEATE-GRACILE COMPLEX: The cuneate-gracile complex is qualitatively large in many primates compared to other mammals, including the related tree-shrews (order Scandentia) (Figures 7 and 8). Tilney conducted a survey of the brainstems in many primates species wherein he selected sections from the same brainstem level and measured the area of nuclei (Tilney, 1927). Based on those measurements, tarsiers had the smallest cuneate nucleus relative to their brainstem, baboons and gorillas had the second largest, and humans had the largest. This could reflect an increase in the importance of hand sensation in these species. For the gracile nucleus, tarsiers had the smallest nucleus relative to their brainstem, the humans had the second largest and howler monkeys (the only member of the Atelidae that was included in Tilney's study) had the largest. The large ratio for the howler monkey might be related to the tactile pad on their tail. Another study highlighted the particularly large gracile nucleus in the spider monkey (Chang, 1947).

The primate cuneate-gracile complex has a distinctive modular structure. In the species in which it has been studied, neural tract tracing has shown that these modules correspond to digits or to glabrous pads on the palmar surface (Florence et al., 1988; Florence et al., 1989; Qi and Kaas, 2006; Strata et al., 2003). These studies and others have revealed that the orientation of the hand representation in the cuneate nucleus in galagos, squirrel monkeys, and marmosets are all similar, but that this arrangement is different in macaques (Figure 10) (Florence et al., 1989; Xu and Wall, 1996; Xu and Wall, 1999). In the former, the distal ends of the digit representations point dorsally and the palm is represented ventrally (Figure 10C, D). In the macaques, the orientation is reversed (Figure 10B). The basic arrangement of the cell-dense modules in the human cuneate nucleus matches the arrangement in the macaques better than it matches the squirrel monkey, suggesting that the human cuneate is organized similar to the macaque (Figure 10A-C) (Florence et al., 1989). Together, these results suggest that in the lineage including the old world monkeys and apes, the orientation of the cuneate flipped.

MAJOR CLADE XENARTHRA, SUPERORDER XENARTHRA

We know of no research on the somatosensory brainstems of any member of the superorder Xenarthra (sloths and anteaters, and armadillos). However, a section of the brainstem of an unidentified sloth species is shown in Figure 3C. This section has a surprisingly large cuneate-gracile complex for a seemingly inactive animal.

MAJOR CLADE AFROTHERIA, ORDER HYRACOIDEA

Hyraxes are terrestrial and arboreal, primarily herbivorous mammals, and inhabit sub-Saharan Africa (Olds and Shoshani, 1982). Of the four extant species within the order Hyracoidea, rock hyraxes (*Procavia capensis*) have been the most extensively studied (Olds and Shoshani, 1982). The body mass for a rock hyrax is approximately 3.8kg for rock hyraxes, with a brain mass of approximately 12.8g (Sarko, unpublished). In addition to pelage fur, rock hyraxes have prominent vibrissae on the face (e.g., mystacial, supraorbital, and submental). Recent evidence has shown that hyraxes also exhibit an expanded distribution of vibrissae covering the entire body (Sarko et al., 2015), an elaboration that is unique to hyraxes and sirenians (Reep et al., 2002). Rock hyrax body vibrissae extend beyond pelage fur as black, elongated hairs that are thought to enhance detection of the boundaries of (and facilitate navigation through) the rocky crevices of their habitat, ultimately aiding survival through predator avoidance (Sarko et al., 2015).

TRIGEMINAL NUCLEI: No barrels have been observed in the rock hyrax neocortex (Woolsey et al., 1975), and although no electrophysiological or tracing data for the rock hyrax somatosensory brainstem currently exist, preliminary histological and histochemical analysis indicates parcellation of PrV and SpV (Sarko and Reep, 2013) (Figure 9). Although barrelettes were not noted in the trigeminal nucleus, previous studies using electrophysiological mapping of primary somatosensory cortex in the hyrax neocortex revealed a large proportion of that cortex dedicated to intraoral and perioral inputs (Welker and Carlson, 1976). This indicates that intraoral and perioral inputs may dominate the trigeminal nucleus as well, and may - in addition to facial vibrissae - constitute functional divisions within the topography of trigeminal parcellation.

CUNEATE-GRACILE COMPLEX: Prominent cuneate and gracile nuclei exhibited parcellation presumably related principally to inputs from body vibrissae (Sarko and Reep, 2013) (Figure 9). The trigeminal, cuneate, and gracile

nuclei appear to be only moderate in size compared to the same nuclei in manatees. The caudal-most extension of the gracile nucleus, related to cutaneous inputs from the tail in other species (Johnson et al., 1968; Ostapoff and Johnson, 1988), was small in hyraxes, as expected given the hyrax's rudimentary tail.

MAJOR CLADE AFROTHERIA, ORDER PROBOSCIDEA

Elephants are the largest extant land mammals, and include African (*Loxodonta africana*) and the slightly smaller Asian (*Elephas maximas*) species. African elephants have a body mass of approximately and 3,000kg and a brain mass of approximately 4,783g (Shoshani et al., 2006). Although the elephant neocortex has not been analyzed for the presence of barrels to date, barrels might not be expected, given that vibrissae are only known to exist on the trunk tip (Laursen and Bekoff, 1978; Rasmussen and Munger, 1996).

TRIGEMINAL NUCLEI: Verhaart noted that the trigeminal nucleus of the African elephant was relatively large and subdivided into at least 4 "gelatinous masses" within SpVc (also see Figure 9). Further parcellation is evident in SpVi, but SpVo appeared relatively small and homogenous with little discernible parcellation. PrV was large and exhibited parcellation (Verhaart, 1962). The tip of the Asian elephant's trunk is relatively sensitive (Dehnhardt et al., 1997) - with a tactile discrimination threshold comparable to that of the manatee's facial vibrissae (Bachteler and Dehnhardt, 1999) – and contains vibrissae as well as Pacinian corpuscles sensitive to pressure and vibration (Rasmussen and Munger, 1996). Therefore, it seems likely that parcellation in the trigeminal nuclei is preferentially dedicated to inputs from the trunk (and the trunk tip in particular).

CUNEATE-GRACILE COMPLEX: Some degree of subdivision was evident in the cuneate-gracile complex, which appear to be relatively small in Verhaart's preparations (Verhaart, 1962) but were noted to be relatively large by Maseko et

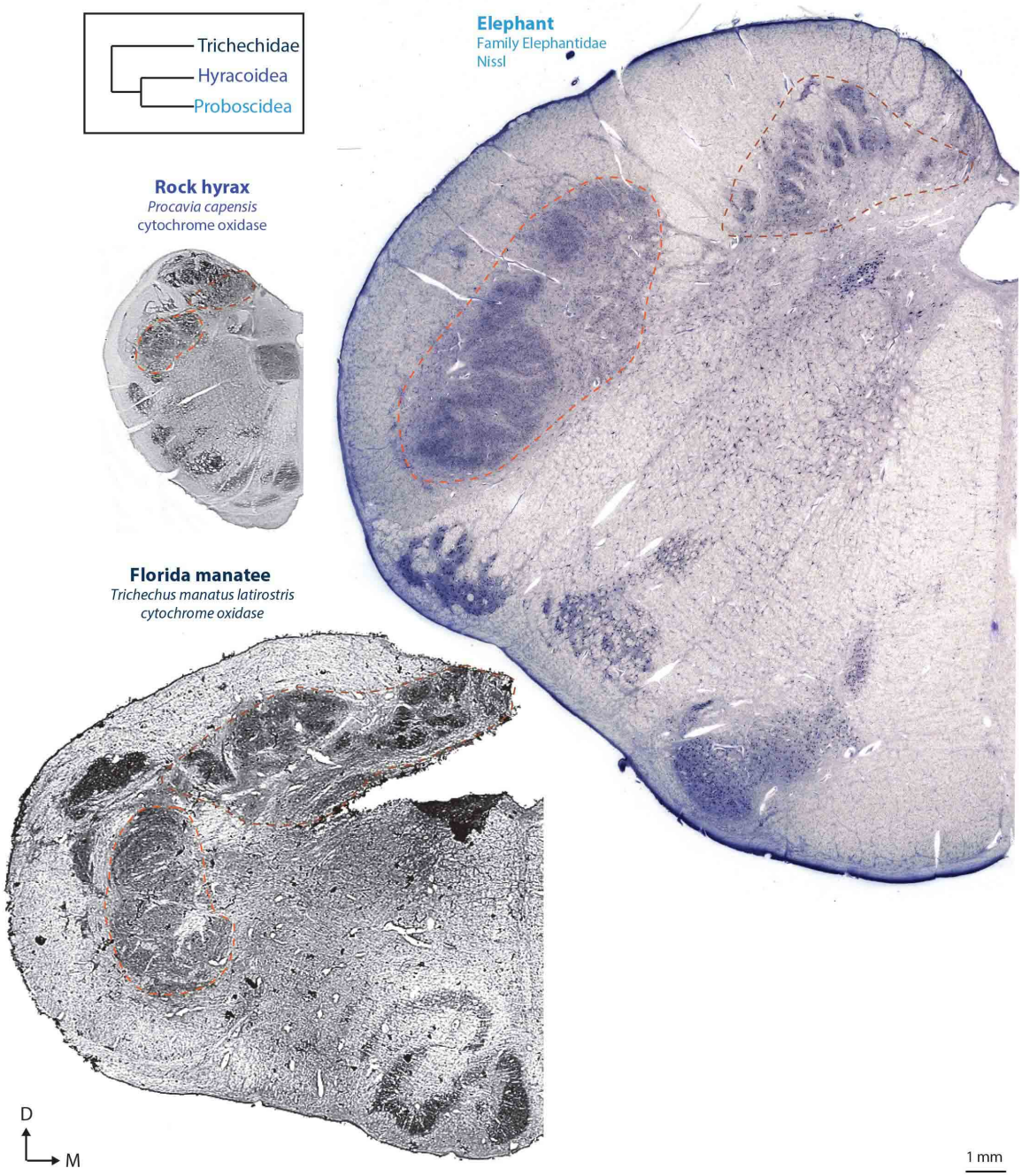
Trichechidae
Hyracoidea
Proboscidea
Elephant
Family Elephantidae
Nissl
Rock hyrax
Procavia capensis
cytochrome oxidase
Florida manatee
Trichechus manatus latirostris
cytochrome oxidase
D
M
1 mm

Fig. 9: A cladogram showing relationships between groups within the Afrotherian clade, with brainstem sections from the orders Trichechidae, Hyracoidea, and Proboscidea. The most species-specific identifier available for the section is given above the photomicrograph, along with the stain shown. Sections stained for myelin and cytochrome oxidase are shown in black and white while sections stained for nissl are shown in color. The shade of the section name matches the groups shown in the cladogram. The spinal trigeminal subnucleus caudalis is outlined in orange, and the cuneate-gracile complex is outlined in red. Although no barrelettes were detected in manatees, elephants, or hyraxes, SpVc did exhibit parcellation in each species shown. Some degree of suborganization was also evident in the cuneate-gracile complex of each species, with punctate cell-dense clusters separated by light septa. The Florida manatee's cuneate-gracile complex qualitatively appears to be disproportionately large, likely to accommodate inputs from tactile hairs located on its entire body. Scale bar is 1 mm, and matches Figures 3 and 5-8. D = dorsal, M = medial.

al. (Maseko et al., 2013) (also see Figure 9). Although elephant skin is quite tough, and generally likely to be relatively insensitive, specific body regions are highly invested with sensory innervation and mechanoreceptors. The Asian elephant's feet are laden with Pacinian corpuscles thought to aid in detection of low-frequency seismic communication with conspecifics (Bouley et al., 2007). Therefore, cuneate and gracile parcellation may be preferentially related to inputs from the feet. The elephant body has a distribution of hairs as well, and although these are not thought to be vibrissae, they likely extend a degree of tactile sensitivity to the sensory surface of the elephant's large body.

MAJOR CLADE AFROTHERIA, ORDER SIRENIA

The order Sirenia includes 3 extant manatee species (one of which is divided into 2 subspecies) and one extant dugong species. Florida manatees (*Trichechus manatus latirostris*) are aquatic herbivores with lissencephalic brains and a low encephalization quotient (O'Shea and Reep, 1990; Reep and O'Shea, 1990). Florida manatees have a body mass of approximately 756kg and a brain mass of approximately 364g (O'Shea and Reep, 1990). Despite their relatively small brain size, manatees possess tactile specializations including fields of facial vibrissae. Like rock hyraxes, manatees have tactile hairs distributed on the entire body as well, although manatees lack pelage fur, making vibrissae the only hair type found on the manatee body. Facial vibrissae are critically important in manatee feeding (specific vibrissae are everted and used in a caliper-like grasping behavior to bring food into the oral cavity) and in tactile exploration of the environment (Marshall et al., 1998a; Marshall et al., 1998b). Manatee body vibrissae are thought to function as a lateral line system, allowing manatees to detect currents and other hydrodynamic stimuli in their murky underwater habitat where visual cues are limited (Gaspard et al., 2013; Reep et al., 2011; Reep et al., 2002). Instead of barrels, the manatee cortex includes Rindenkerne, which are barrel-like clusters found in layer VI (rather than layer IV) (Dexler, 1912; Marshall and Reep, 1995; Reep et al., 1989). Rindenkerne are thought to receive inputs from vibrissae of the manatee face and body (Reep et al., 1989), and may process tactile stimuli together with low-frequency auditory stimuli through body vibrissae deflection underwater (Sarko and Reep, 2007).

TRIGEMINAL NUCLEI: The manatee brainstem includes large, lobulated principal sensory and spinal trigeminal nuclei (Sarko et al., 2007). Because barrelettes were not detected, somatotopic parcellation in these nuclei is thought to be

related to entire facial follicle fields, which work as functional groups, rather than distinctly related to individual vibrissae.

CUNEATE-GRACILE COMPLEX: Extensive somatotopic parcellation was evident in the cuneate and gracile nuclei which may be related to discrete functional representations of body vibrissae (Sarko et al., 2007). The caudal-most extension of the gracile nucleus – the presumptive fluke representation – appears to be disproportionately large in manatees, likely accommodating a large degree of inputs from vibrissae present on the fluke (Sarko et al., 2007). The fluke is thought to play a critical role in underwater navigation, potentially involving extensive sensorimotor feedback as manatees constantly adjust the angle of their fluke during movement.

TRENDS

VOLUMES OF BRAINSTEM SOMATOSENSORY NUCLEI ARE EVOLUTIONARILY PLASTIC

Perhaps the most readily apparent trend upon comparative analysis of the somatosensory brainstem is that the relative sizes of the cuneate-gracile complex, PrV, and SpV subnuclei are variable. This variability seems to reflect the sensory physiology of the animal such that brainstem representations of peripheral sensory structures appear hypertrophied in animals that rely heavily on the corresponding body areas for tactile exploration, and hypotrophied when that area is of less importance (i.e., less behaviorally relevant, with less sensitivity and commensurately less innervation). This is the case with the large trigeminal nuclei in the star-nosed mole, the expansive cuneate nucleus in the apes, and the enormous gracile nucleus in the manatee. While this link between the size of the brainstem nucleus and some measure of the functional capacity of the body region is likely broadly applicable, a more nuanced analysis is not feasible with the current data. For example, is the absolute size of the cuneate directly related to the tactile acuity of the hand by a calculable factor? Does this same factor apply for other body regions in the same animal? Does it apply to closely related animals? It seems likely that the relationship between size and function will be more complicated than a constant relationship and magnification factor.

Mice and rats have a particularly large SpVi with a clear barrelette pattern. However, the SpVi is not necessary for the formation of the expansive cortical barrel pattern seen in these animals, whereas the smaller PrV is required (Killackey and Fleming, 1985). The PrV in rats and mice is surprisingly small given its role in discriminative touch (in mice the PrV is 2/3 of the size of the SpVi, in rats it is 1/3)(Ashwell, 2013). This relative

pattern of a large SpVi and a small PrV does not hold true in species with different trigeminal sensory-motor specializations. For example, the California sea lion has highly innervated mystacial whiskers but in this species the PrV and the SpVi appear more similar in size (Sawyer et al., 2016).In the Florida manatee, highly innervated follicle fields used extensively in "oripulation" and discriminative touch appear to be represented in a large and parcellated PrV, but SpVi is relatively small and lacks clear subdivisions (Sarko et al., 2007). In the platypus, the PrV is nearly two times larger than the SpVi (Ashwell et al., 2006). In the star-nosed mole, not only does the PrV appear larger in volume than the SpVi, but the relative volumes of the representation of the tactile rays is not the same in the PrV and SpVi; the somatosensory fovea has a larger representation in the PrV than it does in the SpVi (Catania et al., 2011a; Sawyer et al., 2014). The difference in the volume of the ray representations in these nuclei might be related to specialized functions for those rays. While the sophisticated experiments conducted in traditional lab animals will be important to ultimately understanding the function of these nuclei, further comparative work, particularly those that include quantitative measurements (ex. (Ashwell et al., 2006; Baron, 1990; Stephan et al., 1981)) could be a useful way to generate hypotheses and assess evolutionary extremes. For example, if there is an animal in which the SpVo is particularly large or specialized, there may be an aspect of that animal's anatomy or behavior that will suggest a function for this subnucleus.

NEW NUCLEI ARE RARE

In this review, the sole example of a novel nucleus was related to a unique sensory modality in the infrared-sensing vampire bat (Kishida et al., 1984). This putative IR nucleus was located just lateral to the descending spinal trigeminal tract. While vampire bats are the only mammal known to detect infrared wavelengths, this ability has also evolved at least two separate times in snakes. Boidae (boas and pythons) and the Crotalinae snakes (pit vipers) also have a trigeminally-mediated infrared sense (Bullock and Cowles, 1952; Gracheva et al., 2010). In both of these groups, the putative IR nucleus is located in nearly the same position as in the vampire bat (Molenaar, 1974; Molenaar, 1978). It is remarkable that a very similar location for the brainstem representation has independently evolved three times. However, a novel sensory modality is not sufficient to result in a novel nucleus. The platypus, and to a lesser extent the echidnas, are remarkable mammals in that they have electroreceptive sensory organs. In these cases, the novel sense mediated by the trigeminal nerve is melded into trigeminal brainstem somatosensory areas. The trigeminal brainstem nuclei of the platypus is large, but there are not separate nuclei for

mechanosensation and electrosensation. It would be interesting to know if the reported electrosensory abilities of dolphins is supported by a dedicated brainstem nucleus (Czech-Damal et al., 2012).

PARCELLATION OF TACTILE NUCLEI IS COMMON IN THE BRAINSTEM

The most stunning anatomically visible somatotopic maps represent a sensory surface with distinct breaks. Be it the digits on a hand, or the punctate distribution of whisker follicles on the snout of a rodent, both have central nervous system representations where cell-sparse septa mark the boundaries of the cell-dense representations of sensory surfaces. This clear organizational pattern demonstrates how the peripheral and central somatosensory systems faithfully match each other as they convey tactile stimuli upstream. Every new example of topographical organization adds more support to this view. However, science progress not through adding support to a hypothesis, but through testing it's critical predictions. Thus, it would be interesting to further investigate the representation of animals with fused limbs, such as the flipper of the sea lion, to better understand why and where septa form if there is not a clear break in the tactile surface.

One recent new example of somatotopic mapping in the brainstem is the barrelettes in the brainstem of the California sea lion. Beyond discovering barrelettes in a new taxa, the barrelettes in the sea lion are notable for their large size. The barrelettes in the sea lion SpVc, SpVi, and PrV are 11, 6, and 10 times larger in cross-sectional area than those found in a mouse (Ma, 1991). While a seal would be expected to have a larger brainstem than a mouse, larger modules representing the whiskers are not a foregone conclusion. A larger brain must overcome the challenge of needing progressively thicker and longer connections to link areas that are farther apart (Striedter, 2005). These wiring challenges increase exponentially with brain size. Increasing the number of similarly sized functional areas is one way to mitigate this problem (Kaas, 2000). It has been suggested that some cortical modules (e.g., barrels in primary somatosensory cortex, blobs in primary visual cortex, entorhinal clusters, and modules in the dolphin insular cortex) all have a similar cross-sectional area despite the range of brain sizes these structures are found in (Manger et al., 1998). However, the presence of such large barrelettes in the sea lion brainstem does not fit the pattern of a size limit on modules. This may indicate that the brainstem and cortex evolve under different constraints.

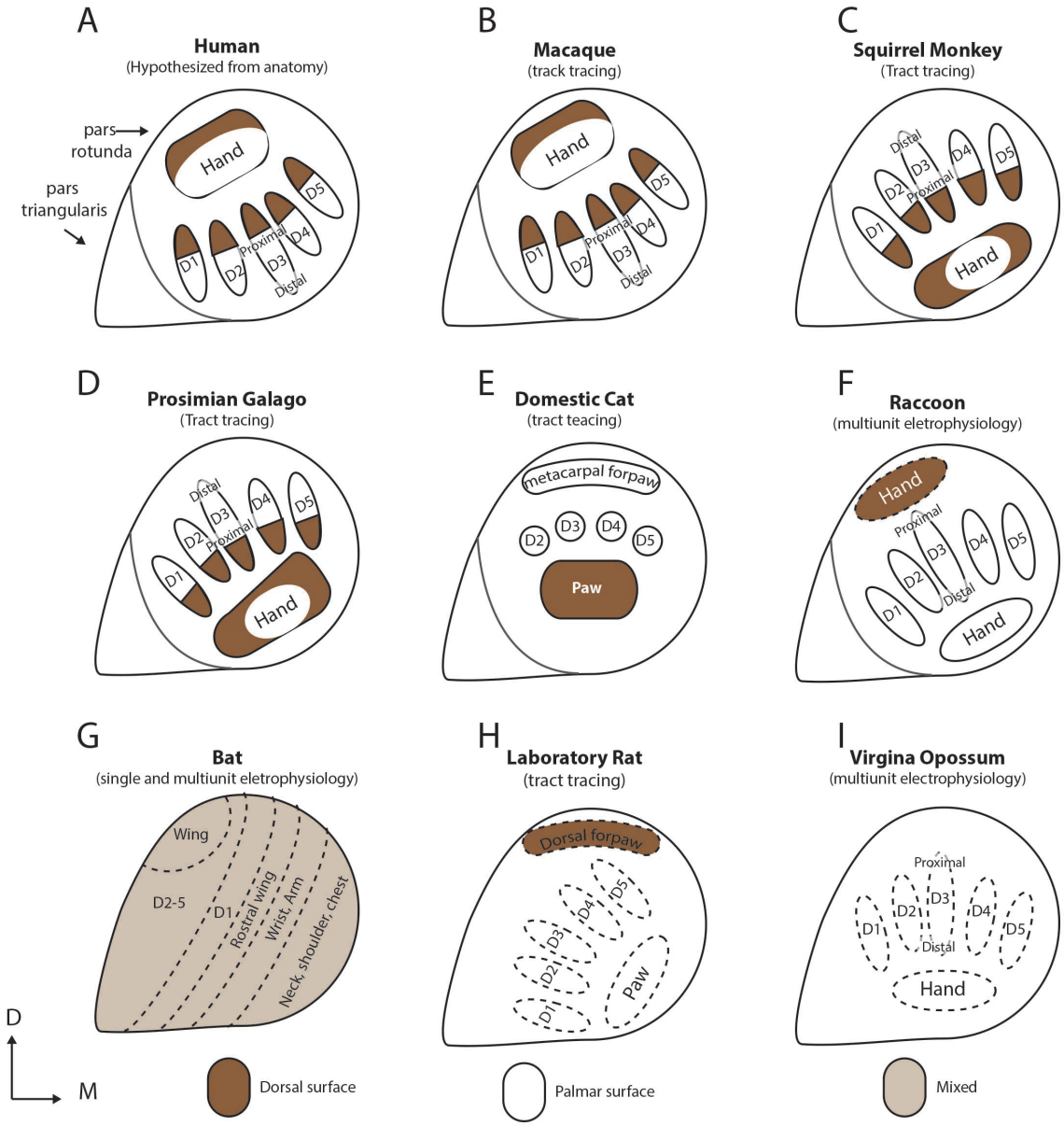
A
Human
(Hypothesized from anatomy)
pars rotunda
pars triangularis
Hand
D1
D2
D3
D4
D5
Proximal
Distal
B
Macaque
(track tracing)
C
Squirrel Monkey
(Tract tracing)
D
Prosimian Galago
(Tract tracing)
E
Domestic Cat
(tract teacing)
metacarpal forpaw
Paw
F
Raccoon
(multiunit eletrophysiology)
G
Bat
(single and multiunit eletrophysiology)
Wing
D2-5
D1
Rostral wing
Wrist, Arm
Neck, shoulder, chest
D
M
Dorsal surface
H
Laboratory Rat
(tract tracing)
Dorsal forpaw
Palmar surface
I
Virgina Opossum
(multiunit electrophysiology)
Mixed

Fig. 10. A schematic summary of the reported organization of the pars rotunda in the cuneate nucleus in several species, showing that the orientation of the somatopographic map appears to vary between species. This Figure is based off of Figure 13 in Florence, Wall and Kaas (1991), but updated to include new information. The species and the main method used to determine somatotopy are displayed on the Figure. The boundary between the pars rotunda and the pars triangularis is marked by a dotted line for those species in which this boundary was defined. **A**: A human (Florence, Wall and Kaas, 1989). **B:** A macaque monkey (Florence, Wall and Kaas, 1989). **C:** A squirrel monkey (Florence, Wall and Kaas, 1991). **D**: A prosimian galago (Strata, Coq, Kaas, 2003). **E**: A domestic cat (Nyberg, 1988). **F**: A raccoon (Johnson et al. 1968). **G**: A bat (little red flying fox) (Martin 1993). **H**: A laboratory rat (Maslany, Crockett and Egger, 1991). **I**: A Virginia opossum (Hamilton and Johnson, 1973). D = dorsal, M = medial.

ORIENTATION OF FUNCTIONAL SUBDIVISIONS WITHIN THE CUNEATE NUCLEUS MAY BE PLASTIC

Many different somatotopic maps of the cuneate nucleus have been reported. Some of these are summarized in Figure 10. The extent of variations seen, if correct, is anomalous for central nervous system somatosensory areas. In all mammals in which the somatosensory cortex has been mapped, only bats exhibit an unusual somatotopic organization (Calford et al., 1985). Furthermore, in the brainstem, the only reported variation of the orientation of the face representation is a slight rotation in the PrV of the star-nosed mole, which is likely related to the large size of that nucleus (Catania et al., 2011a). Other areas do not appear to change as much as the cuneate nucleus.

One explanation may be that at least some of the reported variation would not hold up under further studies with different methods. *In vivo* electrophysiological mapping of small nuclei is problematic because it is difficult to accurately localize and target the electrode during recording, and recording locations must be verified through electrolytic lesions relative to cytoarchitectural boundaries. Neural tract tracing can be more anatomically precise. In addition, the cuneate nucleus is a three-dimensional structure, which adds a level of complexity to mapping the somatotopy. Comparing the cuneate nucleus at different rostro-caudal extents will result in imprecise characterization. These challenges are likely responsible for some of the conflicting reports seen in well-studied animals (Maslany et al., 1991; Nord, 1967), and should be considered before accepting a somatotopic map for a species from just a single source.

However, some of the reported variations are well-supported, such as the inversion of the orientation of the hand representation between the new-world monkeys and the macaques. It is also interesting that the orientation of the digits in raccoons appears similar to macaques. Given the remarkable stability of the organization of the brainstem, these change in orientation stands out. The functional impact of this change in the somatotopy is unknown, and would be an interesting area for future research.

CONCLUSIONS

The basic architecture of the somatosensory brainstem is recognizable within, and even beyond, the mammal group. The stability of the architecture of the mammalian brainstem has led to the hypothesis that variations from the stereotypical mammalian plan are a reflection of the animal's adaptation for its environmental niche (Johnson, 1980; Taber, 1961; Tilney, 1927). This can be seen repeatedly in the individual examples we

highlighted in this chapter. Efforts to add to this understanding could focus on 1) exemptions to normal trends, such as the addition of new nuclei or a change in the orientation of the representation 2) sampleing from poorly represented groups and 3) obtaining quantitate measurements when possible, or if they must be qualitative making an explicit comparison back to an animal with more thoroughly documented anatomy.

ACNKOWLEDGMENTS

We thank the many students and workers of Jon Kaas' laboratory, who over the years processed many of the sections presented here. We also thank Roger Reep, for the sections presented here that were part of his laboratories collection.

REFERENCES

Abbie, A. A. (1934). The Brain-Stem and Cerebellum of Echidna aculeata. *Philosophical Transactions of the Royal Society of London B: Biological Sciences* **224**, 1-74.

Ashwell, K. W., Hardman, C. D. and Paxinos, G. (2006). Cyto- and chemoarchitecture of the sensory trigeminal nuclei of the echidna, platypus and rat. *J Chem Neuroanat* **31**, 81-107.

Ashwell, K. W. S. (2010). The neurobiology of Australian marsupials. Cambridge: Cambridge University Press.

Ashwell, K. W. S. (2013). Neurobiology of monotremes : brain evolution in our distant mammalian cousins. Collingwood, VIC: CSIRO Publishing.

Astrom, K. E. (1953). On the central course of afferent fibers in the trigeminal, facial, glossopharyngeal, and vagal nerves and their nuclei in the mouse. *Acta physiol. scand* **29**, 209-320.

Bachteler, D. and Dehnhardt, G. (1999). Active touch performance in the Antillean manatee: evidence for a functional differentiation of facial tactile hairs. *Zoology* **102**, 61-69.

Badlangana, N. L., Bhagwandin, A., Fuxe, K. and Manger, P. R. (2007). Distribution and morphology of putative catecholaminergic and serotonergic neurons in the medulla oblongata of a sub-adult giraffe, Giraffa camelopardalis. *J Chem Neuroanat* **34**, 69-79.

Baron, G. S., H.; Frahm, H. D. (1990). Comparison of brain structure volumes in Insectivora and primates. IX. Trigeminal complex. *J Hirnforsch* **31**, 193-200.

Belford, G. R. and Killackey, H. P. (1979). Vibrissae representation in subcortical trigeminal centers of the neonatal rat. *J Comp Neurol* **183**, 305-21.

Belford, G. R. and Killackey, H. P. (1980). The sensitive period in the development of the trigeminal system of the neonatal rat. *J Comp Neurol* **193**, 335-50.

Bereiter, D. A., Hirata, H. and Hu, J. W. (2000). Trigeminal subnucleus caudalis: beyond homologies with the spinal dorsal horn. *Pain* **88**, 221-4.

Bininda-Emonds, O. R. P. (2000). Pinniped brain sizes. *Marine Mammal Science* **16**, 469-481.

Bosman, L. W., Houweling, A. R., Owens, C. B., Tanke, N., Shevchouk, O. T., Rahmati, N., Teunissen, W. H., Ju, C., Gong, W., Koekkoek, S. K. et al. (2011). Anatomical pathways involved in generating and sensing rhythmic whisker movements. *Front Integr Neurosci* **5**, 53.

Bouley, D. M., Alarcon, C. N., Hildebrandt, T. and O'Connell-Rodwell, C. E. (2007). The distribution, density and three-dimensional histomorphology of Pacinian corpuscles in the foot of the Asian elephant (Elephas maximus) and their potential role in seismic communication. *J Anat* **211**, 428-35.

Bullock, T. H. and Cowles, R. B. (1952). Physiology of an Infrared Receptor: The Facial Pit of Pit Vipers. *Science* **115**, 541-3.

Cajal, S. R. (1896). Beitrag zum Stndien der Medulla Oblongata, des Kleinhirns und des Ursprungs des Gehirnnerven. Leipzig: J.A. Barth.

Calford, M. B., Graydon, M. L., Huerta, M. F., Kaas, J. H. and Pettigrew, J. D. (1985). A variant of the mammalian somatotopic map in a bat. *Nature* **313**, 477-9.

Catania, K. C. (1995). Magnified cortex in star-nosed moles. *Nature* **375**, 453-4.

Catania, K. C., Catania, E. H., Sawyer, E. K. and Leitch, D. B. (2013). Barrelettes without barrels in the American water shrew. *PLoS One* **8**, e65975.

Catania, K. C., Hare, J. F. and Campbell, K. L. (2008). Water shrews detect movement, shape, and smell to find prey underwater. *Proc Natl Acad Sci U S A* **105**, 571-6.

Catania, K. C. and Kaas, J. H. (1995). Organization of the somatosensory cortex of the star-nosed mole. *J Comp Neurol* **351**, 549-67.

Catania, K. C. and Kaas, J. H. (1997). Somatosensory fovea in the star-nosed mole: behavioral use of the star in relation to innervation patterns and cortical representation. *J Comp Neurol* **387**, 215-33.

Catania, K. C., Leitch, D. B. and Gauthier, D. (2011). A star in the brainstem reveals the first step of cortical magnification. *PLoS One* **6**, e22406.

Catania, K. C. and Remple, M. S. (2002). Somatosensory cortex dominated by the representation of teeth in the naked mole-rat brain. *Proc Natl Acad Sci U S A* **99**, 5692-7.

Chadha, M., Moss, C. F. and Sterbing-D'Angelo, S. J. (2011). Organization of the primary somatosensory cortex and wing representation in the Big Brown Bat, Eptesicus fuscus. *J Comp Physiol A Neuroethol Sens Neural Behav Physiol* **197**, 89-96.

Chang, H.-T. (1944). High level decussation of the pyramids in the pangolin (Manis pentadactyla Dalmanni). *J Comp Neurol* **81**, 333-338.

Chang, H.-T. R., T., C. (1947). Organization of the dorsal columns of the spinal cord and their nuclei in the spider monkey. *J Anat* **81**, 140-149.

Christian, J. J. (1950). Behavior of the Mole (Scalopus) and the Shrew (Blarina). *Journal of Mammalogy* **31**, 281-287.

Crish, S. D., Rice, F. L., Park, T. J. and Comer, C. M. (2003). Somatosensory organization and behavior in naked mole-rats I: vibrissa-like body hairs comprise a sensory array that mediates orientation to tactile stimuli. *Brain Behav Evol* **62**, 141-51.

Culberson, J. L. (1987). Projection of cervical dorsal root fibers to the medulla oblongata in the brush-tailed possum, Trichosurus vulpecula. *Am J Anat* **179**, 232-42.

Czech-Damal, N. U., Liebschner, A., Miersch, L., Klauer, G., Hanke, F. D., Marshall, C., Dehnhardt, G. and Hanke, W. (2012). Electroreception in the Guiana dolphin (Sotalia guianensis). *Proc Biol Sci* **279**, 663-8.

Dammhahn, M. K., P. M. (2005). Social System of Microcebus berthae, the World's Smallest Primate. *International Journal of Primatology* **26**, 407-435.

Dehnhardt, G., Friese, C. and Sachser, N. (1997). Sensitivity of the trunk of Asian elephants for texture differences of actively touched objects. *ZEITSCHRIFT FUR SAUGETIERKUNDE* **62**, 37-39.

Dexler, H. (1912). Das Hirn von Halicore dugong Erxl: Wilhelm Engelmann.

Diamond, M. E., von Heimendahl, M., Knutsen, P. M., Kleinfeld, D. and Ahissar, E. (2008). 'Where' and 'what' in the whisker sensorimotor system. *Nat Rev Neurosci* **9**, 601-12.

Dubner, R. and Bennett, G. J. (1983). Spinal and trigeminal mechanisms of nociception. *Annu Rev Neurosci* **6**, 381-418.

Ebner, F. T. and Kaas, J. H. (2015). Somatosensory System. In *The Rat Nervous System* pp. 675-701 San Diego: Academic Press.

Edwards, L. F. (1937). Morphology of the forelimb of the mole (Scalops aquaticus, L.) in relation to its fossorial habits.

Fleagle, J. G. (2013). Primate adaptation and evolution. Amsterdam ; Boston: Elsevier/Academic Press.

Florence, S. L., Wall, J. T. and Kaas, J. H. (1988). The somatotopic pattern of afferent projections from the digits to the spinal cord and cuneate nucleus in macaque monkeys. *Brain Res* **452**, 388-92.

Florence, S. L., Wall, J. T. and Kaas, J. H. (1989). Somatotopic organization of inputs from the hand to the spinal gray and cuneate nucleus of monkeys with observations on the cuneate nucleus of humans. *J Comp Neurol* **286**, 48-70.

Fox, K. (2008). Barrel Cortex. New York: Cambridge University Press.

Friedman, C. and Leftwich, M. C. (2014). The kinematics of the California sea lion foreflipper during forward swimming. *Bioinspir Biomim* **9**, 046010.

Gaspard, J. C., 3rd, Bauer, G. B., Reep, R. L., Dziuk, K., Read, L. and Mann, D. A. (2013). Detection of hydrodynamic stimuli by the Florida manatee (Trichechus manatus latirostris). *J Comp Physiol A Neuroethol Sens Neural Behav Physiol* **199**, 441-50.

Glaser, N., Wieskotten, S., Otter, C., Dehnhardt, G. and Hanke, W. (2011). Hydrodynamic trail following in a California sea lion (Zalophus californianus). *J Comp Physiol A Neuroethol Sens Neural Behav Physiol* **197**, 141-51.

Godfrey, S. J. (1985). Additional observations of subaqueous locomotion in the california sea lion (Zalophus californianus). *Aquatic Mammals* **11**, 53-57.

Gracheva, E. O., Cordero-Morales, J. F., Gonzalez-Carcacia, J. A., Ingolia, N. T., Manno, C., Aranguren, C. I., Weissman, J. S. and Julius, D. (2011). Ganglion-specific splicing of TRPV1 underlies infrared sensation in vampire bats. *Nature* **476**, 88-91.

Gracheva, E. O., Ingolia, N. T., Kelly, Y. M., Cordero-Morales, J. F., Hollopeter, G., Chesler, A. T., Sanchez, E. E., Perez, J. C., Weissman, J. S. and Julius, D. (2010). Molecular basis of infrared detection by snakes. *Nature* **464**, 1006-11.

Grant, R. A., Haidarliu, S., Kennerley, N. J. and Prescott, T. J. (2013). The evolution of active vibrissal sensing in mammals: evidence from vibrissal musculature and function in the marsupial opossum Monodelphis domestica. *J Exp Biol* **216**, 3483-94.

Graur, D. H., D. G. (1994). Molecular evidence for the inclusion of cetaceans within the order Artiodactyla. *Molecular Biology and Evolution* **11**, 357-364.

Griffiths, M. (1978). The biology of the monotremes. New York: Academic Press.

Haight, J. R. (1988). Marsupials, Nervous System. In *Comparative Neuroscience and Neurobiology*, pp. 63-68: Birkhäuser Boston.

Hamilton, T. C. and Johnson, J. I. (1973). Somatotopic organization related to nuclear morphology in the cuneate-gracile complex of opossums Didelphis marsupialis virginiana. *Brain Res* **51**, 125-40.

Hatschek, R. S., H. (1902). Der hirstamm des Delphinus (Delphinus delphis). *rbeiten aus dem Neurologischen Institute an der Wiener Universitat* **9**, 1–117.

Henry, E. C., Remple, M. S., O'Riain, M. J. and Catania, K. C. (2006). Organization of somatosensory cortical areas in the naked mole-rat (Heterocephalus glaber). *J Comp Neurol* **495**, 434-52.

Henry, E. C., Sarko, D. K. and Catania, K. C. (2008). Central projections of trigeminal afferents innervating the face in naked mole-rats (Heterocephalus glaber). *Anat Rec (Hoboken)* **291**, 988-98.

Herrera, E. A. M., D. W. (1993). Aggression, dominance, and mating success among capybara males (Hydrochaeris hydrochaeris). *Behavioral Ecology* **4**, 114-119.

Hines, M. (1929). The Brain of Ornithorhynchus anatinus. *Philosophical Transactions of the Royal Society of London B: Biological Sciences* **217**, 155-287.

Huffman, K. J., Nelson, J., Clarey, J. and Krubitzer, L. (1999). Organization of somatosensory cortex in three species of marsupials, Dasyurus hallucatus, Dactylopsila trivirgata, and Monodelphis domestica: neural correlates of morphological specializations. *J Comp Neurol* **403**, 5-32.

Iwaniuk, A. N. and Whishaw, I. Q. (1999). How skilled are the skilled limb movements of the raccoon (Procyon lotor)? *Behav Brain Res* **99**, 35-44.

Jacquin, M. F., McCasland, J. S., Henderson, T. A., Rhoades, R. W. and Woolsey, T. A. (1993). 2-DG uptake patterns related to single vibrissae during exploratory behaviors in the hamster trigeminal system. *J Comp Neurol* **332**, 38-58.

Johnson, J. I. (1980). Morphological Correlates of Specialized Elaborations in Somatic Sensory Cerebral Neocortex. In *Comparative Neurology of the Telencephalon*, (ed. S. E. Ebbesson), pp. 423-447: Springer US.

Johnson, J. I., Jr., Welker, W. I. and Pubols, B. H., Jr. (1968). Somatotopic organization of raccoon dorsal column nuclei. *J Comp Neurol* **132**, 1-43.

Jurgens, K. D. (2002). Etruscan shrew muscle: the consequences of being small. *J Exp Biol* **205**, 2161-6.

Kaas, J. H. (1983). What, if anything, is SI? Organization of first somatosensory area of cortex. *Physiol Rev* **63**, 206-31.

Kaas, J. H. (2000). Why is Brain Size so Important:Design Problems and Solutions as Neocortex Gets Biggeror Smaller. *Brain and Mind* **1**, 7-23.

Killackey, H. P. and Fleming, K. (1985). The role of the principal sensory nucleus in central trigeminal pattern formation. *Brain Res* **354**, 141-5.

Kishida, R., Goris, R. C., Terashima, S. and Dubbeldam, J. L. (1984). A suspected infrared-recipient nucleus in the brainstem of the vampire bat, Desmodus rotundus. *Brain Res* **322**, 351-5.

Krubitzer, L., Manger, P., Pettigrew, J. and Calford, M. (1995). Organization of somatosensory cortex in monotremes: in search of the prototypical plan. *J Comp Neurol* **351**, 261-306.

Krubitzer, L. A. and Calford, M. B. (1992). Five topographically organized fields in the somatosensory cortex of the flying fox: microelectrode maps, myeloarchitecture, and cortical modules. *J Comp Neurol* **317**, 1-30.

Kürten, L. S., U. (1982). Thermoperception in the common vampire bat (Desmodus rotundus). *Journal of comparative physiology* **146**, 223-228.

Kürten, L. S., U.; Schäfer, K. (1984). Warm and cold receptors in the nose of the vampire bat Desmodus rotundas. *Naturwissenschaften* **71**, 327-328.

Laursen, L. and Bekoff, M. (1978). Loxodonta africana. *Mammalian Species*, 1-8.

Leitch, D. B., Sarko, D. K. and Catania, K. C. (2014). Brain mass and cranial nerve size in shrews and moles. *Sci Rep* **4**, 6241.

Ma, P. M. (1991). The barrelettes--architectonic vibrissal representations in the brainstem trigeminal complex of the mouse. I. Normal structural organization. *J Comp Neurol* **309**, 161-99.

Ma, P. M. and Woolsey, T. A. (1984). Cytoarchitectonic correlates of the vibrissae in the medullary trigeminal complex of the mouse. *Brain Res* **306**, 374-9.

Manger, P., Sum, M., Szymanski, M., Ridgway, S. H. and Krubitzer, L. (1998). Modular subdivisions of dolphin insular cortex: does evolutionary history repeat itself? *J Cogn Neurosci* **10**, 153-66.

Manger, P. R. and Pettigrew, J. D. (1996). Ultrastructure, number, distribution and innervation of electroreceptors and mechanoreceptors in the bill skin of the platypus, Ornithorhynchus anatinus. *Brain Behav Evol* **48**, 27-54.

Manger, P. R., Rosa, M. G. and Collins, R. (2001). Somatotopic organization and cortical projections of the ventrobasal complex of the flying fox: an "inverted" wing representation in the thalamus. *Somatosens Mot Res* **18**, 19-30.

Marshall, C. and Reep, R. (1995). Manatee cerebral cortex: cytoarchitecture of the caudal region in Trichechus manatus latirostris. *Brain Behav Evol* **45**, 1-18.

Marshall, C. D., Clark, L. A. and Reep, R. L. (1998a). The muscular hydrostat of the Florida manatee (Trichechus manatus latirostris): a functional morphological model of perioral bristle use. *Marine Mamm Sci* **14**, 290-303.

Marshall, C. D., Huth, G. D., Edmonds, V. M., Halin, D. L. and Reep, R. L. (1998b). Prehensile use of perioral bristles during feeding and associated behaviors of the Florida manatee (Trichechus manatus latirostris). *Marine Mamm Sci* **14**, 274-289.

Martin, R. L. (1993). Representation of the body surface in the gracile, cuneate, and spinal trigeminal nuclei of the little red flying fox (Pteropus scapulatus). *J Comp Neurol* **335**, 334-42.

Maseko, B. C., Patzke, N., Fuxe, K. and Manger, P. R. (2013). Architectural organization of the african elephant diencephalon and brainstem. *Brain Behav Evol* **82**, 83-128.

Maslany, S., Crockett, D. P. and Egger, M. D. (1991). Somatotopic organization of the dorsal column nuclei in the rat: transganglionic labelling with B-HRP and WGA-HRP. *Brain Res* **564**, 56-65.

Matsubayashi, H. B., E.; Kohshima, S. (2003). Activity and Habitat Use of Lesser Mouse-Deer (Tragulus javanicus). *Journal of Mammalogy* **84**, 234-242.

McGovern, K. A., Marshall, C. D. and Davis, R. W. (2015). Are vibrissae viable sensory structures for prey capture in northern elephant seals, Mirounga angustirostris? *Anat Rec (Hoboken)* **298**, 750-60.

Mercado III, E. (2014). Tubercles: what sense is there. *Aquat Mamm* **40**, 95-103.

Meredith, R. W., Janecka, J. E., Gatesy, J., Ryder, O. A., Fisher, C. A., Teeling, E. C., Goodbla, A., Eizirik, E., Simao, T. L., Stadler, T. et al. (2011). Impacts of the Cretaceous Terrestrial Revolution and KPg extinction on mammal diversification. *Science* **334**, 521-4.

Molenaar, G. J. (1974). An additional trigeminal system in certain snakes possessing infrared receptors. *Brain Res* **78**, 340-4.

Molenaar, G. J. (1978). The sensory trigeminal system of a snake in the possession of infrared receptors. I. The sensory trigeminal nuclei. *J Comp Neurol* **179**, 123-35.

Moore, J. D., Mercer Lindsay, N., Deschenes, M. and Kleinfeld, D. (2015). Vibrissa Self-Motion and Touch Are Reliably Encoded along the Same Somatosensory Pathway from Brainstem through Thalamus. *PLoS Biol* **13**, e1002253.

Murphy, W. J., Eizirik, E., Johnson, W. E., Zhang, Y. P., Ryder, O. A. and O'Brien, S. J. (2001). Molecular phylogenetics and the origins of placental mammals. *Nature* **409**, 614-8.

Nord, S. G. (1967). Somatotopic organization in the spinal trigeminal nucleus, the dorsal column nuclei and related structures in the rat. *J Comp Neurol* **130**, 343-56.

Noriega, A. L. and Wall, J. T. (1991). Parcellated organization in the trigeminal and dorsal column nuclei of primates. *Brain Res* **565**, 188-94.

Norris, K. S. and Sciences, A. I. o. B. (1966). Whales, Dolphins, and Porpoises: University of California Press.

Nowak, R. M. and Walker, E. P. (1991). Walker's mammals of the world. Baltimore: Johns Hopkins University Press.

Nweeia, M. T., Eichmiller, F. C., Hauschka, P. V., Donahue, G. A., Orr, J. R., Ferguson, S. H., Watt, C. A., Mead, J. G., Potter, C. W., Dietz, R. et al. (2014). Sensory ability in the narwhal tooth organ system. *Anat Rec (Hoboken)* **297**, 599-617.

O'Shea, T. J. and Reep, R. L. (1990). Encephalization quotients and life-history triats in the sirenia. *Journal of Mammalogy* **71**, 534-543.

Olds, N. and Shoshani, J. (1982). Procavia capensis. *Mammalian Species* **171**, 1-7.

Olszewski, J. (1950). On the anatomical and functional organization of the spinal trigeminal nucleus. *J Comp Neurol* **92**, 401-13.

Ostapoff, E. M. and Johnson, J. I. (1988). Distribution of cells projecting to thalamus vs. those projecting to cerebellum in subdivisions of the dorsal column nuclei in raccoons. *J Comp Neurol* **267**, 211-30.

Park, T. J., Comer, C., Carol, A., Lu, Y., Hong, H. S. and Rice, F. L. (2003). Somatosensory organization and behavior in naked mole-rats: II. Peripheral structures, innervation, and selective lack of neuropeptides associated with thermoregulation and pain. *J Comp Neurol* **465**, 104-20.

Peterson, R. S. B., G. A. (1967). The natural history and behaviour of the California sea lion. Stillwater, OK, USA: American Society of Mammalogists.

Pettigrew, J. D., Manger, P. R. and Fine, S. L. (1998). The sensory world of the platypus. *Philos Trans R Soc Lond B Biol Sci* **353**, 1199-210.

Qi, H. X. and Kaas, J. H. (2006). Organization of primary afferent projections to the gracile nucleus of the dorsal column system of primates. *J Comp Neurol* **499**, 183-217.

Ramamurthy, D. L. and Krubitzer, L. A. (2016). The evolution of whisker-mediated somatosensation in mammals: sensory processing in barrelless S1 cortex of a marsupial, Monodelphis domestica. *J Comp Neurol*.

Rasmussen, L. E. and Munger, B. L. (1996). The sensorineural specializations of the trunk tip (finger) of the Asian elephant, Elephas maximus. *Anat Rec* **246**, 127-34.

Reep, R. L., Gaspard, J. C., 3rd, Sarko, D., Rice, F. L., Mann, D. A. and Bauer, G. B. (2011). Manatee vibrissae: evidence for a "lateral line" function. *Ann N Y Acad Sci* **1225**, 101-9.

Reep, R. L., Johnson, J. I., Switzer, R. C. and Welker, W. I. (1989). Manatee cerebral cortex: cytoarchitecture of the frontal region in Trichechus manatus latirostris. *Brain Behav Evol* **34**, 365-86.

Reep, R. L., Marshall, C. D. and Stoll, M. L. (2002). Tactile hairs on the postcranial body in Florida manatees: a Mammalian lateral line? *Brain Behav Evol* **59**, 141-54.

Reep, R. L. and O'Shea, T. J. (1990). Regional brain morphometry and lissencephaly in the Sirenia. *Brain Behav Evol* **35**, 185-94.

Reeve, N. J. (1994). Hedgehogs. London: Hedgehogs.

Remple, M. S., Henry, E. C. and Catania, K. C. (2003). Organization of somatosensory cortex in the laboratory rat (Rattus norvegicus): Evidence for two lateral areas joined at the representation of the teeth. *J Comp Neurol* **467**, 105-18.

Roberts, T. J. (2005). Field guide to the small mammals of Pakistan. Karachi: Oxford University Press.

Sakurai, K., Akiyama, M., Cai, B., Scott, A., Han, B. X., Takatoh, J., Sigrist, M., Arber, S. and Wang, F. (2013). The organization of submodality-specific touch afferent inputs in the vibrissa column. *Cell Rep* **5**, 87-98.

Sarko, D. K., Johnson, J. I., Switzer, R. C., 3rd, Welker, W. I. and Reep, R. L. (2007). Somatosensory nuclei of the manatee brainstem and thalamus. *Anat Rec (Hoboken)* **290**, 1138-65.

Sarko, D. K. and Reep, R. L. (2007). Somatosensory areas of manatee cerebral cortex: histochemical characterization and functional implications. *Brain Behav Evol* **69**, 20-36.

Sarko, D. K. and Reep, R. L. (2013). Somatosensory representations in the central nervous system of rock hyraxes (Procavia capensis). . In *Society for Neuroscience Abstract*, pp. 173.15.

Sarko, D. K., Rice, F. L. and Reep, R. L. (2015). Elaboration and Innervation of the Vibrissal System in the Rock Hyrax (Procavia capensis). *Brain Behav Evol* **85**, 170-88.

Sawyer, E. K., Leitch, D. B. and Catania, K. C. (2014). Organization of the spinal trigeminal nucleus in star-nosed moles. *J Comp Neurol* **522**, 3335-50.

Sawyer, E. K., Liao, C. C., Qi, H. X., Balaram, P., Matrov, D. and Kaas, J. H. (2015). Subcortical barrelette-like and barreloid-like structures in the prosimian galago (Otolemur garnetti). *Proc Natl Acad Sci U S A* **112**, 7079-84.

Sawyer, E. K., Turner, E. C. and Kaas, J. H. (2016). Somatosensory brainstem, thalamus, and cortex of the California sea lion (Zalophus californianus). *J Comp Neurol* **524**, 1957-75.

Shigenaga, Y., Otani, K. and Suemune, S. (1990). Morphology of central terminations of low-threshold trigeminal primary afferents from facial skin in the cat--intra-axonal staining with HRP. *Brain Res* **523**, 23-50.

Shoshani, J., Kupsky, W. J. and Marchant, G. H. (2006). Elephant brain. Part I: gross morphology, functions, comparative anatomy, and evolution. *Brain Res Bull* **70**, 124-57.

Sikich, L., Woolsey, T. A. and Johnson, E. M., Jr. (1986). Effect of a uniform partial denervation of the periphery on the peripheral and central vibrissal system in guinea pigs. *J Neurosci* **6**, 1227-40.

Small, G. L. (1971). The blue whale. New York,: Columbia University Press.

Stephan, H., Baron, G. and Frahm, H. D. (2012). Insectivora: with a stereotaxic atlas of the hedgehog brain: Springer Science & Business Media.

Stephan, H., Frahm, H. and Baron, G. (1981). New and revised data on volumes of brain structures in insectivores and primates. *Folia Primatol (Basel)* **35**, 1-29.

Stephan, H. B., G.; Frahm, H. D. (2012). Insectivora: with a stereotaxic atlas of the hedgehog brain: Springer Science & Business Media.

Strata, F., Coq, J. O. and Kaas, J. H. (2003). The chemo- and somatotopic architecture of the Galago cuneate and gracile nuclei. *Neuroscience* **116**, 831-50.

Striedter, G. F. (2005). Principles of brain evolution. Sunderland, Mass.: Sinauer Associates.

Taber, E. (1961). The cytoarchitecture of the brain stem of the cat. I. Brain stem nuclei of cat. *J Comp Neurol* **116**, 27-69.

Tilney, F. (1927). The brain stem of Tarsius. A critical comparison with other primates. *J Comp Neurol* **43**, 371-432.

Tobias, P. V. (1971). The brain in hominid evolution: Columbia University Press.

Turnbull, B. G. and Rasmusson, D. D. (1987). Sensory innervation of the raccoon forepaw: 3. Cutaneous domains and organization of nerves innervating the raccoon forepaw. *Somatosens Res* **5**, 19-33.

Usunoff, K. G., Marani, E. and Schoen, J. H. R. (1997). The trigeminal system in man. Berlin ; New York: Springer.

Van Dyck, S. and Strahan, R. (2008). The mammals of Australia: New Holland Pub Pty Limited.

Verhaart, W. J. (1962). Anatomy of the brain stem of the elephant. *J Hirnforsch* **5**, 455-524.

Vincent, S. B. (1912). The functions of the vibrissae in the behavior of the white rat: University of Chicago.

Waite, P. M., Marotte, L. R. and Leamey, C. A. (1994). Timecourse of development of the wallaby trigeminal pathway. I. Periphery to brainstem. *J Comp Neurol* **350**, 75-95.

Waite, P. M., Marotte, L. R. and Mark, R. F. (1991). Development of whisker representation in the cortex of the tammar wallaby Macropus eugenii. *Brain Res Dev Brain Res* **58**, 35-41.

Welker, W. I. and Carlson, M. (1976). Somatic sensory cortex of hyrax (Procavia). *Brain Behav Evol* **13**, 294-301.

Weller, W. L. (1993). SmI cortical barrels in an Australian marsupial, Trichosurus vulpecula (brush-tailed possum): structural organization, patterned distribution, and somatotopic relationships. *J Comp Neurol* **337**, 471-92.

Wilson, D. E. and Reeder, D. M. (2005). Mammal species of the world : a taxonomic and geographic reference. Baltimore: Johns Hopkins University Press.

Wilson, R. B. (1933). The anatomy of the brain of the whale (Balaenoptera sulfurea). *J Comp Neurol* **58**, 419-480.

Windle, W. F. (1926). Non-bifurcating nerve fibers of the trigeminal nerve. *J Comp Neurol* **40**, 229-240.

Wise, L. Z., Pettigrew, J. D. and Calford, M. B. (1986). Somatosensory cortical representation in the Australian ghost bat, Macroderma gigas. *J Comp Neurol* **248**, 257-62.

Wohlert, D., Kroger, J., Witt, M., Schmitt, O., Wree, A., Czech-Damal, N., Siebert, U., Folkow, L. and Hanke, F. D. (2015). A Comparative Morphometric Analysis of Three Cranial Nerves in Two Phocids: The Hooded Seal (Cystophora Cristata) and the Harbor Seal (Phoca Vitulina). *Anat Rec (Hoboken)* **299**, 370–378.

Woolsey, T. A., Welker, C. and Schwartz, R. H. (1975). Comparative anatomical studies of the SmL face cortex with special reference to the occurrence of "barrels" in layer IV. *J Comp Neurol* **164**, 79-94.

Woudenberg, R. A. (1970). Projections of mechanoreceptive fields to cuneate-gracile and spinal trigeminal nuclear regions in sheep. *Brain Res* **17**, 417-37.

Xu, J. and Wall, J. T. (1996). Cutaneous representations of the hand and other body parts in the cuneate nucleus of a primate, and some relationships to previously described cortical representations. *Somatosens Mot Res* **13**, 187-97.

Xu, J. and Wall, J. T. (1999). Functional organization of tactile inputs from the hand in the cuneate nucleus and its relationship to organization in the somatosensory cortex. *J Comp Neurol* **411**, 369-89.

Yablokov, A. V. B., V. M.; Borisov, V. I. (1974). Whales and dolphins: Joint Publications Research Service.

Yu, C., Derdikman, D., Haidarliu, S. and Ahissar, E. (2006). Parallel thalamic pathways for whisking and touch signals in the rat. *PLoS Biol* **4**, e124.

CHAPTER V

Conclusions and Future Directions

This dissertation is focused on the comparative anatomy of the trigeminal somatosensory pathways in mammals. This pathway mediates the sensation of touch arising from the face, including the tactile hairs, or whiskers, that are found on most mammals on their cheeks/upper lip areas. In rodents, this pathway has been the subject of a tremendous amount of research, both of the circuit in its own right and of the composition of each relay as an experimentally tractable system that can be used to investigate other aspects of nervous function. One reason the rodent trigeminal somatosensory system is so popular is that the punctate array of whiskers on the face is isometrically represented in a one-to-one fashion by anatomically-distinct units in the brainstem, thalamus, and cortex. My research addresses whether some of the principles we have learned about the neuroanatomical organization of this pathway in rodents, particularly this anatomically visible somatotopic map, can be extended to other mammalian nervous systems.

SOMATOSENSORY SYSTEM OF THE CALIFORNIA SEA LION

In Chapter II, I present results from one of the first histological investigation of the brain of any pinniped. The research presented there investigates the vibrissal follicles, the trigeminal nerve, and the somatosensory areas in the brainstem, thalamus, and cortex. I found three separate clusters of barrelette modules in the brainstem, each located in the same anatomical coordinates as they are found in laboratory rodents. The presence of modules in the brainstem of such a large animal suggests that basic properties organizing the brainstem architecture can scale up, at least within the range of a ~20 g mouse to a 300 kg adult male California sea lion. I found no evidence of distinct anatomical units in the thalamus or the cortex, but that should not be taken as proof they could not be found with variations to the methods used here. Future work could further investigate these areas.

In addition, this research unexpectedly uncovered a clearly subdivided and large cuneate nucleus. This is interesting because within somatosensory areas anatomical modules are often related to divisions in the sensory surface, such as seen for central representations of the digits of the primate hand (see Chapter V) or the rays of the tactile star of a star-nosed mole (see Chapter III). However, at least upon gross examination, the flipper surface of

the sea lion is not subdivided, which leads to the question of why there are distinct subdivisions in the cuneate flipper representation? The segmented flipper representation, if it holds up in further work, challenges the hypothesis that the septa represent breaks in the skin surface. Directly challenging hypotheses is the fastest way to make progress in science. Thus, further studying the representation of the flipper could be more informative to the principals of brain organization than delineating another example of a segmented surface in yet-unstudied animal would be.

Lastly, the pinnipeds as a whole are a group that should be interesting to neurobiologists for many reasons beyond the specifics about their somatosensory system that I have highlighted here. I believe that the nervous systems of pinnipeds deserve more research attention than they have garnered in the past, and I have delineated a few of those reasons below:

1. Pinnipeds have extraordinary sensory adaptations that allow them to function adroitly in terrestrial and aquatic environments, a feat that stresses sensory systems in many ways. The great difference in the viscosity of air and water challenges the somatosensory system to detect patterns of mechanical displacement. Meanwhile their visual system can accommodate from the dark depths of the ocean to the bright mid-day sun on shore, representing huge range in illumination and light frequency. Their ocular musculature also cope with the challenges of focusing light above and below water (Hanke et al., 2009). Like most mammals, their auditory system functions well for airborne signals. However, in pinnipeds, the auditory system also works underwater where sounds travel 4.3 times faster and the basic structure of the mammalian ear transduces sounds less well than in air (Reichmuth et al., 2013). Lastly, their vestibular system copes with a three-dimensional environment that few mammals face, with the exceptions of bats and other marine mammals.

2. Pinnipeds are one of four groups of mammals that have independently evolved a brain that is over 1000g, and as such, they provide an important non-primate example of how mammal brains become large (Manger et al., 2013). The other groups that have reached this mark are humans, elephants, and cetaceans. Of the non-human representatives, pinnipeds may be the most approachable animal for study. Pinnipeds are also a good choice because with 32 extant species that cover a range of brain sizes (the brain of a Phocid largha seal weighs 130g on average, while the brain of a southern elephant seal is about 1500g) that grant us many different states to study (Bininda-Emonds, 2000).

3. Pinnipeds have the greatest sexual dimorphism in body size of any mammal. For example, the average female southern elephant seal is about 550kg, while the males are about 6.3 times heavier. However, his brain is only 1.6 times greater in mass than hers (Bininda-Emonds, 2000; Fitzpatrick et al., 2012). This provides an opportunity to examine how sexual selection may influence brain size and more generally, the allometric relationships between brain size and body size in extremely dimorphic species.

4. Pinnipeds show remarkable resilience to hypoxic stress. Hooded seal neurons in a cortical slice preparation can continue firing for up to an hour in 0% oxygen solutions, whereas the mouse neurons treated the same way are dead in 8 minutes (Folkow et al., 2008). Research in this domain has obvious implications to human health including understanding mechanisms that promote neural survival during times of oxygen deprivation.

5. All the northern elephant seals alive today are decedents of 20 to 100 animals that survived a severe bottleneck caused by human hunting (Bonnel and Selander, 1974; Weber et al., 2000). The living northern elephant seals have extraordinary genetic similarity. However, they have obvious differences in patterns of cortical folding (personal observation). Thus, they are a rare example of a large-brained animal where genetic variation is nearly perfectly controlled. Any intraspecific variation is likely attributable to the role of the environment in development.

SPINAL TRIGEMINAL NUCLEUS OF THE STAR-NOSED MOLE

Chapter III presents the results of research on the somatosensory brainstem of the star-nosed mole. This research directly addresses the assertion that the somatotopic maps in the principal sensory nucleus, the spinal trigeminal subnucleus interpolaris, and the spinal trigeminal subnucleus caudalis are proportionate to each other (Belford and Killackey, 1979). To my knowledge, this assumption had not previously been tested. However, given the hypotheses that the areas of the brainstem that have these maps are specialized for different functions, it seemed possible that they might have different proportions. In rodents, it is difficult to determine if the maps are directly proportional because the large number of whisker modules and the reality of practical histology (as opposed to the best sections that are presented in papers) make it unfeasible to follow an entire array of modules throughout their three dimensional representation (personal observation). However, this task was approachable in the representation of the tactile star of the star-nosed mole, with its array of only 11 appendages on each half of the nose. We found that the representation of the star in subnucleus interpolaris had different proportions than in the principal sensory nucleus; specifically the representation of the medial dorsal ray was larger in the former than in the latter.

The somatosensory star of the star-nosed mole is an unusually quantifiable somatosensory surface; from the Eimer's organs on the star's surface, to the myelinated fibers in the cranial nerve, to the volume of nervous tissue in each ray representation in the brainstem and cortex (Catania, 1995; Catania and Kaas, 1997; Sawyer and Catania, 2016; Sawyer et al., 2014) (and see appendix). Only one link from this pathway remains unmeasured – the thalamic representation in the ventral posterior medial nucleus. Investigation of that link would allow questions about the entire pathway to be addressed, such as where are the origins of "cortical" magnification? This remains a worthwhile goal for future research.

TRIGEMINAL SOMATOSENSORY SYSTEM IN THE PROSIMIAN GALAGO

In Chapter IV, I present an analysis of the trigeminal somatosensory pathway in a prosimian galago, the northern greater galago. Galagos, like most primates, do not have elaborate facial tactile hairs.

Although we examined the trigeminal somatosensory system in particular detail, one of the main findings of this work relates to the representation of the entire body surface. We report on an unusually clear representation of the entire body surface in the ventral posterior nucleus. This representation contained circular modules that appeared to represent the tactile hairs on the face, as well as clear septa marking the hand/face border and the hand/foot border. Within the hand representation were thin, lightly stained septa that separated five darkly stained stripes. As indicated by the cortciothalmic tracers, these stripes represented the individual fingers (see also (Qi et al., 2011)). In our opinion, the anatomical representation we discovered in the ventroposterior nucleus of the thalamus is one of the finest examples of a complete anatomically visible somatotopic map that is known and could be particularly informative of somatosensory organization in the primate lineage.

We found a parcellated SpVi, PrV, and distinct circular modules in the ventral posterior nucleus. These modules likely represented the microvibrissae near the lips of the galago, and not the longer mystacial vibrissae. In addition, cortical mapping experiments found that a large part of the cortical face representation was devoted to those microvibrissae, while it was difficult to locate any cortical receptive field for the mystacial whiskers. This was unexpected because in mice and rats the longer vibrissae have a larger representation in the thalamus and cortex (Haidarliu and Ahissar, 2001; Van der Loos, 1976; Woolsey and Van der Loos, 1970).

Our results make sense in light of the morphology of the whiskers and the galago's sensory requirements. The mystacial vibrissae are small and few in number compared to the sturdy hairs seen in other mammals.

However, the galago microvibrissae do not appear much different than what is seen in a mouse or rat; in all these animals they are short, thin, and in great abundance very close to the mouth (within a few millimeters). In mice and rats, these whiskers are used for very close tasks associated with object recognition, while the mystacial vibrissae are used to determine distance to objects (Brecht et al., 1997). Galagos, and most primates, have excellent vision that can report on objects that are a distance from the face. However, it is more difficult for an animal to visually focus on something directly at its snout. It is possible that primate vision has made the long-distance function of mystacial vibrissa less important but has left the importance of microvibrissa for very near tactiles tasks.

Regardless of if that evolutionary story is correct, the galago provided a lesson in not overlooking small sensory structures. The initial premise of studying the galago was to study an animal with a "mediocre" trigeminal system in order to better relate the impressive tactile arrays of the sea lions, star-nosed moles, and rodents to those from an organism more akin to our primate ancestry. In the end, we found that the tiny hairs near the mouth had an impressive representation in their own right and should not have been underestimated. In the future, it would be valuable to know more about how primates use their vibrissae, and if humans have a similar behavior.

LITERATURE REVIEW OF SOMATOSENSORY BRAINSTEM NUCLEI IN MAMMALS.

The main points of the literature review in Chapter V was to highlight trends in the organization of the somatosensory system in other animals, focusing on the brainstem somatosensory nuclei. These anatomical distinctions are clear from light microscopy-based histological preparations, the largest resource for information on the nervous system of unusual animals. This review highlighted four major trends, these were: (1) volumes of brainstem somatosensory nuclei are evolutionarily plastic, (2) new nuclei are rare, (3) parcellation of tactile nuclei is common in the brainstem, and (4) orientation of functional subdivisions within the cuneate nucleus may be plastic.

Another consequence of the literature review was to highlight the limited distribution of animals in which information about the anatomy of this system is available. Several orders were completely unrepresented. A further point that was made clear in this literature review was that many descriptions of tissue were limited to comparative statements such as "the nucleus appeared large." Statements of this nature rely on the expertise and personal biases of the investigator, which make them difficult to interpret and is especially frustrating when they are used to describe a rare species that is unlikely to be available again. This highlights the usefulness of quantitative

measurements and the recommendation to ground such comparisons to well-known "reference species" (Striedter et al., 2014).

CONSIDERATION OF METHODS

In my graduate career I have had the opportunity to study some of the largest and some of the smallest mammalian brains, and I have come to recognize that this training is a rare in today's biology. While the previous pages have been almost entirely on the concepts and facts, I want to take a moment to share what I have learned about the methods of working with and processing brains from a variety of animals.

Large and small brains each present their own challenges. Large brains require much more effort to cut, space to store, reagents to process and time to reconstruct. Small brains are delicate, harder to manipulate, and any one mistake can damage the entire case. But, with a small brain there is also the comparative luxury that one person can feasibly do every step of processing every section of the tissue. In large brains, processing every section would require a team and a fortune. Instead of acquiring those, there is a common strategy of working with others to process only some sections. In my experience this meant one person cutting the brain into sections that were about 50 um thick, and another person histologically processing every fourth section (galagos) or tenth (sea lions) for a specific stain.

I have found the strategy of using only some sections more useful for the cortex, which does not seem to change substantially over those distances, than for subcortical structures, which do. Many of the subcortical structures I examined were of similar size no mater what animal I was examining (Fig. 1). This may explain why, despite the Kaas and Casagrande lab investigating the galago brain for decades, the anatomically visible somatotopic map I report on in Chapter IV had not been seen before. By only processing every fourth section, hints of the pattern were missed.

Another reason the pattern might not have been seen before is because there is more reluctance to experiment with cutting angle in a large brain than a small one. Convention, not biology, dictates sectioning brains into coronal, horizontal or sagittal planes. In my experience, the fear of ruining a case and wasting resources (including a labmate's time) keeps researchers true to those standards. Because the negatives of an error are greater with larger brains than with small ones, the larger a brain was the more experimentation felt discouraged.

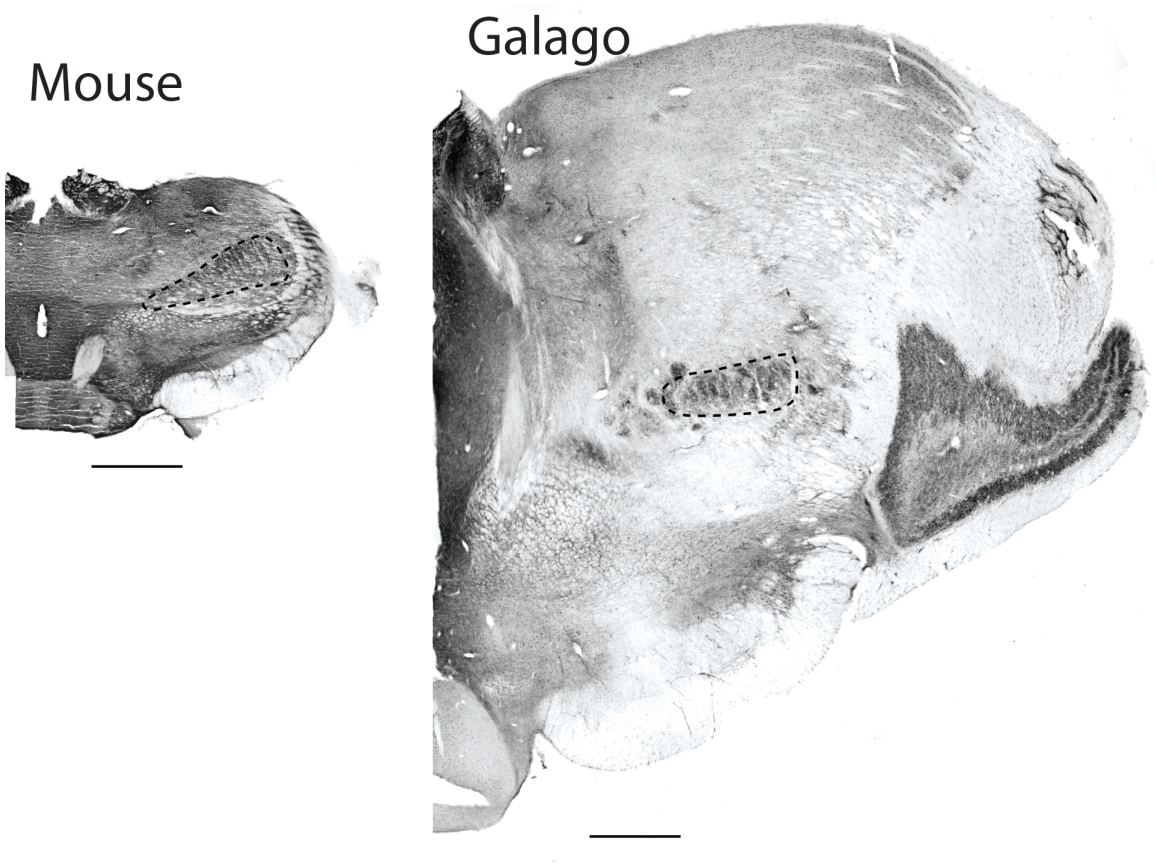

Fig. 1: Coronal sections of the thalamus of a mouse and a galago stained for vesicular glutamate transporter 2 presented at the same scale. The location of the whisker organization in the ventroposterior nucleus of the thalamus is outlined in the black dashed line. Within the outlined area pale vertical stripes that are the septa between the barreloids can be seen. Cutting the brain perpendicular to these stripes, reveals circular pattern of the barreloids. The dorso-ventral extent of this region is similar in these two species, yet they would likely be processed differently due to the overall size of the brain. Scale bar = 1 mm

In the future, high-resolution magnetic resonance images of the brains of unusual animals may better allow novel explorations of these more difficult large specimens. Digital information could be virtually sectioned, put back together, and resectioned with little cost. This could be used to generate hypotheses that could then be checked with more labor-intensive traditional histological investigations. Histological investigations could also be improved with serial block face imaging, which allows virtual resectioning of brains that have already been sectioned and stained (Vandenberghe et al., 2016).

OVERALL CONCLUSIONS

This research investigated the neuroanatomy of the trigeminal somatosensory system in a variety of mammals and specifically searched for the anatomically-distinct units that are sometimes visible in the many stations of this pathway. In the somatosensory brainstem, the presence of these modules was almost always present if the specimen was from the appropriate stage of development. While staging development in different species is beyond the scope of this work, roughly, if the whiskers had sprouted and the fur was just barely breaking the skin, I could almost always see distinct whisker representations in the brainstem (e.g. a seven day old postnatal mouse). I saw these patterns both in the species mentioned in chapter II-IV, as well as unpublished work on other species that I have worked with during my graduate career. In the ventroposterior nucleus of the thalamus, the presence of the pattern in the galago leads me to suspect a visible pattern is common in other animals, but it is likely to be small and most detectable at an unconventional angle that will be very difficult to find in other animals using only traditional histological methods. The somatosensory cortex appears to show great variation in the presence of anatomically-distinct modules.

Beyond individual species, comparative neuroanatomical analyses allow us to understand which variations represent common ways that the central nervous system changes over time and which variations are extraordinary. The strong power of comparative neurobiology lies in no single champion species but in phylogenetically-informed comparisons. This way of thinking could help focus the study of the evolution of the nervous system in the future.

REFERENCES

Belford, G. R. and Killackey, H. P. (1979). Vibrissae representation in subcortical trigeminal centers of the neonatal rat. *J Comp Neurol* **183**, 305-21.

Bininda-Emonds, O. R. P. (2000). Pinniped brain sizes. *Marine Mammal Science* **16**, 469-481.

Bonnel, M. L. and Selander, R. K. (1974). Elephant seals: genetic variation and near extinction. *Science* **184**, 908-9.

Brecht, M., Preilowski, B. and Merzenich, M. M. (1997). Functional architecture of the mystacial vibrissae. *Behav Brain Res* **84**, 81-97.

Catania, K. C. (1995). Magnified cortex in star-nosed moles. *Nature* **375**, 453-4.

Catania, K. C. and Kaas, J. H. (1997). Somatosensory fovea in the star-nosed mole: behavioral use of the star in relation to innervation patterns and cortical representation. *J Comp Neurol* **387**, 215-33.

Fitzpatrick, J. L., Almbro, M., Gonzalez-Voyer, A., Hamada, S., Pennington, C., Scanlan, J. and Kolm, N. (2012). Sexual selection uncouples the evolution of brain and body size in pinnipeds. *J Evol Biol* **25**, 1321-30.

Folkow, L. P., Ramirez, J. M., Ludvigsen, S., Ramirez, N. and Blix, A. S. (2008). Remarkable neuronal hypoxia tolerance in the deep-diving adult hooded seal (Cystophora cristata). *Neurosci Lett* **446**, 147-50.

Haidarliu, S. and Ahissar, E. (2001). Size gradients of barreloids in the rat thalamus. *J Comp Neurol* **429**, 372-87.

Hanke, F. D., Hanke, W., Scholtyssek, C. and Dehnhardt, G. (2009). Basic mechanisms in pinniped vision. *Exp Brain Res* **199**, 299-311.

Manger, P. R., Spocter, M. A. and Patzke, N. (2013). The evolutions of large brain size in mammals: the 'over-700-gram club quartet'. *Brain Behav Evol* **82**, 68-78.

Qi, H. X., Gharbawie, O. A., Wong, P. and Kaas, J. H. (2011). Cell-poor septa separate representations of digits in the ventroposterior nucleus of the thalamus in monkeys and prosimian galagos. *J Comp Neurol* **519**, 738-58.

Reichmuth, C., Holt, M. M., Mulsow, J., Sills, J. M. and Southall, B. L. (2013). Comparative assessment of amphibious hearing in pinnipeds. *Journal of Comparative Physiology A* **199**, 491-507.

Sawyer, E. K. and Catania, K. C. (2016). Somatosensory organ topography across the star of the star-nosed mole (Condylura cristata). *J Comp Neurol* **524**, 917-29.

Sawyer, E. K., Leitch, D. B. and Catania, K. C. (2014). Organization of the spinal trigeminal nucleus in star-nosed moles. *J Comp Neurol* **522**, 3335-50.

Striedter, G. F., Belgard, T. G., Chen, C.-C., Davis, F. P., Finlay, B. L., Güntürkün, O., Hale, M. E., Harris, J. A., Hecht, E. E. and Hof, P. R. (2014). NSF workshop report: discovering general principles of nervous system organization by comparing brain maps across species. *Brain Behav Evol* **83**, 1-8.

Van der Loos, H. (1976). Barreloids in mouse somatosensory thalamus. *Neurosci Lett* **2**, 1-6.

Vandenberghe, M. E., Herard, A. S., Souedet, N., Sadouni, E., Santin, M. D., Briet, D., Carre, D., Schulz, J., Hantraye, P., Chabrier, P. E. et al. (2016). High-throughput 3D whole-brain quantitative histopathology in rodents. *Sci Rep* **6**, 20958.

Weber, D. S., Stewart, B. S., Garza, J. C. and Lehman, N. (2000). An empirical genetic assessment of the severity of the northern elephant seal population bottleneck. *Curr Biol* **10**, 1287-90.

Woolsey, T. A. and Van der Loos, H. (1970). The structural organization of layer IV in the somatosensory region (SI) of mouse cerebral cortex. The description of a cortical field composed of discrete cytoarchitectonic units. *Brain Res* **17**, 205-42.

Appendix

Somatosensory organ topography across the star of the star-nosed mole (*Condylura cristata*)

This appendix is reproduced with permission from the published work by Sawyer, E. K. and Catania, K. C. 2016 Somatosensory organ topography across the star of the star-nosed mole (*Condylura cristata*). Journal of Comparative Neurobiology 524 (5) 917-929. It is unaltered in content.

ABSTRACT

Quantifying somatosensory receptor distribution in glabrous skin is usually difficult due to the diversity of skin receptor subtypes and their location within the dermis and epidermis. However, the glabrous noses of moles are an exception. In most species of moles, the skin on the nose is covered with domed mechanosensory units known as an Eimer's organs. Eimer's organs contain a stereotyped array of different mechanosensory neurons, meaning the distribution of mechanosensitive nerve endings can be inferred by visual inspection of the skin surface. Here we detail the distribution of Eimer's organs on the highly derived somatosensory star on the rostrum of the star-nosed mole (*Condylura cristata*). The star consists of 22 fleshy appendages, or rays, that are covered in Eimer's organs. We find that the density of Eimer's organs increases from proximal to distal along the length of the star's rays with a ratio of 1: 2.3: 3.1 from the surface nearest to the nostril, to the middle part of ray, to the ray tip, respectively. This ratio is comparable to the increase in receptor unit density reported in the human hand, from the palm to the middle of the digits, to the distal fingertips. We also note that the tactile fovea of the star nosed mole, located on the medial ventral ray, does not have increased sensory organ density, and we describe these findings in comparison to other sensory fovea.

INTRODUCTION

Investigations of somatosensory receptor arrangement in most skin surfaces require multiple visualization techniques and must account for distortions caused by cutting and staining tissue (Li et al., 2011; Miller et al., 1958; Nolano et al., 2003; Novotny and Gommert-Novotny, 1988). Because quantifying skin somatosensory receptors is

difficult, efforts to describe the topography of mechanoreceptor distribution lag behind similar observations in the visual system, where flattened retinal preparation have been used to determine photoreceptor distribution (Curcio et al., 1987; Curcio et al., 1990; Packer et al., 1989). Unlike the mechanoreceptors which densely innervate the fingertips, lips, and oral cavity of many vertebrates (Dixon, 1961; Halata and Munger, 1983; Pare et al., 2002), the somatosensory Eimer's (EOs) of the mole display distinctive morphology that is easily visible on the superficial sensory epithelium. The superficial shape of EOs on the glabrous rostrum of moles provides an opportunity to map sensory units on a tactile surface to a level of detail comparable to flattened retinal preparations.

EOs are domed papillae that house clusters of multiple mechanosensory cell types (Eimer, 1871). These organs are present on the noses of most members of the mole family (*Talpidae*) (Catania, 2000). However, star-nosed moles (*Condylura cristata*, Fig. 1A) have the greatest number of EOs, and individual EOs in this species are smaller in diameter than those of other species (Catania, 1995a). These EOs cover the entire surface of the star, which is composed of 22 extensions, or rays (See Fig. 1B for the ray numbering convention). EOs consist of a stereotyped arrangement of at least 4 kinds of mechanoreceptor endings, including a laminated corpuscle, a Merkel cell-neurite complex, a class of presumptive light-touch mediating free nerve endings, and a class of presumptive nociceptive free nerve endings (Marasco et al., 2006). The cellular anatomy of an EO of a star-nosed mole is shown in Figure 1C (Catania, 1995b; Catania, 1996). Externally, each EO of a star-nosed mole appears as a raised papilla with a dimple in the center (Fig. 1D, E). The highly specialized rostrum of the star-nosed mole is covered in these papillae, making this skin surface a star-shaped sheet of discrete somatosensory organs.

The star of the star-nosed mole is additionally noteworthy for the special properties of ray 11, the medial ventral ray. There is a behavioral preference to use this ray. For example when another part of the star touches a potential food item, the mole reorients its head and star so that ray 11 makes contact with the item prior to ingestion (Catania and Remple, 2004). Furthermore, the extensive use of ray 11 is reflected in the central nervous system where, despite the small surface area of the ray, its representation takes up 25 percent of the total star representation in primary somatosensory cortex (Catania and Kaas, 1997). In addition, cortical multiunit receptive fields are smaller on ray 11 than on other rays – 0.58 mm^2 on ray 11 compared to 0.82 mm^2 on the other rays – implying a difference in tactile resolution (Sachdev and Catania, 2002). For these reasons, ray 11 has been called a "somatosensory fovea." Sensory foveae have been described in other sensory systems. Often they are marked by a difference in tactile resolution (Sachdev and Catania, 2002). For these reasons, ray 11 has been called a

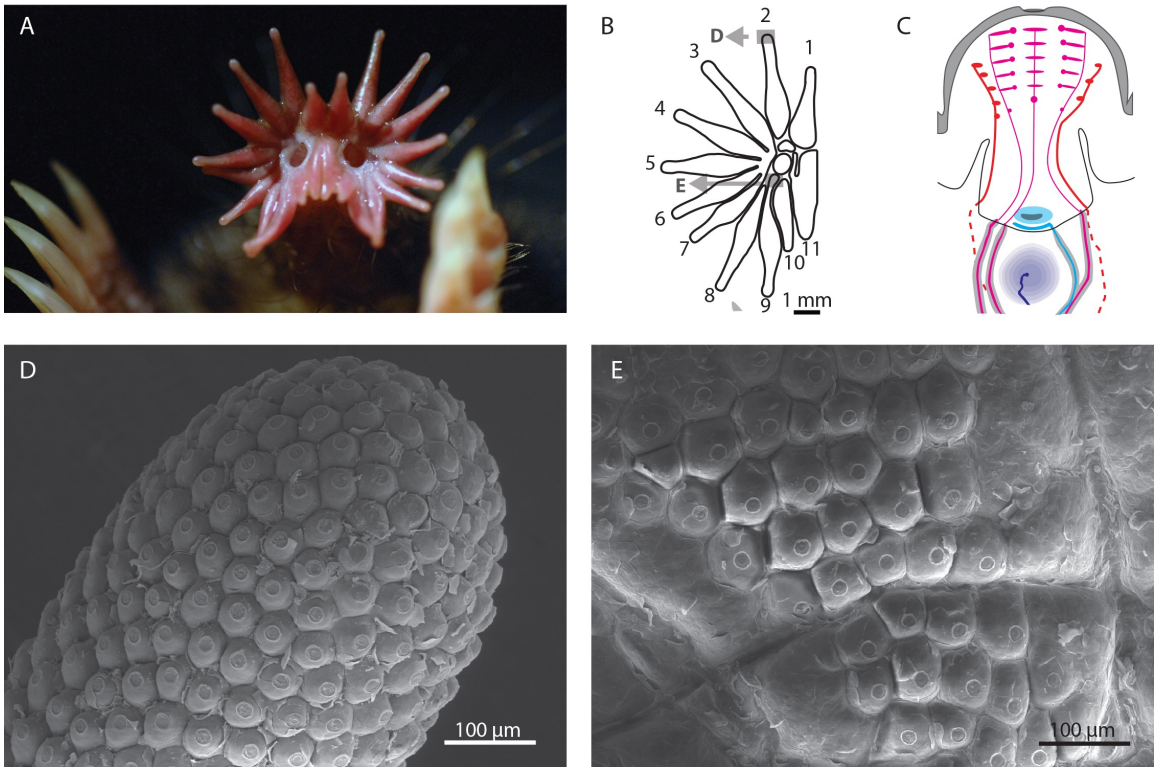

Fig. 1: The somatosensory surface of the star of a star-nosed mole (*Condylura cristata*). (A) The star of a star-nosed mole. (B) A schematic of the star. On the left, the rays are numbered according to the conventional numbering system. On the right two small grey rectangles show the location D and E. (C) A schematic of the dermal innervation of an Eimer's organ, the repeated somatosensory unit on the star based on Catania 1995c. Each Eimer's organ has one laminated corpuscle (dark blue) and one Merkel cell-neurite complex (light blue). The free-nerve endings are pink and red. There are seven or eight presumptive light touch mediating fibers (pink) and an unquantified number of presumptive pain-mediating fibers (red). (D) and (E) Scanning electron micrographs from the tip of a ray, and base of a ray, respectively.

"somatosensory fovea." Sensory foveae have been described in other sensory systems. Often they are marked by a higher density of sensory receptors compared to contiguous sensory surfaces (Bacelo et al., 2008; Pettigrew and Frost, 1985) yet no specialization in the arrangement of EOs has been found for ray 11 in star-nosed moles.

Variation in the size and density of EOs in the star-nosed mole has been previously noted but not thoroughly quantified (Catania, 1995b; Van Vleck, 1965). More specifically the EOs on the tips of the rays were reported to be smaller and more densely packed than those at the base of the rays (Fig. 1 C-E) and EOs on ray 11 have a density similar to that on other rays (Catania, 1995b; Van Vleck, 1965). Here we quantify the distribution of EOs on the forward-facing star surface to further test these observations. We chose to focus on only the rostral surface of the star (although EO's ring the distal portion of most rays) because the front of the star is the part that comes into most frequent contact with the substrate as the mole explores its environment (Catania and Remple, 2004). Also, the rostral surface of the star is where the majority of receptive fields were found and measured during electrophysiological recordings in somatosensory areas in the brainstem and cortex (Catania and Kaas, 1995; Catania et al., 2011; Sawyer et al., 2014). Our goals were to document the receptor distribution to a level not possible in other glabrous skin surfaces and to determine whether the distribution of EOs on ray 11 differed from that of the other rays.

MATERIALS AND METHODS

ANIMALS

No animals were sacrificed for this project. Star skin surfaces were obtained from stored samples from adult star-nosed mole (*Condylura cristata*) that were sacrificed for other research projects. Those projects conformed to the National Institutes of Health standards concerning the use and welfare of experimental animals and were approved by the Vanderbilt University Animal Care and Use Committee (Animal Welfare Assurance Number A-3227-01).

Stars with obvious scars and abrasions indicating natural use-dependent injury/damage were excluded. Fifteen stars were used in total. These were all from adult individuals that had been collected in Potter County, Pennsylvania (Pennsylvania Game Commission permit # 112-2011). Moles had been euthanized with an overdose of sodium pentobarbital (120 mg/kg) and transcardially perfused with phosphate buffered saline (PBS) (pH 7.3)

followed by 4% paraformaldehyde. The star had been removed and placed in 4% paraformaldehyde for at least 2 months before being retrieved for use in this project.

WHOLE STAR MEASUREMENTS

For all samples, stars were rinsed in PBS, and the muscle tissue around the star was trimmed away to leave only the glabrous star skin surface. For measurements of the shape and sizes of the rays, the star was placed on a light box and under glass slides to gently press the star flat. A photo of the star and a scale bar was taken from directly above the star with an Olympus TG-2 camera.

SCANNING ELECTRON MICROSCOPY (SEM)

Four stars were again rinsed in PBS, trimmed, and gently pressed flat. The sample was then dehydrated in an ethanol series (50%, 70%, 95% and 100%), critical point dried in an E3000 drier (Quorum Technologies, Guelph, ON, Canada), and coated with gold in a Cressington 108 sputter coater (Cressington Scientific Instruments Ltd, Watford, UK). Specimens were imaged in a Tescan Vega II scanning electron microscope (Tescan USA, Cranberry Twp, PA, USA).

IMAGE ANALYSIS

For measurements of the size and shapes of rays, the images were imported into Adobe Illustrator (version 17) and the rays were outlined using the pen tool. Rays were numbered as shown in Fig. 1C. The outline of the ray was defined at the medial end as areas where there was a break in the receptor sheet, or the where receptor sheet of one ray merged with another ray. Tissue with EOs was more opaque than areas where there were breaks in the receptor sheet, making the breaks visible as brighter areas when the star was illuminated from behind.

The image was imported into ImageJ (RRID:nif-0000-30467) and scaled to fit the scale in the image (Schneider et al., 2012). The rays were measured for area and circularity using the *analyze particles* function. Circularity, defined as 4π * area/perimeter^2, is a dimensionless value that describes how circular a shape is (Russ and DeHoff, 2000). A value of one indicates a perfect circle, while a value closer to zero indicates a more elongated shape. Circularity is used to describe biological shapes from neurons to maple leaves (Majumdar and Mallick, 2005; Royer et al., 2009).

The photography, outlining, and measurement of one half star was repeated three times. The coefficient of variation was 3.5% for area measurements and 2.5% for circularity calculations. For five stars, both the left and right sides were measured, but no laterality effect was detected so only one side of the remaining stars were measured.

For four stars SEM photomicrographs were analyzed for measurements of individual organs. In these preparations, only those organs on the forward face of the star and which were completely visible (judged by seeing the outline of the entire organ) were measured. Organs were defined as domes that contained the distinctive round dimple, indicating the mechanosensory column (Catania, 1995b). All the Eimer's organs on 5 rays were marked three times, and the coefficient of variation for the total number of EOs marked was 1.5%, indicating that we were consistently selecting the same EOs as being on the forward face of the star. The surface area of each EO on two half stars and the density of EO for four whole stars were measured.

To measure surface area, the SEM images were imported into Adobe Illustrator, and EOs were outlined using the pen tool. The image of all the outlined rays was then imported into ImageJ. The image was rotated so that the long axis of the ray was vertical, and only the *y* coordinate of the EOs was used for the analysis. The area of each EO and its *y* coordinate along the ray was found using the *analyze particles* function. The y coordinate was used to calculate "eccentricity", which we defined here as the distance from the most medial EO on the ray. Percent eccentricity was found for each ray using the following formula: percent eccentricity = 100 x (distance from base/ length of ray). Percent eccentricity facilitated comparisons between rays of different lengths.

To measure the density of EOs, SEM images were imported into Adobe Illustrator and a single dot was placed on the central disk-shaped region of every completely visible individual EO. The image of the dots was then imported into ImageJ. The heat density maps were created in ImageJ by importing this image, using a *mean filter*, and then implementing the *Look Up Table* feature for coloring. The raw image was also further analyzed for the density measurements used in the statistical analyses. For this, every EO not on a ray was placed in the "center" group. For every EO on a ray, the rays were divided into 20 sections with approximately equal numbers of EOs in each section. Each section was outlined and the area of each section found using ImageJ. The density was calculated as the number of EOs in that portion of the star divided by the area.

Statistical analysis was done on SPSS version 22 (RRID:rid_000042)

RESULTS

The areas of the rostral star surface varied between individuals, but the relative sizes of this surface of each ray on their respective stars were consistent. Ray 10 had the smallest surface area, and many rays were grouped as having similarly large surface areas. Rays 2, 8, and 9 were the most elongated (most eccentric), and Ray 1 was the most circular (least eccentric). EOs covered the star in a hexagonal array. EOs were larger and less densely packed toward the base of the rays than towards the tips.

SIZE AND SHAPE OF THE STAR: The area and circularity of the frontal surface area of the rays are shown in Table 1 and Figure 2. A one-way ANOVA revealed that there was an effect of ray on rostral surface area of the star ($F= (10, 110)=11.259$, $p <0.01$). A post-hoc Tukey's HSD revealed that ray 10 had the smallest surface area. The test grouped rays 1, 2, 3, 4, 8, and 11 as having the largest rostral surface area. The rostral surface area of a ray was related to the rostral surface area of the other rays on the star (e.g., a large ray 1 was from a star that also had large rays 2 through 11). This relationship was seen in that the area of each ray was positively related to the overall size of the rest of the star (e.g., the sum of the areas of the other 10 rays) so that $p < 0.01$ for all 11 linear regressions. The coefficient of variation for individual rays, which represents within-species variation, was between 15.0% and 21.4%, and was 15.6% for the overall size of the star. The body mass and length of the individual animals from which the stars originated were unknown, so no further analysis of how stars varied with body size could be completed.

Ray number also had a significant effect on circularity (ANOVA df=10, f=108.458, p=0.000). Ray 1 was the most circular, followed by rays 10 and 11. Not captured in these measurements is that the receptor sheet is continuous from ray 11 on one side and its contralateral counterpart. This is not the case for ray 1, the other midline ray. Rays 8, 9 and 2 had the most elongated shapes.

DENSITY OF EIMER'S ORGANS: In the four complete stars analyzed for EO density, EOs were most tightly packed at the tips of the rays and were less dense at the base of the rays and near the nostril (Fig. 3 A, C, E, G). When the density of EOs was plotted against the percent eccentricity, the curve of every ray on each star fit both a linear function and a cubic function ($p <0.01$). The r-squared for the linear equations were between 0.21 and 0.82, and for the cubic equations were between 0.51 and 0.90. In all cases the value of R-squared for the cubic function was

greater than the value of R-squared for the linear functions. The cubic function described a curve where EO density was lowest at the base of the ray and increased to an eccentricity of about 25% (Fig. 3B, D, F, H). The density then plateaued until increasing again in the most distal 10% of the ray. The shape of the curve was used as a guide to group the measurements of density into three parts on the ray and the base area near the nostrils. Pooling all stars and rays, the average density and standard deviation were 228.35 +/- 45.6 EO/mm^2 for the center of the star, 390.7 +/-74.6 EO/mm^2 for the base of the ray, 515.6 +/- 84.7 EO/mm^2 for the middle portion of the ray, and 718.0 +/- 106.3 EO/mm^2 for tip of the ray. Following these subdivisions, the ratio of densities for EOs at the center portion of the star (not on a ray) to the base of a ray (5-25% eccentricity) to the middle portion of the star (30-85% eccentricity) to the tip of the ray (90-100% eccentricity) was 1: 1.3: 2.6: 3.1.

Those groupings were used when comparing the density of the organs on different rays. A one-way ANOVA for EO density with ray as a factor showed no difference between the density of the rays when grouped by ray base, middle, and tip. There was no difference between rays when the areas were pooled. The average number of EOs on the surface of the rays was 8169 +/- 414.

SIZE OF EIMER'S ORGANS: The trends for EOs' size mirrored the findings for density. In all rays, EOs were largest at the base of the rays, appeared moderately sized throughout the middle half of the ray, and then smallest at the tip of the ray (Figs. 4, Table 2). The histograms in Figure 4 B and D show the frequencies of the area measurements of EOs in the two stars in either the center portion of the star, rays 1-10, or ray 11. The histograms show 1) the sizes of EO on the rays fall into a slightly right shifted distribution 2) within a star the distribution of sizes is similar between ray 11 and all the other rays 3) The size of the EOs not on a ray is not right shifted, and 4) EOs on star A had a larger range of sizes than EOs on star B. Some of this variation could be due to differences in tissue shrinkage during preparation for scanning electron microscopy.

In all rays the relationship between eccentricity and the surface area of the EOs was well described by a linear function (p <0.01 for all linear regressions, R-squared values ranging from 0.42 to 0.78). The shape of the curves again suggested a cubic relationship, which was also tested and found to be significant (p <0.01 for all cubic regressions, R-squared values ranging from 0.47 to 0.79). For each ray the R-squared values for the cubic functions were always greater than for the linear function.

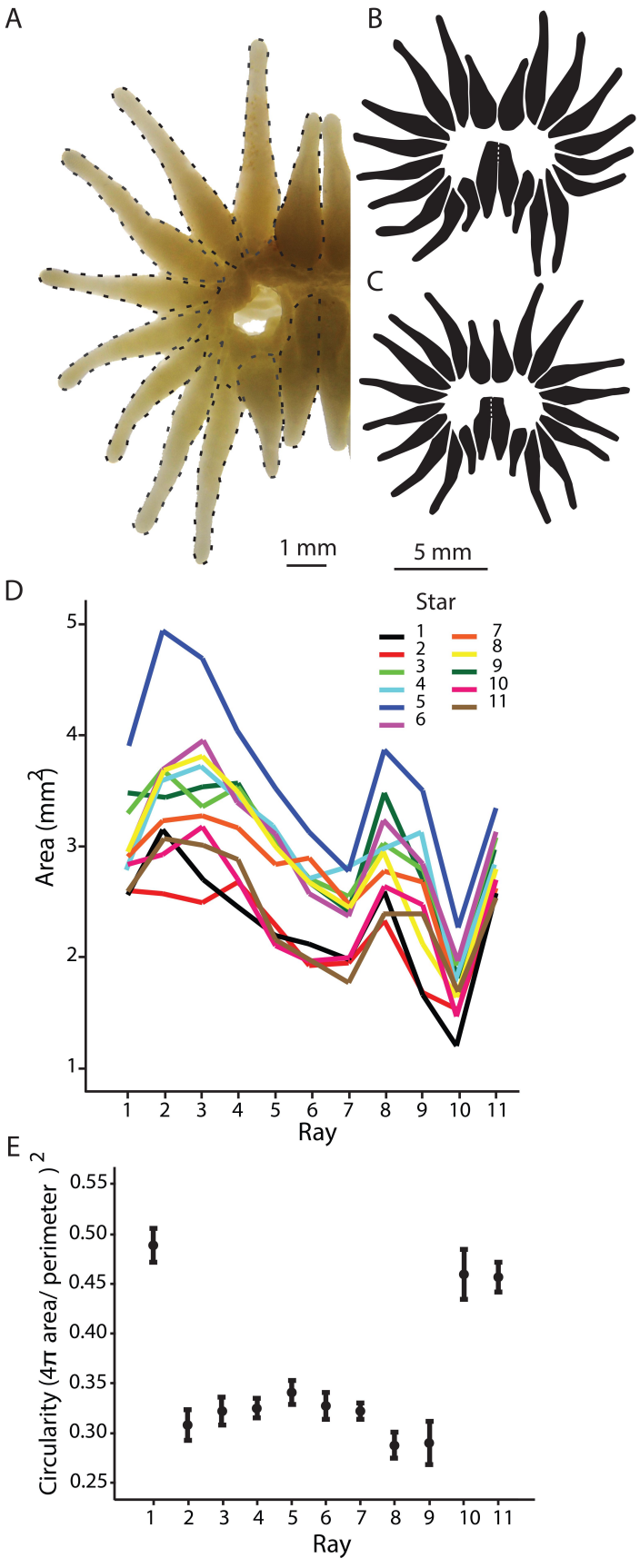
A
B
C
1 mm
5 mm
D
Star
1
2
3
4
5
6
7
8
9
10
11
Area (mm2)
Ray
E
Circularity (4π area/ perimeter 2)
Ray

Fig. 2: The shape and size of the rays. (A) An example image showing the definitions of the rays. (B) and (C): Two images of traced stars shown as example results. (D) A graph of the frontal surface area of individual rays from 11 different arrays of stars. (E): A graph of the average circularity measurements of the frontal surface of individual rays from 11 stars. The bars indicate the 95% confidence interval.

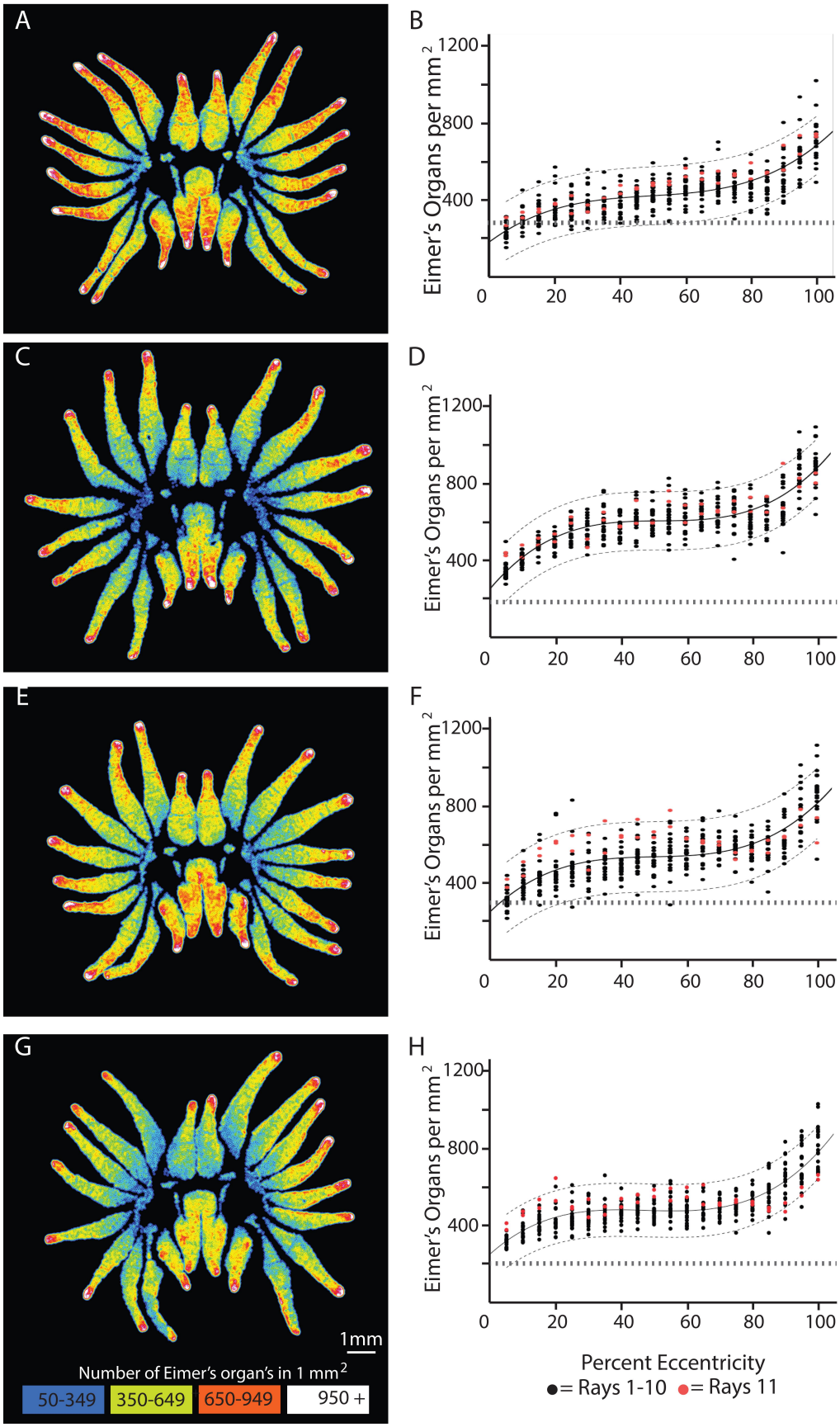
A
B
C
D
E
F
G
H
1mm
Number of Eimer's organ's in 1 mm2
50-349
350-649
650-949
950 +
Eimer's Organs per mm2
1200
800
400
0
20
40
60
80
100
Percent Eccentricity
●= Rays 1-10 ●= Rays 11

Fig. 3: The density of Eimer's organs on the star surface. (A), (C), (E), (G) Colored heat maps of the density of Eimer's organs on the flattened surface of four stars for stars A, B, C and D, respectively. (B), (D), (F), (H): The density of Eimer's organs plotted against the normalized distance from the base of the ray, for stars A, B, C, and D, respectively. Percent eccentricity= 100 x (distance from base/ length of ray). Solid lines are the best-fit cubic equation for all rays. Black dashed lines are 95% confidence interval around the best fit curve, and the grey dotted lines are the average density of the Eimer's organs on the base portion of the star around the nostrils. The density of organs on the somatosensory fovea, ray 11, is similar to that of other rays.

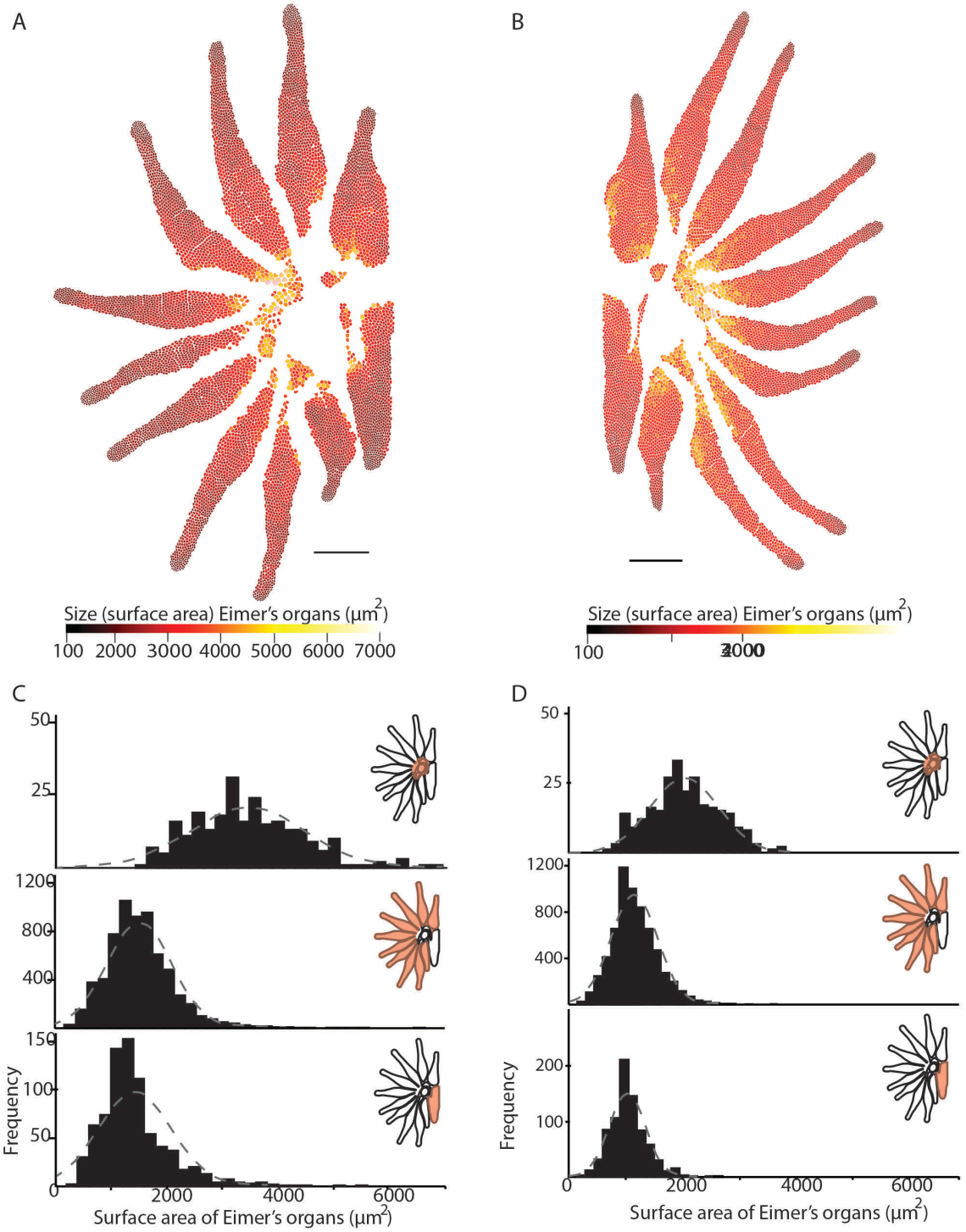
A
B
Size (surface area) Eimer's organs (µm2)
100 2000 3000 4000 5000 6000 7000
Size (surface area) Eimer's organs (µm2)
100
C
D
Frequency
Surface area of Eimer's organs (µm2)
Frequency
Surface area of Eimer's organs (µm2)

Fig. 4: The size (surface area) of the Eimer's organs on the flattened surface of of a sensory star.

(A) and (B) One half of the sensory star from case A and B, respectively. The size of the Eimer's organ is represented with color, as shown in the key below each image. (C) and (D): Histograms displaying the frequency of Eimer's organs with different surface areas in star A and B, respectively. In each column the topmost histogram displays the results for the base area of the star, the middle histogram for rays 1-10, and the bottom histogram for ray 11. The dotted line shows a normal distribution. Scale bar = 1 mm.

Ray		Area (mm^2)	Percent of total star area	Circularity
1	Mean (SD)	2.61 (0.4)	9.95 (0.54)	0.48(0.03)
	Coefficient of Variation	15.33	5.43	
2	Mean (SD)	2.93 (0.48)	11.15 (0.82)	0.29 (0.02)
	Coefficient of Variation	16.38	7.35	
3	Mean (SD)	2.91 (0.54)	11.05 (0.77)	0.31 (0.02)
	Coefficient of Variation	18.56	6.97	
4	Mean (SD)	2.74 (0.43)	10.43 (0.55)	0.32 (0.02)
	Coefficient of Variation	15.69	5.27	
5	Mean (SD)	2.34 (0.45)	8.87 (0.70)	0.32 (0.02)
	Coefficient of Variation	19.23	7.89	
6	Mean (SD)	2.09 (0.39)	7.93 (0.68)	0.31 (0.02)
	Coefficient of Variation	18.66	8.58	
7	Mean (SD)	2.00 (0.36)	7.58 (0.64)	0.31 (0.01)
	Coefficient of Variation	18.00	8.44	
8	Mean (SD)	2.55 (0.42)	9.69 (0.50)	0.28 (0.02)
	Coefficient of Variation	16.47	5.02	
9	Mean (SD)	2.2 (0.47)	8.32 (1.12)	0.28 (0.03)
	Coefficient of Variation	21.36	13.46	
10	Mean (SD)	1.52 (0.24)	5.79 (0.57)	0.43 (0.05)
	Coefficient of Variation	15.79	9.84	
11	Mean (SD)	2.4 (0.36)	9.18 (0.74)	0.44 (0.03)
	Coefficient of Variation	15.00	8.06	
Total	Mean (SD)	26.29 (4.1)		
	Coefficient of Variation	15.60		

Table 1: The area and shape of the surface of nasal rays of the star-nosed mole.

The area and shape of the surface of rays on one half of a star (6 right, 5 left). The average value is given with standard deviation in the parentheses. Circularity describes how like a circle the shape is. A value of one indicates a perfect circle, while a value closer to zero indicates a more elongated shape. The equation for circularity is: circularity = 4π*area/perimeter^2 .

		Base			Middle			Tip			Full ray		
Star	Ray	Mean Area (μm^2)	N	SD	Mean Area (μm^2)	N	SD	Mean Area (μm^2)	N	SD	Mean Area (μm^2)	N	SD
A	1	2358.37	190	737.72	1662.79	495	441.94	841.57	49	236.43	1788.02	734	656.05
A	2	2166.02	154	553.54	1519.92	641	403.07	676.48	90	184.66	1546.57	885	564.38
A	3	2223.8	192	536.05	1561.01	569	400.57	792.38	72	197.2	1647.34	833	569.09
A	4	2555.13	127	864.91	1473.07	522	399.79	709.58	71	242.59	1588.64	720	709.68
A	5	2357.19	108	657.3	1435.49	467	306.07	826.86	65	179.03	1529.22	640	562.44
A	6	2143.67	70	521.33	1307.67	375	314.15	634.4	65	162.05	1336.6	510	515.58
A	7	2202.81	108	588.89	1327.85	438	384.11	731.9	63	188.66	1421.36	609	578.56
A	8	2286.86	114	465.04	1534.85	462	412.07	748.97	72	259.63	1579.83	648	576.63
A	9	2738.45	40	594.91	1709.96	428	424.33	969.83	65	347.49	1696.88	533	575.57
A	10	1831.74	104	644.18	1448.35	306	420.24	585.1	41	147.7	1458.28	451	564.26
A	11	2138.42	125	632.67	1369.53	588	540.66	673.85	72	174.89	1428.16	785	648.23
A	Center										3389.2	255	996.65
A	Full star	2255.04	1332	659.29	1490.51	5291	429.31	744.98	725	238.45	1617.04	7603	709.43
B	1	1449.71	217	364.64	1207.31	529	343.28	502.84	49	146.66	1230.05	795	402.49
B	2	1500.63	150	345.08	1102.23	572	273.27	522.53	70	157.8	1126.45	792	371.16
B	3	1439.77	198	277.41	999.45	571	223.61	647.98	60	117.91	1079.18	829	320.42
B	4	1552.98	189	299.23	1086.2	439	242.22	592.45	66	159.58	1166.36	694	374.12
B	5	1620.01	144	408.27	1080.61	417	236.14	581.68	56	155.64	1161.21	617	403.3
B	6	1621.52	104	460.89	992.22	359	208.41	616.1	51	153.37	1082.23	514	401.85
B	7	1803.97	90	336.37	1046.77	328	240.8	524.83	60	148.65	1123.82	478	447.32
B	8	1801.66	91	380.24	1279.5	389	270.05	714.23	70	189.13	1293.95	550	406.77
B	9	1855.83	87	391.44	1321.13	386	320.35	747.85	67	222.96	1336.15	540	436.59
B	10	1768.98	101	361.6	1150.46	382	288.85	477	36	153.96	1224.11	519	434.61
B	11	1359.78	138	263.58	1020.1	605	273.52	582.67	58	120.94	1046.95	801	320.12
B	Center										2005.01	264	594.02
B	Full star	1573.41	1509	380.16	1111.34	4977	288.57	599.92	643	179.94	1193.09	7393	434.833

Table 2: The mean surface area of Eimer's organs on the star of the star-nosed mole.

The area, sample size, and standard deviation for Eimer's organs on various parts of the star. The base (percent eccentricity between 0 and 25), middle (percent eccentricity between 25 and 85), and tip (percent eccentricity between 85 and 100) groupings are based on the pattern of density change along the ray.

For star A, the largest EO was 26.6 times larger in area than the smallest; in star B, they were 25.5 times larger in area. However, the variation within two standard deviations of the mean was more modest, with EOs at the 97.5 percentile being 6.1 and 4.8 times larger than those at the 2.5 percentile for cases A and B, respectively. Values for the mean size of the Eimer's organs on the different regions of the ray (base, middle, and tip as defined in above) are shown in Table 2. The maximum size of EOs in case A was larger than in case B.

DISCUSSION

Our results take advantage of the punctate distribution of Eimer's organs to document the distribution of somatosensory units on a glabrous skin surface with great precision. We show that in the star-nosed mole the area of the dome of an EO usually varies over a factor of about 5.5 (but can vary over a larger range), with larger and less densely distributed EOs near the nostrils and smaller more densely distributed EOs near the tips of the rays. The variation of EO size and density could have effects on the sensitivity and resolving power of different portions of the sensory star. However, we found no evidence that the fovea-like properties of ray 11, which include smaller cortical receptive fields and greater cortical magnification in that ray compared to other rays, are related to the density of sensory organs on the star surface.

COMPARISON TO PREVIOUS WORK ON THE STAR

Variation in EO density has been recognized in the star surface of the star-nosed mole. Van Vleck suggested that EOs on the sides of the rays are larger than those on the flat, forward-facing portion of the star (1965). It has also been noted that the EOs at the tips of the rays are smaller in diameter, and thus denser, than those at the base of the rays (Catania, 1995). Our general findings that 1) EOs are larger and less dense at the base of the rays than at the tips of the rays, and 2) the distribution of EOs on ray 11 appears the same as on other rays, is consistent with previous reports (Catania, 1995b; Van Vleck, 1965). The current more detailed analysis allows for more comprehensive comparisons to other somatosensory sensory epithelia.

A priori mapping EOs on a star might suggest the distal tips of each ray, with their high density of EOs, as the likely candidate sites for elaborated somatosensation. However, previous behavioral, neuroanatomical, and electrophysiological investigations instead highlight the significance of ray 11 (Catania and Kaas, 1997; Catania and Remple, 2004). Together these results suggest that the behavioral significance and central nervous system

elaboration of ray 11 do not arise solely from the distribution of EOs on the receptor sheet. The results lead to two separate questions. First, why doesn't the fovea have more smaller and denser EOs? Second, why do the tips of the rays have smaller and more dense EOs.

WHY DOESN'T THE FOVEA HAVE THE HIGHEST CONCENTRATION OF EIMER'S ORGANS?

Fovea is Latin for "pit." This term was employed as an anatomical designation of the dip in the center of the retina, the *fovea centralis* in primates. The concept of a sensory fovea as a region of a sensory epithelium that is adapted for high spatial resolution has since been expanded and applied to other sensory systems. Outside of the visual system, sensory foveae have been reported in the auditory, somatosensory, and electrosensory systems (e.g., (Bacelo et al., 2008; Catania and Kaas, 1997; Corfield et al., 2011; Covey, 2005; Iggo et al., 1996; Muller et al., 1992; Pettigrew and Frost, 1985)). Definitions of the term *sensory foveae* vary, but usually include at least the following requirements: 1) A higher density of sensory receptors in the foveal area than the surrounds, 2) a specialized (disproportionally large) central representation, and 3) a sensorimotor system that directs the fovea to the stimuli of interest (Bacelo et al., 2008; Pettigrew and Frost, 1985). The extent to which the reported examples of sensory fovea fit all these points varies.

Star-nosed moles clearly meet the second and third criteria (Catania and Kaas, 1997), but, intriguingly, the sensory organs are equally dense on all rays. The acute sensory resolution does not seem to be reflected by sensory organ distribution,. This could be an underappreciated phenomenon in biology as identifying other examples would require a level of detailed neuroanatomical and physiological study that is rarely done in most species (but may also be seen in the auditory system of the big brown bat (Casseday and Covey, 1992; Covey, 2005; Dear et al., 1993)). In the case of the star-nosed mole, how localized differences in touch acuity can be supported by a sensory surface with a uniform sensory organ density is at least partly explained by the innervation of the star.

Differences in innervation of the rays, not the EO density itself, very likely explains part of the high-resolution properties of Ray 11. There is specialization of the sensory array that is not visible from the external surface of the star. This hypothesis is already supported by previous work (Catania and Kaas, 1997). Nerve counts show that ray 11 has a higher ratio of myelinated nerve fibers to EOs in comparison to other rays, with about seven fibers per EO on ray 11 compared to four fibers per EO on the others. This demonstrates that at the level of the

primary sensory axons there is less convergence in ray 11 than in the other rays, and hence an anatomical basis for greater resolution (Catania and Kaas, 1997).

Another reason that EOs might be of similar size on all the rays is if their size is dictated by a structural constraint of covering the surface of the star and not functional one. If the size of the EO were purely based on a structural constraint then we would not expect a difference in the size of EOs on ray 11. This idea is expanded upon in the next section.

Our finding of equal sensory organ density on all the rays does not fit neatly into a broad intra-modality intraspecific definition of a sensory fovea.. The example of the star-nosed mole shows that a strict criterion for a sensory fovea to have a higher density of sensory receptors at the foveal region than at other regions of the sensory epithelium could overlook interesting biology. This also highlights the challenges and utility of trying to define analogous specializations across diverse sensory systems and species. Definitions are perhaps most useful when they point out exceptions.

WHY DO THE TIPS OF THE RAYS HAVE THE HIGHEST CONCENTRATION OF EOS?

The distribution of EOs seen in the adult may reflect a mechanical constraint. The star is covered in a hexagonal array of Eimer's organs. Hexagonal arrays are a common solution to the problem how to completely cover a surface (Schwann, 1847). The hexagonal pattern naturally arises in proliferating epithelia (Gibson et al., 2006). This conformation has been described in sensory epithelia such as the array of hair cells in a cochlea, the ommatidia of compound eyes, the distribution of rods and cones on the retina, the distribution of chemosensory cells on the barbels of fish (Kiyohara et al., 2002), as well as in non-sensory surfaces such as the hairs on *Drosophila* wings, honeycombs, and the epidermises of plant leaves (Gibson et al., 2006). The problems of tiling a ray base and a ray tip may call for units of a different size.

Alternatively, it could be that the small organs are an adaptation for sensitivity (not resolution), and are clustered at the tips of the rays because these are areas specialized for highest sensitivity. Sensory fovea is a term used for a specialization for high spatial resolution, but there is no term for the area of the sensory epithelium that is optimal for high sensitivity. A dense distribution of sensory cells could be indicative of a specialization for high sensitivity ex. (de Busserolles et al., 2014). This idea is also supported by the internal structure of Eimer's organs. While the arrangement of mechanoreceptors within an EO is constant across the star (Catania, 1995b), smaller EOs

necessarily have less tissue surrounding the sensory nerve endings than larger EOs. This may endow the smaller EOs with better sensitivity to mechanical deformations. If this is the case than the high density of sensory organs at the tip of the ray could be a specialization for high sensitivity.

The high density of EOs at a location other than the high-resolution fovea suggests that observations of non-uniform distribution of mechanoreceptors taken alone is insufficient to distinguish a high-resolution fovea in the somatosensory system.

COMPARISON TO OTHER SENSORY SURFACES

A star-nosed mole EO is consistently composed of 7 to 8 presumptive light-touch-mediating free nerve endings, 1 lamellated corpuscle, 1 Merkel cell-neurite complex, and an un-quantified population of presumptive pain-mediating fibers (Catania, 1995b). The average EO density at the tips of the rays is 718 per mm^2 (+/- 106.2). Therefore the distal tip of each ray is predicted to have 718 lamellated corpuscles per mm^2, 718 Merkel cells per mm^2 and 5385 presumptive light touch-mediating free nerve endings per mm^2. This estimate for the density of nerve endings is greater than approximations and direct measurements from the vast majority of other vertebrate somatosensory surfaces. For example, it is also far denser than the measured values for mechanoreceptors in the primate hand. The density of Meissner's corpuscles in a macaque fingertip has been estimated at 57.6 per mm^2, Pacinian corpuscles at 1.2 per mm^2 (Pare et al., 2002), and free nerve endings at 50 to 57 per mm^2 (Arthur and Shelley, 1959; Novotny and Gommert-Novotny, 1988). Even the most densely-innervated tissue in humans, the cornea, contains only 525 terminals per mm^2 (He et al., 2010).

One of our findings was that the Eimer's organs were most dense at the tips of the rays. A concentration of mechanoreceptors at the distal end of an appendage is also found in other taxa. In echidnas, platypus, crocodilians, and several classes of birds the tip of the snout or bill has the highest density of somatosensory units (Cunningham; Cunningham, 2013; Iggo et al., 1996; Leitch and Catania, 2012; Manger and Pettigrew, 1996; Pettigrew and Frost, 1985; Swennen, 2004). Another relevant comparison is to the digits of the hand. The increase in Eimer's organ density along a ray is reminiscent of the distribution of mechanoreceptor units in the human hand. The density of mechanoreceptor units in the human hand has been estimated by systematically recording single unit receptive fields from the median nerve, which showed that the density of low threshold mechanoreceptor units increases from the palm to the tip of the finger (Johansson and Vallbo, 1979). There is a slight increase in unit density from the palm to

the base of the finger, and a sharp increase from the main part of the finger to the tip. The relative density of units in the palm to the main part of the finger and then to the fingertip is 1:1.6: 4.2 (Johansson and Vallbo, 1979). This ratio is similar to that found in the current study for the density of EO near the nostrils, in the middle part of the ray, and the ray tip of 1: 2.3: 3.1. In humans, the increase in unit density was attributed almost entirely to an increased density of Meissner's corpuscles at the tips of the fingers, while lamellated corpuscles retain a uniform distribution over the hand. In the mole's star, unlike in the primate's hand, lamellated corpuscles are more densely distributed at the tips of the appendages than at the base. The non-uniform distribution and high density of lamellated corpuscles could be related to differences in how moles and humans use their mechanosensory appendages to detect textures. Humans do so by moving their hands across a surface, and moles appear to perform this tasks by rapidly (up to 13 taps/sec) probing surfaces (Catania and Remple, 2004).

Lastly, the measurements of variation in the star can be compared to other species. Variation within a species is important to document because such heterogeneity within a species is the raw material from which natural selection works.

Within the somatosensory system in mammals, measures of variation within a species are limited, but include analyses of whisker distributions (Muchlinski, 2010; Van der Loos et al., 1984; Welker and Van der Loos, 1986), and histological studies of primate hands (Kelly et al., 2005). In other mammalian sensory systems, inter-individual variation has been documented in the composition of the retina (Curcio et al., 1990; Packer et al., 1989) and the morphology of the semicircular canal (Billet et al., 2012; Welker et al., 2009). In non-mammalian species, there is within-species variation in the distribution of the neuromasts of the lateral line system (Schmitz et al., 2008; Wark and Peichel, 2010), electrosensory pit organs (Peach, 2003), and the size and distribution of facets of compound eyes (Spaethe and Chittka, 2003).

Some studies have used high coefficients of variation (CVs) to suggest that a sensory system is under relaxed selection. The logic for this is that sensory systems that are vital for an animal's survival should be constrained by strong stabilizing selection, while less important sensory systems are free to vary more. For example, measurements of the morphology of the semicircular canals in sloths have CVs near 15%, which is larger than the CVs of closely related species (Billet et al., 2012). This suggests that vestibular system of the ponderous sloth is under less intense stabilizing selection than in closely related species (Billet et al., 2012). A similar interpretation of relaxed selection was suggested for inter-individual variation of 10%-20% for the number of

ampullary organs in some sharks and rays (Peach, 2003). Yet, the even greater degree of variation in the density of cones in primate retinas (up to 46% inter-individual variation in cone density in the human fovea) has not yet been ascribed an evolutionary explanation (Curcio et al., 1987; Curcio et al., 1990; Packer et al., 1989; Song et al., 2011). The inconsistency in interpretations is partly due to a lack of information about what are "normal" levels of within-species variation for different sensory systems and also due to the different focuses of the studies. Here we show that the active sensory surface of the star-nosed mole's tactile star varies in surface area by about 15%, and in number or EOs per star by about 5%, between adults. A likely explanation is that the somatosensory system is able to accommodate this level of peripheral variation and still produces a high functioning sensory system; it seems unlikely that the specialized tactile star is under minimal selection pressure. In the future it might be interesting to compare the level of variation found here to other somatosensory surfaces.

CONCLUSION

Our results document the distribution of somatosensory organs on a sensory epithelium with great precision. We find that the pattern of sensory organ density varies along the star-nosed moles' star appendages similarly to the organization of somatosensory surfaces and the distribution of specialized tactile organs of other animals, most notably along the fingers of humans. We calculate the nerve endings in the mole's star are remarkably dense, peaking at about 7180 nerve endings per mm^2. In addition, we find no direct evidence that the remarkable spatial resolution of the somatosensory fovea is related to the density of EOs, an intriguing finding for behaviorally significant sensory surfaces.

Our finding that the 11^{th} ray of the star-nosed mole does not have a higher concentration of EOs, despite meeting other important qualities of previous definitions of a sensory fovea is noteworthy. The 11^{th} ray of the star nosed mole is special for its role in high-resolution touch and in some ways it is like the pit in the center of the primate retina. In other ways, as shown here in the distribution of sensory organs, it is different. Our results show that focusing on sensory organ density alone is insufficient to assess the resolving power of a somatosensory epithelium. These results may be applicable to other vertebrate skin surfaces.

ACKNOWLEDGMENTS

We would like to thank Elizabeth Catania and Duncan Leitch for assistance trapping moles in the field, and Jon Kaas and Duncan Leitch for their input in the editing of this manuscript.

REFERENCES

Arthur, R. P. and Shelley, W. B. (1959). The innervation of human epidermis. *J Invest Dermatol* **32**, 397-411.

Bacelo, J., Engelmann, J., Hollmann, M., von der Emde, G. and Grant, K. (2008). Functional foveae in an electrosensory system. *J Comp Neurol* **511**, 342-59.

Billet, G., Hautier, L., Asher, R. J., Schwarz, C., Crumpton, N., Martin, T. and Ruf, I. (2012). High morphological variation of vestibular system accompanies slow and infrequent locomotion in three-toed sloths. *Proc Biol Sci* **279**, 3932-9.

Casseday, J. H. and Covey, E. (1992). Frequency tuning properties of neurons in the inferior colliculus of an FM bat. *J Comp Neurol* **319**, 34-50.

Catania, K. C. (1995a). A comparison of the Eimer's organs of three North American moles: the hairy-tailed mole (Parascalops breweri), the star-nosed mole (Condylura cristata), and the eastern mole (Scalopus aquaticus). *J Comp Neurol* **354**, 150-60.

Catania, K. C. (1995b). Structure and innervation of the sensory organs on the snout of the star-nosed mole. *J Comp Neurol* **351**, 536-48.

Catania, K. C. (1996). Ultrastructure of the Eimer's organ of the star-nosed mole. *J Comp Neurol* **365**, 343-54.

Catania, K. C. (2000). Epidermal sensory organs of moles, shrew moles, and desmans: a study of the family talpidae with comments on the function and evolution of Eimer's organ. *Brain Behav Evol* **56**, 146-74.

Catania, K. C. and Kaas, J. H. (1995). Organization of the somatosensory cortex of the star-nosed mole. *J Comp Neurol* **351**, 549-67.

Catania, K. C. and Kaas, J. H. (1997). Somatosensory fovea in the star-nosed mole: behavioral use of the star in relation to innervation patterns and cortical representation. *J Comp Neurol* **387**, 215-33.

Catania, K. C., Leitch, D. B. and Gauthier, D. (2011). A star in the brainstem reveals the first step of cortical magnification. *PLoS One* **6**, e22406.

Catania, K. C. and Remple, F. E. (2004). Tactile foveation in the star-nosed mole. *Brain Behav Evol* **63**, 1-12.

Corfield, J., Kubke, M. F., Parsons, S., Wild, J. M. and Koppl, C. (2011). Evidence for an auditory fovea in the New Zealand kiwi (Apteryx mantelli). *PLoS One* **6**, e23771.

Covey, E. (2005). Neurobiological specializations in echolocating bats. *Anat Rec A Discov Mol Cell Evol Biol* **287**, 1103-16.

Cunningham, S. J. C., I.; Potter, M.A.; Jensen, T. . Bill morphology of ibises suggests a remote-tactile sensory system for prey detection. *Auk* **127**, 308-316.

Cunningham, S. J. C., J. R.; Iwaniuk, N. A.; Castro, I.; Alley, M. R.; Birkhead, T. R.; Parsons, S. (2013). The Anatomy of the bill Tip of Kiwi and Associated Somatosensory Regions of the Brain: Comparisons with Shorebirds. *PLoS One* **8**, e80036.

Curcio, C. A., Sloan, K. R., Jr., Packer, O., Hendrickson, A. E. and Kalina, R. E. (1987). Distribution of cones in human and monkey retina: individual variability and radial asymmetry. *Science* **236**, 579-82.

Curcio, C. A., Sloan, K. R., Kalina, R. E. and Hendrickson, A. E. (1990). Human photoreceptor topography. *J Comp Neurol* **292**, 497-523.

de Busserolles, F., Fitzpatrick, J. L., Marshall, N. J. and Collin, S. P. (2014). The influence of photoreceptor size and distribution on optical sensitivity in the eyes of lanternfishes (Myctophidae). *PLoS One* **9**, e99957.

Dear, S. P., Fritz, J., Haresign, T., Ferragamo, M. and Simmons, J. A. (1993). Tonotopic and functional organization in the auditory cortex of the big brown bat, Eptesicus fuscus. *J Neurophysiol* **70**, 1988-2009.

Dixon, A. D. (1961). Sensory nerve terminations in the oral mucosa. *Arch Oral Biol* **5**, 105-14.

Eimer, T. (1871). Die Schnauze des Maulwurfes als Tastwerkzeug. *Arch. Mikr. Anat.* **7**, 181–191.

Gibson, M. C., Patel, A. B., Nagpal, R. and Perrimon, N. (2006). The emergence of geometric order in proliferating metazoan epithelia. *Nature* **442**, 1038-41.

Halata, Z. and Munger, B. L. (1983). The sensory innervation of primate facial skin. II. Vermilion border and mucosa of lip. *Brain Res* **286**, 81-107.

He, J., Bazan, N. G. and Bazan, H. E. (2010). Mapping the entire human corneal nerve architecture. *Exp Eye Res* **91**, 513-23.

Iggo, A., Gregory, J. E. and Proske, U. (1996). Studies of mechanoreceptors in skin of the snout of the echidna Tachyglossus aculeatus. *Somatosens Mot Res* **13**, 129-38.

Johansson, R. S. and Vallbo, A. B. (1979). Tactile sensibility in the human hand: relative and absolute densities of four types of mechanoreceptive units in glabrous skin. *J Physiol* **286**, 283-300.

Kelly, E. J., Terenghi, G., Hazari, A. and Wiberg, M. (2005). Nerve fibre and sensory end organ density in the epidermis and papillary dermis of the human hand. *Br J Plast Surg* **58**, 774-9.

Kiyohara, S., Sakata, Y., Yoshitomi, T. and Tsukahara, J. (2002). The 'goatee' of goatfish: innervation of taste buds in the barbels and their representation in the brain. *Proc Biol Sci* **269**, 1773-80.

Leitch, D. B. and Catania, K. C. (2012). Structure, innervation and response properties of integumentary sensory organs in crocodilians. *J Exp Biol* **215**, 4217-30.

Li, L., Rutlin, M., Abraira, V. E., Cassidy, C., Kus, L., Gong, S., Jankowski, M. P., Luo, W., Heintz, N., Koerber, H. R. et al. (2011). The functional organization of cutaneous low-threshold mechanosensory neurons. *Cell* **147**, 1615-27.

Majumdar, S. and Mallick, B. N. (2005). Cytomorphometric changes in rat brain neurons after rapid eye movement sleep deprivation. *Neuroscience* **135**, 679-90.

Manger, P. R. and Pettigrew, J. D. (1996). Ultrastructure, number, distribution and innervation of electroreceptors and mechanoreceptors in the bill skin of the platypus, Ornithorhynchus anatinus. *Brain Behav Evol* **48**, 27-54.

Marasco, P. D., Tsuruda, P. R., Bautista, D. M., Julius, D. and Catania, K. C. (2006). Neuroanatomical evidence for segregation of nerve fibers conveying light touch and pain sensation in Eimer's organ of the mole. *Proc Natl Acad Sci U S A* **103**, 9339-44.

Miller, M. R., Ralston, H. J., 3rd and Kasahara, M. (1958). The pattern of cutaneous innervation of the human hand. *Am J Anat* **102**, 183-217.

Muchlinski, M. N. (2010). A comparative analysis of vibrissa count and infraorbital foramen area in primates and other mammals. *J Hum Evol* **58**, 447-73.

Muller, M., Laube, B., Burda, H. and Bruns, V. (1992). Structure and function of the cochlea in the African mole rat (Cryptomys hottentotus): evidence for a low frequency acoustic fovea. *J Comp Physiol A* **171**, 469-76.

Nolano, M., Provitera, V., Crisci, C., Stancanelli, A., Wendelschafer-Crabb, G., Kennedy, W. R. and Santoro, L. (2003). Quantification of myelinated endings and mechanoreceptors in human digital skin. *Ann Neurol* **54**, 197-205.

Novotny, G. E. and Gommert-Novotny, E. (1988). Intraepidermal nerves in human digital skin. *Cell Tissue Res* **254**, 111-7.

Packer, O., Hendrickson, A. E. and Curcio, C. A. (1989). Photoreceptor topography of the retina in the adult pigtail macaque (Macaca nemestrina). *J Comp Neurol* **288**, 165-83.

Pare, M., Smith, A. M. and Rice, F. L. (2002). Distribution and terminal arborizations of cutaneous mechanoreceptors in the glabrous finger pads of the monkey. *J Comp Neurol* **445**, 347-59.

Peach, M. B. (2003). Inter- and intraspecific variation in the distribution and number of pit organs (free neuromasts) of sharks and rays. *J Morphol* **256**, 89-102.

Pettigrew, J. D. and Frost, B. J. (1985). A tactile fovea in the Scolopacidae? *Brain Behav Evol* **26**, 105-95.

Royer, D. L., Meyerson, L. A., Robertson, K. M. and Adams, J. M. (2009). Phenotypic plasticity of leaf shape along a temperature gradient in Acer rubrum. *PLoS One* **4**, e7653.

Russ, J. C. and DeHoff, R. T. (2000). Practical stereology. New York: Kluwer Academic/Plenum.

Sachdev, R. N. and Catania, K. C. (2002). Receptive fields and response properties of neurons in the star-nosed mole's somatosensory fovea. *J Neurophysiol* **87**, 2602-11.

Sawyer, E. K., Leitch, D. B. and Catania, K. C. (2014). Organization of the spinal trigeminal nucleus in star-nosed moles. *J Comp Neurol* **522**, 3335-50.

Schmitz, A., Bleckmann, H. and Mogdans, J. (2008). Organization of the superficial neuromast system in goldfish, Carassius auratus. *J Morphol* **269**, 751-61.

Schneider, C. A., Rasband, W. S. and Eliceiri, K. W. (2012). NIH Image to ImageJ: 25 years of image analysis. *Nat Methods* **9**, 671-5.

Schwann, T. (1847). Microscopical Researches into the Accordance of Structure and Growth in Animals and Plants London: Syndenham Society.

Song, H., Chui, T. Y., Zhong, Z., Elsner, A. E. and Burns, S. A. (2011). Variation of cone photoreceptor packing density with retinal eccentricity and age. *Invest Ophthalmol Vis Sci* **52**, 7376-84.

Spaethe, J. and Chittka, L. (2003). Interindividual variation of eye optics and single object resolution in bumblebees. *J Exp Biol* **206**, 3447-53.

Swennen, C. Y., Y.-T. (2004). Notes on feeding structures of the Black-faced Spoonbill Platalea minor. *Ornithological Science* **3**, 119-124.

Van der Loos, H., Dorfl, J. and Welker, E. (1984). Variation in pattern of mystacial vibrissae in mice. A quantitative study of ICR stock and several inbred strains. *J Hered* **75**, 326-36.

Van Vleck, D. (1965). The anatomy of the nasal rays of *Condylura cristata*. *Journal of Mammalogy* **248-253.**, 248-253.

Wark, A. R. and Peichel, C. L. (2010). Lateral line diversity among ecologically divergent threespine stickleback populations. *J Exp Biol* **213**, 108-17.

Welker, E. and Van der Loos, H. (1986). Quantitative correlation between barrel-field size and the sensory innervation of the whiskerpad: a comparative study in six strains of mice bred for different patterns of mystacial vibrissae. *J Neurosci* **6**, 3355-73.

Welker, K. L., Orkin, J. D. and Ryan, T. M. (2009). Analysis of intraindividual and intraspecific variation in semicircular canal dimensions using high-resolution x-ray computed tomography. *J Anat* **215**, 444-51.